An Integrated Site and Device Selection Methodology for the Ocean Wave Energy Sector

A thesis

submitted in fulfilment

of the requirements for the degree

of

Doctor of Philosophy in Engineering

at

The University of Waikato

by

DANIELLE VALERIE BERTRAM

THE UNIVERSITY OF
WAIKATO
Te Whare Wānanga o Waikato

2021

Abstract

The ocean covers approximately 70 % of the earth's surface and contains an immense source of renewable energy, in terms of ocean waves. However, this resource is unevenly distributed throughout the world, and so, therefore, converting waves into a useful form of energy will require the identification of potential Wave Energy Farm (WEF) locations. This should be undertaken in tandem with selecting an appropriate Wave Energy Converter (WEC), as the characteristics of these devices are critical in capturing the available wave power.

This thesis presents a novel integrated methodology to select and assess potential installation sites for WEFs, identify appropriate WECs, and overcome the limitations of current methods. Original contributions of this thesis include: (i) a robust method for identifying generic WEF sites based on the dimensions of sustainability, which includes a cultural dimension, and utilises limiting conditions to reduce large study areas; (ii) a suite of MATLAB tools—which thoroughly assesses potential WEF sites, in terms of the available resource as well as temporal, directional, and spectral characteristics; (iii) a WEC database which identifies all devices currently in development; and (iv) a WEC classification scheme that classifies devices in a practical and meaningful manner in order to streamline the selection process of WECs for wave energy projects.

Several of the developed methods have been applied to a New Zealand (NZ) case study. Results confirm that with the application of the proposed site selection method, that 12 suitable WEF sites, clustered within four regions along the west and south coast of NZ, were identified from the initial study area of approximately 4.1 million km^2. In terms of site assessment, the utilisation of the MATLAB tools established that a higher-energy area comprised the south of NZ and that as expected, the available resource at all sites was subjected to seasonal variability, with a maximum and minimum wave power available in the winter and summer months, respectively. Furthermore, it was determined that due to the westerly wind flow that dominates the wave generation and direction of wave propagation in NZ, that the prevailing wave approach direction at all the sites was between South-South-West and West-North-West. With regards to the spectral characteristics, it was further determined that a wide range of wave conditions were experienced at each site.

The development of the WEC database identified that 116 companies were actively developing 130 devices. These devices were then classified according to five main categories, which included a technology maturity class. Moreover, 41 devices were identified as being at an advanced technology level.

Acknowledgements

A large amount of work, research, and dedication was needed to complete this project, and the execution thereof would not have been possible if I did not have the support of a substantial number of individuals.

First and foremost, I would like to express my sincerest gratitude to my chief supervisor Professor Michael R. W. Walmsley, for his continued support and guidance throughout this journey whilst encouraging me to develop into an independent researcher. I would also like to acknowledge and thank my co-supervisors, Dr Martin J. Atkins, Dr Graeme D.E. Glasgow, and especially Dr Amir H. Tarighaleslami. Amir, your endless patience, comments, and suggestions were greatly appreciated. I would also like to take the opportunity to thank Dr James R. Neale for his continuous encouragement, and Professor Mark Dyer, Dean of Engineering, for piquing my interest in pursuing a PhD during my undergrad in Ireland and then giving me the opportunity to pursue my academic dream here in New Zealand. Andrzej and I really appreciated your warm welcome when we arrived in the country and your continued support.

As a large amount of external data was required for this research, I would like to take this opportunity to thank all the individuals, private and governmental organisations, and wave energy developers for the assistance they have provided over the last three years. Dr Helen Bostock and Mr William Dick, thank you for your continued support, mentorship, and invaluable advice. Mr João Albuquerque, thank you for developing the brilliant NZ Wave Data Tool and making it freely available. Also, thank you very much to the following organisations for providing free data so that I was able to complete my analysis: Ministry for Primary Industries, Maritime NZ, MetOcean Solutions (especially Dr Brett Beamsley for providing the wave energy resource contour lines), NIWA, Environment Canterbury, Trustpower NZ, and Fisheries NZ (especially Ms Anna Cochran for going above and beyond to source AIS data, and Mr Bruce Barton for allowing me access and the use of his AIS data).

I am also grateful to past and present members of the Sustainable Energy, Water & Resilient Systems Group, especially: Dr Benjamin Ong, Dr Nathan Lal, Mr Yihan Wu, Mr Lance Wong, Mr Mohammed Kariri and Ms Marianne Hull-Cantillo. Thank you for the lively discussions, laughs, continued support, and, most importantly, the baked treats.

Thank you to all the amazing friends that I have made at the University of Waikato, especially Dr Rachael Tighe, Dr Mark Lay, Dr Chanelle Gavin, Mr Yousef Alshammari, and Ms Natalie Shaw. Natalie, thank you also for 'Natalie'ing' my thesis and for being such a great friend. Also, I would like to thank the school administrator Ms Mary Dalbeth and the subject librarians, Ms Cheryl Ward and Ms Debby Dada, for always being on hand to help; it was much appreciated.

To my sister, Natasha (Tash), for her endless support, assisting with my figures, proofreading my thesis, and just being an all-round amazing person. To the rest of my family, Miriam (mom), George (dad), Georgie, Leigh-Anne, and Eoghan, thank you for all unconditional support, laughter, smart remarks (Georgie and Tash!), and for keeping me on my toes. Thank you so much for sending me a PhD care package, and more importantly, making sure it was full of my favourite treats! You may be across the ocean, but you are always close to my heart, and I miss you all dearly.

Do moich polskich rodzin Błaszczyków i Stefanków. Naprawdę doceniam to, że zostałam przyjęta z otwartymi ramionami oraz waszą nieustającą miłością i z wsparciem przez lata. To, czego nie można było przekazać słowami, na pewno zostało pokazane poprzez wasze wsparcie.

Lastly, and most importantly, to my beloved husband, Andrzej Błaszczyk, for his unwavering support, encouragement, as well as unconditional love. You have been my absolute rock these last twelve years, and without your endless support and encouragement, I would have never achieved my childhood dream of becoming an engineer. Kocham cię bardzo.

Contributing Publications

The majority of the proposed methods and results in this thesis have been published in an international journal and peer-reviewed conference papers. Chapter 3 is comprised of an article published in Renewable and Sustainable Energy Reviews [1] as well as a peer-reviewed conference paper published in the Australasian Coasts and Ports 2019 conference proceedings [2]. Part of Chapter 4 is published in Renewable and Sustainable Energy Reviews [1]. Chapter 5 is comprised of the article published in Renewable and Sustainable Energy Reviews [1] and a peer-reviewed conference paper published in the proceedings of the 22nd Conference on Process Integration, Modelling and Optimisation for Energy Saving and Pollution Reduction (PRES'19) [3].

The research comprising this thesis has been presented at several local and international conferences, namely, the Waikato Young Research Engineers Symposium [4], the PRES'19 Conference, and the Australasian Coasts and Ports Conference [5] through both oral and poster presentation. Most notably, Chapter 3 was awarded the New Zealand Coastal Society 'Coasts and Ports' Student Award for best student paper presented at the 2019 Australasian Coasts and Ports Conference, and Chapter 5 was awarded the best poster award (1st place) at the PRES 2019 Conference.

Research Publications

[1] **Bertram DV**, Tarighaleslami AH, Walmsley MRW, Atkins MJ, Glasgow GDE. A systematic approach for selecting suitable wave energy converters for potential wave energy farm sites. Renewable and Sustainable Energy Reviews. 2020;132:110011.

[2] **Bertram DV**, Bostock H, Walmsley MR, Atkins MJ, Glasgow G. Geospatial multi-criteria analysis for site selection of wave energy farms in New Zealand. Australasian Coasts and Ports 2019 Conference: Future directions from 40 [degrees] S and beyond; 2019 10-13 Sep; Hobart, Australia: Engineers Australia.

[3] **Bertram DV**, Oskartiz O, Tarighaleslami AH, Walmsley MRW, Atkins MJ, Glasgow GDE. A systematic approach for selecting suitable wave energy converters for potential wave energy farm sites. In: Varbanov PS, Seferlis P, Voutetakis SS, Walmsley TG, Klemeš JJ, editors. PRES'19: Proceedings of the 22nd Conference on Process Integration, Modelling and Optimisation for Energy Saving and Pollution Reduction; 2019 20–23 Oct; Crete, Greece.

Conference Presentations

[4] **Bertram DV**. Selecting suitable wave energy converters for the New Zealand wave climate. Waikato Young Research Engineers Symposium 2018 1 Nov; Hamilton, New Zealand, *accepted for oral presentation*.

[5] **Bertram DV**. Geospatial multi-criteria analysis for site selection of wave energy farms in New Zealand. Australasian Coasts and Ports 2019 Conference: Future directions from 40 [degrees] S and beyond; 2019 10-13 Sep; Hobart, Australia.

Table of Contents

List of Figures

List of Tables

Nomenclature

Abbreviations

A1	Auckland 1
A2	Auckland 2
A3	Auckland 3
AEP	Annual Electricity Production [kWh]
AIS	Automatic Identification System
AoI	Area of Interest
CA	Class A: Larger Vessels
CAPEX	CAPital EXpenditure
CO_2	Carbon Dioxide
COV	Coefficient of Variation
CRF	Capital Recovery Factor
CWR	Capture Width Ratio
DD	Decimal Degrees
EEZ	Exclusive Economic Zone
ENSO	El Niño-Southern Oscillation
ESBI	Electricity Supply Board International
G1	Greymouth 1
G2	Greymouth 2
G3	Greymouth 3
GIS	Geographic Information System
I1	Invercargill 1
I2	Invercargill 2
I3	Invercargill 3
IEA-OES	International Energy Agency — Ocean Energy Systems
IoA	Willmott Index of Agreement
LCOE	Levelised Cost of Electricity
LINZ	Land Information New Zealand
MDA	Multi-Dimensional Analysis
MPA	Marine Protected Area
MV	Monthly Variability Index
NaN	Not a Number
NIWA	National Institute of Water and Air
NP1	New Plymouth 1
NP2	New Plymouth 2
NP3	New Plymouth 3
NZ	New Zealand
NZCS2000	New Zealand Continental Shelf Lambert Conformal 2000
NZGD2000	New Zealand Geodetic Datum 2000
O&M	Operations and Maintenance
OPEX	OPerating EXpenditure
OWC	Oscillating Water Column
PIA	Potential Installation Areas
PTO	Power Take-Off
R&D	Research & Development
RfI	Request for Information
RMSE	Root-Mean-Square-Error

SI	Scatter Index
SQL	Standard Query Language
SS	Suitability Scale
SV	Seasonal Variability Index
SWAN	Simulating WAves Nearshore
SWL	Still Water Level
TPL	Technology Performance Level
TRL	Technology Readiness Level
UK	United Kingdom
USA	United States of America
USD	United States Dollars
WAVEPLAM	WAVe Energy PLAnning and Marketing
WEC	Wave Energy Converter
WEF	Wave Energy Farm
WGS84	World Geodetic System 1984

Roman Symbols

A_f	Availability factor
a	Wave amplitude [m]
B	WEC characteristic dimension [m]
C	Constraint [%]
C_f	Capacity factor
c	Wave celerity [m/s]
c_g	Group celerity [m/s]
d	Water depth [m]
$d_{critical}$	Deep-water limit [m]
dr	Discount rate [%]
E_k	Kinetic energy [MWh/m]
E_p	Potential energy [MWh/m]
E_{wave}	Total wave energy per unit area of sea surface [MWh/m]
f	Wave frequency [Hz]
g	Gravity [m/s^2]
H	Wave height [m]
H_{m0}	Spectral significant wave height [m]
k	Wavenumber [m^{-1}]
M_{max}	Most energetic month [kW/m]
M_{min}	Least energetic month [kW/m]
m	Median
m_n	N'th spectral moment
N	Number of data points
n	Project life expectancy [years]
P_E	Average power output [kW]
P_{occ}	Resource-characterisation matrix [%]
P_T	Wave-power matrix [kW/m]
P_{wave}	Wave power per metre width of wave crest [kW/m]
P_{WEC}	WEC power matrix [kW]
R	Restriction [%]
R_C	WEC rated capacity [kW]
r	Pearson correlation coefficient
$S(f)$	Wave-variance spectrum [m^2/Hz]
S_{max}	Most energetic season [kW/m]

S_{min}	Least energetic season [kW/m]
T	Wave period [s]
T_e	Energy wave period [s]
T_{m01}	Mean wave period [s]
T_{m02}	Mean wave period [s]
T_p	Peak wave period [s]
t	Year from start of project
WEF_c	Project capacity [kW]
w	Weighting [%]
x_o	Observed measurements
$\bar{x}_o$	Average of observed measurements
x_m	Modelled measurements
$\bar{x}_m$	Average of modelled measurements
y	Minimum value
z	Maximum value

Greek symbols

α	Fixed conversion factor
γ	Peak enhancement factor
σ	Standard deviation
θ_m	Mean wave direction [°]
θ_p	Peak wave direction [°]
λ	Wavelength [m]
μ	Mean
Π	Product
ρ	Density [kg/m³]
Σ	Sum

Chapter 1

Introduction

1.1 Background

Access to energy is fundamental in developing the economy of a country, alleviating poverty, and ensuring human wellbeing [6, 7]. However, as the population continues to grow, so does the demand for energy (Figure 1.1). In a recently published report by the International Energy Agency [8], it was established that the global energy consumption growth rate had almost doubled in 2018 compared to that of 2010. This increased consumption led to the additional demand for fossil fuels, resulting in emissions rising to a historic high of 33.1 Gt CO_2 (carbon dioxide), a 1.7 % increase since 2010. This significant increase in demand was attributed to being driven by a robust global economy and the effects of climate change (increased cooling and heating demands throughout the world).

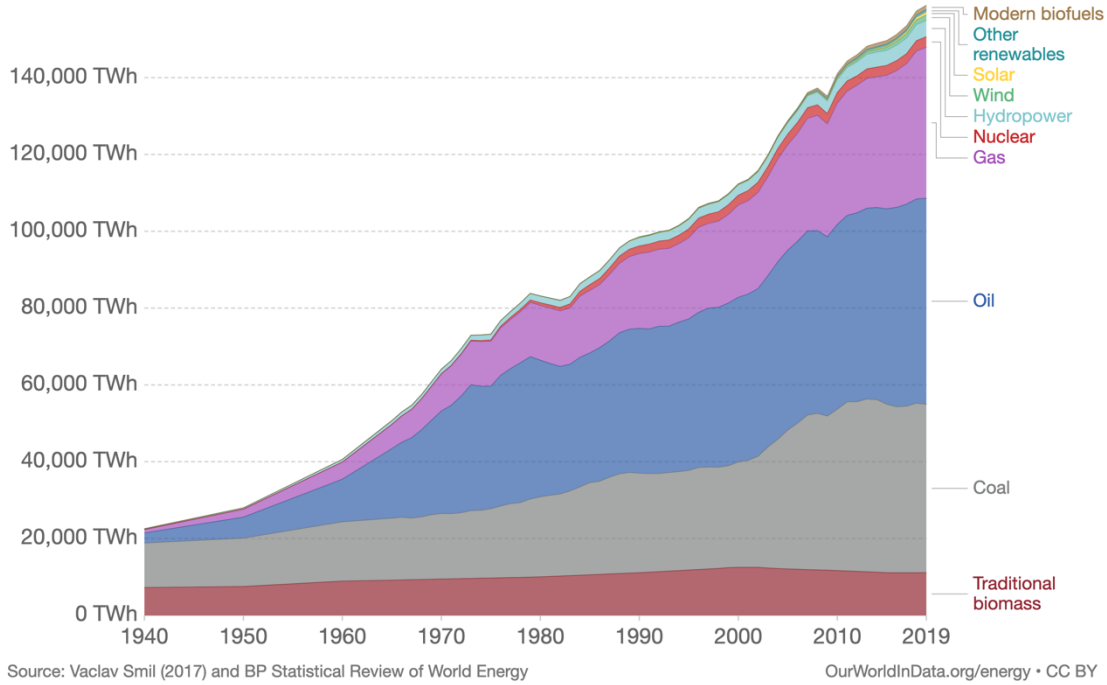

Figure 1.1. Global direct primary energy consumption from 1940 to 2019 (image source: Our World in Data, licensed for re-use under CC BY 4.0) [6].

Fossil fuels comprised approximately 80 % of the primary global energy demand [9]. As current energy systems are still dominated by these fuels (coal, oil, and gas) [6], it is unsurprising that the energy sector accounted for approximately two-thirds of global CO_2

emissions [8]. As CO_2 is the primary driver of global climate change, a substantial and concerted transition to affordable, sustainable, low emissions energy systems is required.

Just as essential, however, is the need to secure access to energy for quality of life and economic development. Hence, the United Nation's established Sustainable Development Goal 7, which calls for ensuring global access to affordable, reliable, and clean energy by 2030. However, the world is currently falling short on all of the clean energy targets. As a result, approximately one billion people are still living without access to electricity [10]. Furthermore, the COVID-19 pandemic has highlighted the central role that energy has in responding to emergencies, as inadequate energy access has quickened the spread of the virus [11].

As ocean wave energy is considered to be one of the most promising sources of clean, reliable, and renewable energy [12], it has the potential to play an important role in the world's efforts to combat climate change. Potentially decreasing CO_2 emissions by 1–2 billion tons per year if it displaced conventional fossil fuel sources [13]. Furthermore, it is estimated that there is a theoretical global wave energy potential of 32,000 TWh available per year [14], which is approximately 1.2 times the global electricity supply in 2019 (27,004.7 TWh/yr) [15]. Moreover, with approximately 40 % of the world's population residing in coastal areas [16], this provides additional opportunities for the deployment of Wave Energy Converters (WECs) for distributed generation.

Compared to other renewable energy sources, wave energy is more predictable, more constant, has a lower visual and environmental impact, and most significantly, a higher energy intensity [17]. However, this sector is still relatively immature compared to that of wind and solar [18], and despite considerable research and development, there are a significant number of competing technologies, which show no sign of converging to a preferred design [19]. Another limitation is that the performance of the device is site dependent, and therefore, it will behave differently at different locations [20].

Furthermore, as seen in Figure 1.2, wave energy is also unevenly distributed throughout the world, where the best locations for extracting wave power would be in north and south temperature zones (latitudes of ±30° to ±60°) [21]. Therefore, a key stage in developing a Wave Energy Farm (WEF) is to identify and assess potential deployment locations [22].

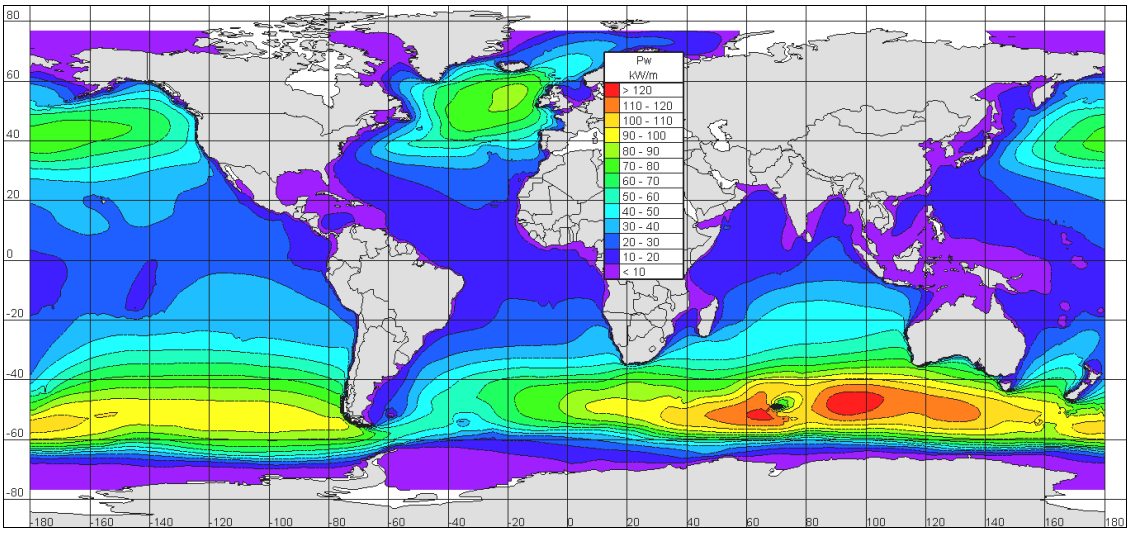

Figure 1.2. Global distribution of mean wave power, from 1997 to 2006 [21]. Reprinted with permission from A. Cornett (personal communication, June 26, 2020).

1.2 Research Aim

This environmental engineering thesis aims to develop a framework that can be implemented in order to identify optimal WEF sites (that is applicable at multi-scale) and subsequently, the most suitable WEC(s) for these locations. The approach proposes the use of five main dimensions, based on the pillars of sustainability, to assist in determining the relevant site selection criteria. Limiting conditions will then be applied to reduce the initial area of interest, and thereafter, spatial Multi-Dimensional Analysis (MDA) will be utilised to conduct the analysis. Once the most suitable locations have been identified, the available resource will be quantified, and the temporal, directional, and spectral characteristics of the wave climate will be examined at each site for several timescales (where relevant). The proposed site selection and site assessment methodology will be applied to a Southern Hemisphere case study; New Zealand (NZ).

A review of the current wave energy technologies in development will also be undertaken, and five main categories (with appropriate descriptors) will be proposed to classify these devices in a meaningful way. An initial screening of the WECs based on advanced maturity level will then be applied, and if applicable, devices will be screened further based on site-specific considerations. Thereafter, performance comparison metrics will be proposed and discussed.

1.2.1 Key Research Questions

Key research questions include:

1. How to determine appropriate site selection criteria?
2. How to identify suitable WEF locations from large areas, such as the Exclusive Economic Zone (EEZ) of a country?
3. How to determine the suitability of a marine area for the installation of a WEF?
4. How to thoroughly assess the wave climate at potential WEF sites?
5. How to classify devices in a practical and meaningful manner?

1.3 Thesis Outline

Chapter 2 thoroughly reviews the key literature and advances in WEC development, WEF site selection, and WEC site matching, which are most relevant to the thesis aim. It examines the current state of the art for both WEF site selection and WEC site matching methods. This review highlights that these two separate approaches are intrinsically linked and should be integrated to form a holistic and systematic methodology that should be applied in order to determine the most optimal WEF site. The chapter also provides a brief overview of the theory relating to ocean wave energy, as a fundamental understanding of the wave transformation processes is required to exploit the wave energy resource effectively.

Chapter 3 develops a novel methodology for selecting appropriate sites for wave energy projects, utilising MDA within a Geographic Information System (GIS) framework. It highlights the importance of sustainability and that the dimensions of sustainable development should be integral in identifying appropriate site selection considerations. Furthermore, it emphasises the need for cultural considerations, as coastal indigenous communities are intrinsically linked with the marine environment. This chapter also shows that with the selection of appropriate limiting conditions (based on the constraints of the current technology), the proposed approach can be applied to a large study area. The new method is applied to an NZ case study, utilising geoprocessing tools within ArcGIS applications to conduct the analysis.

Chapter 4 presents an effective and efficient method for assessing the wave climate at the potential WEF sites. It highlights that the most optimal solution is not necessarily the site with the greatest resource. In this chapter, the available resource is quantified, and the

directional, temporal, and spectral characteristics at each site are examined using the range of developed MATLAB tools.

Chapter 5 develops a method for selecting the most appropriate WEC(s) for a potential WEF site. All WECs currently under development are identified and the relevant information collated into an Excel spreadsheet database. It highlights the importance of classifying devices appropriately in order to streamline the process and that ultimately the most suitable location for a WEF is WEC dependent. This chapter also emphasises that as the wave energy sector is continually evolving, the developer database will have to be continuously updated.

Chapter 6 summarises the major findings of the research and provides recommendations for areas of future work.

Chapter 2
Literature Review

2.1 Introduction

Converting the energy within waves into usable energy has been attempted since the 18th century, where the Girard's filed the first known patent in France, in 1799 [23], for a shoreline device that was designed to mechanically extract energy from ocean waves [24].

Since that initial design over 200 years ago, the development of wave energy devices has been sporadic [24]. The next notable wave energy device was developed in the late 1940s by Yoshio Masuda, a Japanese naval officer, and is considered to be the first (floating) Oscillating Water Column (OWC) [23]. This device was a navigation buoy, which used an air turbine to power its lamp, and since 1965 over 1,000 of these devices have been produced and marketed worldwide [25].

Ocean wave energy was only earnestly considered an alternative energy source during the oil shortage crisis in the early 1970s [23, 24]. This renewed interest was due to a landmark paper published by Stephen Salter in 1974 regarding the Salter Duck WEC [26], which is still renowned as the most efficient device (measured at 90 % [27]) ever designed [28]. This renewed interest led to both the British and Norwegian governments starting Research and Development (R&D) programmes in wave energy in 1975 [23], with the first conferences taking place in England in 1976 and 1978 [23].

However, by the early 1980s, funding for R&D decreased markedly, especially in England [23], due to declining oil prices [29] and the lack of commercially viable devices [28]. This absence of public finance virtually halted the considerable progress that was occurring [28].

The focus shifted back to wave energy in 1991 when the European Commission included ocean energy in their R&D program regarding renewable energies [23]. Canada and the United States of America (USA) followed suit over a decade later with the formation of collaborative programs to demonstrate ocean energy conversion (focused mainly on tidal and wave energy) in North America [30]. Whilst wave energy R&D began in earnest in the early 2010s in Japan, Korea and China [31, 32], which culminated in the first Asian Wave and Tidal Energy Conference in 2012 [33].

In recent years the wave energy sector has suffered a number of major setbacks, which have been attributed to the delayed progress in developing viable technologies [34]. These setbacks ranged from original equipment manufacturers withdrawing from the sector in 2012 and 2013 [34] to the business failure of advanced wave energy developers, Wavebob [35], Pelamis Wave Power [34], Oceanlinx [36] and Aquamarine Power [34], in 2013 and 2014. Despite these significant setbacks, the sector started to recover in 2016 [34], and there are currently over 100 WECs in various stages of development around the world [1].

2.2 Developmental Stages

In order to standardise the ad hoc approach to WEC development that led to this divergence in technology, slow rate of development as well as numerous device failures and considerable investment losses over the years, the International Structured Development Plan was established by the International Energy Agency — Ocean Energy Systems (IEA-OES) group [37]. This plan incorporates Technology Readiness Levels (TRLs) into a five-stage approach, which sets out the requirements for a WEC concept to achieve commercialisation (Figure 2.1(a)). TRLs are internationally recognised and widely accepted as a benchmarking tool for tracking the advancement of emerging technologies [37] and are commonly comprised of nine development levels, with the ninth level representing the most mature technology.

As seen in Figure 2.1(b), utility companies, Electricity Supply Board International (ESBI) and Vattenfall, further proposed that TRLs should not only be defined in terms of the technology's readiness to convert ocean wave energy and export it to the grid ('functional readiness') but also address the project's lifecycle requirements such as operational and supply chain readiness, and risk and cost reduction ('lifecycle readiness') [38].

Each of the stages proposed in the IEA-OES structured programme can be equated to specific ESBI and Vattenfall defined TRL(s) (with the exception of TRL 1, 2, and 9). This has been shown in Figure 2.1 by utilising a distinct colour for each of the five development stages in the IEA-OES structured programme and relating it to the relevant ESBI and Vattenfall TRLs.

(a)

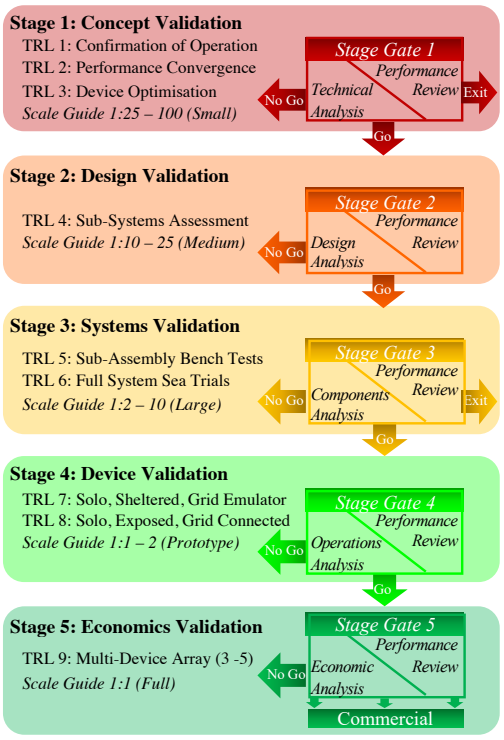

(b)

TRL	Functional Readiness	Lifecycle Readiness
1	Basic principles observed and reported.	Potential uses of technology identified.
2	Technology concept formulated.	Market and purpose of technology identified.
3	Analytical and experimental critical function and/or characteristic proof-of concept *(Scale Guide 1:25 - 100)*	Initial capital cost and power production estimates/targets established.
4	WEC component and/or basic WEC subsystem validation in laboratory environment. *(Scale Guide: >1:25)*	Preliminary lifecycle design: targets for manufacturable, deployable, operable and maintainable technology.
5	WEC component and/or basic WEC subsystem validation in relevant environment. *(Scale Guide 1:4 - 15)*	Supply-chain mobilisation: Procurement of subsystem design, installation feasibility studies, cost estimations, etc.
6	WEC prototype demonstration in relevant environment. *(Scale Guide >1:4)*	Customer interaction: consider customer requirements to inform design. Inform customer of likely project site constraints.
7	WEC prototype demonstration in operational environment. *(Scale Guide 1:2)*	Ocean operational readiness: management of ocean scale risks, marine operations, etc.
8	Actual full-scale WEC completed and qualified through test and demonstration. *(Scale Guide 1:1)*	Actual marine operations completed and qualified through test and demonstration.
9	Operational performance and reliability demonstrated for an array of WECs. *(Scale Guide Multiple 1:1)*	Fully de-risked business plan for utility scale deployment of arrays.

Figure 2.1. Industry proposed WEC development protocols: (a) the international structured five-stage development protocol, modified from Holmes and Nielsen [37]; (b) ESBI and Vattenfall Wave Energy Systems TRLs, defined in terms of both functional readiness and lifecycle readiness [38, 39].

Whilst TRLs are predominately used to rate the technical maturity of a device, Weber [40] introduced the complementary Technical Performance Levels (TPLs). This scale evaluates the techno-economic potential of a WEC by assessing cost drivers such as: environmental, social and legal acceptability; power absorption and conversion; system availability (including the device's survivability mode); capital expenditure as well as lifecycle operational expenditure [40]. Similarly to the TRL scale, TPLs are categorised into nine levels, with the ninth level representing an economically viable and competitive device.

2.3 Classification Schemes

As wave energy technology development stages vary widely, so do the proposed classification schemes. Traditionally WECs have been classified according to operating principle (overtopping device, OWC, and wave-activated bodies) [41], location (shoreline, nearshore and offshore; floating, submerged or bottom-standing), directional alignment (terminators, attenuators, and point absorbers) and Power Take-Off (PTO) systems (mechanical, hydraulic, pneumatic, and directly electrical) [42].

However, as the sector has advanced, numerous approaches have been proposed in the literature that attempts to adapt this traditional WEC classification system to include the development of novel and unconventional devices. Drew et al. [43] introduced a variation of the traditional classification scheme with the addition of the submerged pressure differential and oscillating wave surge converter and the removal of the wave-activated bodies from the operating principle category. Whereas the European Marine Energy Centre [44] and Li and Yu [45] identified eight and five main WEC types, respectively. These classification schemes appear to be various combinations of the main categories proposed by Falcão [41], Falnes [42], and Drew et al. [43], with the addition of the rotating mass [44], bulge wave [44] and membrane [45] device types.

More recently, Lehmann et al. [46] have proposed that a wide range of wave energy technology can be classified by using five main categories: working principle (OWC, heaving buoy, submerged pressure differential, wave activated bodies, bulge wave, oscillating wave surge, rotating mass and cycloidal wave absorber); location (shore-based, nearshore, and offshore); orientation (point absorber, attenuator, and terminator); PTO system (hydraulic, direct drive, hydro, and pneumatic); and TRLs.

Alternative categorisation based on the referencing configuration (self-referencing or seabed/shoreline referencing) and mode(s) of motion (heave, pitch, and/or surge) of the WECs primary conversion component has been proposed by the EquiMar project [47]. Whereas Margheritini et al. [48] recommended a classification scheme based on the WECs expected environmental impact. This scheme classified the devices by: location (onshore, intermediate, and offshore); stability elements (anchors/moorings and foundations); PTO system; as well as the obstruction to the water column and sea surface. Whilst many WECs can be accommodated within these numerous classification schemes, there are still a large number of device concepts that cannot be captured.

The lack of an all-encompassing taxonomy is an issue because a WEC will not perform the same in different locations, and likewise, different WEC designs perform differently at the same location [20]. This is due to the characteristics and tuning of the device [49]. Design characteristics such as the WEC's operational range and efficiency at various sea states are critical in quantifying the amount of energy that can be harvested at a specific site [50]. Whilst the technology's ability to be tuned to the dominant wave frequency will maximise its energy capture [51]. Therefore, in determining if a wave energy project is feasible, it is vital that the most suitable WEC is selected for the potential WEF site [20], and this selection process can be streamlined by classifying devices appropriately.

2.4 Site Selection

Before attempting to determine the most suitable device(s) for a potential site, initial deployment locations need to be identified and assessed, as wave energy is unevenly distributed throughout the world [18]. Bedard et al. [52], Zubiate et al. [53] and Kim et al. [54] identified an accurate assessment of the wave energy resource as the most important factor with regards to determining a suitable location for the installation of a WEF. This is because wave energy projects are only considered viable in locations where the potential annual wave power is greater than 20 kW/m [55, 56]. Furthermore, in order to effectively exploit the wave energy resource, a fundamental understanding of the wave transformation processes is required.

2.4.1 The Wave Resource

Wave Parameters

Wave motion can be simply described as a regular, sinusoidal (monochromatic) wave with the characteristics depicted in Figure 2.2. Monochromatic waves have constant height H, wavelength λ, and period T [24].

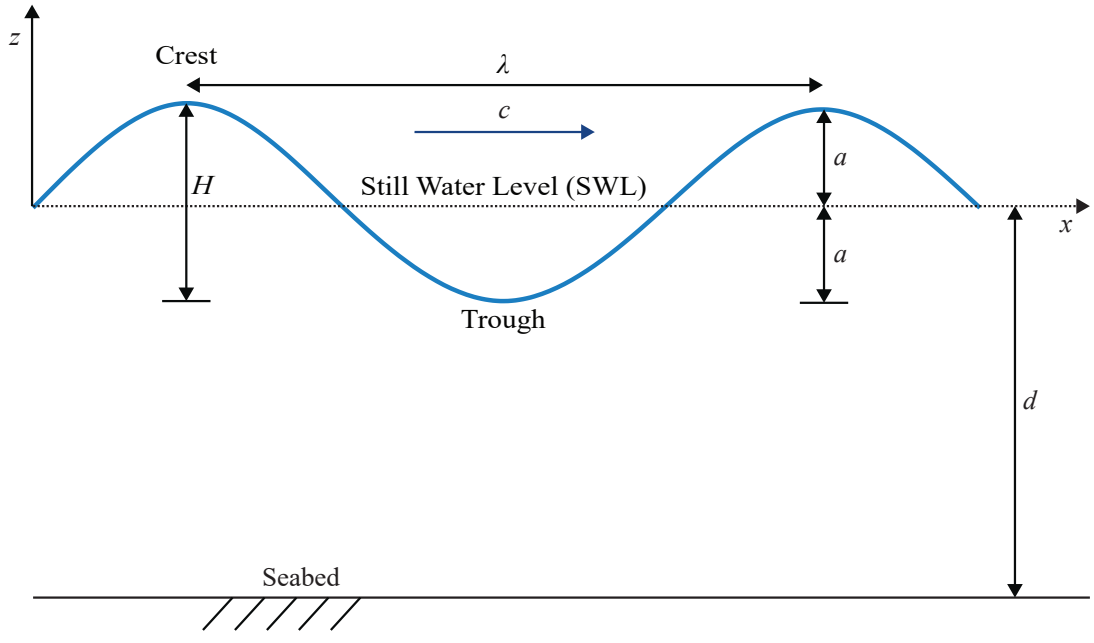

Figure 2.2. A monochromatic wave propagating at celerity *c* on water of depth *d*, adapted from [57] and [58].

The important wave parameters (including those depicted in Figure 2.2), have been defined in Table 2.1.

Table 2.1. Definition of wave parameters.

Parameter	Description
Crest	Highest part of the wave [59]
Trough	Lowest part of the wave [59]
Water depth d [m]	Vertical distance between the SWL and seabed
Wave amplitude a [m]	Vertical distance between the SWL and crest (or trough) [57]
Wave height H [m]	Vertical distance between the crest and adjacent trough ($H = 2a$) [57]
Wavelength λ [m]	Horizontal distance between two successive crests (or troughs) [57]
Wave period T [s]	Time it takes two successive crests (or troughs) to pass a fixed point (wave cycle) [59]
Wave frequency f [Hz]	Number of wave cycles that are completed in a second (therefore the reciprocal of the wave period: $f = 1/T$) [59]
Wavenumber k [m^{-1}]	Number of wave cycles per metre ($k = 2\pi/\lambda$) [57]
Wave celerity c [m/s]	The speed at which the wave crest (or trough) travels [58], calculated as follows [60]: $$c = \frac{\lambda}{T} = \frac{gT}{2\pi}\tanh\left(\frac{2\pi d}{\lambda}\right) \quad (2.1)$$ where g is acceleration due to gravity (9.81 m/s^2). In deep water [60]: For $d/\lambda > 0.5$, $\tanh\left(\frac{2\pi d}{\lambda}\right) \cong 1$, therefore, Equation (2.1) reduces to: $$c = \frac{gT}{2\pi} \quad (2.2)$$ In shallow water [60]: For $d/\lambda < 0.05$, $\tanh\left(\frac{2\pi d}{\lambda}\right) \cong \frac{2\pi d}{\lambda}$, therefore Equation (2.1) reduces to: $$c = \sqrt{gd} \quad (2.3)$$
Group celerity c_g [m/s]	The speed at which the wave train, and wave energy, travels [58], calculated as follows [61]: $$c_g = \frac{1}{2}\left[1 + \frac{4\pi d/\lambda}{\sinh(4\pi d/\lambda)}\right]c \quad (2.4)$$ In deep water: For $d/\lambda > 0.5$, $\frac{4\pi d/\lambda}{\sinh(4\pi d/\lambda)} \cong 0$, therefore, Equation (2.4) reduces to: $$c_g = \frac{c}{2} = \frac{gT}{4\pi} \quad (2.5)$$ In shallow water: For $d/\lambda < 0.05$, $\frac{4\pi d/\lambda}{\sinh(4\pi d/\lambda)} \cong 1$, therefore, Equation (2.4) reduces to: $$c_g = c = \sqrt{gd} \quad (2.6)$$

The Wave Resource

When the ocean surface is disturbed by wind, gravity, seafloor landslides or seismic disruptions (disturbing forces) [59], waves are generated (Figure 2.3). As the wave passes, the surface of the ocean is returned towards its original flat state by gravity or, in the case of ripples, surface tension (restoring forces) [59]. As seen in Figure 2.3, the majority of the energy available in the various types of waves is concentrated in wind waves [59]. Therefore, these are the most suitable for energy utilisation [62], and thus the focus of the wave energy sector [24].

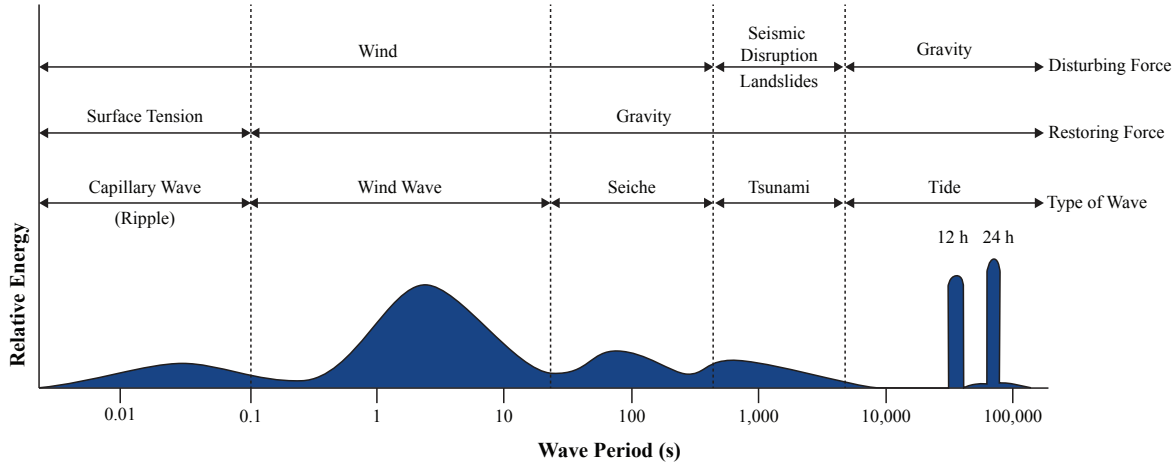

Figure 2.3. The formation of, and the distribution of energy in, the various types of ocean waves, adapted from [59].

Wind Waves

Wind waves form as a result of energy being transferred from the wind (produced by the differential heating of the earth by the sun) to the water surface as it blows over the ocean [62]. At each stage of the conversion process, power is spatially concentrated. The original solar energy with a typical power intensity of 0.1 kW/m^2–0.3 kW/m^2 (area perpendicular to the sun's rays) is transformed into wind energy with an intensity of approximately 0.5 kW/m^2 (area perpendicular to wind direction). Further spatial concentration occurs as wind energy is converted into wave energy, resulting in an increased power intensity of typically 2–3 kW/m^2 (area perpendicular to wave propagation) [42]. Therefore, wave energy can be considered a concentrated form of solar energy [62].

The energy contained within a wave is stored equally in the mass of water displaced from the SWL (potential energy E_p) and in the motion of water particles (kinetic energy E_k) [58, 62]. Thus the total energy per unit area of sea surface is [63]:

$$E_{wave} = E_p + E_k = \frac{1}{8}\rho g H^2 \quad (2.7)$$

where ρ is the density of seawater (1,025 kg/m^3).

As the wave passes, there is no significant net advancement of water mass because the water particles located in the wave crest move up and forward, whilst the water particles in the wave trough will move down and backwards (Figure 2.4). Thus the average position of the water particle does not change, and therefore, wave energy and waveform (shape of the wave), not water particles, are transmitted across the ocean surface [59].

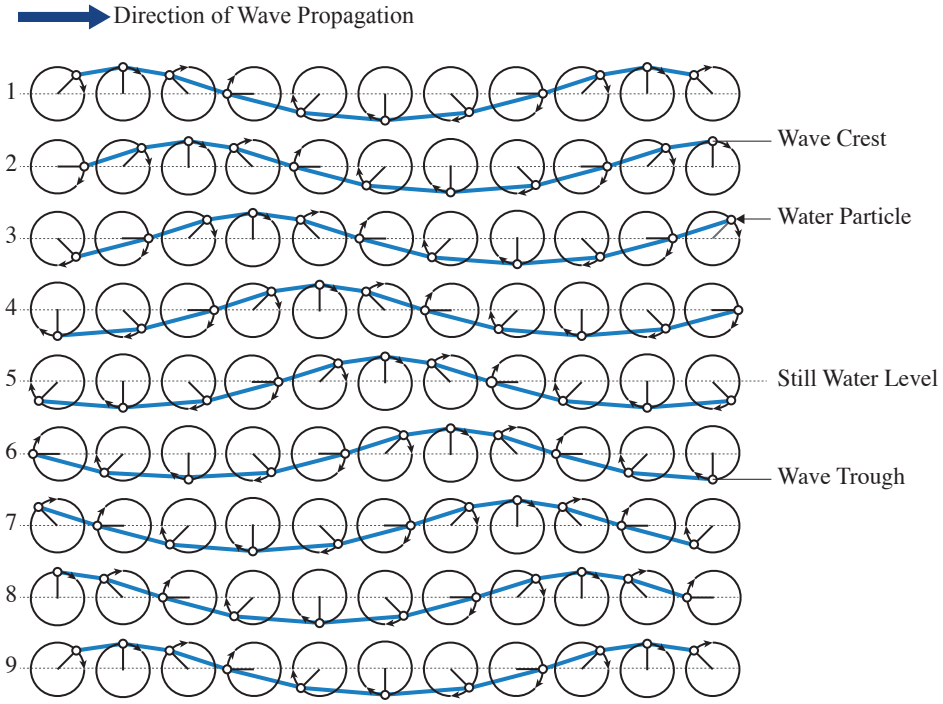

Figure 2.4. Nine snapshots depicting the orbital motion of the water particles as a wave is transmitted across the ocean surface, adapted from [58].

Generation of Wind Waves

As the wind blows over a calm ocean surface, small variations in the wind speed result in air pressure fluctuations above the water surface, which produce ripples (capillary waves) [57]. The slopes of these small capillary waves are further acted upon by the wind causing additional wave growth and leading to the development of complex, irregular wind seas (as illustrated by the wave profile in Figure 2.5) [57]. This chaotic surface forms due to the interaction (constructive and destructive wave interference) of numerous waves of varying wavelengths, periods, and heights travelling in different directions and at different speeds [64].

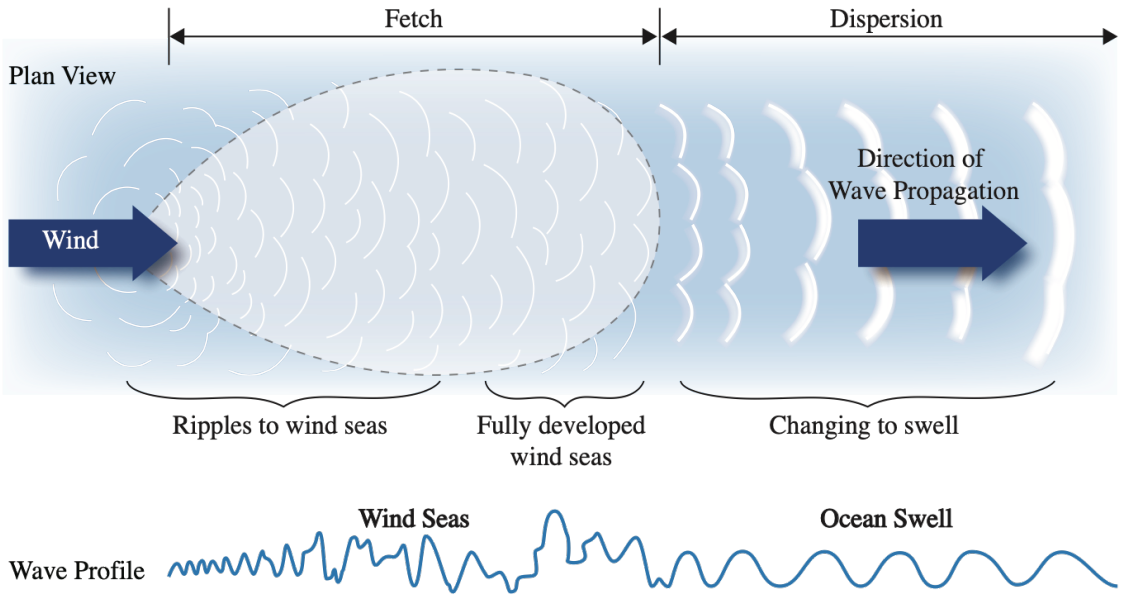

Figure 2.5. The generation and growth of wind waves, adapted from [64] and [59].

The quantity of wind energy transferred, and therefore the variety and size of the resulting waves is a function of the wind speed (or wind strength) [59], the length of time the wind blows (wind duration) [59], the uninterrupted distance over which the wind blows in a single direction (fetch) [59], and the original state of the sea surface [64]. Therefore, larger, more powerful waves (increased wave height, period and length [59]) are generated by high wind speeds blowing for an extended period of time over a vast expanse of water [65].

The wind seas continue to grow in size within the fetch area until a steady-state condition has been achieved for the prevailing wind conditions (wind speed, duration, and fetch) [64]. This is referred to as a fully developed sea (Figure 2.5); the waves cannot grow further in size under the existing wind conditions because the rate of energy supplied by the wind equals that dissipated by the waves breaking [66].

Once the waves travel outside the fetch area, the wind imparts no further energy, and so, therefore, the length, speed (celerity), and period of the waves remain unchanged [64]. As the celerity is directly proportional to the wavelength (Equation (2.1)), groups of waves (wave trains) with longer wavelengths will travel faster than wave trains comprised of shorter wavelengths [59]. Although each individual wave advances at a celerity corresponding to its wavelength λ, the wave train advances at a group velocity c_g [59], which is dependent on the relative water depth (d/λ) (Equation (2.4)). The group velocity is also the rate with which the wave energy is transmitted (wave power) [59]. Thus the wave power P_{wave} per metre width of wave crest is given by [67]:

$$P_{wave} = E_{wave} c_g \quad (2.8)$$

This process of wave separation (dispersion) of the faster, longer waves from the shorter, slower waves leads to the development of ordered and regular ocean swells [64], depicted in Figure 2.5. Ocean swells can travel vast distances (up to ten thousand kilometres or more), with virtually no loss of energy in deep water [62].

Wave Transformations

In Figure 2.6, it can be seen that as the ocean swells propagate in deep water, the orbital paths of the water particles travel in vertical circles [59]. At the water surface, the diameter of the water particle's circular orbit is equal to the wave's height *H* [64]. The orbital diameters then decrease exponentially with increasing depth [58] until the motion of the water particles ceases at a water depth approximately equal to half the wavelength (wave base) [64]. Consequently, the energy also decreases as the depth increases, where up to 95 % of the wave energy is located between the water surface and a quarter of the wavelength below it [32].

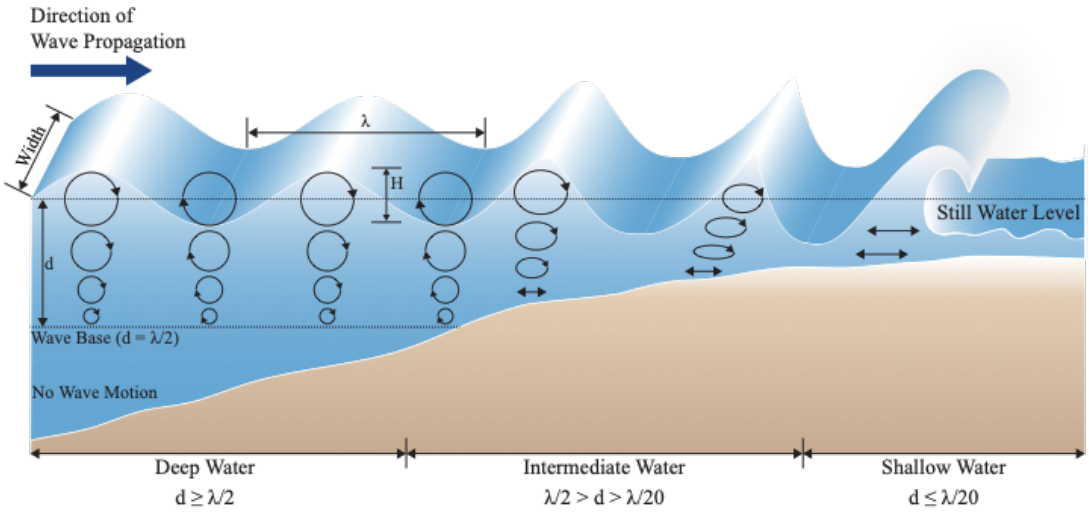

Figure 2.6. The behaviour of a wave is dependent on its wavelength *λ* relative to the water depth *d* it is propagating through (where the size and shape of the orbital path are determined by *λ* and *d*, respectively). Adapted from [59], [64] and [68].

When the wave train propagates into water with a depth less than its wave base (intermediate water), interaction with the seafloor occurs [64]. As seen in Figure 2.6, the circular motion of the water particles deforms and becomes progressively flatter until, in water depths less than one-twentieth of the original wavelength (shallow water), the water near the seabed is restricted to a rapid back and forth movement [59]. This frictional resistance between the water particles and seafloor (bottom friction) results in the

dissipation of energy, which increases with the roughness of the ocean bottom and the width of the continental shelf [62].

The bottom interference also causes the wave celerity to decrease [60]. However, as the advancing wave slows, the trailing wave continues towards the shore at its original speed, thereby shortening the wavelength as it moves closer to the slower leading wave (shoaling) [66]. As the water depth decreases, the waveform is also modified. The wave height increases whilst the troughs become flattened, which leads to an asymmetric wave profile (Figure 2.6) [64]. The changing waveform and increasing wave height is the redistribution of wave energy that occurs with decreasing water depth [64].

In shallow water, the bottom of the wave slows because, as previously stated, the movement of these water particles is severely limited near the ocean floor [66]. However, the motion of the water particles at the surface is not reduced as no contact with the seabed has occurred. Therefore, the upper segment of the wave overtakes the lower segment, resulting in the disintegration of the wave as it falls over and breaks [66], dissipating all its order and energy (Figure 2.6) [59].

Due to the interaction with the ocean bottom, and in some cases, structures, the energy available in intermediate and shallow water waves may also be redistributed and/or redirected through processes such as refraction, diffraction and reflection [69].

In refraction, as the wave trains approach the coast, the wave crests bend in order to become more parallel to the depth contours (isobaths) and shoreline (Figure 2.7(a)) [62]. When the wave is travelling in intermediate or shallow water, the wave celerity varies along the wave crest, causing the shallower section of the wave to propagate at a slower rate than the deeper section of the wave [60]. This results in the wave crests bending to align with the orientation of the isobaths [60]. Consequently, wave energy converges in convex bathymetric and coastal formations, such as submarine ridges and headlands, which could potentially lead to “hot spots” (localised high concentration of energy) [62]. Conversely, wave energy diverges in concave formations, such as submarine canyons and bays, thereby resulting in a local decrease in wave energy [62].

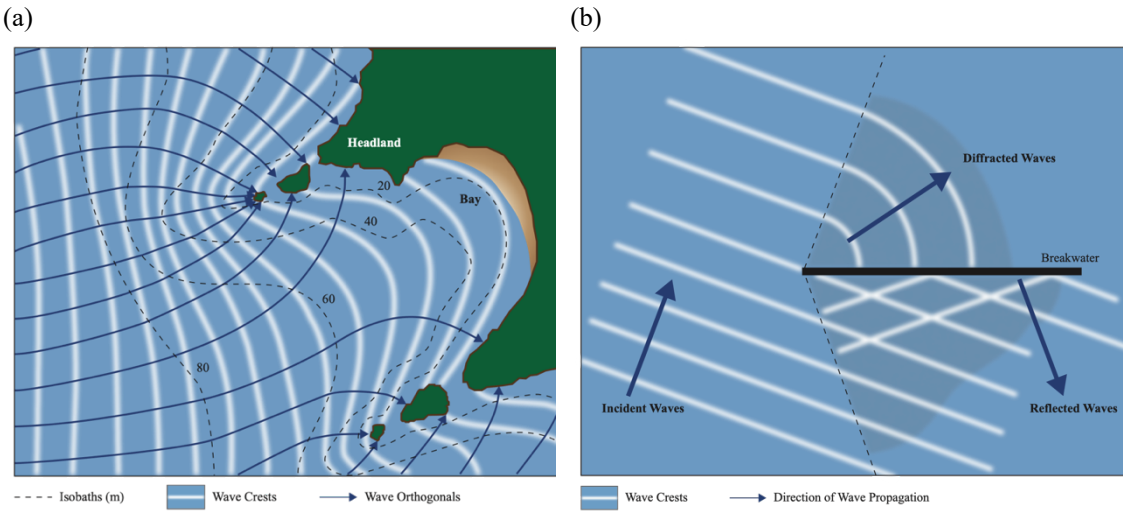

Figure 2.7. (a) The wave refraction which occurs along an irregular shoreline. The orthogonal lines illustrate the concentration of wave energy on the headlands and its dispersion in the bays, adapted from [70]. (b) As a wave encounters an obstacle, both wave diffraction and reflection can occur, adapted from [63].

Diffraction is the process by which the waves curve around and behind impermeable structures [62], such as breakwaters and jetties (Figure 2.7(b)). As the wave passes the obstacle, wave energy is transferred laterally along the wave crests to the sheltered region (shadow zone) behind the structure [60]. These diffracted wave crests will travel into the shadow zone in approximately concentric circular arcs with exponentially decreasing wave heights along the crests [60]. Thereby defocusing (spreading out) the wave energy [62].

As seen in Figure 2.7(b), when a wave encounters an obstacle, a portion of the wave energy is reflected [70]. The quantity and direction of the reflected energy is dependent upon the amount of energy absorbed by the obstacle, as well as the angle of approach [69]. In the case of impermeable structures with steep faces, approximately 100 % of the wave energy will be reflected [70]. Whilst a sloping structure that has a porous surface will reflect significantly less wave energy as the majority of the energy is absorbed or dissipated [69]. The reflected waves could also potentially constructively or destructively interfere with the incoming waves [66], thereby resulting in a localised increase or decrease in wave energy concentration.

2.4.2 Extreme Wave Climate

It is essential to know how these wave parameters vary in time at a specific location (wave climate), as WECs are tuned for maximum efficiency for particular ranges of wave heights and periods and cease operations in stormy seas [71]. Extreme wave events have

the potential to cause significant damage [72, 73], and therefore, the severity of the wave climate extremes should be investigated, and a threshold wave height value clearly defined [74].

In the literature, however, the threshold for an extreme wave condition is not clearly defined, which has resulted in a wide range of values being proposed. Liberti et al. [75], Amrutha et al. [76], and Bozzi et al. [71] utilised a single significant wave height H_{m0} (a measure of H) threshold of 4 m, 4.5 m, and 7 m, respectively. Whilst Rusu and Onea [73] utilised an 'extreme index' to identify the highly energetic sea states in terms of H_{m0} at each of the 21 sites being analysed, which ranged from 6.2 m to 12.4 m. Whereas Zheng et al. [77] proposed using the Gumbel Curve Method to determine the extreme wave heights, which ranged from 6 m to 20 m, depending on the site being analysed.

Moto and Pinto [78] proposed using a wave power cut-off value of 120 kW/m, whilst Folley and Whittaker [79] introduced the concept of maximum exploitable P_{wave}, which was defined as being four times the average P_{wave}. In this case, the maximum exploitable P_{wave} was considered the threshold power level, and any sea states larger than this value were deemed unexploitable.

Lastly, Morim et al. [80] assumed that WECs only operated within the range of sea states specified on the device's corresponding power matrix. Thus, sea states greater than the maximum specified H_{m0} were not taken into consideration in this approach [80].

This lack of consistency in the literature is an issue as these conditions are hazardous to WEC systems [73].

2.4.3 Existing Site Selection Methodologies

Nobre et al. [81], Galparsoro et al. [82], and the European Union's WAVEPLAM (WAVe Energy PLAnning and Marketing) project [83] proposed using multi-criteria analysis within a GIS framework to produce maps that depicted areas of varying suitability for generic WEFs. Nobre et al.'s [81] approach, implemented along the Portuguese south-west coast, classified the relevant site selection criteria as restrictions or weighted factors. These restrictions represented non-installation areas and were omitted from the analysis, whereas the weighted factors were assessed on their ability to affect the installation of a WEF. This differed slightly from the methods proposed by Galparsoro et al. [82], demonstrated within the Basque Continental Shelf (Spain), and the WAVEPLAM project [83], which both firstly used three main categories (socioeconomic, environmental, and

technical) to identify the relevant site selection factors, and instead of omitting the exclusion factors from further analysis, these areas were assigned a value of zero. In addition, as a generalised site selection methodology was introduced by the WAVEPLAM project [83], a comprehensive list of all necessary information was provided, whereas Galparsoro et al. [82] and Nobre et al. [81] proposed site-specific selection criteria.

Subsequently, studies conducted by Le et al. [84], Chakraborty [13], and Ghosh [17] integrated multi-criteria decision making techniques with GIS to determine optimal generic WEF locations. Le et al.'s [84] method, implemented in Tasmanian coastal waters, classified the identified site selection criteria as ocean features, marine uses and facilities. However, the factors in this method were all considered to be limiting, and so, therefore, potentially the most suitable WEF location could be in direct conflict with an existing marine use. Whilst the approach outlined by Chakraborty [13], demonstrated at multiple marine energy test sites (in Australia, England, and Spain), and Ghosh [17], implemented at specific locations within the coastal environments of Japan and the USA, only considered site selection criteria which would influence the wave energy potential (such as wave height, wave period, depth, and so forth). Neither attempted to incorporate social or economic impacts, environmental aspects, or existing marine uses into the analysis.

None of these case studies was applied to an initial large area, and in fact, the WAVEPLAM guidance document [83] actively discouraged assessing large areas, such as a country's entire marine territory. However, the majority of these methodologies recognised that the available resource is not the only aspect to be used in the analysis because the selection of an appropriate WEF site also requires an assessment of the technical limitations, potential economic and social impacts, and environmental considerations.

2.5 Site Matching

As stated in Section 2.3, an important aspect to consider when selecting a suitable location for the deployment of a WEF is determining which wave energy technology would be more appropriate for the particular conditions encountered at that potential site [85]. A review of the literature identified four main methods for matching wave energy devices to potential marine energy sites:

1. Method 1—Evaluating and comparing the performance of a single device at a single location.
2. Method 2—Evaluating and comparing the performance of a single technology type at different locations.
3. Method 3—Evaluating and comparing the performance of a range of technology types in a specific area.
4. Method 4—Evaluating and comparing the performance of different technology types at a range of sites.

If multiple locations were investigated within a country's EEZ, this was defined as a single 'specific area' (Method 1 and Method 3). Table 2.2 provides an overview of the literature pertaining to the four site matching methodologies.

Table 2.2. Review of the scientific literature focused on the four methods of site matching. For each method, the studies have been listed in reverse chronological order.

Study / Year	Device(s)	Performance Indicator(s)	Location(s)
Method 1			
Margheritini & Kofoed [86] / 2019	[ii]WEPTOS	Energy: Power Production, Capacity Factor	[iii]Denmark
Carballo & Iglesias [87] / 2012	[ii]Generic shoreline OWC	Energy: Power Production, Capacity Factor, Equivalent Hours, Over-Rated Time Percentage	[iii]Spain
Method 2			
Dalton et al. [88] / 2010	Pelamis[a] — only WEC to have published power performance data (at the time).	Energy: Power Production Economic: Cost of Electricity, Net Present Value, Internal Rate of Return	Ireland, Portugal, Canada, USA
Method 3			
Amrutha et al. [76] / 2019	[ii]Oyster[a], Wave Dragon, Wave Star[a] —selected WECs that were suitable for nearshore locations.	Energy: Power Production, Capacity Factor, Capture Width	[iv]India
[i]Iuppa et al. [89] / 2015	[ii]AquaBuoy[a], Pelamis[a], Wave Dragon, as well as seven generic devices numerically modelled by Babarit et al. [90].	Energy: Power Production, Capacity Factor	[iv]Italy
Veigas et al. [91] / 2015	[ii]Archimedes Waveswing, Pelamis[a], Wave Dragon, generic OWC	Energy: Power Production	[iv]Spain
Bozzi et al. [71] / 2014	AquaBuoy[a], Pelamis[a], Wave Dragon—WECs that had a range of operating principles, reached an advanced stage of development and had published performance data.	Energy: Power Production, Capacity Factor, Coefficient of Variation	[iv]Italy

Study / Year	Device(s)	Performance Indicator(s)	Location(s)
Method 3 – Continued			
Mota & Pinto [78] / 2014	[ii]Archimedes Waveswing, Pelamis[a], Wave Dragon—WECs that had a range of operating principles.	Energy: Power Production, Capacity Factor	[iii]Portugal
[i]Sierra et al. [92] / 2014	[ii]AquaBuoy[a], Pelamis[a], Wave Dragon	Energy: Power Production, Capacity Factor	[iv]Spain
[i]Aoun et al. [93] / 2013	[ii]AquaBuoy[a], Pelamis[a], Wave Dragon—selected range of WECs that had published performance data.	Energy: Power Production, Capacity Factor	[iii]Lebanon
[i]Silva et al. [94] / 2013	[ii]AquaBuoy[a], Oyster[a], Pelamis[a], Seawave Slot-Cone Generator[a], Wave Dragon— selected range of WECs.	Energy: Power Production	[iii]Portugal
Vaquero et al. [95] / 2013	[ii]Ceto, Oceantec, Oyster[a], Pelamis[a], Pontoon Power Converter, Seabased, Seawave Slot-Cone Generator[a], Wave Dragon, Wave Star[a] —selected range of WECs.	Energy: Power Production, Capacity Factor, Capture Width	[iv]Spain
Dunnett & Wallace [50] / 2009	AquaBuoy, Pelamis[a], Wave Dragon— selected range of WECs that had undergone full-scale testing.	Energy: Power Production, Capacity Factor Economic: Net Present Value, Simple Payback Period	[iv]Canada
Method 4			
[i]Rusu & Onea [96] / 2017	Ceto[b], Ocean Energy Buoy, Oceantec[b], Pelamis[a], Pontoon Power Converter, Seabased, Sea Power, Wavebob[a], Wave Dragon, Wave Star[a]—selected range of WECs at an advanced stage of development.	Energy: Power Production, Capacity Factor, Capture Width	[iv]Angola, Australia, Brazil, Canada, Chile, China, Denmark, Greenland, Iceland, Ireland, India, Indonesia, Madagascar, Mexico, NZ, Papua New Guinea, Peru, Philippines, Portugal, Russia, Senegal, South Africa, United Kingdom (UK), Uruguay, USA
[i]Vannucchi & Cappietti [97] / 2016	Archimedes Waveswing, Oyster[a], Pelamis[a], Wave Dragon, Oyster[a], Wave Star[a]—selected range of WECs at an advanced stage of development.	Energy: Power Production, Capacity Factor, Capture Width	[iv]Ireland, Italy, France, Portugal

Study / Year	Device(s)	Performance Indicator(s)	Location(s)
Method 4 – Continued			
[i]Rusu & Onea [73] / 2015	Archimedes Waveswing, AquaBuoy, Ceto[b], Ocean Energy Buoy, Oceantec[b], Pelamis[a], Pontoon Power Converter, Wavebob[a], Wave Dragon, Wave Star[a]—selected range of WECs at an advanced stage of development and designed to operate in the offshore environment.	Energy: Power Production, Capacity Factor, Capture Width	[iv]Bulgaria, France, Ireland, Italy, Norway, Portugal, Romania, Spain, UK
[i]Rusu [85] / 2014	AquaBuoy[a], Pelamis[a], Wave Dragon—selected range of WECs.	Energy: Power Production, Capacity Factor, Capture Width	[iv]Portugal, Spain
O'Connor et al. [20] / 2013	[ii]Pelamis[a], Wave Star[a]	Energy: Power Production, Capacity Factor Economic: Cost of Electricity, Net Present Value, Internal Rate of Return	[iv]Denmark, Greece, Ireland, UK, Spain, Portugal
[i]Babarit et al. [90] / 2012	[ii]Eight generic numerically modelled devices inspired by Ceto[b], Langlee[a], Ocean Energy Buoy, Oyster[a], Pontoon Power Converter, Seabased, Wavebob[a], Wave Star[a].	Energy: Power Production, Capture Width Ratio	[iv]Ireland, France, Portugal, UK

[i.] An external body funded the study.
[ii.] The initial WEC selection was not discussed in the study.
[iii.] The initial selection of the locations was not disclosed.
[iv.] The selection of the sites was based on the available resource and/or limited to technical parameters.
[a] Abandoned technology.
[b] Technology has evolved significantly since the publication of the study.

As seen in Table 2.2, a significant number of the case studies were based in the Northern Hemisphere (predominately along the Atlantic coast of Europe) and were limited to assessing the energy performance of the WEC(s) only. Furthermore, the majority of these case studies selected the locations based solely on the available resource and/or technical limitations (ocean depth, distance to shore, etc.). Whilst the initial selection of the wave energy technology, existing or generic, was generally not discussed, and as this is a rapidly evolving sector, the development of several of the 'existing' WECs has since been abandoned.

2.6 Conclusions

Three main gaps have been identified from the literature. Firstly, the absence of an adaptable taxonomy, which has distinct containing classes, that is both analytical and able to accommodate future wave energy technologies. Secondly, a lack of a flexible broad-based method that determines optimal locations, from an initial large study area, for

generic wave energy projects. Thirdly, the need for a systematic site matching methodology, which includes the initial identification of devices that could potentially be suitable for these deployment locations.

Chapter 3
Stage 1: Site Selection

3.1 Introduction

As wave energy is unevenly distributed throughout the world [18], the first step in establishing a WEF would be to identify suitable locations [22]. A number of site selection methodologies proposed in the literature (Section 2.4.3) converge to a common approach of utilising a form of multi-criteria analysis within a GIS framework. The majority of these methods recognised that even though an energetic resource is vital, it is not the only aspect to be considered because an assessment of the technical limitations, potential socio-economic impacts, and environmental considerations is also required. However, determining feasible locations to deploy, operate, and maintain a WEF is a considerable undertaking, and an extensive amount of information is required to conduct an informed evaluation [83]. Hence, the previous case studies were limited to small study areas.

The aim of this chapter is, therefore, to develop a systematic approach for the identification of suitable WEF locations that is applicable at any scale. This will include breaking down the critical processes into three main stages. The first stage will define the study area, identify the relevant site selection criteria (based on the dimensions of sustainability), and gather and prepare the relevant geospatial data. The second stage will integrate this information in GIS to identify suitable WEF locations, regardless of the size of the initial study area. The third stage will then assess the robustness of the results obtained in the second stage.

3.2 Methodology

As seen in Figure 3.1, the principal steps in the site selection procedure were grouped into three distinct sub-stages: Stage 1.1: Data Acquisition and Preparation, Stage 1.2: GIS Analysis, and Stage 1.3: Scenario Analysis. In the Data Acquisition and Preparation sub-stage, the general area of interest was established, and the relevant geospatial data was identified, assembled, and prepared. This spatial data was then integrated and modelled in a GIS system in Stage 1.2 to identify suitable areas for wave energy projects, regardless of the size of the initial study area. In the last sub-stage, the robustness of the results acquired from the GIS model was evaluated. The proposed methodology was applied to an NZ case study.

ArcGIS Desktop 10.5.1 [98] was used to implement the proposed site selection approach. It is an appropriate tool for spatial analysis as it is able to capture, store, maintain, process, analyse, and display geospatial data [99]. This software package is comprised of numerous applications; however, only ArcCatalog and ArcMap were utilised. ArcCatalog is a data-management application, whereas ArcMap's functionalities range from creating maps to spatially modelling and analysing the geographic data [99].

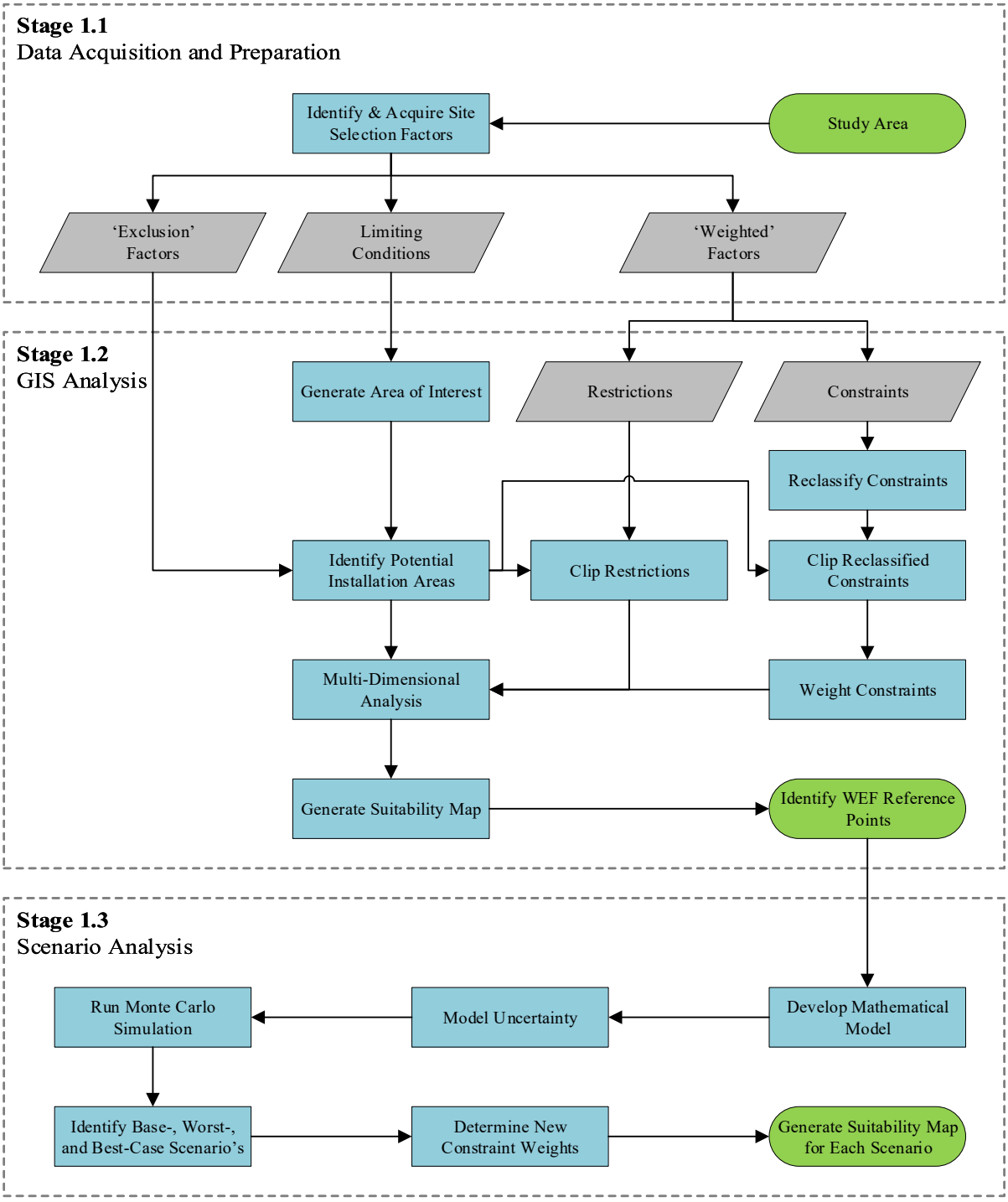

Figure 3.1. The site selection methodology utilised to identify and assess optimal WEF locations.

3.2.1 Stage 1.1: Data Acquisition and Preparation

The steps proposed in the first sub-stage defined the study area, and to encourage a sustainable outcome, by avoiding the development of projects in inappropriate areas, all pertinent and available information was identified and gathered. Sustainability in reference to sustainable development is commonly defined as "development that meets the needs of the present without compromising the ability of future generations to meet their own" [100] and is comprised of the integration of three main dimensions: social inclusion, economic prosperity, and environmental protection [101]. These dimensions, with the addition of a technical and cultural dimension, form the framework for identifying the relevant site selection criteria.

Cultural Dimension. Approximately 27 million people from 87 different countries make up the coastal indigenous communities around the world [102]. These communities are intrinsically linked with the marine environment as it forms part of their cultural heritage and identity [102]. Therefore, marine areas of cultural significance or that contribute to the food sovereignty of these communities were considered cultural factors.

Economic Dimension. For the purpose of this study, economic factors were defined as activities that occur in, or uses, the marine environment, which made a direct economic contribution to the study area.

Environmental Dimension. Due to the immature nature of the ocean energy sector, the effects of a WEF on the marine environment, such as the risk of collision between marine animals and the moving parts of WECs, are currently unknown [22]. Furthermore, these potential environmental impacts will also vary depending on the former condition of the receiving environment. For instance, a number of maritime areas have severely deteriorated due to industrial marine activities, whilst untouched marine environments are regarded as more vulnerable. Hence, their protection and preservation are prioritised [83]. Therefore, Marine Protected Areas (MPAs), which were established to protect and maintain marine ecosystems and biodiversity, were considered environmental factors.

Social Dimension. The coastal and marine environment provides opportunities for discovery, leisure and contemplation. However, a WEF could potentially interact with or transform these activities, thereby impacting the local lifestyle and negatively influencing public perception [83]. In this approach, only submarine archaeology was considered. However, once suitable WEF locations have been identified, it is recommended that areas of popular recreational

activities, such as bathing, fishing, and surfing, should be identified and used to refine the site selection further.

Technical Dimension. Technical parameters that could influence a WEF installation include the wave climatology (wave resource), ocean features (bathymetry), infrastructure and logistics (grid availability and port facilities), as well as existing marine applications (dredged areas, dumping grounds, military exercise areas, and submarine cables and pipelines) [83].

These site selection factors were then further classified as 'Limiting Conditions', 'Exclusion Factors' and 'Weighted Factors'. The Limiting Conditions delineated the preliminary areas which were viable for wave energy projects, and therefore reduced the size of the initial study area. The Exclusion Factors were considered incompatible with a WEF and were eliminated from further analysis, whilst the Weighted Factors were criteria that had the potential to impact a WEF (either negatively or positively) and were weighted according to their relevance.

As part of this sub-stage, once the relevant site selection considerations were identified and further categorised, the corresponding spatial datasets had to be sourced and assembled into a database in ArcCatalog. Geospatial data are commonly stored in either a raster or vector structure [99]. In a vector structure, coordinates are used to establish the locations of points, lines, and polygons, which represent discrete map features [99]. Whereas in a raster structure, the geographic space is divided into a regular grid of cells, and each cell is allocated the value of the map feature that dominates that cell [99].

Each of these geographic datasets, which were stored in a vector structure, were then reviewed to determine which required further processing. This included ensuring that the dataset was accurate and up-to-date, projecting datasets to the recommended coordinate system for the study area, as well as splitting or merging existing datasets. Developing the database was a crucial and time-consuming aspect of the procedure, as the completeness and quality of the datasets utilised in the spatial analysis determined the accuracy of the resulting suitability map.

3.2.2 Stage 1.2: GIS Analysis

The GIS analysis was conducted in ArcMap, where the vector datasets assembled in Section 3.2.1 were displayed as layers. In this sub-stage, the initial processing and analysis procedures were conducted using input layers with a vector structure, whilst the final operation, spatial MDA, required raster input layers.

The first process to be undertaken was to generate a smaller, more manageable Area of Interest (AoI) vector layer from the initial broad study area. Therefore, only regions with ocean depths less than 250 m and a resource greater than 20 kW/m were considered for further analysis. These parameters were selected as the limiting conditions, as the maximum ocean depth suitable for the installation of WECs ranges from 50 m [84] to 500 m [55] in the literature, and WEFs are only considered viable in locations where the potential wave power is greater than 20 kW/m [55, 56].

Then in order to determine the potential areas for the installation of WECs, the exclusion factors were merged to create a single non installation areas layer. This layer was spatially removed from the AoI layer, resulting in a Potential Installation Areas (PIA) vector layer.

To perform the final process, spatial MDA required the development of a suitability model (Equation (3.1)). This model combined the weighted factors, further categorised as constraints and restrictions, to generate a suitability map that identified the most optimal WEF locations by utilising a Suitability Scale (SS), which ranged from 1 (unsuitable locations) to 100 (very suitable locations).

The SS equation is defined as follows:

$$SS = \left(\sum_{i=1}^{n} w_i C_i\right) \prod_{j=1}^{m} R_j \tag{3.1}$$

where C_i and R_j referred to the (reclassified) constraints and restrictions, which were stored in a raster structure, with w_i representing the weight assigned to the individual constraints. These weightings were based on the importance of each constraint, and the total weight for all constraints was equal to 100 %.

Constraints. Practical constraints associated with a WEF took into account the relative ease with which the WEC arrays could be installed, operated and maintained (distance to a port); the ability of the technology to generate electricity from the natural resource (available wave energy resource); and exporting the electricity to the local distribution network or the national transmission grid (distance to the power grid). As these constraints contain different features and measuring units, they had to be reclassified to a common comparable scale. In this scale, low values represented areas of poor resource or great distances from the ports or power grid, whilst high values represented areas with an excellent resource or close proximity to ports or power grid.

These reclassified constraints were then assigned a weight in accordance with their relative economic impact on the project (Table 3.1). The available wave resource received the highest weighting as it has the greatest influence on the economics of the project. This was followed by the distance to ports, as a WEF will require servicing over its lifespan. The distance to power grid constraint was ranked the lowest as the costs associated with connecting to the power grid (underwater and overland transmission lines) are considered one-off capital costs. The proposed weightings were provided by a wave energy expert (W. Dick, personal communication, April 29, 2019), which also corresponded with the values provided in the literature [81]. However, it should be noted that these values are quite subjective and should be adjusted according to the situation being analysed (small island community vs coastal country) and also potentially as the sector matures.

Table 3.1. The project constraints that are considered instrumental in determining the most optimal sites for wave energy projects.

Constraint	Weight (%)
Available Wave Energy Resource	60
Distance to Ports	30
Distance to Power Grid	10

Restrictions. Factors that were not incompatible with a WEF but could negatively influence the local economy or public perception were considered restrictions. Therefore, these locations were considered less suitable for wave energy projects and were assigned a limiting value based on the perceived importance of these areas with the local stakeholders.

Before applying the suitability model, new raster layers had to be created from the restriction and reclassified constraint raster layers that were contained within the PIA vector layer. The resulting 'clipped' (cropped) restriction and reclassified constraint raster layers were then inputted into Equation (3.1) to identify the most optimal WEF locations.

3.2.3 Stage 1.3: Scenario Analysis

In order to determine the robustness of the results obtained from the suitability model, a scenario analysis was conducted utilising a Monte Carlo simulation. The Monte Carlo method is a relatively simple and proven mathematical technique for the inclusion of uncertainty in quantitative models [103]. A calculation is executed multiple times in this approach, each time with a unique set of inputs randomly selected from pre-specified probability functions [103].

Therefore, the first process to be undertaken was to develop a mathematical model that best captured the current uncertainties with the suitability model; the subjectivity of the constraint weightings depicted in Table 3.1. As the initial weight assigned to each of the constraints was in accordance with the relative economic impact on the WEF, it was determined that the Levelised Cost of Electricity (LCOE) would be the most appropriate model.

LCOE is a standard cost metric for quantifying the economic performance of an electricity-generating technology [104]. This parameter takes into consideration the capital costs, the Operations and Maintenance (O&M) costs over the project's lifespan, as well as the technology's cumulative energy yield.

$$LCOE = \frac{CAPEX + \sum_{t=1}^{n} \frac{OPEX_t}{(1+dr)^t}}{\sum_{t=1}^{n} \frac{AEP_t}{(1+dr)^t}} \tag{3.2}$$

where CAPEX refers to the project's Capital Expenditures and OPEX the project's Operational Expenditures, dr refers to the discount rate, t is the year from the start of the project, and n is the project life expectancy. AEP is the Annual Electricity Production and is calculated as follows [104]:

$$AEP = WEF_C \times C_f \times 365\ (days) \times 24(hours) \times A_f \tag{3.3}$$

where WEF_C is the installed capacity of the WEF project, which is calculated by multiplying the number of WECs in the WEF by the device's rated capacity R_C. C_f refers to the capacity factor, whilst A_f is the WEF's availability factor (the maximum potential time that the WEF is available to produce electricity annually).

However, the standard LCOE calculation depicted in Equation (3.2) cannot be used directly in the Monte Carlo approach, and so, therefore, the annualised cost of producing electricity was modelled instead. This was achieved by multiplying the CAPEX in Equation (3.2) by a Capital Recovery Factor (CRF):

$$CRF = \frac{dr(1+dr)^n}{(1+dr)^n - 1} \tag{3.4}$$

resulting in an annualised cost assessment model that could be utilised in the Monte Carlo simulations.

$$LCOE = \frac{(CAPEX)(CRF) + OPEX}{AEP} \quad (3.5)$$

Once the quantitative model was established, the input variables that were uncertain and therefore crucial in assessing the suitability model had to be identified. The uncertainty was modelled by specifying the likely probability distribution. For the annualised LCOE model (Equation (3.5)), it can be clearly seen that the major variables that determine the economics of the power generation are the amount of electricity generated (AEP) and the associated costs (CAPEX and OPEX). For the purposes of this study, it was assumed that the AEP was a fixed point value and that the uncertainty associated with the CAPEX and OPEX values was best described by a normal distribution [103, 105].

Before the simulation could be run, the LCOE input variables had to be linked to the constraints used in the suitability model. This required each model input to be broken down further (Table 3.2) so that it could be determined which constraints were best described by the LCOE input(s).

Table 3.2. Breakdown of the LCOE model inputs (where relevant), adapted from [104].

Model Input	Description
AEP (kW/year)	Amount of electricity generated by the WEF.
CAPEX (currency/kW)	Majority of the CAPEX costs are incurred at the beginning of the project.
Project Development (currency/kW)	Project costs, such as environmental impact assessment and site surveys. Usually incurred before WEF deployment and operation.
Grid Connection (currency/kW)	Cost of connecting the WEF to the power grid (dependent on the distance to a suitable grid connection point [106]).
Device (currency/kW)	Cost of materials and fabrication of the structure.
Moorings and Foundations (currency/kW)	Cost of all the components required to hold the device in place.
Installation (currency/kW)	Cost of pre-assembly, transporting, installing moorings and/or foundations, as well as attaching the device to the appropriate fixings.
OPEX (currency/kWyear)	OPEX costs are distributed throughout the project's lifetime.
O&M (currency/kWyear)	Cost of all planned maintenance and repair requirements associated with maintaining the WEF (includes service vessel requirements).
Insurance (currency/kWyear)	Cost of insuring the technology against all risks during its deployment and operational life.
Seabed lease rates (currency/kWyear)	Cost of renting the seabed at the chosen site of deployment.

As the amount of power that a device can generate is directly dependent on the available resource (this relationship is captured by the C_f parameter, which is discussed further in Section 5.2.3), it was determined that the AEP input best represented the Available Resource constraint.

In terms of the cost inputs, several cost centres were identified for both CAPEX and OPEX. However, not all these cost components are relevant in terms of the suitability model. On further inspection, it was determined that the Distance to Grid constraint would be represented well by the grid connection cost (CAPEX). Whereas the installation cost (CAPEX) and O&M costs (OPEX) would best reflect the Distance to Ports constraint.

As the overall CAPEX and OPEX inputs could not be directly linked to the suitability model constraints, the contribution of the relevant cost centres to these model inputs had to be determined. As seen in Table 3.3, only the values for the relevant CAPEX cost categories were shown. This is because the majority of the studies only reported the OPEX in terms of the O&M cost component if reported at all. Therefore, for this study, it was assumed that 100 % of the OPEX cost was comprised of this O&M component.

Table 3.3. Percentage of the grid connection and installation cost components to the overall CAPEX of a wave energy project. Studies have been listed in reverse chronological order.

Study / Year	Grid Connection [%]	Installation [%]
de Andres et al. [107] / 2017	8	6
Guardiola Moliner [108] / 2016	15	15–20
Chozas [104] / 2015	10	–
[i]SI Ocean [106] / 2013	6	22
Ocean Energy Systems [109] / 2012	15	20–25
[i]Carbon Trust [110] / 2011	12	10

[i.] The cost values provided in these reports were a percentage of the project lifetime costs, which included the O&M costs. Therefore, these reported values had to be recalculated in terms of each cost components percentage contribution to the overall CAPEX. These recalculated percentage contributions are the values depicted in the table.

In the case of the grid connection cost centre, it can be seen that a range of values has been reported in the literature (Table 3.3). However, for the purpose of this investigation, the value provided by Chozas [104] was utilised, as the input data required for the LCOE model was obtained from this report.

Similar to that of the grid connection cost component, a wide range of values was recorded in the literature with regards to the contribution of the installation costs to the overall CAPEX (Table 3.3). As 20 % was the most commonly reported value, it was determined that this would be the percentage of the CAPEX assigned to the installation cost centre. However, as shown in Table 3.2, the installation cost is comprised of four main sub-components, only one of which is relevant to the distance to port constraint, namely transportation. As no further information could be obtained about the installation sub-components, it was assumed that each component

contributed equally. Therefore, the installation cost centre, in terms of transportation, was assigned the value of 5 %.

Once the percentages of each of the relevant cost centres were defined, the Monte Carlo simulation could be run. The simulation modelled 500 different combinations of the input variables in an Excel spreadsheet, where these combinations were randomly selected from the pre-defined probability distribution for the CAPEX and OPEX model inputs.

The Monte Carlo simulation resulted in a distribution of possible LCOE values, which were used to determine three cost scenarios, namely:

1. Base-case scenario–Ordinary/typical scenario (i.e. average LCOE value)
2. Worst-case scenario–Most unfavourable projected outcome (i.e. maximum LCOE value)
3. Best-case scenario–Most favourable projected outcome (i.e. minimum LCOE value)

For each scenario, a new set of weights was ascertained for the suitability model constraints. It should be noted that the AEP parameter could not be utilised to determine the weight of the Available Resource constraint. Therefore, the weight of this constraint was calculated by subtracting the percentage contribution of the annual grid connection costs, installation (in terms of transport) costs, and O&M costs from 100 %. This ensured that the sum of the constraint weights would always equal 100 %, which is an important requirement of the suitability model.

The final process in this sub-stage required the suitability model to be rerun for all three scenarios. The suitability maps generated from these scenarios were then compared to the initial suitability map obtained in Stage 1.2 in order to determine the sensitivity of the suitability model.

3.3 New Zealand Case Study

The procedures proposed in Stage 1 were applied to a case study in the Southern Hemisphere, namely, NZ. The selection of a Southern Hemisphere case study was twofold. Firstly, as seen in Table 2.2, the case studies published on site matching were rarely conducted in the Southern Hemisphere. Secondly, it is well established that although the wave power values are similar in the two hemispheres, the Southern Hemisphere has considerably less temporal variation (at all timescales) [21], thereby making it more suitable for the installation of WEFs.

NZ is an island country that is comprised of two main landmasses (the North and South Islands separated by Cook Strait) and over seven hundred smaller islands [111]. It is an ideal case study as it is in a prime position to develop wave energy projects. Firstly, as this island nation is quite isolated, its shores are exposed to high energy wave conditions (Figure 3.2), approximately 25 kW/m [112], from the surrounding Southern and Pacific oceans and the Tasman Sea [113].

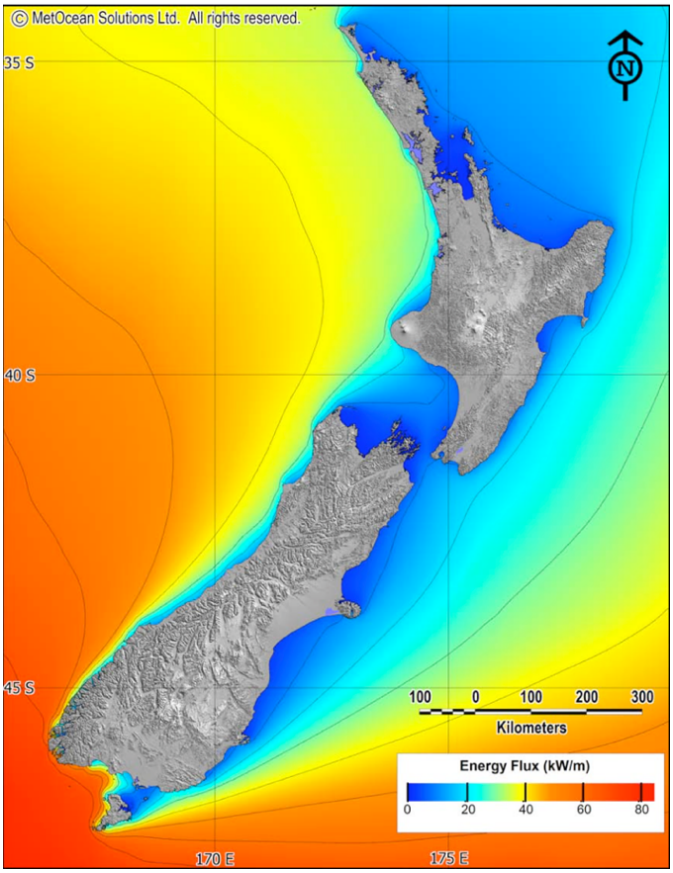

Figure 3.2. Distribution of mean wave power in NZ, from 1998–2007 [114]. Reprinted with permission from MetOcean Solutions Ltd. (personal communication, July 24, 2020).

Secondly, NZ has an extensive marine area, as it has the sixth-largest EEZ in the world [115], and lastly, over 70 % of the population resides within 10 km of the coast [116], which provides additional opportunities for distributed generation.

3.3.1 Stage 1.1: Data Acquisition and Preparation

To demonstrate that the proposed site selection methodology is valid at any scale, especially large scale, the initial study area (Figure 3.3) was defined as all the marine waters contained between NZ's coastline and EEZ; approximately 4.1 million km^2.

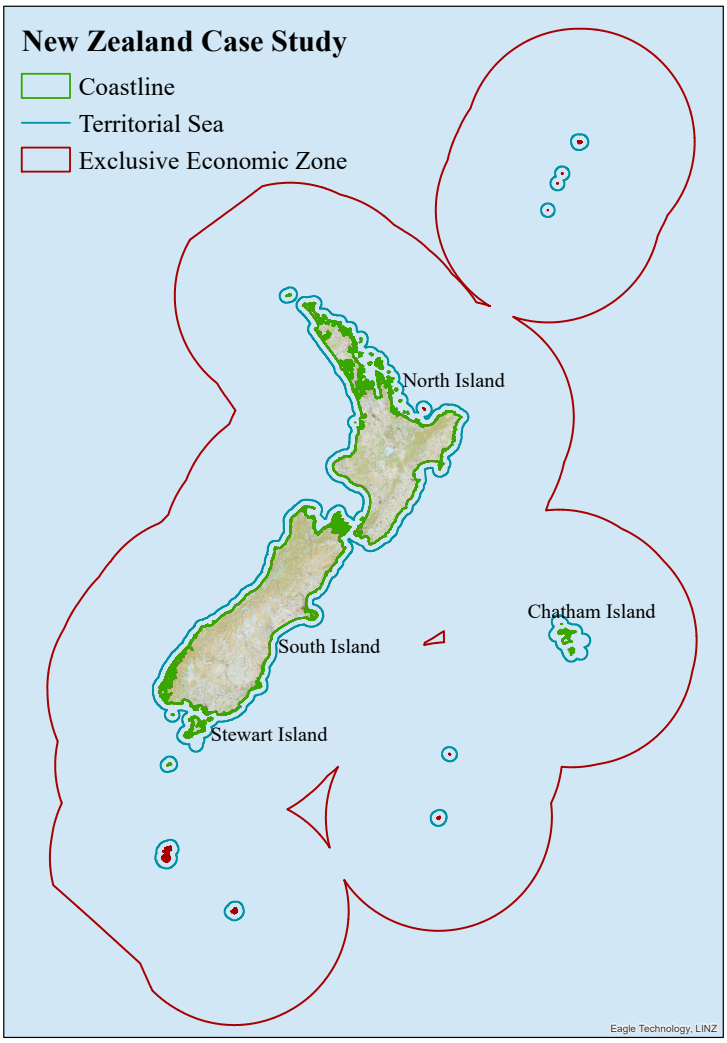

Figure 3.3. The initial marine area proposed for the NZ case study.

The site selection considerations applicable to this case study are depicted in Table 3.4. These criteria were identified according to the five main dimensions proposed in Section 3.2.1, and depending on its potential to condition or influence the project, were classified further as limiting conditions, and exclusive or weighted factors. Based on the site selection factors proposed by Galparsoro et al. [82], Le et al. [84], Nobre et al. [81], and the WAVEPLAM project [83], it was found that the proposed economic, social and technical criteria were widely applicable, whilst the recommended cultural and environmental factors are unique to NZ.

Table 3.4. The relevant site selection factors identified according to the proposed cultural, economic, environmental, social, and technical dimensions.

Dimension	Factor	Classification	Data Type	Data Source
Study Area	Coastline	—	Polygon	[117]
	EEZ	—	Line	[118]
Cultural	Mātaitai Reserves	Exclusion	Polygon	a
	Taiāpure	Exclusion	Polygon	[119]
Economic	Marine Farms (Aquaculture)	Exclusion	Polygon	[120]
	Settlement Areas (Aquaculture)	Exclusion	Polygon	[121]
	Commercial Fisheries	Exclusion	Raster	b
	Offshore Platforms	Exclusion	Point	[122, 123]
	Seabed Mining	Exclusion	Polygon	[124]
	Shipping (Routes)	Exclusion	Line	c
Environmental	Benthic Protection Areas	Exclusion	Polygon	[125]
	Hauraki Gulf Marine Park	Weighted (*Restriction*)	Polygon	b
	Marine Mammal Sanctuaries	Weighted (*Restriction*)	Polygon	[126, 127]
	MPAs	Exclusion	Polygon	[128]
	Marine Reserves	Exclusion	Polygon	[129]
	Seamount Closure Areas	Exclusion	Polygon	[130]
Social	Submarine Archaeology	Weighted (*Restriction*)	Point	[131-136]
Technical	Bathymetry	Limiting Condition	Line	[137]
	Dredged Areas	Exclusion	Polygon	[138-140]
	Dumping Grounds	Exclusion	Polygon	[141-143]
	Grid Availability	Weighted (*Constraint*)	Point	d
	Military Exercise Areas	Exclusion	-	[144]
	Commercial Ports	Weighted (*Constraint*)	Point	[145]
	Submarine Cables	Exclusion	Line	[146]
	Submarine Cables & Pipelines Protection Zones	Exclusion	Polygon	[128, 147-150]
	Wave Energy Resource	Limiting Condition; Weighted (*Constraint*)	Line	e

[a] Ministry for Primary Industries, personal communication, December 22, 2018
[b] Fisheries NZ, personal communication, March 12, 2019
[c] Maritime NZ, personal communication, March 4, 2019
[d] Transpower NZ Ltd., personal communication, May 6, 2019
[e] MetOcean Solutions Ltd., personal communication, November 23, 2017

NZ Cultural Factors. The importance of oceans to the Māori tribes, NZ's indigenous people, is managed through the establishment of mātaitai reserves (traditional fishing grounds) and taiāpure (traditional fishing grounds as well as areas of special cultural or spiritual significance) [151].

NZ Environmental Factors. There are three levels of marine protection in NZ: Type 1 Marine Reserves (the highest protection level); Type 2 MPAs; and Type 3 Other Marine Protection Tools (which includes benthic protection areas, seamount area closures, marine mammal sanctuaries and the Hauraki Gulf marine park) [152]. Additional environmental aspects that should be considered, once these general WEF installation regions have been identified, are coastal areas of outstanding natural character, features, and landscapes [153].

The corresponding GIS database was then developed using spatial data from the sources referred to in Table 3.4. The majority of these site selection factors were readily available in a GIS format but required further preparation before the analysis could be conducted. The main geodata pre-processing steps included: transforming the geospatial data into the same projected coordinate system, ensuring the features within the shapefiles were up-to-date (by referring to the relevant NZ nautical charts, legislation [154], and/or gazette notices[1][155]), and clipping the features to the defined study area.

In general, the shapefiles that could be obtained were defined in the WGS84 (World Geodetic System 1984) geographic coordinate system. However, as this proposed methodology will be applied to an NZ case study, the recommended projected coordinate system for NZ's continental shelf was used; NZCS2000 (NZ Continental Shelf Lambert Conformal 2000) [156]. All the datasets were converted to this projected coordinate system because, for multiple spatial datasets to work together correctly in ArcMap, the coordinate systems have to be consistent. Furthermore, if spatial analysis is to be undertaken, the map layers should be transformed into a projected coordinate system as opposed to a geographic coordinate system [157]. To convert the coordinate system, the 'Project' tool in ArcMap was employed, and as the input and output coordinate systems had different datums (WGS84 and NZGD2000[2], respectively), the NZGD_2000_To_WGS_1984_1 geographic transformation parameter[3] was applied. It should be noted that this is effectively a null transformation [158] (the coordinates are not adjusted),

[1] The NZ Gazette is the official newspaper of the NZ Government, which contains official commercial and government notifications [155].

[2] NZGD2000 (New Zealand Geodetic Datum 2000) is NZ's national geodetic system [156], which is used to define map projections such as NZCS2000.

[3] Data alignment and accuracy issues may occur if the correct transformation is not applied when converting between coordinate systems comprised of different datums.

as the WGS84 and NZGD2000 reference frames are very closely aligned (to approximately a 1 m accuracy level) [159].

The data preparation undertaken for each site selection criterion is expanded on below. With the exception of the site selection factors classified as either a limiting condition or a constraint, the datasets to be utilised in the GIS Analysis stage had to be comprised of polygon features. Geographic features represented by polygon data are two dimensional, and therefore the area and perimeter can be measured. Whereas line data can only be used to measure length, whilst point data can measure neither length nor area. Therefore, the relevant spatial datasets that initially contained point or line features required further pre-processing to achieve this required outcome.

Study Area

To generate the initial study area required the spatial data pertaining to NZ's coastline (inner boundary of the study area) and EEZ (outer boundary of the study area). Before the study area shapefile could be created, both the coastline and EEZ spatial data had to be transformed from the WGS84 coordinate system to the NZCS2000 reference system. Thereafter, the EEZ features had to be converted from polylines to a polygon, which was achieved by employing the 'Feature to Polygon' tool (this tool only generates polygons if the areas are fully enclosed by the input line features). However, as seen in Figure 3.4(a), this resulted in a polygon that included the landmasses. Therefore the 'Erase' tool was used to remove the coastline polygons from the EEZ polygon (in Figure 3.4(b)), resulting in the initial study area polygon depicted in Figure 3.4(c), which contained all the marine waters between NZ's coastline and EEZ.

To calculate the area and perimeter of this polygon required the addition of two new fields, of type double, to be added to the attribute table[4] (by utilising the 'Add Field' function). Then with the aid of the 'Calculate Geometry' function, the area and perimeter were calculated.

[4] The information regarding the features contained within a layer (dataset) is stored in a table. Each row in this table represents a single feature record, and each column represents the category of information (feature attribute).

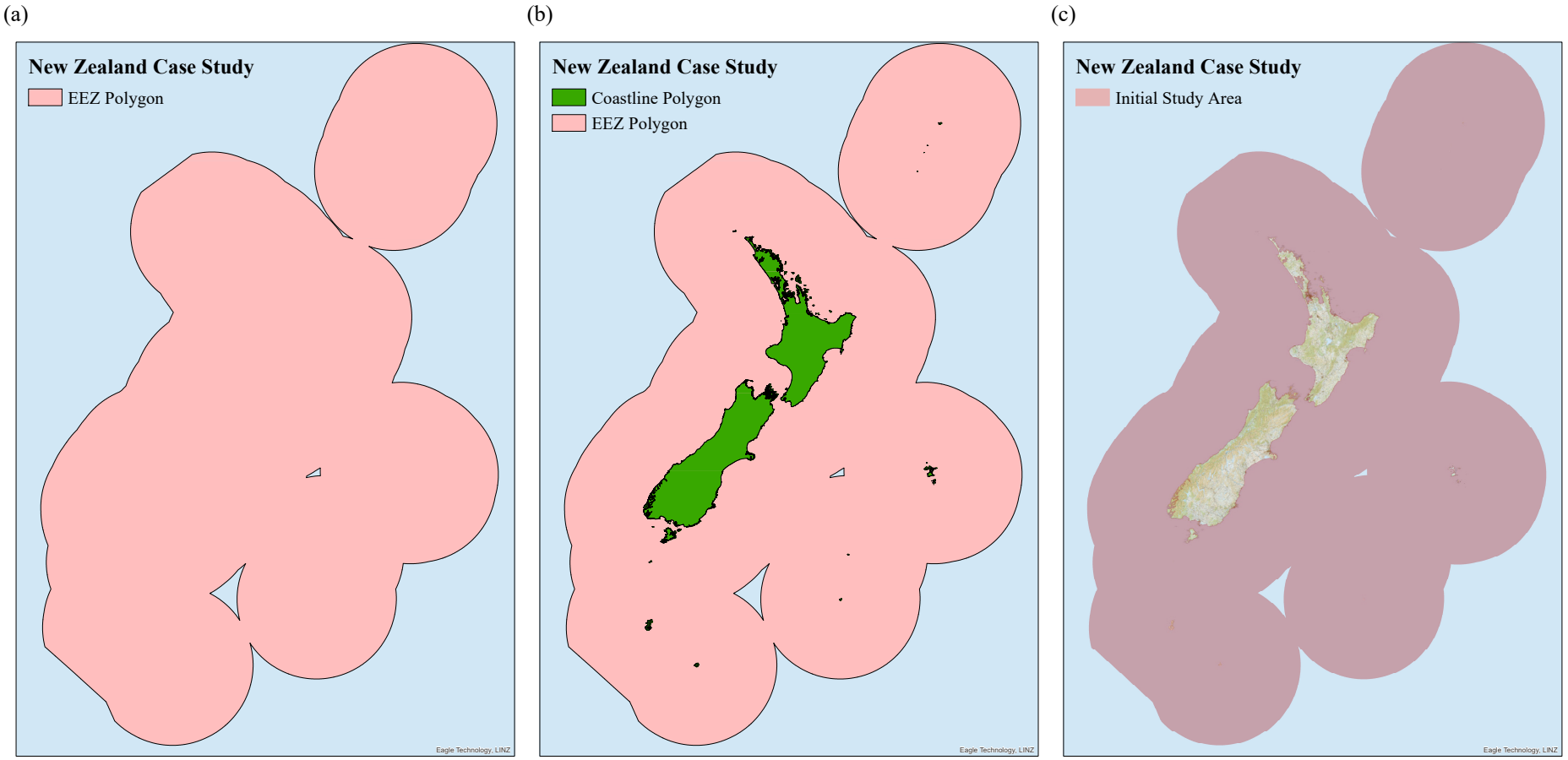

Figure 3.4. The (a) EEZ polylines were converted to a polygon to form an initial study area, which contained NZ's landmasses. Therefore the (b) coastline polygons were spatially removed from the EEZ polygon, resulting in the (c) initial study area polygon, which was used to process the datasets pertaining to the site selection factors further.

As part of the data preparation, the spatial datasets depicted in Table 3.4 were clipped to this Initial Study Area layer (by utilising the 'Clip' tool) to ensure that only features contained within the study area would be analysed in the next stage. Unless stated otherwise, it can be assumed that this was the last pre-process undertaken in the Data Acquisition and Preparation stage.

Cultural Dimension

Mātaitai Reserves / Taiāpure. Even though the cultural site selection factors, Mātaitai Reserves and Taiāpure, were obtained from separate sources (Table 3.4), these datasets required minimal preparation. Both shapefiles were transformed from the WGS84 geographic coordinate system to the required NZCS2000 projected coordinate system, and the respective features were compared with the relevant legislation and gazette notices.

Economic Dimension

Aquaculture (Settlement Areas / Marine Farms). The geodata pertaining to NZ's aquaculture were obtained through ArcGIS online, which was accessed directly through the ArcMap application. Both datasets had to be converted from the projected Mercator 41 coordinate system to the required NZCS2000 projected coordinate system. As Mercator 41 is based on the WGS84 datum, a null transformation was applied.

Commercial Fisheries. A geographical dataset pertaining to the most popular commercial fishing locations is not publicly available. However, an official information act [160] application[5] was made by the author to Fisheries NZ requesting the geodata corresponding to Figure 3.5(a), which depicts the commercial fishing intensity spanning the past ten years (2007-2018). This geodata was provided in a raster format, which was comprised of grid cells that ranged from 5 km^2 to 50 km^2 (Figure 3.5(b)). Each of these cells was assigned an intensity ranking value that ranged from 1 (low catch) to 10 (high catch). This ranking system was developed using the actual catch weights per km^2.

[5] The Official Information Act 1982 makes official information available to the general public in NZ.

(a) (b)

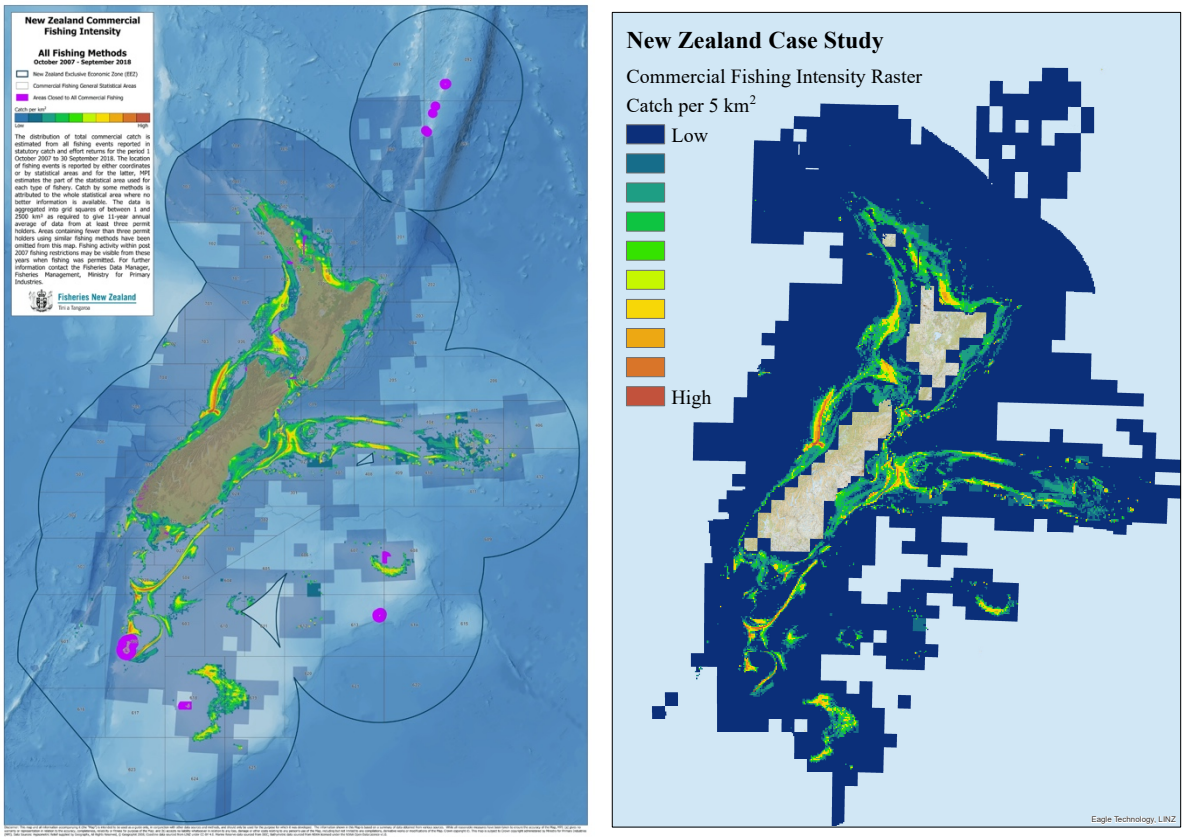

Figure 3.5. The (a) commercial fishing intensity map available from the Fisheries NZ website [161] (image source: Ministry for Primary Industries, licensed for re-use under CC BY 4.0) with the (b) corresponding raster image containing grid cells that ranged from 5 km^2 to 50 km^2.

In order to generate the commercial fisheries vector dataset, the 'Raster to Polygon' tool was utilised. This resulted in a shapefile comprised of multiple polygons, which depicted all commercial fishing areas regardless of popularity. Therefore, to determine the most popular commercial fishing locations, polygons containing a high-intensity ranking (values ranging from 7–10) were identified by implementing a SQL (Standard Query Language) query (feature with an attribute value ≥ 7) performed by the 'Select by Attributes' tool. The selected polygons were exported to a new shapefile and then further processed by merging all the features that shared a boundary into one polygon (Figure 3.6). It should be noted that to merge features within the same dataset requires the use of the 'Merge' function available from the Editor menu, as opposed to the 'Merge' tool, which combines multiple datasets into a single output dataset. As the initial projected coordinate system assigned to the raster was Albers Equal Area, this was inherited by the newly generated vector dataset. Therefore, this coordinate system was converted to the appropriate NZCS2000 coordinate system. Similar to the Mercator 41 projected coordinate system, Albers Equal Area is based on the WGS84 datum, therefore a null transformation was applied.

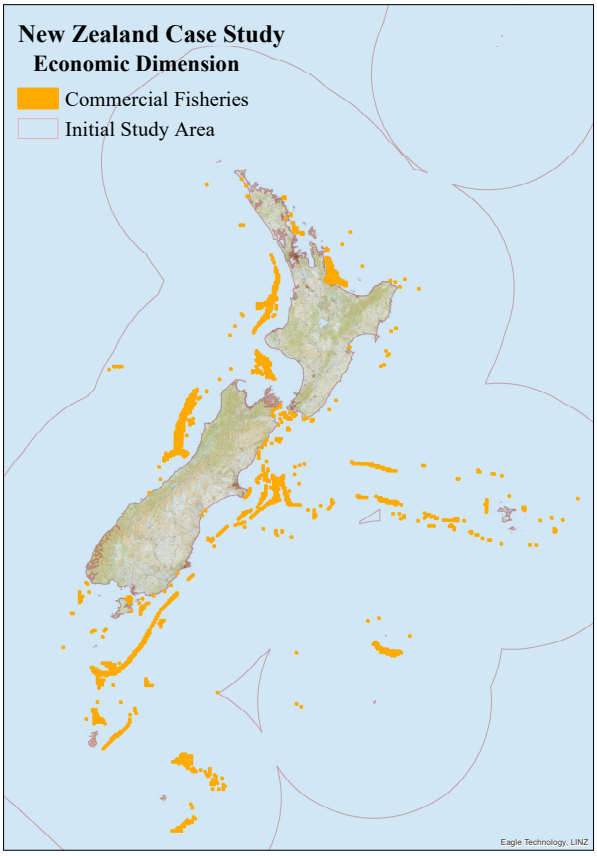

Figure 3.6. Finalised shapefile depicting the most popular commercial fishing locations, which was generated from a raster image.

Offshore Installations. The offshore installation dataset utilised in the GIS Analysis stage was created from two existing shapefiles, which were obtained from separate sources (Table 3.4). Before these shapefiles could be merged to create a single dataset, the spatial data required pre-processing. The Offshore Platform Points (Hydro, 1:90k - 1:350k) [122] shapefile only required minimal preparation, which was limited to transforming its coordinate system from WGS84 to NZCS2000. Whereas the data preparation regarding the second shapefile, Petroleum Wells [123], was more substantial.

Firstly, the projected coordinate system, Transverse Mercator, was reprojected to NZCS2000. As the Transverse Mercator projection is based on the NZGD2000 datum, no transformation was required. Secondly, as seen in Figure 3.7, the data had to be cleaned up, as this shapefile contained records for both on- and offshore wells, which had statuses that ranged from 'producing' to 'plugged and abandoned'. Therefore, for this analysis, only wells that were located offshore and that had the status of 'producing', 'confidential' or 'unknown' were selected and exported to a new shapefile. These features were selected with the following SQL

attribute query: “WaterDepth” <> ‘ ’ AND (“Status” = ‘Confidential’ OR “Status” = ‘producing’ OR “Status” = ‘unknown’).

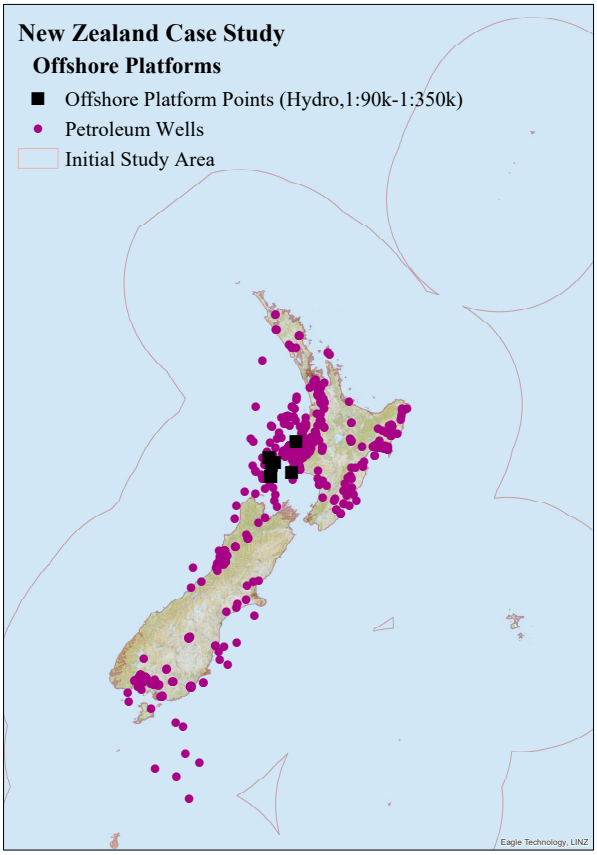

Figure 3.7. Two shapefiles were identified as containing relevant offshore installation data.

This new shapefile was combined with the modified Offshore Platform Points (Hydro, 1:90k - 1:350k) dataset by utilising the ‘Merge’ tool, resulting in a single dataset referred to as Offshore Platforms. The duplicate records contained in the newly generated Offshore Platforms dataset were then deleted. In some cases, the records indicated multiple overlapping wells in the same area; therefore, these offshore platforms were compared with relevant NZ nautical charts in order to identify the correctly located well(s). Once this dataset was cleaned up, 500 m polygons were generated around each well point utilising the ‘Buffer’ tool, resulting in the processed dataset depicted in Figure 3.8. These were created as both Article 60 of the United Nations Law Convention on the Law of the Sea [162] and NZ’s Continental Shelf Act 1964 [163] require the establishment of 500 m safety zones around offshore installations. Exclusion zones are established in order to protect these offshore installations and minimise the risk of an accident occurring, which could potentially result in marine pollution.

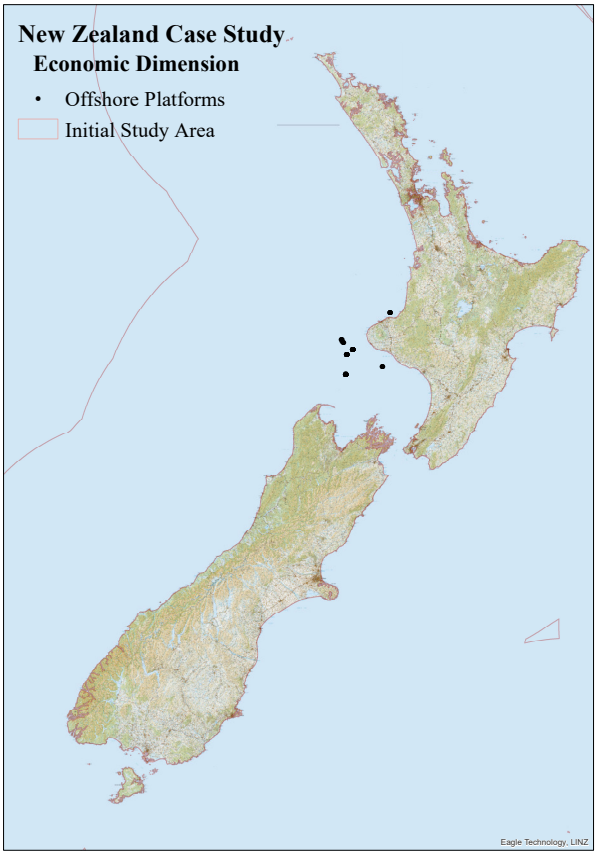

Figure 3.8. The finalised Offshore Platforms dataset that was prepared for the GIS Analysis stage.

Seabed Mining. The Seabed Mining dataset was generated from the Mineral Active Permits shapefile, which was published by New Zealand Petroleum and Minerals [124]. This shapefile contained information regarding the currently registered mining and exploration permits as well as the continental shelf licences.

As the Mineral Active Permits geodata was defined in the Transverse Mercator coordinate system, this had to be reprojected to the required NZCS2000 coordinate system. Similar to that of the Petroleum Wells dataset discussed above, the Mineral Active Permits dataset also contained records for both on- and offshore licenses and permits (Figure 3.9(a)). Therefore, in order to generate the Seabed Mining shapefile, the active offshore permits were identified and selected utilising the SQL attribute query: ("Status" = 'Active' OR "Status" = 'Active - Change Pending') AND "PERMIT_OFF" = 'Offshore'. These selected features were then exported to a new shapefile, resulting in the Seabed Mining shapefile depicted in Figure 3.9(b).

(a) (b)

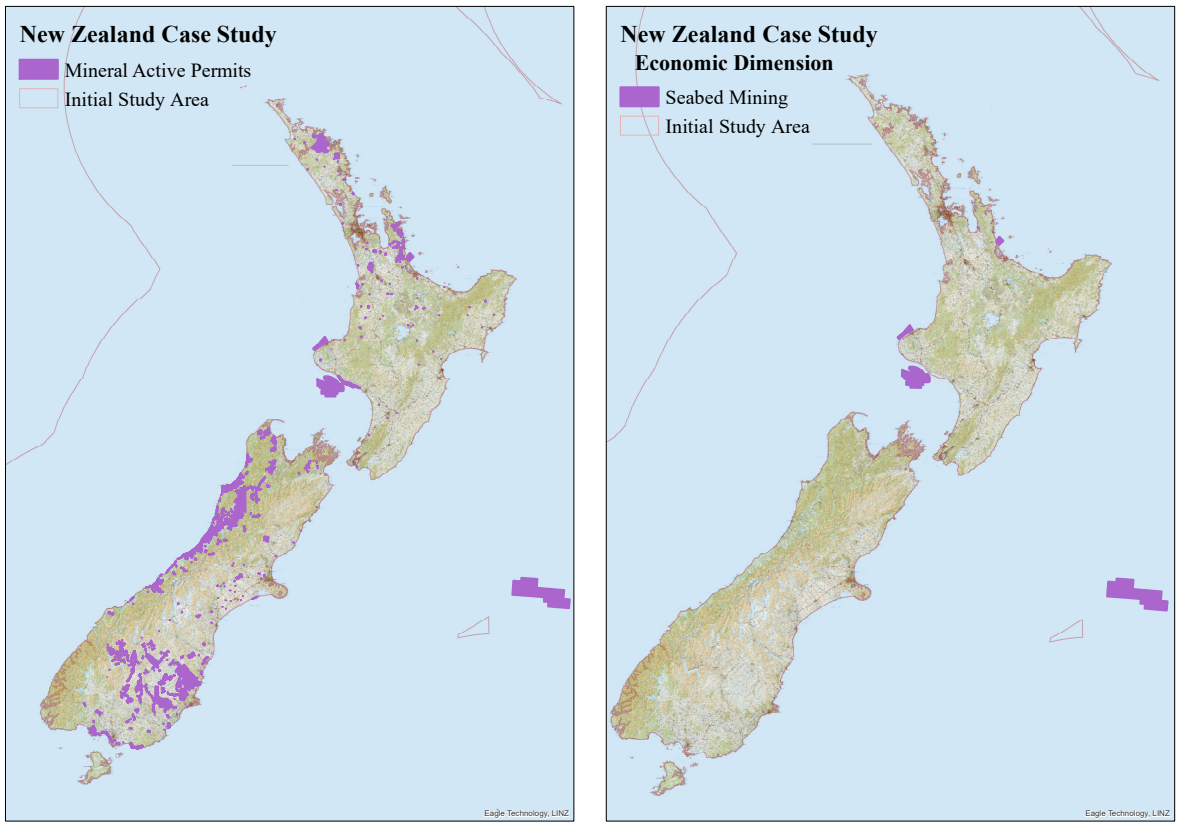

Figure 3.9. The (a) Mineral Active Permits dataset was utilised to generate the (b) Seabed Mining shapefile.

Shipping (Routes). NZ does not have mandatory shipping lanes, and so, therefore, in order to generate a popular shipping routes dataset instead, an official information act application was made to Maritime NZ requesting Automatic Identification System (AIS) ship tracking data. The request could not be processed as this information is not managed or maintained by the government (R. Gabara, personal communication, February 25, 2019). However, two months (October and November 2018) of AIS track data was obtained directly from Maritime NZ (personal communication, March 4, 2019); each month of track data was provided as a separate dataset.

To create the final Popular Shipping Lanes shapefile from these datasets required extensive data preparation and processing. The first issue encountered was that the ArcMap application did not recognise the coordinate system assigned to the dataset. This was because the datasets were assigned the coordinate system WGS 84 instead of GCS_WGS_1984; WGS 84 is denoted by GCS_WGS_1984 in ArcGIS applications. Therefore, in ArcCatalog, the coordinate system had to be updated to the recognisable coordinate system name. Once this was rectified, then both datasets were converted to the required NZCS2000 coordinate system.

Another issue with regards to these initial spatial datasets was that when the ship track lines were generated from the AIS data, superfluous horizontal lines were also generated each time a track line intersected with the 180th meridian (Figure 3.10). Thus, before any further processing could be done, these horizontal lines had to be identified and removed from both sets of data.

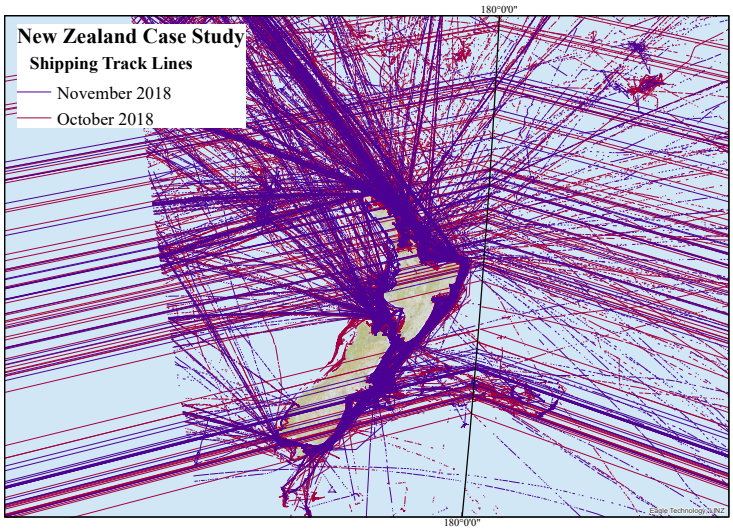

Figure 3.10. The initial datasets containing the ship track line features also contained additional horizontal lines. The horizontal lines appear to be at an angle due to the reprojection of the line features from a geometric coordinate system to that of a projected coordinate system.

In order to determine which lines features were the actual ship track lines in both datasets, the following SQL attribute query was utilised: "shape_length" <= 359. This query selected all line features with a length less than or equal to 359°, which were then exported to two new shapefiles; corresponding to each month (Figure 3.11).

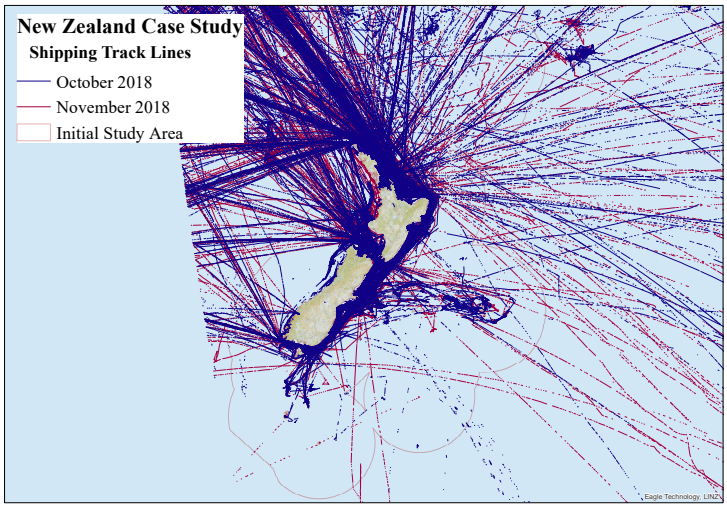

Figure 3.11. The November and December spatial datasets comprised of only the ship tracking line features.

Before a single dataset could be created, the commercial vessels had to be identified, selected, and exported to new shapefiles for each month. This was achieved by implementing a SQL attribute query that selected features with a class corresponding to 'CA' (Class A: Larger Vessels). The month of November only consisted of data relating to larger vessels, whilst October also contained data regarding smaller (leisure) vessels. These cleaned monthly shapefiles were then merged into a single dataset and clipped to the initial study area, thereby resulting in a combined shipping routes dataset.

To generate a dataset that contained information with regards to just popular shipping routes required the use of statistical analysis. In order to conduct the statistical analysis required the track lines to be aggregated within a specific area. Therefore, a 5 km^2-resolution polygon grid, which covered the entire study area, was developed utilising the 'Create Fishnet' tool. Initially, a grid with a higher resolution (1 km^2) was generated, but as the grid was required to cover the entire study area (approximately 4.1 million km^2) it was found to be too computationally expensive. Therefore, similar to that of the Commercial Fisheries shapefile, a resolution of 5 km^2 was selected instead.

The grid was then clipped to the Initial Study Area polygon to ensure that the results would not be skewed. For instance, when aggregating the track lines to the relevant cells, cells that did not contain track lines would be assigned a value of zero. Therefore, if the landmasses and the marine waters outside of the EEZ were not removed before the statistical analysis was undertaken, the cells contained within these areas would be assigned a zero value instead of a null value. This would skew the results as zero values indicated that ships did not travel in these areas and would be included in the analysis, whereas null values represented an area of 'no data' and therefore would not be included in the analysis.

The last step to be undertaken before conducting the statistical analysis was to aggregate the ship track lines in each cell. This was achieved by utilising the 'Join Data' tool, which has a range of functionalities. Firstly, it was utilised to calculate the number of track lines contained within the grid cells, and then a new shapefile was generated, which contained each cell in the grid with the corresponding count data.

The 'Hot Spot Analysis' tool, which is based on the Getis-Ord Gi* statistic, tested the null hypothesis of complete spatial randomness (i.e., how likely is it that the spatial cluster of track lines is the result of a random spatial process?). This resulted in the identification of statistically significant spatial clusters of high values (hot spots) and low values (cold spots) [164]. Once

the tool completed its analysis, a new dataset was generated, which contained each grid cell that was within the initial study area, with its corresponding count value (the number of track lines contained in the cell), z-score (measures of standard deviation) and p-value (probability that the null hypothesis was falsely rejected). Therefore, in order to identify the most popular shipping routes, a SQL attribute query was implemented that selected cells with a z-score >= 2.58 (99 % likelihood that the clustering of high values is statistically significant) and a p-value <= 0.01 (1 % probability that the spatial cluster is the result of a random spatial process). These selected cells were then exported to a new shapefile and merged to create a single polygon that represented the most popular commercial shipping routes (Figure 3.12).

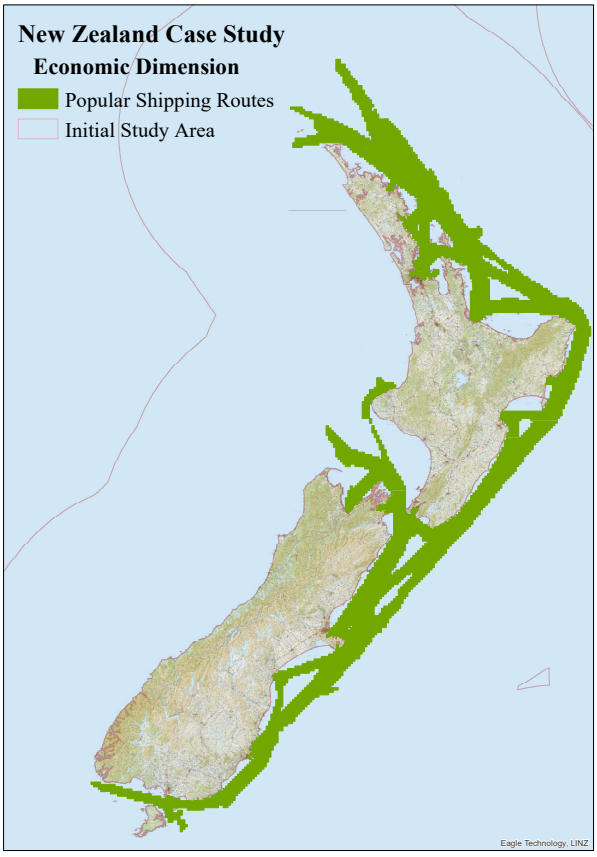

Figure 3.12. The Popular Shipping Routes dataset generated from two months of AIS data.

Even though the resulting Popular Shipping Routes shapefile was created from only two months of data, when it is compared with the 2017 Density Map from MarineTraffic (Figure 3.13), it could be seen that the most travelled sea routes were, in general, captured quite well. Except in the case of the shipping routes that were most frequently travelled west and south of the South Island (Figure 3.13). However, as shown in Figure 3.6, these locations were captured in the Commercial Fisheries layer instead.

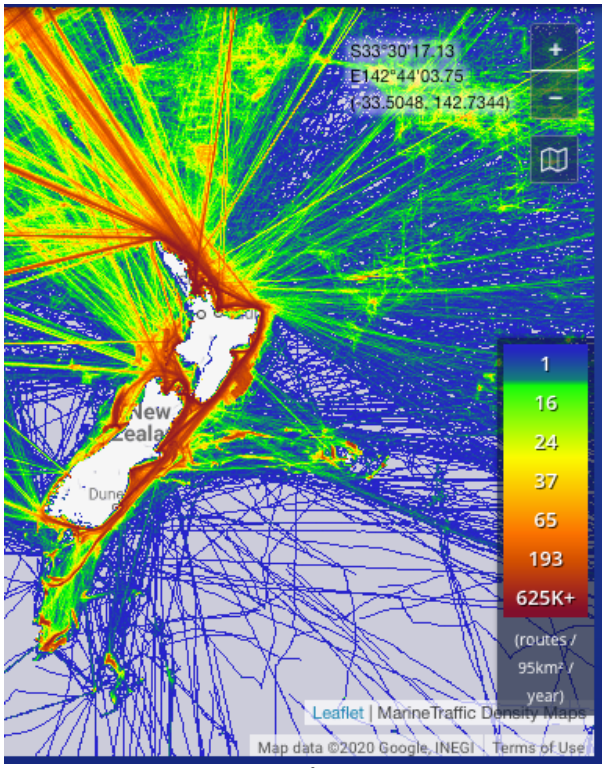

Figure 3.13. Screenshot of the 2017 Density Map[6] from the MarineTraffic website [165]. Printed with permission from MarineTraffic (personal communication, February 21, 2019).

Environmental Dimension

Benthic Protection Areas / Marine Areas / Seamount Closures. The shapefiles with regards to the Marine Reserves, Benthic Protection Areas, and Seamount Closures were obtained from Ministry for the Environment Data Service (Table 3.4). These datasets only required minimal preparation, which included transforming the geographic WGS84 coordinate system to that of the projected NZCS2000 reference system, and ensuring that all the records contained within the respective datasets were up-to-date by referring to the relevant legislation and gazette notices.

Hauraki Gulf Marine Park. An official information act application was made to Fisheries NZ requesting the Hauraki Gulf Marine Park shapefile (Table 3.4). The spatial data received had been digitised from registered images, as no coordinates have been provided in the relevant

[6] A request for the spatial data relating to the Density Maps (Figure 3.13) was made to MarineTraffic (www.marinetraffic.com, personal communication, February 21, 2019). However, the author was informed that these maps had been designed specifically for the MarineTraffic Live Map, and due to technological limitations, could not be provided in the requested format.

legislation to describe the exact boundaries of the marine park [166]. In terms of pre-processing, this shapefile only required the coordinate system to be converted from WGS84 to NZCS2000.

Marine Mammal Sanctuaries. The Department of Conservation Marine Mammal Sanctuaries shapefile was acquired from the Ministry for the Environment Data Service (Table 3.4). However, only six of the eight sanctuaries that provide protection for marine mammals were included in this dataset. Therefore, the shapefile was amended to include the Te Rohe o Te Whānau Puha Whale Sanctuary and the Ōhau NZ Fur Seal Sanctuary, which were established by the Kaikōura (Te Tai o Marokura) Marine Management Act 2014 [127]. As the Ōhau NZ Fur Seal Sanctuary is contained within the Te Rohe o Te Whānau Puha Whale Sanctuary, it was only necessary to create the larger whale sanctuary.

Before amending the initial Marine Mammal Sanctuaries shapefile, the coordinate system had to be converted from WGS84 to NZCS2000. Then to create the additional polygon, the coordinates regarding the Te Rohe o Te Whānau Puha Whale Sanctuary, provided in Schedule 3 of the Kaikōura (Te Tai o Marokura) Marine Management Act 2014, were inputted into an Excel spreadsheet. These coordinates were defined in the WGS84 coordinate system and provided in the format of degrees and minutes, which had to be converted to Decimal Degrees (DD). Once the Excel spreadsheet was prepared, it was imported into a new ArcMap file, which was defined in the WGS84 coordinate system. As seen in Figure 3.14 (a), the Excel data was then used to generate a point feature class by utilising the 'Display XY Data' function, which was exported to a new shapefile. The coordinate system of this new point shapefile was converted from WGS84 to NZCS2000.

To create the additional sanctuary, the initial Marine Mammal Sanctuaries dataset and the point shapefile were imported into a new ArcMap file with NZCS2000 specified as the coordinate system. Then by utilising the 'Create Features' tool in combination with the polygon endpoints (the features contained within the point shapefile) as well as the description of the Te Rohe o Te Whānau Puha Whale Sanctuary provided in Schedule 3 of the Kaikōura Marine Management Act, the missing feature was created in the Marine Mammal Sanctuary dataset (in Figure 3.14 (b)).

(a) (b)

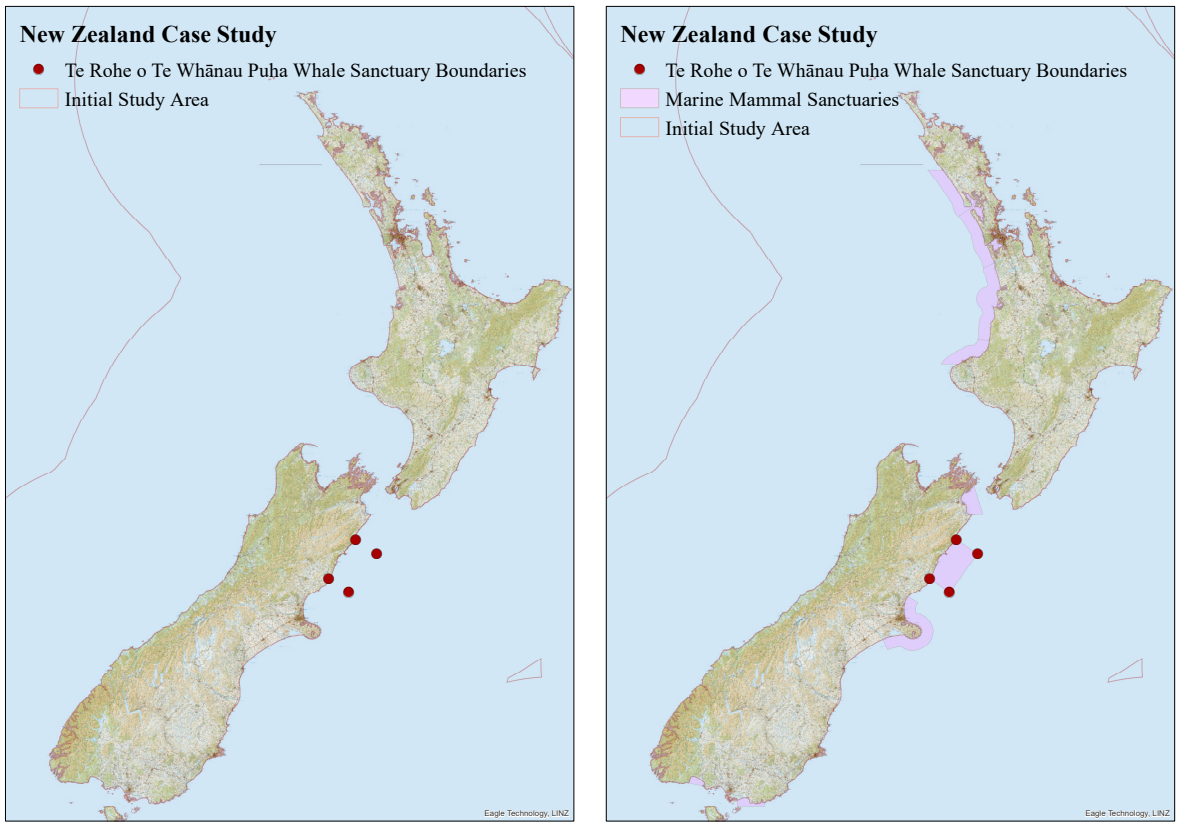

Figure 3.14. The (a) coordinates provided in the relevant legislation were utilised to create a point shapefile, which in turn was employed to create the boundaries of the Te Rohe o Te Whānau Puha Whale Sanctuary.

Marine Protected Areas. The Type 2 MPAs dataset was also obtained from the Ministry for the Environment Data Service. Similar to that of marine reserves, MPAs are established to protect marine habitats and ecosystems [167]. Areas that met the Protection Standard for Type 2 MPAs and, therefore, included in this dataset were the Fiordland Marine Area, marine parks, fisheries closures, a Mātaitai Reserve, as well as submarine cable and pipeline protection zones [167].

In this approach, Mātaitai Reserves and submarine cable and pipeline protection zones were considered cultural and technical factors, respectively. Therefore, the record classified as 'Type II MPA Mataitai' was deleted. Whilst the features assigned the MPA type 'Type II MPA Cable or Pipeline Zone' were selected by a SQL attribute query and exported to a new shapefile (which was later used in the generation of the submarine cable and pipeline dataset). Thereafter, the coordinate system of the environmental MPA dataset was converted from the assigned WGS84 to NZCS2000, and the records compared with the relevant NZ legislation and gazette notices.

Social Dimension

Submarine Archaeology. As no single dataset contained all the relevant information regarding shipwrecks in NZ, a total of six shapefiles (Figure 3.15) were merged in an attempt to create a single complete dataset (which was comprised of 333 records). These six shapefiles were obtained from the LINZ (Land Information New Zealand) Data Service and were all defined in the WGS84 coordinate system, which was inherited by the newly created dataset. The coordinate system of this newly created dataset was then converted from WGS84 to NZCS2000.

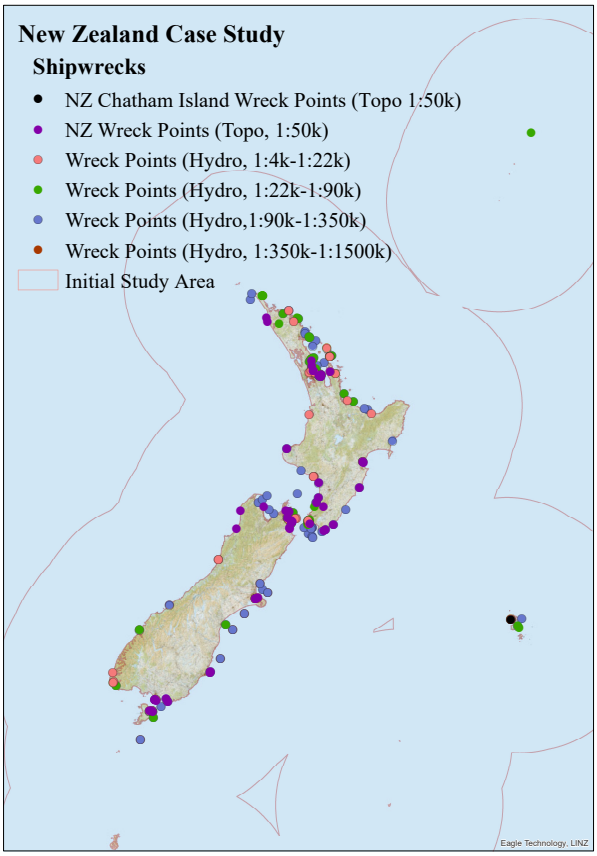

Figure 3.15. Six separate datasets were merged to a single shipwreck shapefile.

As several shapefiles were merged to create the single dataset, a number of records were duplicated, which were subsequently deleted. Furthermore, in several instances, the records indicated multiple overlapping shipwrecks in the same area. Therefore, these features were compared with relevant NZ nautical charts in order to identify the correctly located wrecks. It should be noted that there was no single identifying value that could be utilised in a SQL query. This meant that every single one of the 333 records in the dataset had to be manually reviewed, and during this process, a total of 65 nautical charts were consulted.

Once this dataset was cleaned up, 158 records remained, and similar to that of the offshore platforms, 500 m buffers were generated around each shipwreck point.

Technical Dimension

Bathymetry. The Bathymetry shapefile was obtained from NIWA (National Institute of Water and Air), which was defined in the Mercator 41 projected coordinate system. The first step in preparing the spatial data was to convert the coordinate system to NZCS2000 and then clip the dataset to the study area polygon.

As the 250 m isobath (Figure 3.16 (a)) was identified as a limiting condition (Section 3.2.2), the bathymetry shapefile required extensive pre-processing to prepare it for the analysis stage. Similar to that of the Initial Study Area layer, line features (the 250 m isobath in this case) were used to create a corresponding polygon. However, the 'Feature to Polygon' tool could not be used directly on this spatial data, as the 250 m isobath line features only fully enclosed areas in some locations (Figure 3.16 (b)).

(a) (b)

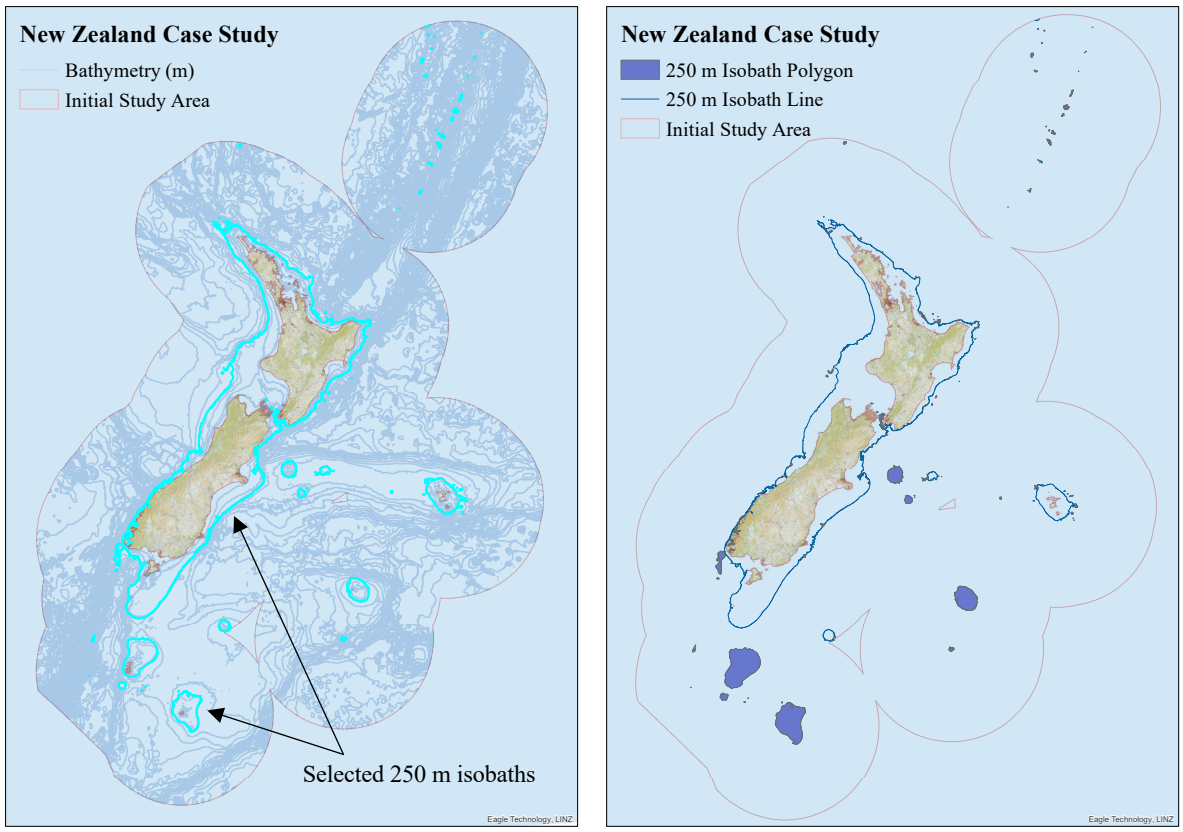

Figure 3.16. The (a) 250 m isobath was selected, utilising a SQL attribute query, and inputted into the 'Feature to Polygon' tool. This resulted in (b) an incomplete polygon dataset, as the 250 m line features did not fully enclose all the relevant areas.

Therefore, the line features that overlapped, intersected, and dangled had to be identified and managed in order to prepare the spatial data sufficiently for the 'Feature to Polygon' tool. This required the creation of a topology, based on the 250 m line features, in ArcCatalog. Where the following line topology rules were utilised: must not dangle, must not intersect, must not overlap. Once the topology was generated (Figure 3.17(a)), then each of the 512 rule violations was inspected individually in ArcMap and rectified if necessary (i.e., joining line features, splitting intersecting lines, and deleting overlapping lines). Once all the topology errors were repaired, the 'Feature to Polygon' tool was utilised to create the bathymetry polygons. However, these polygons included the landmasses. Therefore the 'Erase' tool was used to remove the coastline polygons. Then this spatial dataset was refined further by only retaining the 250 m isobath polygons that surrounded the inhabited islands (North and South Island, Chatham Island, and Stewart Island [168]), resulting in the Bathymetry Limiting Condition dataset depicted in Figure 3.17 (b).

(a) (b)

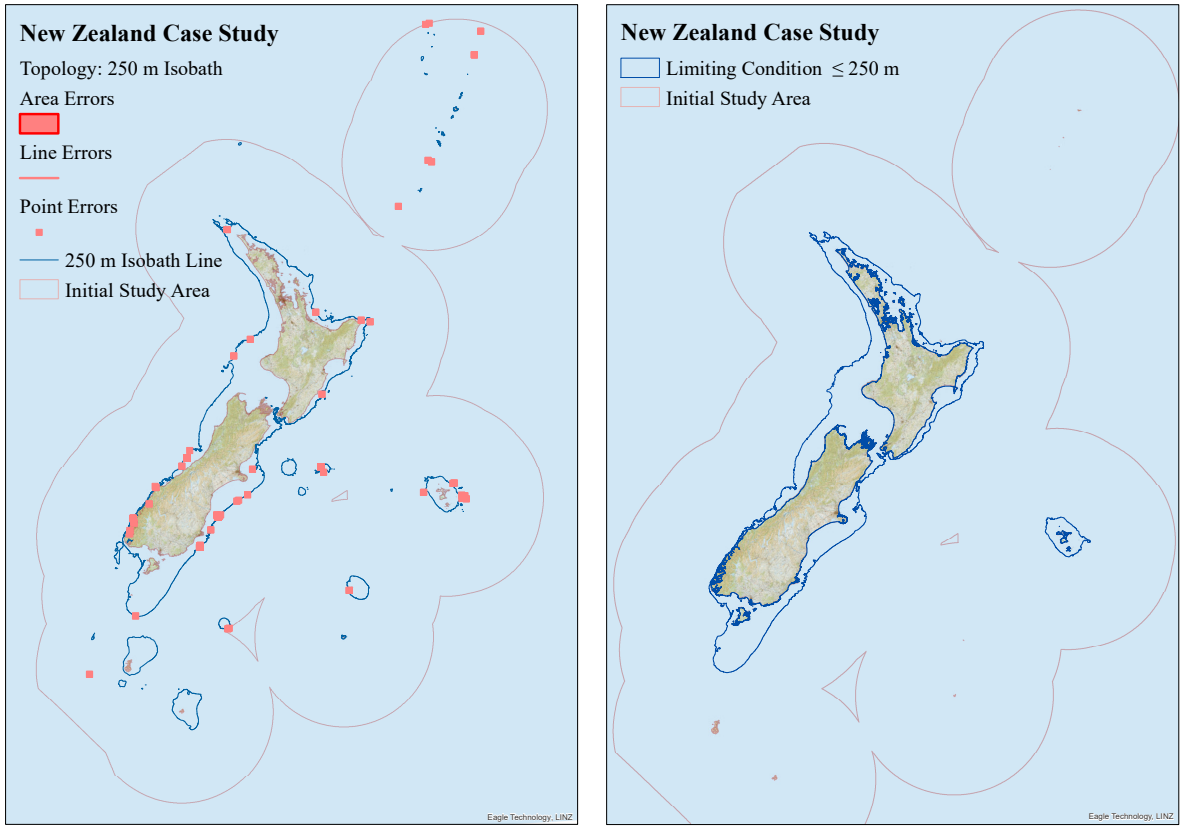

Figure 3.17. (a) A topology was created in order to identify and rectify errors in the dataset. Once this investigation was complete, then (b) the 250 m isobath polygon dataset was generated.

Dredged Areas. Three shapefiles (Table 3.4), with a WGS84 coordinate system, were merged to create a single Dredged Areas dataset with the same geographic coordinate system. The

coordinate system of this newly generated shapefile was then converted to the appropriate coordinate system for this case study.

As this dataset was created from several existing shapefiles, duplicate records occurred. These were identified manually and then deleted. Furthermore, each record was compared to the relevant nautical charts, of which several had to be amended to reflect the correct dredged depth and corresponding nautical chart.

Dumping Grounds. Similar to the development of the Dredged Areas dataset, the Dumping Grounds shapefile was also created by merging three shapefiles (Table 3.4). This newly formed Dumping Grounds shapefile inherited the WGS84 coordinate system associated with the existing shapefiles. Therefore, it was transformed to the required NZCS2000 reference system before further data preparation was undertaken.

As this dataset was generated from shapefiles at three different scales, it was expected that data would be duplicated. Consequently, each record was manually checked, and the replicated data deleted.

Grid Availability. The Grid Connection Points shapefile obtained from Transpower NZ Ltd (Table 3.4) contained point data with regards to the grid injection points and grid exit points. As the grid availability has been classified as a constraint (Table 3.4), the layer retained its point features. Therefore, in terms of data preparation, only the coordinate system was transformed (from Transverse Mercator to NZCS2000). It should be noted that the grid exit points were included in the dataset, as electricity can flow in as well as out at these points (K.J. Hodges[7], personal communication, December 16, 2019).

Military Exercise Areas. A geospatial dataset relating to the military exercise areas in NZ could not be obtained. Therefore, a military exercise areas vector layer was created from the coordinates provided in the Annual NZ Notices to Mariners regarding the firing and bombing practices as well as defence exercises that take place off the coast of NZ [144].

To create the new shapefile, the relevant coordinates from the Annual NZ Notices to Mariners were inputted into an Excel spreadsheet. These coordinates were defined in the WGS84 coordinate system and provided in the format of degrees, minutes, and seconds, which had to

[7] Kevin Hodges, Principal Electrical Engineer at AECOM

be converted to DD. Once the Excel spreadsheet was prepared, it was imported into a new ArcMap file, which was defined in the WGS84 coordinate system. As seen in Figure 3.18(a), the Excel data was then used to generate a point feature class, which was exported to a new shapefile. The coordinate system of this new point shapefile was converted from WGS84 to NZCS2000.

(a) (b)

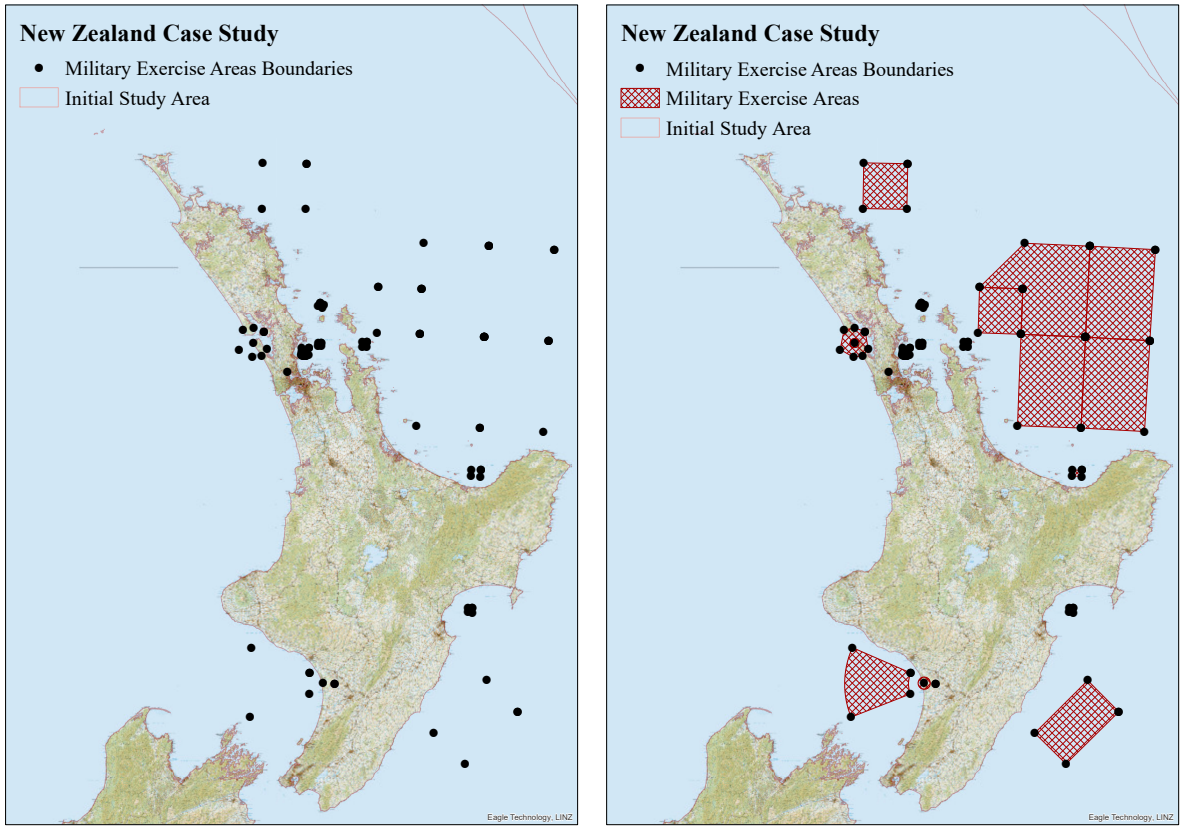

Figure 3.18. The coordinates provided in the relevant documentation were utilised to create (a) a point shapefile, which in turn was employed to create (b) the boundaries of the military exercise areas.

A new polygon shapefile was then created in ArcCatalog (assigned the NZCS2000 coordinate system), which was imported with the point feature shapefile into a new ArcMap file. Then by utilising the 'Create Features' tool in combination with the polygon endpoints as well as the description of each military exercise area provided in 5 Firing Practice, Exercise and Submarine Safe Bottoming Areas of the Annual NZ Notices to Mariners, the polygon features were generated (Figure 3.18 (b)).

Commercial Ports. The data pertaining to NZ's commercial ports were obtained through ArcGIS online, which was accessed directly through the ArcMap application. This spatial data

was defined in the WGS84 coordinate system and, therefore, converted to the required NZCS2000 coordinate system.

A closer inspection of the dataset revealed that it contained both inland ports and seaports and, thus, had to be processed further. A SQL attribute query was utilised to identify and select all the inland ports (Figure 3.19), which were subsequently deleted. In addition, after consulting the World Port Index [169] it was found that Port Opua was absent from the dataset. Therefore, utilising the details provided in this document, an additional point feature was created in the Commercial Ports layer, which represented this missing port.

As the Commercial Ports dataset was considered a constraint (Table 3.4), it was required to keep the port features as point data for the GIS Analysis stage.

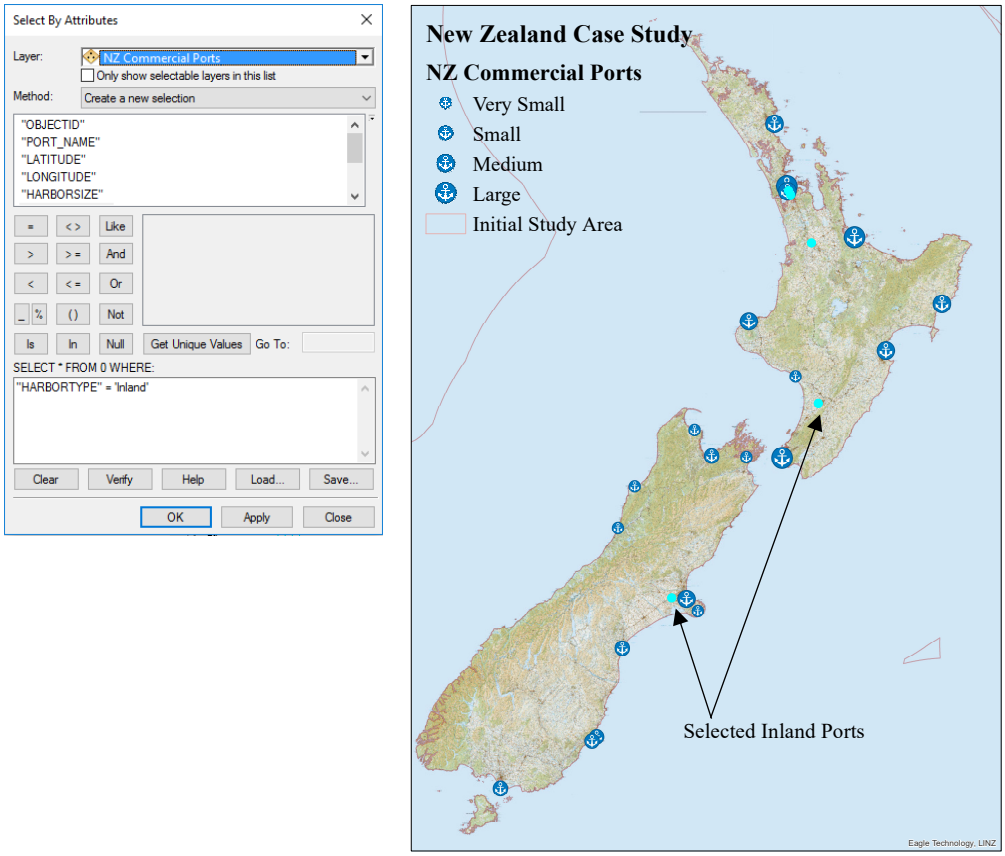

Figure 3.19. The SQL attribute query (left) that was implemented in order to identify the inland port's records (right), which were required to be deleted from the dataset.

Submarine Cables & Pipelines Protection Zones / Submarine Cables. NZ has designated cable and pipeline protection zones [170] within its territorial seas, several of which qualify for 'Type 2 MPA' status, as defined by NZ's Ministry of Fisheries and Department of Conservation [152]. However, for this study MPAs are categorised as environmental factors, which, as stated in Section 3.2.1, are areas that have been established to protect marine habitats and ecosystems.

Therefore, the cable protection zones included in the original MPA spatial dataset were exported to a new vector layer (Figure 3.20), and the coordinate system was transformed from WGS84 to NZCS2000. Not all the cables and pipelines protection areas are classified as Type 2 MPAs, and, therefore, these additional protection zones were identified from the relevant NZ legislation (Table 3.4).

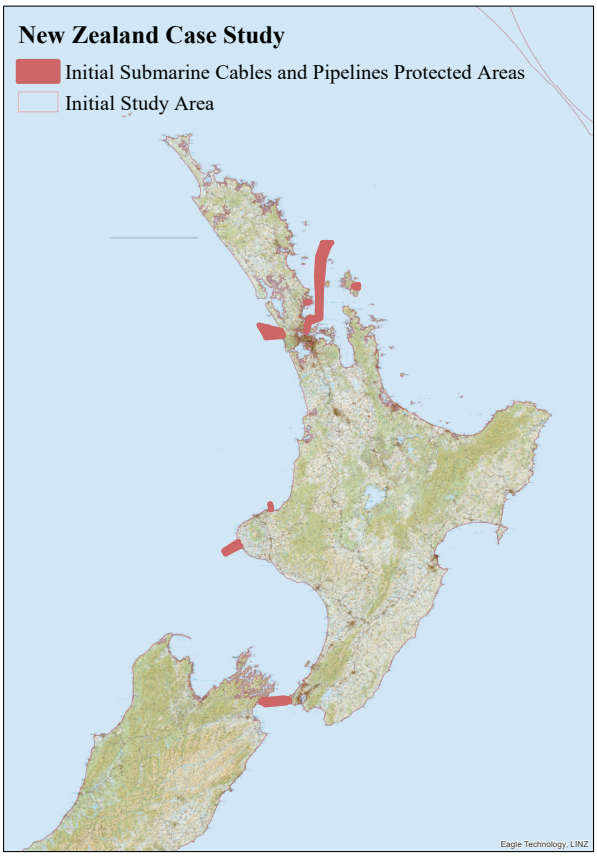

Figure 3.20. The submarine cables and pipelines protection areas which were classified as Type 2 MPAs.

The coordinates regarding the absent submarine cable protection zones were collated into a single Excel spreadsheet and were obtained from the following legislative instruments: Submarine Cables and Pipelines Protection (Tui Area Development) Order 2007 [147]; Submarine Cables and Pipelines Protection (Kupe Gas Project) Order 2008 [148]; Submarine Cables and Pipelines Protection (Maari Development) Order 2008 [149]; as well as the Submarine Cables and Pipelines Protection Order 2009 [150]. It should be noted that the majority of the protected areas described in the Submarine Cables and Pipelines Protection Order 2009 were also classified as Type 2 MPAs, with the exception of Area 6–Taharoa, Area 9–Hawke Bay, and Area 10–Maui & Maui B pipelines [150].

The coordinates were defined in the WGS84 coordinate system and provided in the format of degrees, minutes, and seconds, which had to be converted to DD. Once the Excel spreadsheet was prepared, it was imported into a new ArcMap file, which was defined in the WGS84 coordinate system. The Excel data was then utilised to generate point data, which was exported to a new shapefile. The coordinate system of this new point shapefile was converted from WGS84 to NZCS2000.

In order to generate the additional polygon features, the initial cable protection zones layer (Figure 3.20) and the newly generated point shapefile were imported into a new ArcMap file with NZCS2000 specified as the coordinate system. Similar to that of the marine mammal sanctuary and the military exercise areas datasets, the additional features were created by utilising the description provided in the relevant documentation in combination with the polygon endpoints; the point data (Figure 3.21).

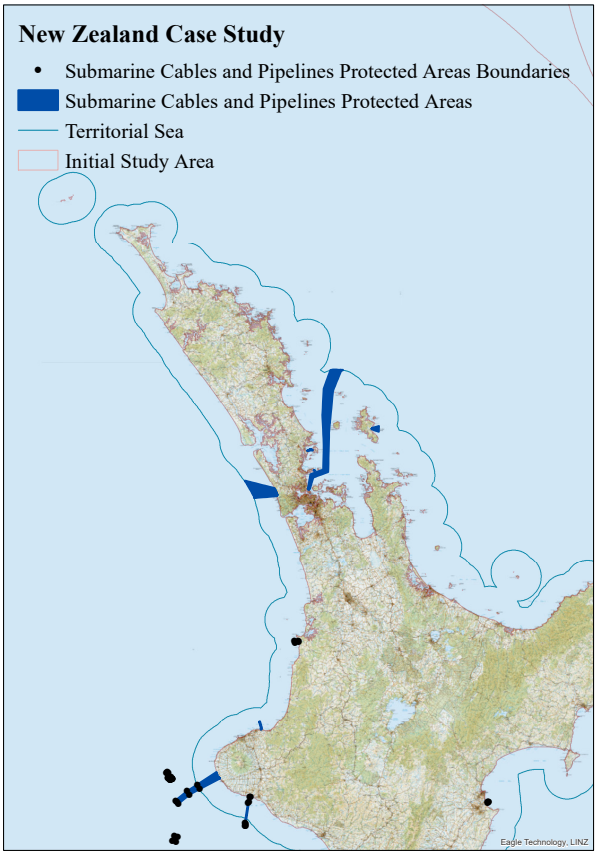

Figure 3.21. The coordinates provided in the relevant legislation were used to establish polygon features for each of the missing protected areas.

As designated cable protection zones have not been delineated between NZ's territorial seas and EEZ, a shapefile with the recommended one nautical mile buffer [171] on either side of the relevant submarine cables was generated. The spatial dataset pertaining to these submarine

cables was obtained from the LINZ Data Service, which was defined in the WGS84 coordinate system. The layer was transformed to the NZCS2000 projected coordinate system before any pre-processing was undertaken.

As seen in Figure 3.22(a), these cable line features extended into the open sea as well as the territorial waters. Therefore, before the buffer zones could be generated, the cables were clipped to the initial study area using the 'Clip' tool, thereby removing the cables that were located outside the study area. As the territorial seas dataset was comprised of line features, it could not be used in conjunction with the 'Clip' tool.

Therefore, in order to remove the cables that occurred within the territorial waters, the 'Split' tool was employed to split the cable lines at the territorial sea boundaries. Then the cables that occurred within the territorial waters were manually removed (Figure 3.22(b)). Once this dataset was cleaned up, one nautical mile buffer polygons were generated on either side of the remaining cables.

(a) (b)

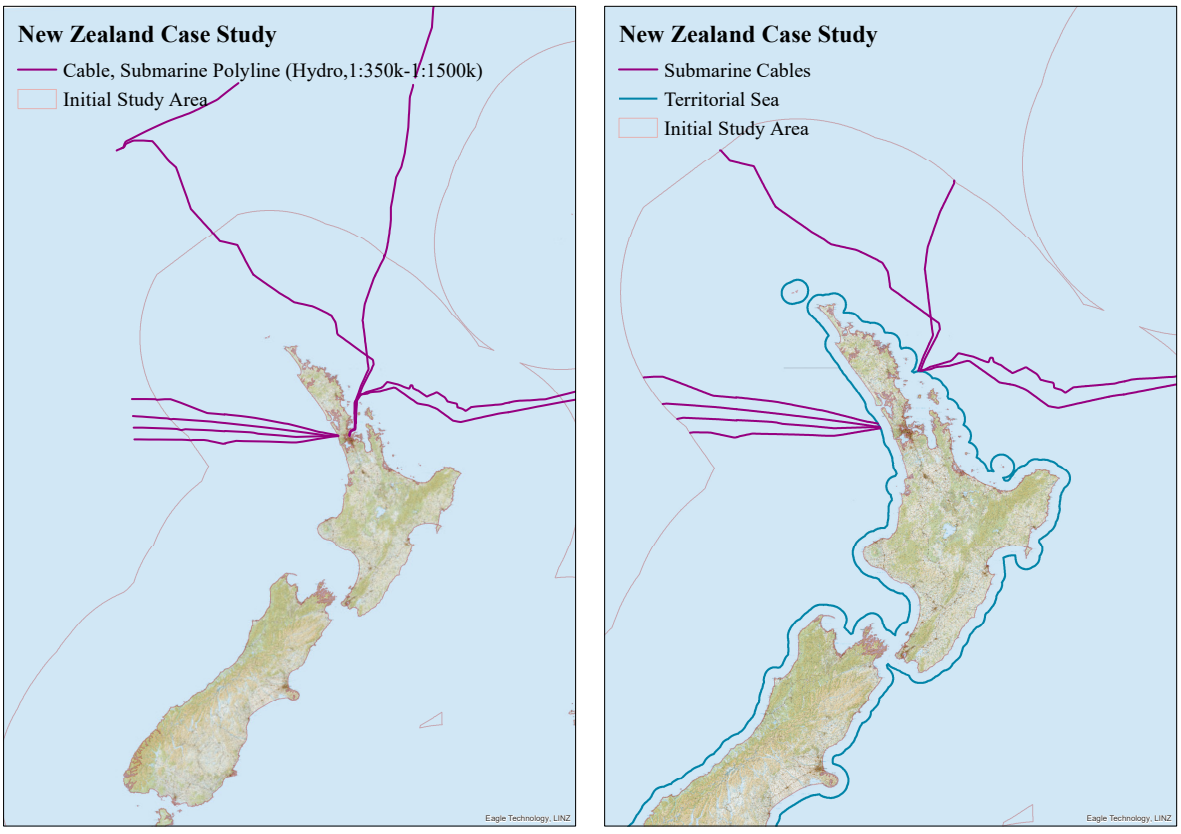

Figure 3.22. The (a) initial submarine cables spatial dataset was comprised of line features that extended into the open and territorial seas. Therefore, (b) the cables that were not located between the territorial seas and EEZ were removed from the layer.

Wave Energy Resource. As the wave energy resource has been classified as both a limiting condition and a weighted factor (Table 3.4), the layer retained its line features. Therefore, this dataset required minimal processing, which was limited to converting the WGS84 coordinate system assigned to the shapefile to the appropriate NZCS2000 coordinate system.

However, there was a slight issue in transforming the coordinate system. The ArcMap application did not recognise the initial coordinate system assigned to the dataset, even though the dataset was assigned the GCS_WGS_1984 reference frame. Therefore, this was rectified by reassigning the GCS_WGS_1984 coordinate system to the layer in ArcCatalog.

3.3.2 Stage 1.2: GIS Analysis

In order to generate the AoI, the 'Split Polygons' tool available from the Advanced Editing toolbar was utilised. This tool allows the user to split a polygon using an overlapping line or polygon feature [172]. Therefore, the Bathymetry Limiting Condition shapefile (Figure 3.23(b)), comprised of polygon features (Figure 3.17(b)), was split into multipart polygons by selecting the 20 kW/m contour line features from the Wave Energy Resource dataset (Figure 3.23(a)). These contour lines were selected by utilising the SQL attribute query: "Value" = 20. Once the bathymetry polygons were split, all polygons that were not within the minimum (resource $\geq$ 20 kW/m) and maximum (depth $\leq$ 250 m) limiting conditions were removed from the dataset. Thereby resulting in the AoI depicted in Figure 3.23(c).

By applying the limiting conditions, the initial study area of 4,163,866 km^2 was significantly reduced to a reasonable AoI of only 131,613 km^2 in size (approximately 3 % of the initial study area). Furthermore, as seen in Figure 3.23(c), the AoI is predominately limited to the north-west and southern coastal areas of North and South Island, whilst almost entirely surrounding Stewart and Chatham Island. Most areas along the north- and south-east coasts (of North and South Island) were excluded due to the combination of low wave resource and large ocean depths. These areas also coincided with the majority of marine applications in NZ, as seen in Figure 3.24(b) and (d), and thus would have been excluded from further analysis regardless.

(a) (b) (c)

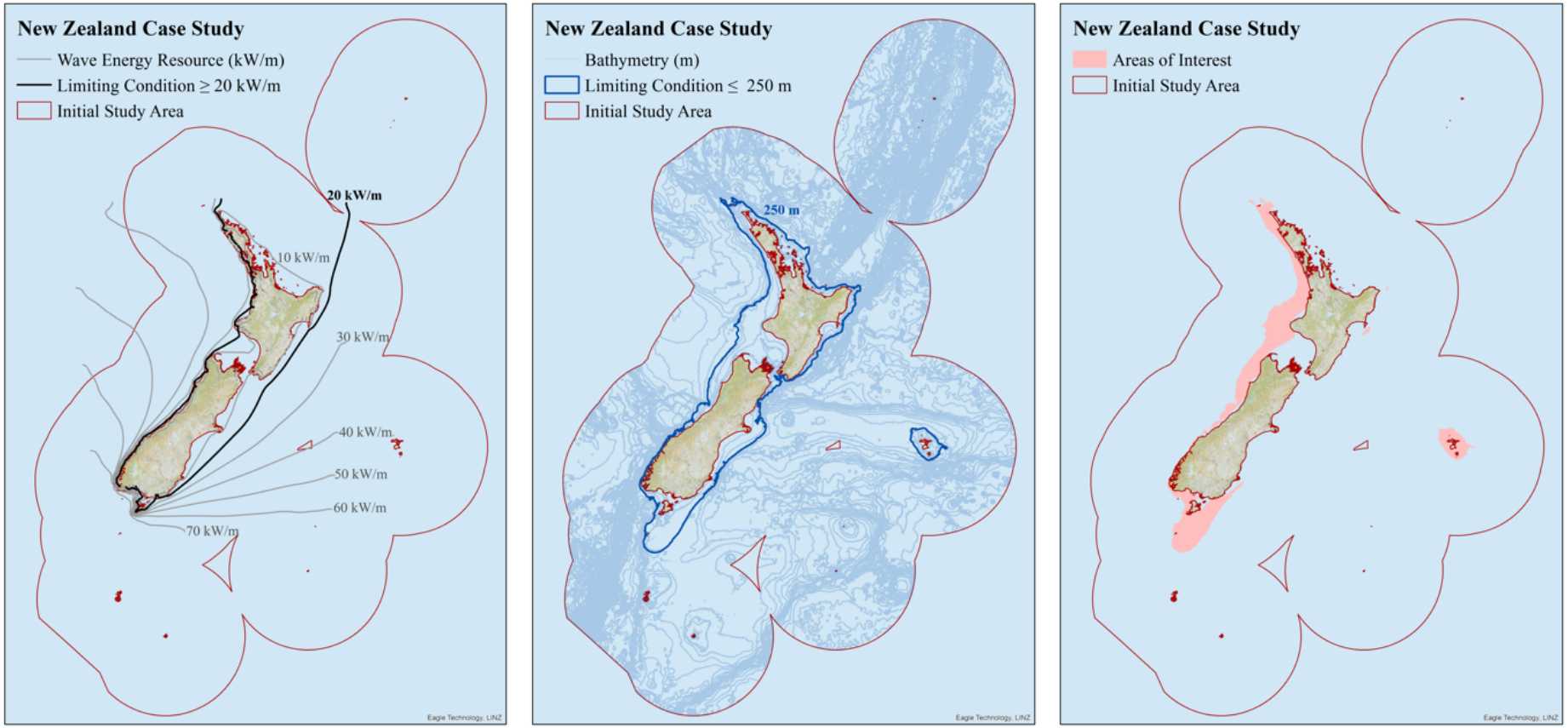

Figure 3.23. The (a) minimum and (b) maximum limiting conditions that were applied to generate the significantly reduced (c) AoI layer.

As seen in Figure 3.24(a–d), a large proportion of NZ's coastal and shallow waters are committed to other uses, which are considered incompatible with WEFs.

(a)

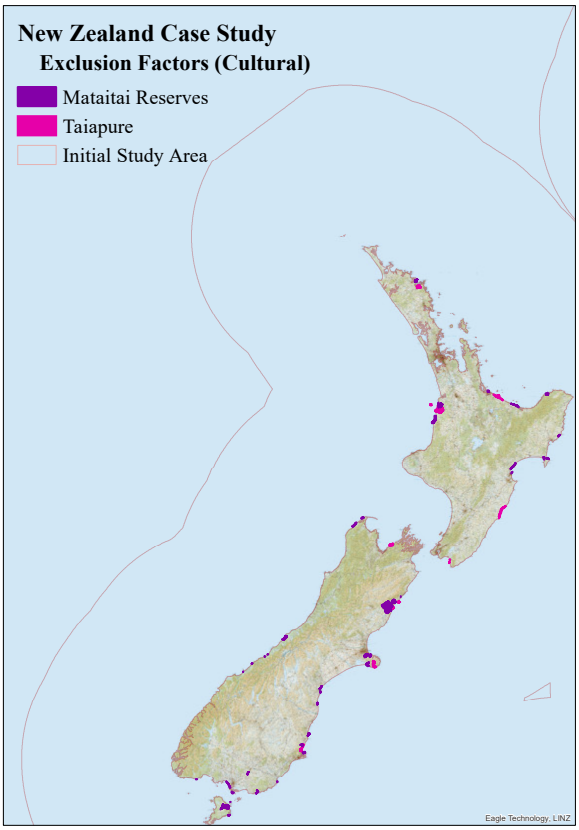

(b)

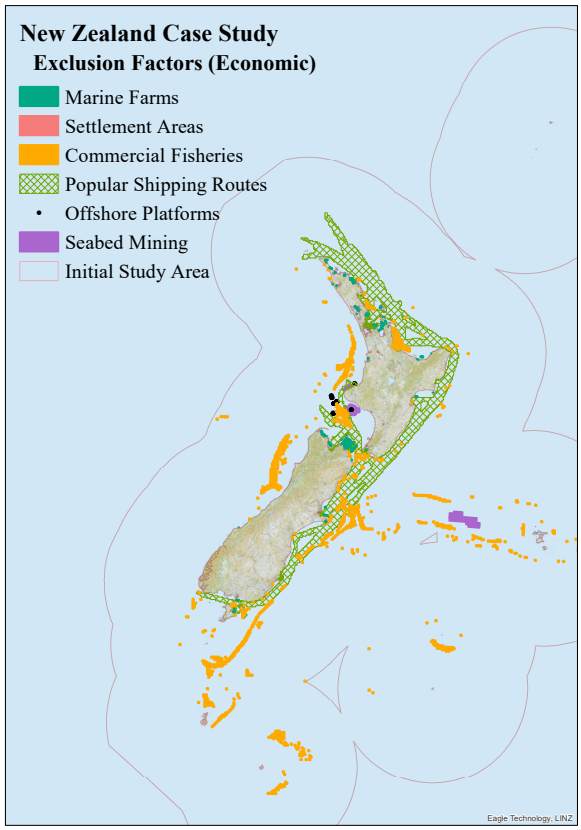

(b)

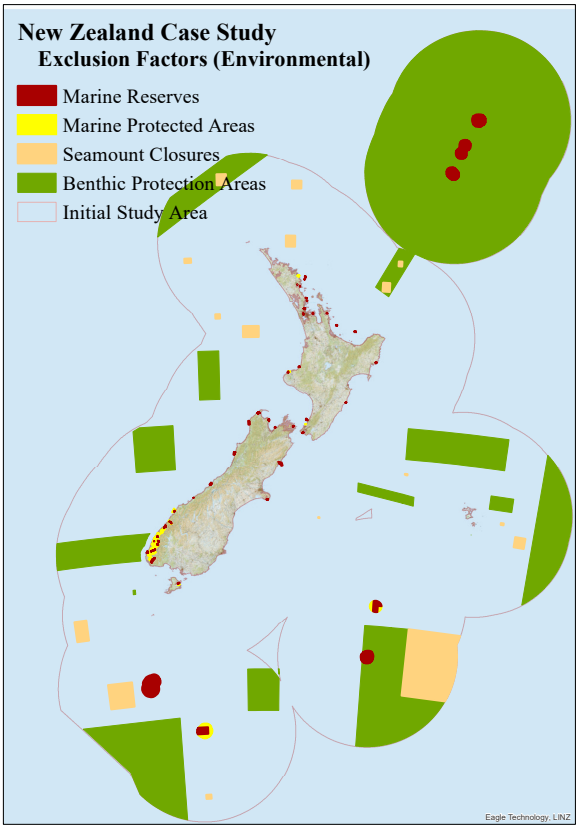

(d)

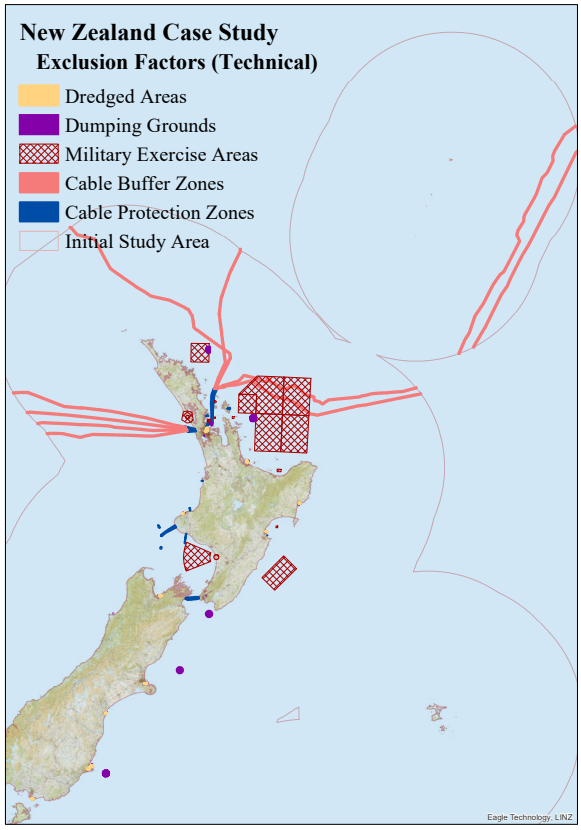

Figure 3.24. Visualisation of the (a) cultural, (b) economic, (c) environmental, and (d) technical activities incompatible with a WEF.

The individual exclusion factors depicted in Figure 3.24 were clipped (with the 'Clip' tool) to the AoI layer and then combined (using the 'Union' tool) to create a new layer that depicted areas in direct conflict with wave energy projects; Figure 3.25(a). The incompatible areas were then erased from the AoI layer using the 'Erase' tool, Figure 3.25(b), thereby resulting in the PIA layer depicted in Figure 3.26.

(a) (b)

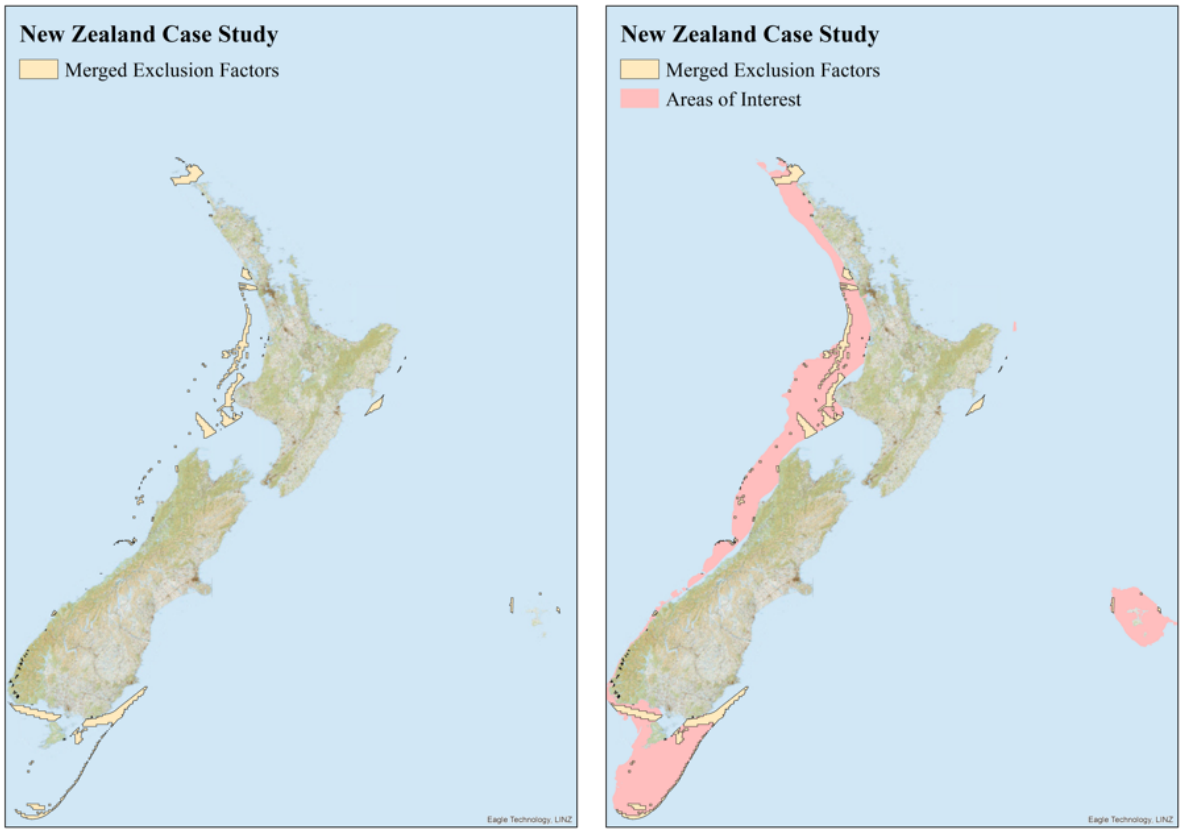

Figure 3.25. The (a) exclusion factors were merged to create a non-installation areas layer, which was (b) spatially removed from the AoI layer.

The elimination of the exclusion factors decreased the area for further analysis from 131,613 km^2 to 111,529 km^2; an additional 15 % reduction.

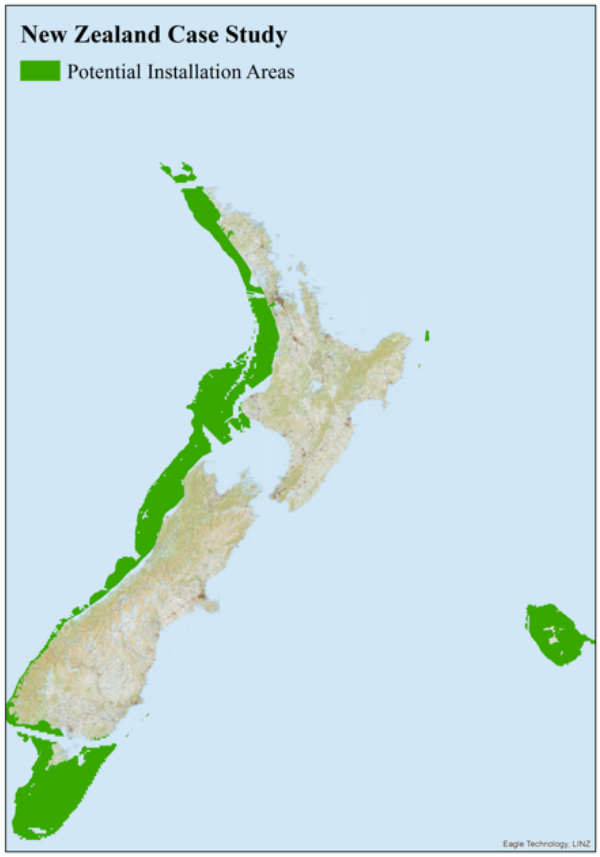

Figure 3.26. The PIAs generated for the NZ case study.

The weighted factors, categorised as constraints and restrictions (Table 3.4), were then combined to develop the WEF suitability map.

Constraint. The constraint raster layers were generated from the vector datasets pertaining to grid availability, commercial ports, and the wave energy resource. A straight line ('Euclidean Distance') tool was applied to the ports and grid connection points that were within 50 km of the PIAs. These newly generated constraint layers contained distance data (in km) from the grid/port location to 100 km offshore (at a 1 km resolution). Whereas the wave energy resource contour lines were interpolated (by using the 'Topo to Raster' tool) in order to determine the available resource (in kW/m), at any location, within the extent of the PIA (also at a 1 km resolution). It should be noted that access to these two tools requires a Spatial Analyst license.

In order to reclassify the constraints, the Equal Interval classification scheme was used to divide the range of attribute values, of each constraint layer, into 10 equally sized classes. Then the 'Reclassify' tool (which also requires a Spatial Analyst license) was utilised to reclassify the constraints to a common preference scale from 10 to 100, with 100 being the most favourable. It should be noted that the preference values are on a relative scale, and these values should be assigned relative to each other within the same dataset as well

as across all the relevant datasets. For example, the value of 100 represents distances within 10 km of a grid connection point or port and a wave energy resource greater than 66 kW/m (Figure 3.27–Figure 3.29).

Thereafter, the reclassified constraint layers were clipped to the PIA layer (using the 'Clip' function within the Image Analysis window), resulting in the layers depicted in Figure 3.27–Figure 3.29.

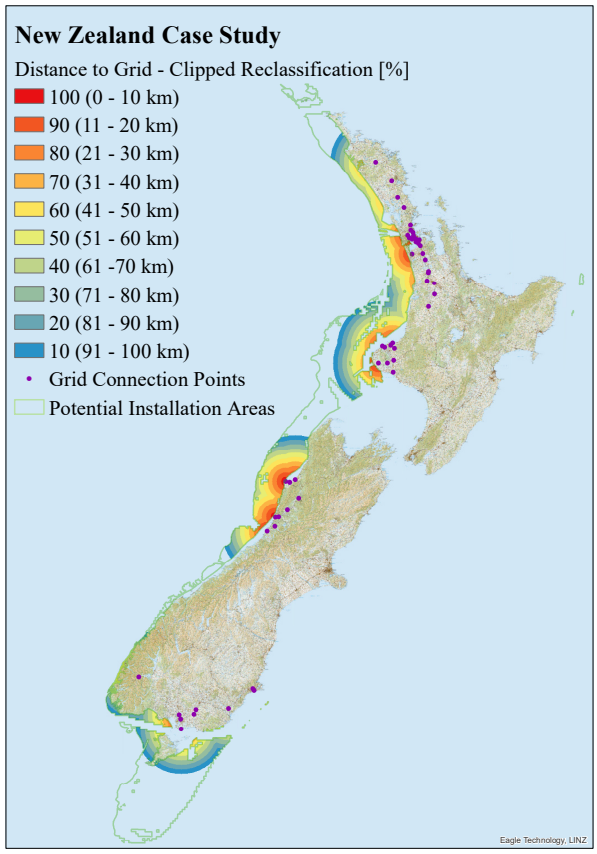

Figure 3.27. The reclassified and clipped Distance to Grid constraint.

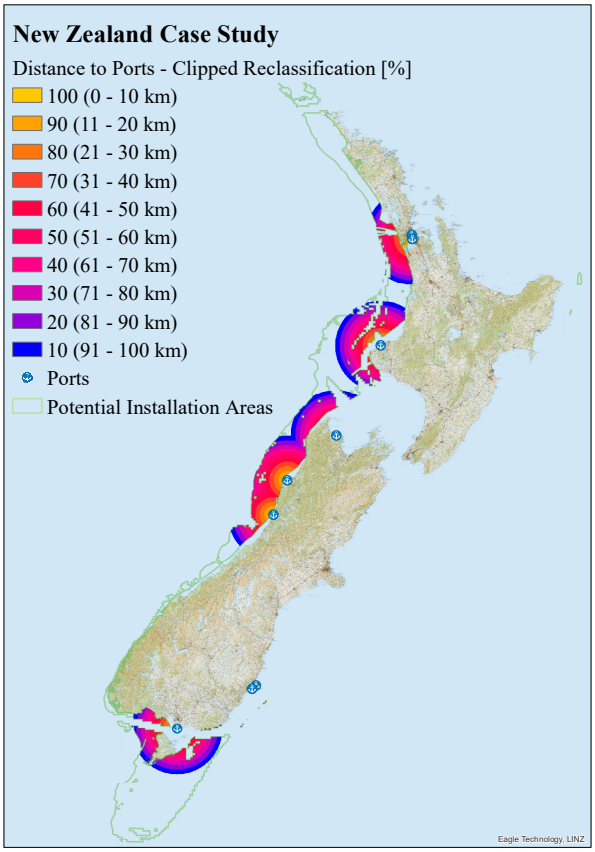

Figure 3.28. The reclassified and clipped Distance to Ports constraint.

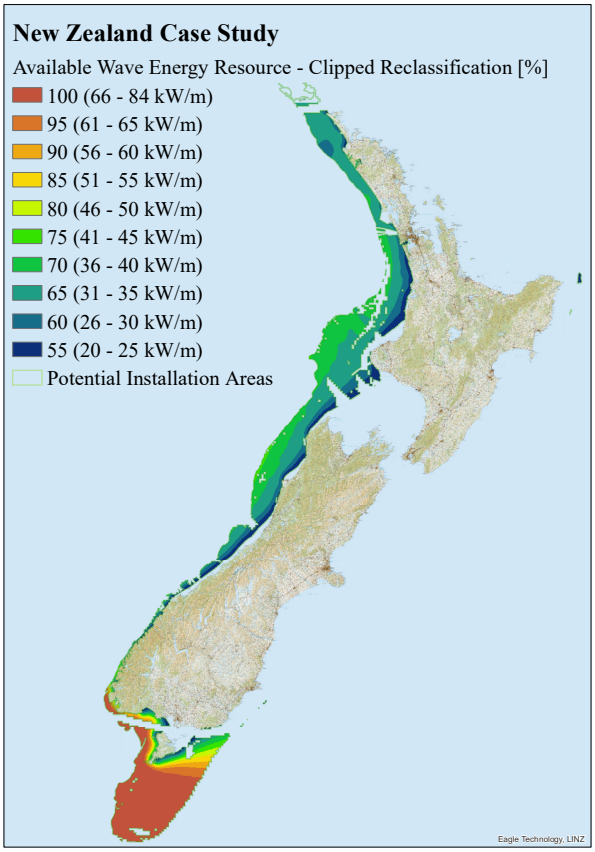

Figure 3.29. The reclassified and clipped Available Wave Energy Resource constraint.

Restriction. The Hauraki Gulf Marine Park, marine mammal sanctuaries, and NZ's submarine archaeology (shipwrecks) were identified as potential restrictions. However, as seen in Figure 3.30, the Hauraki Gulf Marine Park does not fall within the PIAs, and therefore, was not included in the suitability model.

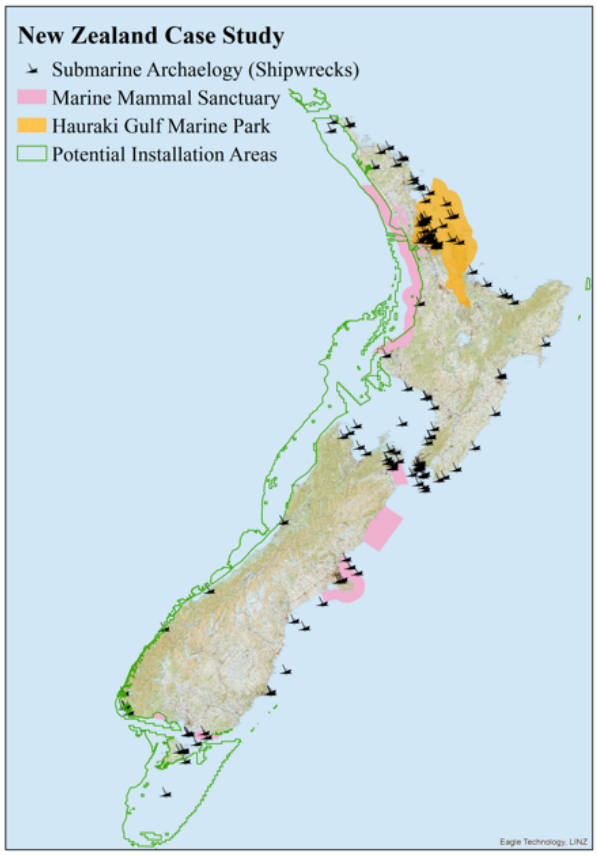

Figure 3.30. The social and environmental factors classified as potential restrictions.

The remaining marine mammal sanctuary and submarine archaeology vector layers had to be processed further to generate the restriction raster layers required for the SS equation.

Firstly, the marine mammal sanctuaries were clipped to the PIA layer (Figure 3.31(a)). The multiple features within this layer were then merged (using the 'Merge' function available from the Editor toolbar) to create a dataset containing only one feature. This polygon layer was converted to a raster, with a 1 km resolution, utilising the 'Feature to Raster' tool. As the suitability map would be contained within the PIA, the 'Is Null' function was used to identify cells within the Marine Mammal Sanctuary raster that contained no data within the PIA extent. Cells that contained no data were assigned a value of 1, whereas the cells that contained a sanctuary were assigned a value of 0. Thereafter, the 'Con' tool was used to change the value of 0 assigned to the sanctuary cells to a limiting value of 0.8 (as more detailed information was not available), resulting

in the clipped restriction raster to be utilised in the suitability model (Figure 3.31(b)). The value of 0.8 is representative of a 20 % reduction in the final SS values.

(a) (b)

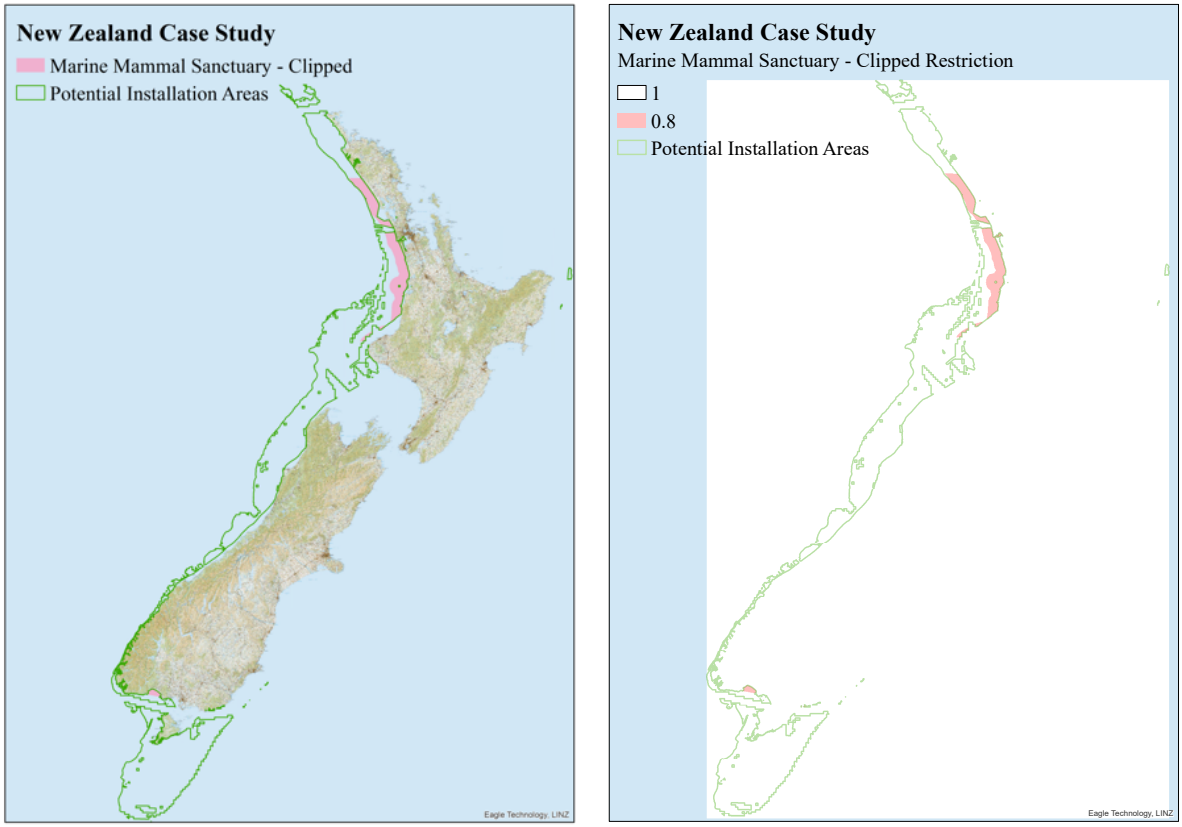

Figure 3.31. The (a) clipped Marine Mammal Sanctuary layer was further processed to generate the (b) raster restriction dataset.

In terms of the submarine archaeology, a new vector layer containing shipwrecks within 500 m of the PIA layer was generated. It was attempted to convert this polygon layer to a raster using the 'Feature to Raster' tool. However, as the resolution of the suitability map was 1 km, the polygon features contained within this layer did not convert to the corresponding raster cells. Therefore, the shipwrecks could not be analysed further in the suitability model.

To produce the final suitability map depicted in Figure 3.32, the SS model, Equation (3.1), was executed in two parts. The first part of the equation used the 'Weighted Overlay' tool to sum the weighted clipped and reclassified constraints, which generated a preliminary suitability raster layer. The second part of the equation then used the Raster Calculator to multiply the clipped Marine Mammal Sanctuary restriction, and the preliminary suitability raster, which resulted in the final suitability map (Figure 3.32) with SS values lowered accordingly in the restriction zones.

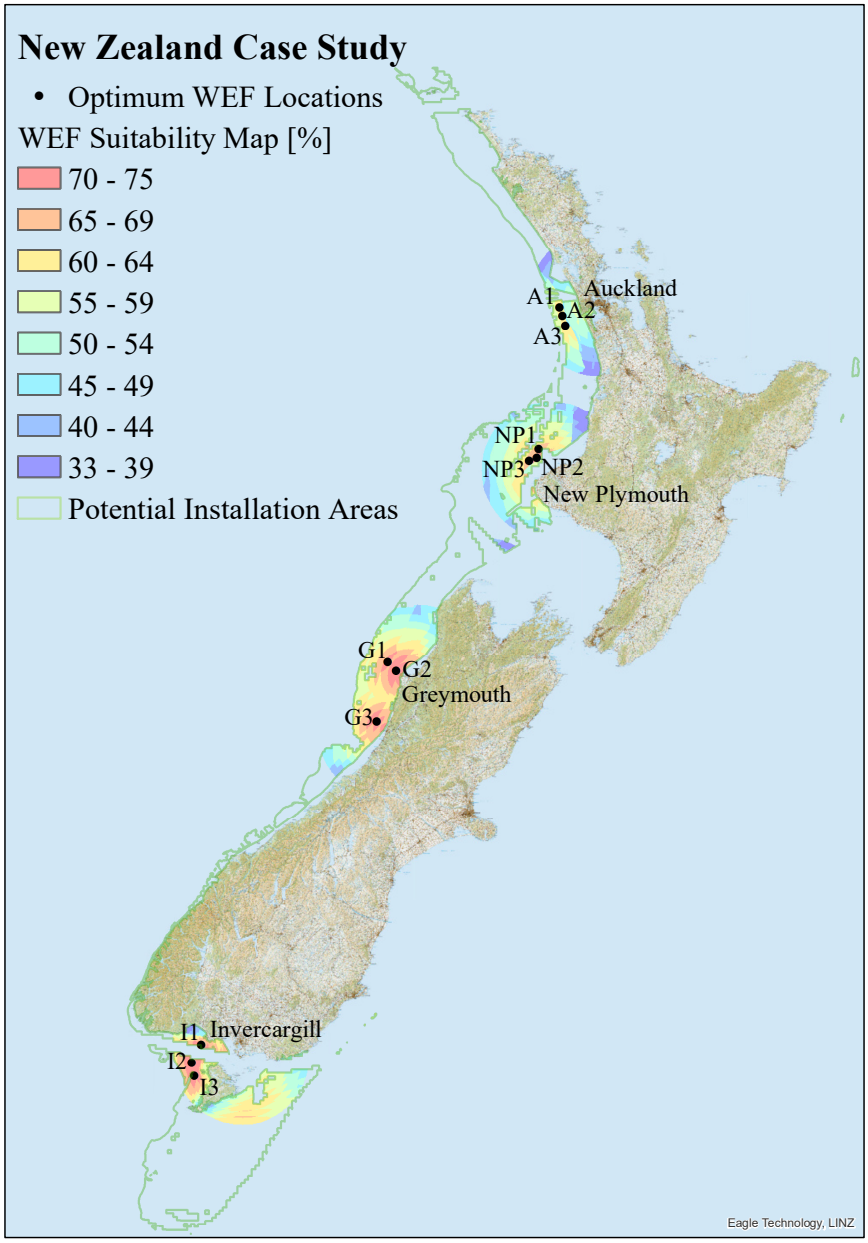

Figure 3.32. The final suitability map indicating the most optimal locations for WEFs in NZ are offshore Auckland, New Plymouth, Greymouth, and Invercargill.

These SS values were only calculated for areas that contained all three constraints. Therefore, PIAs surrounding Chatham Island were excluded from the suitability model as the relevant spatial datasets could not be acquired.

3.3.3 Stage 1.3: Scenario Analysis

To perform a Monte Carlo estimate of LCOE, the annualised cost estimate model (Equation (3.5)) was used and quantified with the relevant point values. As values pertaining to both a small and large commercial-scale WEF could be acquired (Table 3.5), it was determined that the three cost scenarios would be obtained for both projects.

Table 3.5. The mean value of each parameter associated with the first small (2,000 kW) and large (75,000) commercial-scale wave energy projects, adapted from [104]. These values, where relevant, where provided in United States Dollars (USD).

Parameter	2,000 kW Wave Energy Project	75,000 kW Wave Energy Project
WEF_C (kW)	2,000	75,000
CAPEX (USD/kW)	2,700	9,100
OPEX (USD/kWyear)	70	380
A_f	0.95	0.98
C_f	0.35	0

Before the simulation could be run, the relevant distribution parameters had to be obtained. As it was determined that the uncertainty associated with the CAPEX and OPEX values was described well by a normal distribution, the mean and standard deviation had to be specified for each of these model inputs.

Only the mean values (Table 3.5) were provided in the report produced by Chozas [104], and so, therefore, the standard deviation had to be determined somehow. The approach proposed by Hozo et al. [173] was identified as a potential method to calculate the standard deviation of the relevant model inputs.

$$\sigma \approx \begin{cases} \frac{1}{\sqrt{12}}\left[(z-y)^2 + \frac{(y-2m+z)^2}{4}\right]^{1/2} & N \leq 15 \\ \frac{z-y}{4} & 15 < N < 70 \\ \frac{z-y}{6} & N > 70 \end{cases} \tag{3.6}$$

where σ is the standard deviation, z and y refer to the maximum and minimum value in the dataset, respectively. Whilst m refers to the median of the dataset.

If the dataset contained less than 15 data points and was symmetric, then $y + z \approx 2m$ and Equation (3.6) could be simplified to:

$$\frac{1}{\sqrt{12}}\left[(z-y)^2 + \frac{(y-2m+z)^2}{4}\right]^{1/2} \approx \frac{(z-y)}{\sqrt{12}} \tag{3.7}$$

As stated previously, only the mean values could be obtained. However, according to Chozas, the range of cost uncertainty for the reported values was in the order of -30 % to +30 % [104]. Therefore, to generate the variables required for Equation (3.7), 30 % was added to and subtracted from the relevant mean values in Table 3.5 to determine the maximum and minimum values, respectively. Once these values were obtained, then the standard deviation could be calculated (Table 3.6).

Table 3.6. The input variables required for the small and large commercial-scale project.

Parameter	Minimum	Maximum	Mean	Standard Deviation
2,000 kW Wave Energy Project				
CAPEX (USD/kW)	1,890	3,510	2,700	468
CAPEX (USD)	3,780,000	7,020,000	5,400,000	935,307
CRF	0.117	0.117	0.117	
CAPEX (USD/year)	443,997	824,567	634,282	109,861
[i]Grid Connection (USD/year)	44,400	82,457	63,428	10,986
[ii]Installation (USD/year)	22,200	41,228	31,714	5,493
[iii]Other (USD/year)	377,398	700,882	539,140	93,382
OPEX (USD/kWyear)	49	91	70	12
OPEX (USD/year)	98,000	182,000	140,000	24,249
A_f	0.95	0.95	0.95	
C_f	0.35	0.35	0.35	
n (year)	20	20	20	
dr	0.10	0.10	0.10	
AEP (kW)	5,825,400	5,825,400	5,825,400	
75,000 kW Wave Energy Project				
CAPEX (USD/kW)	6,370	11,830	9,100	1,576
CAPEX (USD)	477,750,000	887,250,000	682,500,000	118,212,468
CRF	0.117	0.117	0.117	
CAPEX (USD/year)	56,116,336	104,216,052	80,166,194	13,885,192
[i]Grid Connection (USD/year)	5,611,634	10,421,605	8,016,619	1,388,519
[ii]Installation (USD/year)	2,805,817	5,210,803	4,008,310	694,260
[iii]Other (USD/year)	47,698,885	88,583,644	68,141,265	11,802,413
OPEX (USD/kWyear)	266	494	380	66
OPEX (USD/year)	19,950,000	37,050,000	28,500,000	4,936,345
A_f	0.98	0.98	0.98	
C_f	0.40	0.40	0.40	
n (year)	20	20	20	
dr	0.10	0.10	0.10	
AEP (kW)	257,544,000	257,544,000	257,544,000	

[i.] It is assumed that the grid connection cost accounts for 10 % of the overall CAPEX.
[ii.] It is assumed that the installation cost centre (in terms of the transportation sub-component) accounts for 5 % of the overall CAPEX.
[iii.] The other cost centre is comprised of all the CAPEX cost components, which were not relevant for determining the constraint weights. i.e. costs relating to the development of the project, device, as well as the moorings and foundations (Table 3.2). Therefore, it is assumed that these costs account for the remaining 85 % of the overall CAPEX.

The generated model inputs depicted in Table 3.6 were used to calculate a distribution of possible LCOE values by performing a Monte Carlo simulation. These estimated LCOE values were then used to determine the base case, worst case, and best case cost scenarios for the 2,000 kW and 75,000 kW projects by identifying the mean, maximum, and minimum LCOE values (and the corresponding CAPEX and OPEX) from the 500 trial runs (Table 3.7).

Table 3.7. Scenario Analysis for a small and large commercial-scale wave energy project.

Parameter	Base Case	Worst Case	Best Case
2,000 kW Wave Energy Project			
CAPEX (USD/kW)	2,812	4,295	1,076
CAPEX (USD)	5,624,494	8,590,315	2,151,065
CAPEX (USD/year)	660,651	1,009,015	252,663
Grid Connection (USD/year)	66,065	100,902	25,266
Installation (USD/year)	33,033	50,451	12,633
Other (USD/year)	561,553	857,663	214,764
OPEX (USD/kWyear)	58	73	65
OPEX (USD/year)	115,417	146,107	129,895
AEP (kW)	5,825,400	5,825,400	5,825,400
LCOE (USD/kWh)	0.13	0.20	0.07
75,000 kW Wave Energy Project			
CAPEX (USD/kW)	8,767	12,934	4,939
CAPEX (USD)	657,500,914	970,066,386	370,420,427
CAPEX (USD/year)	77,229,811	113,943,634	43,509,444
Grid Connection (USD/year)	7,722,981	11,394,363	4,350,944
Installation (USD/year)	3,861,491	5,697,182	2,175,472
Other (USD/year)	65,645,339	96,852,089	36,983,028
OPEX (USD/kWyear)	419	442	315
OPEX (USD/year)	31,461,972	33,118,733	23,601,808
AEP (kW)	257,544,000	257,544,000	257,544,000
LCOE (USD/kWh)	0.42	0.57	0.26

To establish the new constraint weights depicted in Table 3.8, the relevant CAPEX and OPEX costs for each cost scenario was used (Table 3.7). In the case of the Distance to Grid constraint, the new weight was determined to be the percentage contribution of the grid connection cost to the annualised cost of the project (for each of the cost scenarios), where the project cost was defined as:

$$Project\ Cost\ (USD/year) = CAPEX(USD/year) + OPEX\ (USD/year) \quad (3.8)$$

Whereas the new weights associated with Distance to Ports constraint were established as the percentage contribution of the combined installation and OPEX costs to the annualised project costs.

Table 3.8. The new weights assigned to each constraint based on the base case, worst case, and best case scenario analysis results.

Project Capacity (kW)	Constraint	Weight (%)		
		Base Case	**Worst Case**	**Best Case**
2,000	Distance to Grid	9	9	7
	Distance to Ports	19	17	37
	Available Resource	72	74	56
75,000	Distance to Grid	7	8	6
	Distance to Port	32	26	38
	Available Resource	60	66	55

The suitability model requires the weights of the constraints to total 100 %. Therefore, the Available Resource constraint weight for the three cost scenarios was calculated by subtracting the weight determined for the Distance to Grid and Distance to Ports constraints from 100 %.

The suitability model was then rerun for the three cost scenarios of both the small and large commercial-scale project, with the newly generated constraint weights shown in Table 3.8. This resulted in the suitability maps depicted in Figure 3.33 and Figure 3.34.

For comparison purposes, the optimal WEF locations identified in Stage 1.2 (depicted by black dots) were included in the newly generated suitability maps (Figure 3.33 and Figure 3.34). From a visual inspection of these maps, it can be clearly seen that the initial optimal wave energy project locations are closely aligned with the areas depicted as the most suitable for WEFs (across both projects and all cost scenarios).

As varying the constraint weights had a minor effect on determining optimal WEF locations, it was concluded that the suitability model developed in this thesis is a robust method for determining the most suitable areas for wave energy projects.

It should be noted that the initial weight of the constraints in the suitability model was not determined by using scenario analysis in conjunction with Monte Carlo simulation due to the high uncertainty associated with the reported values. However, once wave energy projects are more well-established, it is recommended that the constraint weights should be generated using this approach.

(a)

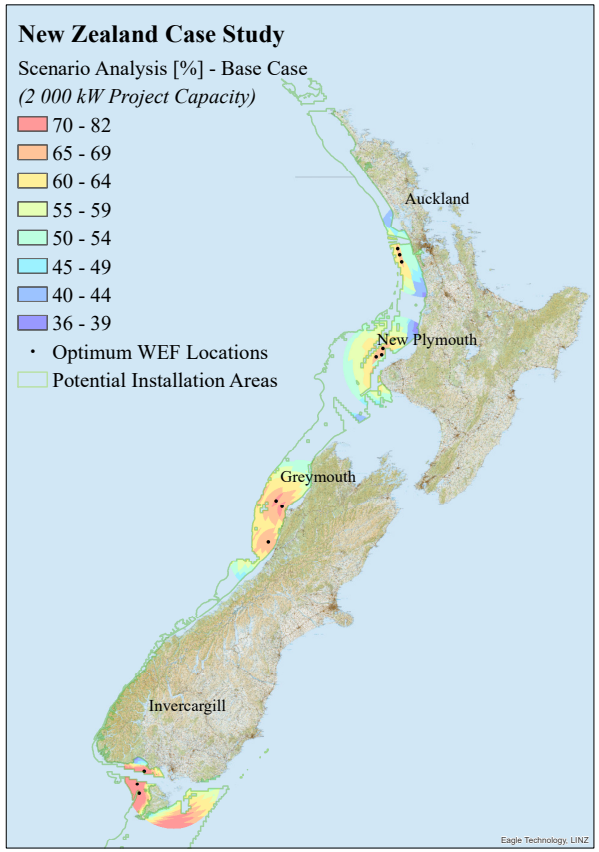

(b)

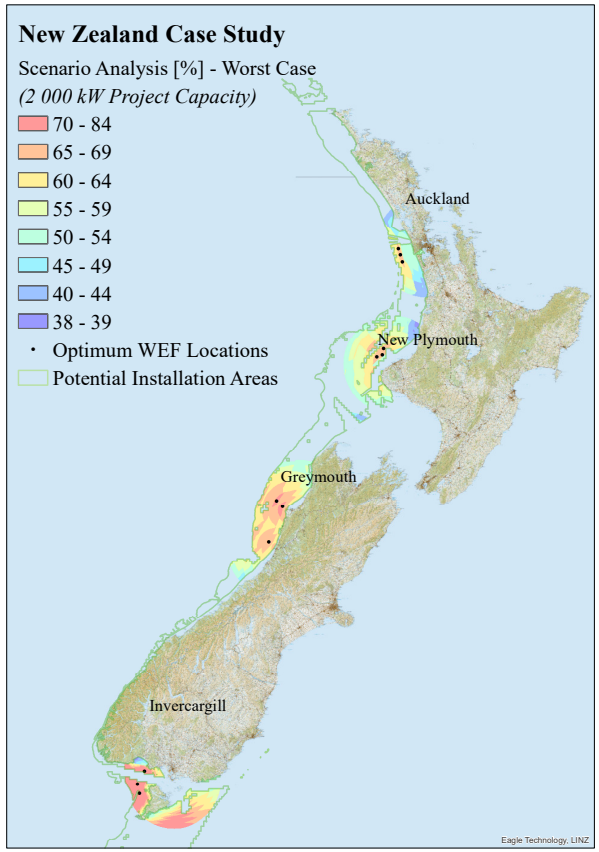

(c)

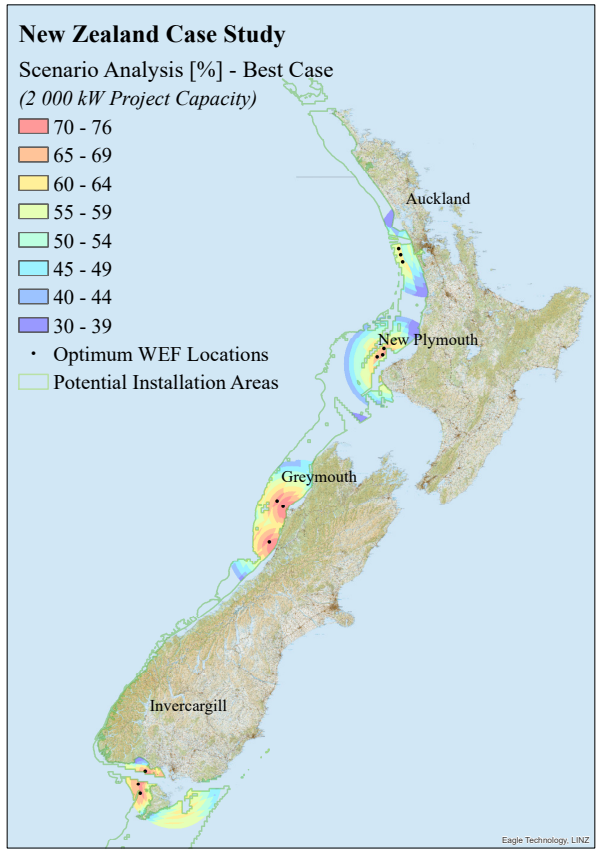

Figure 3.33. The scenario analysis conducted on the 2,000 kW project capacity, which modelled the: (a) base case scenario, (b) worst case scenario, and (3) best case scenario.

(a)

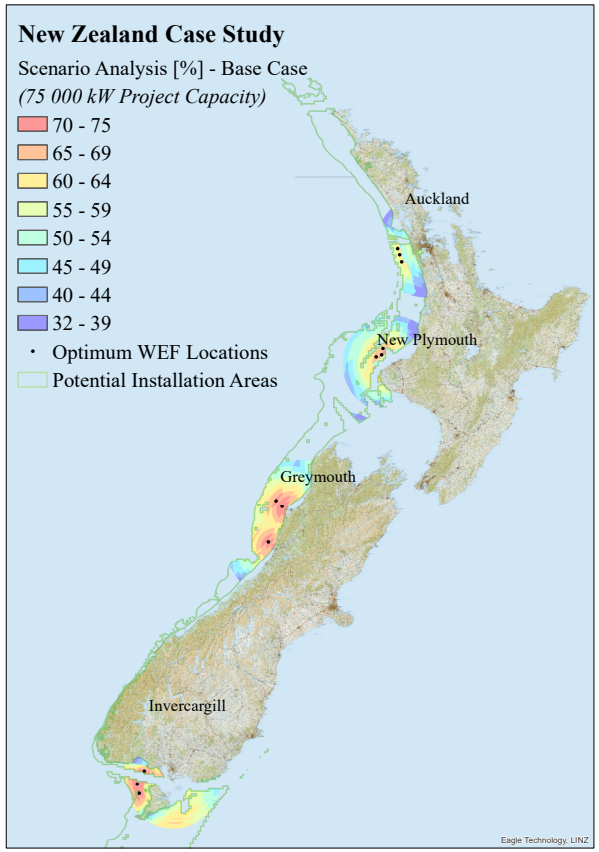

(b)

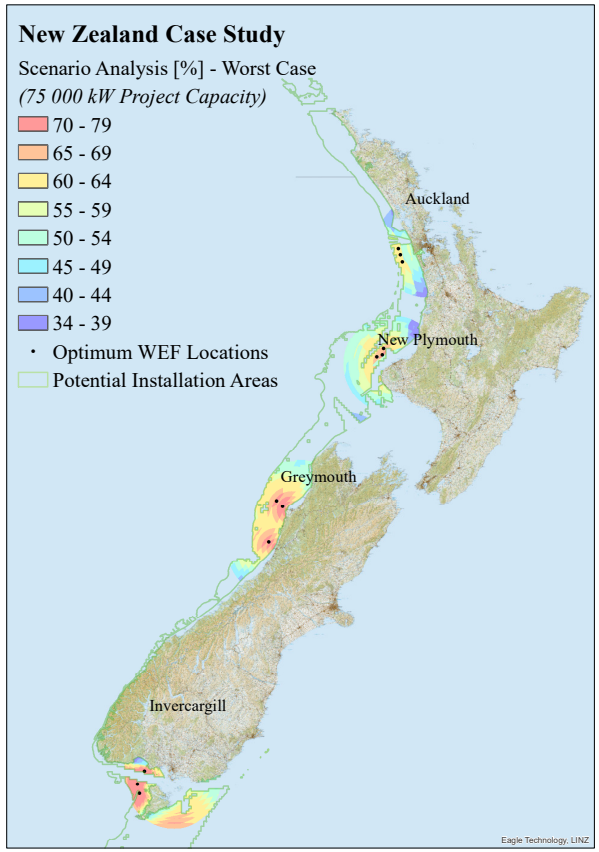

(c)

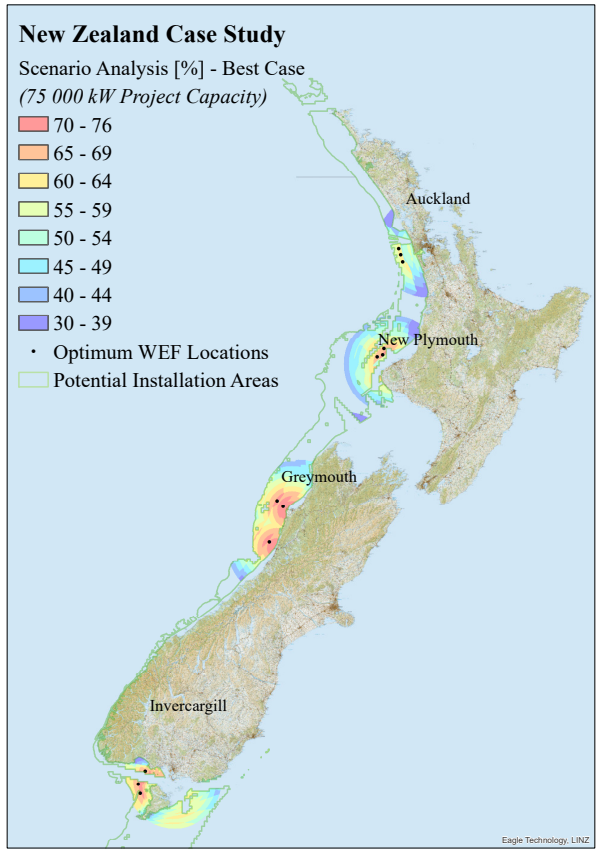

Figure 3.34. The scenario analysis conducted on the 75,000 kW project capacity, which modelled the: (a) base case scenario, (b) worst case scenario, and (3) best case scenario.

3.4 Conclusions

A site selection methodology has been developed and demonstrated in this chapter, which was applicable at any scale and applied to an NZ case study. This approach was comprised of three sub-stages, namely, Stage 1.1: Data Acquisition and Preparation, Stage 1.2: GIS Analysis, and Stage 1.3: Scenario Analysis.

The first sub-stage utilised five main dimensions, based on the pillars of sustainability, in order to determine the relevant site selection criteria. A new cultural dimension was also included to ensure that access to marine resources and ocean spaces were prioritised with respect to coastal indigenous communities. These criteria were then further classified as limiting conditions and exclusion or weighted factors. The corresponding geospatial datasets were then sourced in order to create a database. This aspect of the method was the most time-consuming, as it involved the implementation of a range of pre-processing procedures to ensure that the datasets were in a form that could be readily and accurately analysed.

The second sub-stage used the limiting conditions (based on the constraints on the current technology) to reduce the study area. Whereas the exclusion factors were eliminated from further analysis. A SS, which represented the spatial distribution of each area's suitability for a WEF, was then developed by combining the relevant weighted factors. Based on these analyses, 12 optimal WEF locations, clustered in four regions, were identified along NZ's west and south coast. Namely, offshore Auckland (North Island), New Plymouth (North Island), Greymouth (South Island), and Invercargill (South Island).

The last sub-stage developed an annualised cost assessment model that best captured the uncertainties with the suitability model established in the second sub-stage. The Monte Carlo approach was then utilised to identify the base case, worst case, and best case cost scenarios in order to produce new constraint weights. These new weights were used to generate a suitability map for each cost scenario. Based on these results, it was determined that the suitability model was a robust method for determining optimal WEF locations.

Chapter 4

Stage 2: Site Assessment

4.1 Introduction

In Chapter 3, a multi-dimensional methodology was proposed to identify suitable locations for WEFs in a socially responsible and sustainable manner. One of the critical dimensions of this approach was taking technical factors into consideration, such as the available wave resource. The resource is an essential criterion as only locations with an average wave power greater than 20 kW/m are considered feasible for WEF installations [55, 56].

As previously stated, the wave energy resource spatial dataset that was utilised in the site selection stage was received from MetOcean Solutions Ltd (personal communication, November 23, 2017). This dataset was comprised of mean wave power contour lines (in kW/m), which were interpolated from a ten-year numerical wave hindcast (1998–2007) that was developed specifically for NZ waters [114].

However, the potential electricity production from a specific site is not just a function of the available wave power. The steadiness of the supply (the variability of the resource at different timescales) and the composition of the resource in terms of its sea states (resource characterisation) are also essential technical parameters that influence the siting of a WEF [21, 71].

The aim of this chapter is, therefore, to develop an effective and efficient method for assessing the wave climate at the sites that have been identified as suitable for WEF installations. This will include developing a suite of tools in MATLAB that will quantify the amount of available resource as well as examine the temporal, directional, and spectral characteristics of the ocean waves at the potential deployment sites.

4.2 Methodology

The proposed approach is comprised of three sub-stages, Stage 2.1: Resource Quantification, Stage 2.2: Resource Variability, and Stage 2.3: Resource Characterisation. The first sub-stage computed the wave energy resource available at the area(s) of interest; for different timescales. The second sub-stage quantified the temporal and directional variability of the available resource at these locations, whilst the third and final sub-stage

decomposed and summarised the wave climate in terms of the frequency and intensity of the wave conditions that occurred at the potential WEF sites. This proposed methodology was applied to an NZ case study.

MATLAB 9.6.0.1072779 (R2019a) [174] was used to implement the proposed site assessment approach, as it has been designed specifically for engineers and scientists. It is a high-level programming language and interactive environment for developing algorithms, performing extensive data analysis and visualisation, as well as conducting numerical computations [175].

4.2.1 Data Sources

In order to effectively assess a potential WEF site, the wave climate needs to be determined, which is inferred from statistical wave data [83]. The three primary sources of wave data are: observed, measured, and modelled (hindcast) [58, 62].

Visual observations of the wave height, period, and direction is the simplest method to characterise waves [58]. These observations are typically from vessels participating in the Voluntary Observing Ship Programme [176]. The main limitations with regards to this type of data are that it is subject to fair weather bias (ships avoid bad weather) [62, 177], the lack of spatial coverage in the Southern Hemisphere (the major trade routes are located in the Northern Hemisphere) [176], and inaccurate observations [176] (visually observed wave periods are considerably less accurate than instrumentally measured wave periods [58]). Therefore, visual wave observations are generally not utilised in the determination of the wave climate [177]. However, it is very valuable for validating numerical models and calibrating remotely sensed data, especially in the open ocean [176, 177].

The two general methods for measuring ocean waves are in-situ and remote sensing systems, which are comprised of a variety of measurement instruments (Table 4.1). As there is no universal instrument suitable for measuring all wave parameters [58], the selection of the measurement system is dependent on the application for which the wave data is required [58], as well as other factors such as access, water depth, and the wave conditions at the measurement location [62].

Table 4.1: Accurate information regarding the wave climatology can be obtained by utilising a wide range of in situ and remote sensing measuring devices, adapted from [61].

Method	Instrument	Key Characteristics
In-situ	Seabed pressure sensor	Relatively cheap, limited to shallow water depths, deployed in an array, can give directional characteristics, also measures variation in water depth
	Acoustic Doppler current profiler	Relatively expensive, suitable for water depths up to 50 m, also measures marine currents, recovery required to extract data
	Surface-following buoy	Relatively expensive, accuracy well established, affected by currents, limited accuracy in steep waves, suitable for long-term deployment
Remote sensing	Radar (land-based)	Deployed on land away for aggressive environment, typically requires calibration for each site, often limited to wave height measurement
	Radar (satellite)	Large geographical coverage with low spatial and temporal resolution, typically limited to wave height measurement

For the wave energy sector, in-situ measurements are preferred (specifically obtained from surface-following buoys or acoustic Doppler current profilers [22]) as these systems provide the most accurate and detailed assessment of the wave climate [83]. However, these data are limited due to the expense and difficulties of maintaining offshore buoys and equipment over an extended period of time [83]. Furthermore, as a minimum of ten years of wave climate information is required to reliably assess the seasonal and inter-annual variation of the resource at a particular location, it is necessary to obtain wave data by utilising numerical modelling [22].

Numerical wave models are able to forecast, nowcast, and hindcast wave parameters by simulating the generation, propagation, and dissipation of ocean waves [178]. Wave nowcasts and forecasts predict wave conditions in real-time and in the future, respectively [68]. These data will be instrumental in integrating wave energy into the grid once the WEF is generating electricity, as it will allow the system operator to predict the energy supply and therefore calculate the reserve requirements [179].

Wave hindcasts compute past wave conditions based on historical meteorological data [83]. In terms of site assessment, this wave model is the most useful, as it generates long-term and uniformly distributed (in space and time) wave data, which is critical in quantifying the spatial and temporal variation of the wave climate at a potential WEF site [58]. However, to ensure the quality and accuracy of the hindcast data, it is calibrated as

well as validated against available in-situ measurements and/or satellite altimeter data [22, 58].

4.2.2 Stage 2.1: Resource Quantification

The first step in assessing the locations identified in Figure 3.32 was to quantify the available resource, thereby identifying the most attractive sites in terms of potential electricity production. In Section 2.4.1 the wave power flux was described by $P = Ec_g = \frac{1}{8}\rho g H^2 c_g$ (Equation (2.8)), where H referred to a single wave height. This equation calculates the wave power for monochromatic waves, whereas real seas are complex and contain a multitude of waves that are random in height, period, and direction [62] (Figure 4.1).

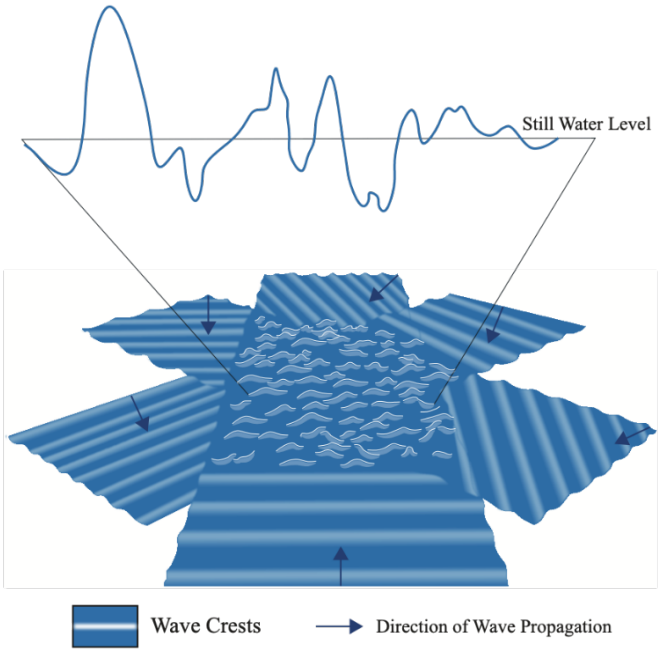

Figure 4.1. In contrast to a monochromatic wave propagating in a single direction, a real sea wave is comprised of several regular sinusoidal waves of varying frequencies and directions, adapted from [66].

However, the characteristics of real seas remain relatively constant for a short duration of time, thereby comprising a sea state that can be described by a wave spectrum [62]. The spectrum plots the wave energy (variance) as a function of frequency, as it is assumed that an irregular sea surface can be decomposed into multiple monochromatic waves of varying frequencies, heights, and directions by Fourier analysis (Figure 4.2) [58, 61].

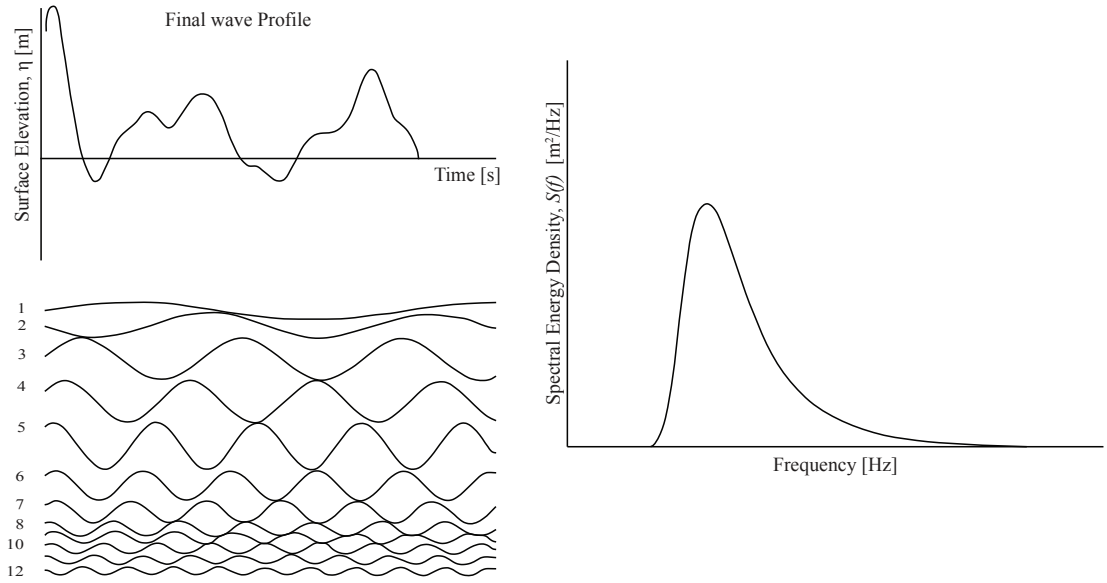

Figure 4.2. An ocean surface with a random appearance (top left) can be represented by a wave spectrum (right), which assumes that irregular waves can be described as a sum of a large number of regular sinusoidal waves (bottom left), adapted from [61].

Therefore, the omnidirectional wave power (per metre of wave crest) P_{wave} for a real sea wave, expressed in terms of the wave spectrum [180] is calculated as follows:

$$P_{wave} = \rho g \int_0^\infty S(f) c_g(f) df \tag{4.1}$$

where $S(f)$ is the wave-variance spectrum.

In deep water, the group celerity reduces to $c_g = \frac{g}{4\pi f}$ (Equation (2.2)), and as a result, Equation (4.1) can be rewritten in terms of the two parameters that are most widely used to characterise a sea state, H_{m0} and the energy period T_e [180]:

$$P_{wave} = \frac{\rho g^2}{64\pi} H_{m0}^2 T_e \tag{4.2}$$

where H_{m0} is an approximation of the average height of the highest one-third of waves that occur during a certain period of time, and is calculated from the moments of the measured spectra [180]:

$$H_{m0} = 4\sqrt{m_0} \tag{4.3}$$

and T_e is defined as being equivalent to the period of a regular sinusoidal wave, which has the same energy as the sea state being considered [181]. This summary statistic is calculated from the spectrum as follows [180]:

$$T_e = \frac{m_{-1}}{m_0} \tag{4.4}$$

where the m_{-1} and m_0 are spectral moments of the variance spectrum. This is defined as [180]:

$$m_n = \int_0^\infty f^n S(f) df \tag{4.5}$$

where m_n refers to the n'th spectral moment.

Once the wave power has been calculated, the total wave energy (per metre of wave crest), E_{wave}, over a given time period (from $t = t_1$ to $t = t_2$) can be computed by integrating the power with respect to time [182]:

$$E_{wave} = \int_{t1}^{t2} P_{wave}(t)\, dt \tag{4.6}$$

4.2.3 Stage 2.2: Resource Variability

The temporal and directional variability of the wave energy resource should also be considered, as it could potentially affect the performance of a WEC and so, therefore, the viability of a prospective wave energy project [61].

The available resource varies at all timescales, from wave to wave (in the order of seconds) to over periods of days, months, seasons and even years [62]. These variable wave conditions could significantly decrease the power generation of a WEF, as WECs tend to be tuned for maximum efficiency in a particular range of sea states [21, 61]. These devices operate optimally, with high efficiency, when the prevailing wave conditions remain consistent within this range [21, 61]. Therefore, locations with a fairly steady, moderate resource may be better suited for wave energy production than locations with a more energetic but unstable and, thus, less reliable resource [21].

In order to determine the magnitude of the wave power temporal variability, the indicators proposed by Cornett [21] were utilised: the Coefficient of Variation (COV), the Seasonal Variability index (SV), and the Monthly Variability index (MV).

COV estimates the magnitude of the inter-annual fluctuation [75] and is calculated as follows [21]:

$$COV = \frac{\sigma_{P_{wave}}}{\mu_{P_{wave}}} \tag{4.7}$$

where $\sigma_{P_{wave}}$ and $\mu_{P_{wave}}$ are defined as the standard deviation and the mean of the yearly average wave power, respectively.

SV describes the maximum range of seasonal mean wave power relative to the annual mean wave power [21]:

$$SV = \frac{P_{wave(S_{max})} - P_{wave(S_{min})}}{P_{wave(year)}} \tag{4.8}$$

where $P_{wave(S_{max})}$ is the average wave power for the most energetic season (usually winter), $P_{wave(S_{min})}$ is the average wave power for the least energetic season (usually summer), and $P_{wave(year)}$ refers to the yearly average wave power [21].

Similar to that of the SV parameter, MV is obtained by dividing the maximum range of monthly mean wave power by the annual mean wave power [21]:

$$MV = \frac{P_{wave(M_{max})} - P_{wave(M_{min})}}{P_{wave(year)}} \tag{4.9}$$

where $P_{wave(M_{max})}$ is the average wave power for the most energetic month, and $P_{wave(M_{min})}$ is the average wave power for the least energetic month.

If the COV, SV, and MV are equal to zero, this indicates that there is no inter-annual, seasonal, or monthly variability. Whereas values less than one signifies that the resource is only moderately unsteady at the various time scales, whilst values greater than one denotes considerable variability. Therefore relatively lower COV, SV, and MV values, in combination with a sufficiently energetic wave resource, indicates that a location is promising for stable wave energy production [97] [183].

The operational feasibility of a WEF can also critically depend on the directional distribution of wave power, as devices such as line absorbers (discussed further in Section 5.2.2) are required to be installed at a certain angle to the wave propagation direction [42]. Therefore, these devices cannot take advantage of all the incoming wave trains. If there is an increase in the resource directional variation, this will lead to a further reduction in the WEF power generation as the WECs will be even less optimally aligned [61]. Therefore, in order to examine the wave power directional variability and thus determine

the prevailing wave direction and optimal alignment for a WEF, wave power roses should be developed [183].

A wave power rose is a polar bar chart, which graphically displays the direction and distribution of the wave power at a particular site for a specific timescale. It is typically comprised of 8, 16 or 32 radiating spokes. Each spoke represents the relative frequency of occurrence of wave power: within a pre-defined P_{wave} range (depicted by colour bands); and the direction from which the waves propagate (in terms of the cardinal and intermediate directions) [184].

4.2.4 Stage 2.3: Resource Characterisation

The resource quantification provided by parameters such as the mean P_{wave} and total E_{wave} is useful for identifying attractive locations for wave energy production [71, 75]. However, these parameters convey insufficient information to harness the resource, as the amount of energy that can be harvested from a location is dependent on the characteristics of the device being considered for deployment at that site. As each WEC has different efficiencies at various sea states and operational ranges that span specific intervals of wave heights and periods, the most suitable WEC for a specific location is a device that has maximum efficiency at the prevailing sea states [94, 185].

WECs do not operate in all sea states but instead cease to function when subjected to calm or extreme wave conditions [185]. A calm sea state is characterised by H_{m0} less than 0.5 m, and it is assumed that a device is unable to produce power when H_{m0} is below this value [181, 183].

In the case of extreme wave conditions, P_{wave} associated with the most energetic sea states can be more than one order of magnitude larger than the values of P_{wave} corresponding to the typical wave conditions [75]. Consequently, the productivity of WECs drastically decreases in these sea states [97, 181], as extreme wave conditions can result in poor performance, equipment damage, and significant downtime [72]. These extreme sea states occur very rarely and so, therefore, hardly contribute to the overall resource [182]. However, it is essential to take these energetic wave events into account when investigating the WEC's reliability and survivability [87].

As stated in the literature review (Section 2.4.2), a wide variety of approaches have been proposed to define the threshold variable and value(s) for the extreme sea states. In this thesis, Morim et al.'s [80] method was utilised, which assumed that WECs only operate

within the range of sea states specified on its corresponding power matrix, and consequently, sea states larger than the maximum specified H_{m0} were considered extreme events. Therefore, as a first approach, wave conditions with H_{m0} larger than 8 m were considered extreme sea states. The value of 8 m corresponds to the upper limit of the Wave Dragon's H_{m0} operating range. This WEC was selected as a reference device as it is actively being developed (Table 5.2), its power matrix is publicly available, and it has been extensively analysed in the literature (Section 2.5).

To match, or tune, a WEC to a potential WEF site, it is, therefore, necessary to characterise the local resource in terms of the individual sea states that provide the P_{wave} [57]; H_{m0} and T_e (Equation (4.2)). This is accomplished by generating a resource-characterisation matrix [67], which is also commonly referred to as a scatter diagram in the wave energy industry [22, 61, 178].

A resource-characterisation matrix is a bivariate distribution, which plots H_{m0} against T_e in tabular form. Each cell (bin) in the table represents the relative frequency of occurrence of a particular sea state [22], with bin dimensions no larger than 0.5 m for H_{m0} and 1.0 s for T_e [186]. The table should also cover the complete range of H_{m0} and T_e values that occur at the site being analysed [178].

4.3 New Zealand Case Study

4.3.1 Data Sources

There are two primary sources of long-term wave data widely available in NZ, both of which simulated wave parameters by utilising the SWAN (Simulating WAves Nearshore) wave model. The first is a 38-year hindcast (1979–2016) generated by MetOcean Solutions (personal communication, June 5, 2019). The wave parameters generated by this model are limited to peak period T_p, peak wave direction θ_p, and H_{m0}, which are at a spatial and temporal resolution of 0.05°x 0.05° and 3 h, respectively [187]. These historical datasets are requested, for specific locations, directly from MetOcean Solutions and are provided at no charge for PhD research purposes. Furthermore, MetOcean Solutions provides access to site-specific hindcast statistics through their interactive MetOceanView platform [188]. However, on this platform, the three wave parameters are limited to frequency of occurrence charts/tables for either a typical year or a typical month of a year for a single location, and no time series data are available for export.

The second data source is the recently published interactive NZ Wave Data Tool developed by Albuquerque et al. [189]. This tool is a 20-year hindcast model (1993–2012) that also generated a range of 3-hourly wave parameters but at a slightly lower spatial resolution of 9 km (~0.09°).

In comparison to MetOcean Solutions, the NZ Wave Data Tool allows the user more flexibility. Firstly, the user has a more extensive range of wave parameters to select from, such as (but not limited to): H_{m0}, mean wave direction θ_m, θ_p, the mean wave periods T_{m01} and T_{m02}, T_e, T_p, and λ. Both T_e and λ, which are not available from the MetOcean Solutions hindcast, are essential for assessing potential WEF sites. λ is required to determine if the region of interest is located in deep water (Figure 2.6) and T_e is fundamental in calculating the available P_{wave} at a deep-water site (Equation (4.2)). Secondly, the user has the option to select multiple (neighbouring) sites at the same time, and lastly, the user is also able to select the time range of the time series data to the closest 3-h interval (within the time span of the hindcast).

Therefore, the wave variables obtained from the NZ Wave Data Tool were utilised to conduct the site assessment even though it was a shorter hindcast and at a slightly lower spatial resolution than the hindcast produced by MetOcean Solutions.

4.3.2 Model Validation

As hindcast data from the NZ Wave Data Tool was utilised to assess the 12 sites identified in Stage 1.2, it was necessary to validate the model in order to provide confidence in its performance as well as determine if the model under or overestimates the wave resource [57, 190]. Validation of the model is dependent on the availability of suitable measurements, preferably from the area of interest [57]. However, this is not essential, as if a model performs well in one location, this can provide confidence in the performance of the model in a different location [57]. As it is also necessary to verify the variability of the wave climate, at least one year of in-situ measurements was required to validate the hindcast [57].

Validation Metrics

Although no single set of statistics can quantify the performance of a model perfectly [191], the bias, Root-Mean-Square Error (RMSE), Scatter Index (SI), and Pearson correlation coefficient (r) are the most commonly used indicators to determine how accurately a model has simulated reality [57, 190].

Bias. The bias (also referred to as mean error) describes the overall direction of the model's error; the hindcast's tendency to under or overpredict the wave parameters [57]:

$$Bias = \frac{1}{N}\sum_{i=1}^{N}(x_{o_i} - x_{m_i}) \tag{4.10}$$

where N, x_{o_i}, and x_{m_i} refer to the number of data points, the observed (wave buoy) measurements, and the modelled (hindcast) data for the same location and time interval. Negative values indicate underestimation, positive values indicate overestimation, and bias values approaching zero signify good model performance [190].

Root-Mean-Square Error. RMSE quantifies the magnitude of the average error associated with the model, in the units of the variable being considered [192], and is determined by [57]:

$$RMSE = \sqrt{\frac{1}{N}\sum_{i=1}^{N}\left(x_{m_i} - x_{o_i}\right)^2} \tag{4.11}$$

where an RMSE value approaching zero demonstrates good agreement between the observed and modelled values [190].

Scatter Index. As RMSE is scale-dependent, it cannot be used to make comparisons between variables of different units [57]. Therefore, the RMSE was normalised by the mean of the measured values to produce a nondimensional indicator SI:

$$SI = \frac{RMSE}{\bar{x}_o} \tag{4.12}$$

where $\bar{x}_o$ is the average of the observed measurements, calculated as follows:

$$\bar{x}_o = \frac{1}{N}\sum_{i=1}^{N}(x_{o_i}) \tag{4.13}$$

SI values closer to zero indicate good performance [190].

Pearson correlation coefficient. The Pearson correlation coefficient is a measure of the strength and direction of the linear relationship between the modelled and observed values, and is defined as [57]:

$$r = \frac{\sum_{i=1}^{N}\left(x_{o_i} - \bar{x}_o\right)\left(x_{m_i} - \bar{x}_m\right)}{\sqrt{\sum_{i=1}^{N}\left(x_{o_i} - \bar{x}_o\right)^2\left(x_{m_i} - \bar{x}_m\right)^2}} \tag{4.14}$$

where $\bar{x}_m$ is the average of the modelled data, calculated as follows:

$$\bar{x}_m = \frac{1}{N}\sum_{i=1}^{N}(x_{m_i}) \tag{4.15}$$

An *r* value that is equal to one indicates a perfect positive linear relationship (the values of both variables increase or decrease concurrently with the same magnitude), whilst *r* equal to negative one signifies a perfect negative linear relationship (as the value of one variable increases, the value of the other variable decreases with the same magnitude). Lastly, *r* equal to zero indicates a completely random simulated value [57]. As *r* is a measure of correlation, not the accuracy of the model, an additional parameter was utilised, namely the Willmott index of agreement.

Willmott Index of Agreement (IoA[8]). IoA demonstrates the degree to which the observed value is accurately simulated by the model [192]:

$$IoA = 1 - \left[\frac{\sum_{i=1}^{N}\left(x_{m_i} - x_{o_i}\right)^2}{\sum_{i=1}^{N}\left(|x_{m_i} - \bar{x}_o| + |x_{o_i} - \bar{x}_o|\right)^2}\right] \tag{4.16}$$

where IoA equal to one indicates perfect agreement between the observed and modelled values, whilst a value of zero indicates no agreement at all [192].

As SI, *r*, and IoA are unit free; these indicators were used to compare performances between variables with different units.

In-situ Measurements

In-situ measurements are not readily available in NZ. However, it was possible to obtain wave buoy data for Manu Bay (Tonkin & Taylor, personal communication, April 8, 2020), Kaikoura (North Canterbury Transport Infrastructure Recovery Alliance, personal communication, April 8, 2020), and Banks Peninsula (Environment Canterbury, personal communication, April 9, 2020). As seen by Figure 4.3, the wave buoy moored at Manu Bay would have been ideal for validating the model as it is located near two regions identified as optimal for WEFs. However, the data available from this wave buoy were

[8] It should be noted that the Willmott Index of Agreement is typically denoted by the letter *d*. However, in this thesis, *d* is the notation utilised for depth. Hence, the use of *IoA* instead.

limited to only three weeks, and it was not within the same time span as the hindcast. A similar issue occurred with the measurements available from Kaikoura.

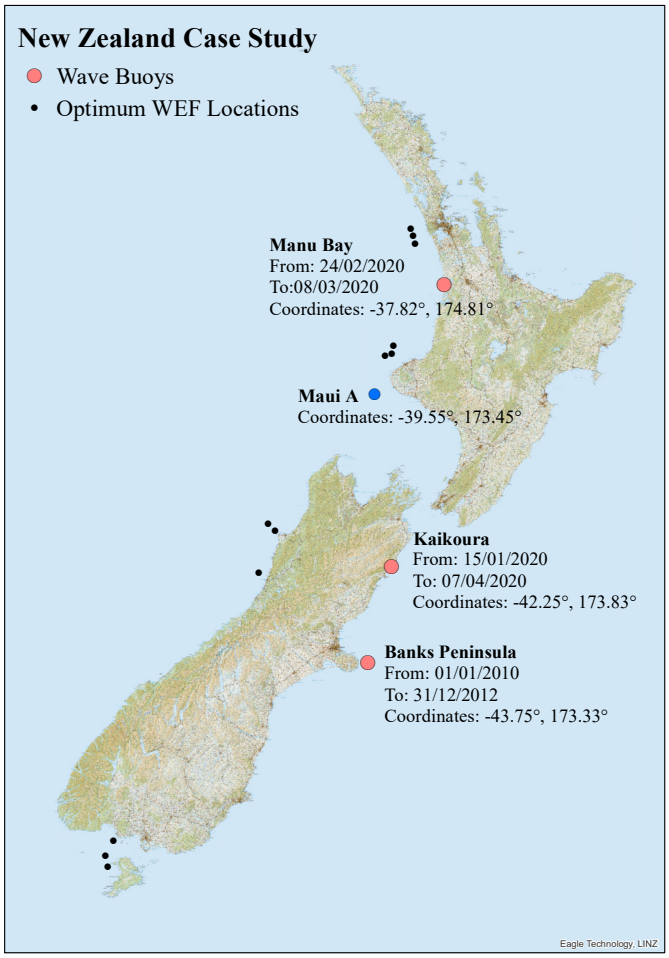

Figure 4.3. The locations of the wave buoys considered for validating the wave hindcast (represented by salmon coloured dots), as well as the location of the wave buoy that was used in the Chiswell & Kibblewhite [193] study (represented by the blue dot).

In the case of the wave buoy moored approximately 17 km off the coast of Banks Peninsula, in a water depth of 76 m, 36 months of wave data could be obtained within the time span of the NZ Wave Data Tool. Therefore, although not ideally located for the purpose of this study, wave parameters obtained from this buoy were utilised to validate the performance of the hindcast.

The validation was performed from 1 January 2010 to 31 December 2012 against 30-minute wave buoy time series for H_{m0}, T_{m02}, and θ_m. As a non-linear relationship exists between H_{m0} and P_{wave}, small errors in the modelled H_{m0} values may result in an inaccurate assessment of the average P_{wave} [194]. Therefore, to further validate the performance of the NZ Wave Data Tool, P_{wave} was calculated for both the model and wave buoy.

The P_{wave} associated with the measured and modelled primary wave parameters were also compared in order to determine if the model under or overestimates the available wave resource. As λ was not one of the wave parameters obtained from the wave buoy, the type of waves occurring at this location could not be defined (i.e., deep-, intermediate-, or shallow-water waves). However, NIWA utilises the measurements from this wave buoy to validate their Canterbury wave model for deep-water wave conditions [195]. Therefore, it was assumed to be a deep-water site, and hence Equation (4.2) was used to determine P_{wave} for both the measured and simulated data.

In order to calculate P_{wave} for a deep-water site, the wave parameters H_{m0} and T_e are required. However, it a widely known issue that T_e is rarely specified [92, 196], as was the case for the data obtained from all three wave buoys. The author believes that this is to do with the disconnect between the different disciplines which operate within the marine sector, as ocean modellers are not aware of the importance of this parameter to the wave energy industry.

Therefore, in order to determine T_e, a fixed conversion factor α can be employed, which is dependent on the theoretical spectral shape considered to be representative of the prevalent wave conditions at the area of interest [196]:

$$T_e = \alpha T_{m02} \tag{4.17}$$

The JONSWAP spectrum best describes the wave conditions in NZ (MetOcean Solutions, personal communication, May 24, 2019), and so, consequently, the theoretical value of α is further dependent on a peak enhancement factor γ [196]:

$$\alpha = \left(\frac{4.2 + \gamma}{5 + \gamma}\right)\left(\frac{11 + \gamma}{5 + \gamma}\right)^{\frac{1}{2}} \tag{4.18}$$

where Chiswell & Kibblewhite [193] determined that γ for a location along the west coast of NZ (Maui A, depicted in Figure 4.3) was best represented by a value of 1.55, thereby resulting in $\alpha = 1.215$. However, Cahill & Lewis [196] showed that the theoretical value of α can vary significantly from that determined from real seas, depending on the geographical region and the prevailing wave climate.

As the Maui A site is along North Island's west coast and the Banks Peninsula wave buoy is along South Island's east coast, it was determined that if the numerical model

performed well, that α would be calculated directly from the NZ Wave Data Tool, as T_e can be obtained from the hindcast [196]:

$$\alpha = \frac{1}{N}\sum_{i=1}^{N}\frac{(T_e)_i}{(T_{m02})_i} \tag{4.19}$$

Results

Before evaluating the hindcast's performance, the wave buoy data required pre-processing. Firstly, the time series of the observed and simulated H_{m0} were plotted to visually observe the behaviour of the data. As seen in Figure 4.4(a), there was an initial phase difference between the two datasets, which was 13 h. However, this was not an issue, as the resource available at a location is dependent on H_{m0} and T_e (Equation (4.2)), and not the wave phase. Therefore, the wave buoy data were adjusted by shifting the time series by 13 h (Figure 4.4 (b)).

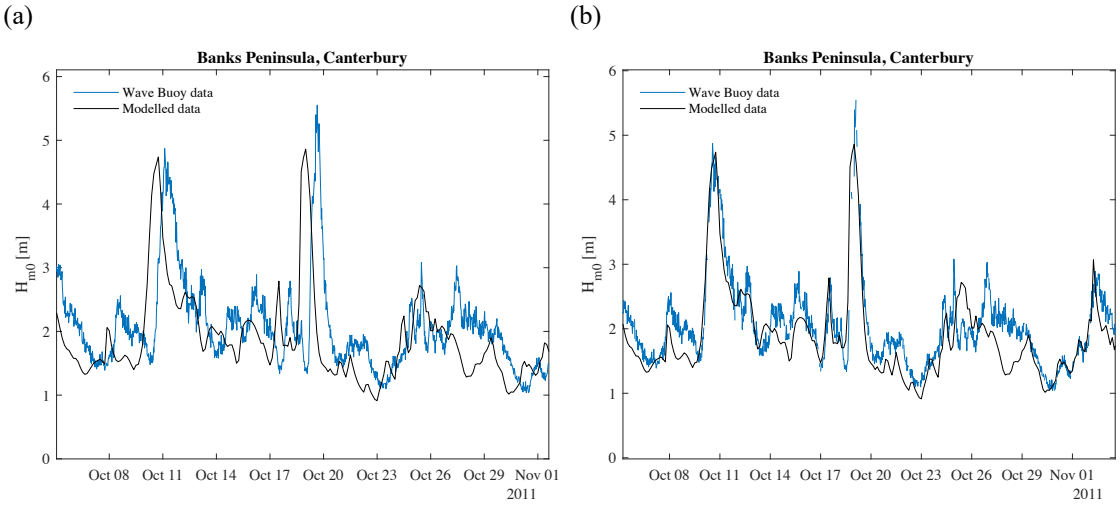

Figure 4.4. Time series plots of the observed and modelled H_{m0}, which illustrates the (a) initial 13 h phase difference between the datasets and (b) adjusted wave buoy measurements.

Secondly, in-situ datasets are often incomplete, which was the case with the measurements received from the Banks Peninsula wave buoy. Therefore, the missing data points had to be located, and corresponding timestamps, assigned NaN (Not a Number) values, created. (A NaN value is commonly used to define a missing data point in a time series.) This was required, because lastly, the wave buoy record was provided in 30-min intervals, as opposed to the hindcast data, which were in 3-h intervals. Therefore, to be able to compare the observed and modelled measurements, the wave buoy dataset was downsampled to 3-hourly intervals by averaging the relevant data points. The use of NaN values to define missing measurements ensured that the resampling of the wave buoy

parameters required all six relevant data points to contain numerical values in order to calculate the equivalent single 3-hour variable. For example, if any of the six values being resampled was a NaN value, then the corresponding 3-hour data point was not calculated, and the timestamp was removed from both the modelled and measured dataset. This ensured that the integrity of the observed dataset was preserved, especially in the case of extended gaps in the wave buoy record (i.e., when large waves interfered with the buoy or it was removed for maintenance).

Once the pre-processing of the wave buoy record was completed, the five statistical parameters discussed in the Validation Metrics section were computed to evaluate the performance of the model. The values are reported in Table 4.2, which indicated that the simulated measurements (H_{m0}, T_{m02}, and θ_m) were in good agreement with the observed measurements, as the SI values were fairly low (especially in the case of H_{m0} and T_{m02}) and the *r* and IoA values were sufficiently high.

Table 4.2. Comparison of wave parameters H_{m0}, T_{m02}, θ_m, and P_{wave} obtained from the Banks Peninsula wave buoy and the NZ Wave Data Tool hindcast.

Wave Parameters	Bias	RMSE	SI	r	IoA
H_{m0}	-0.07 m	0.38 m	0.18	0.90	0.95
T_{m02}	0.22 s	0.93 s	0.14	0.76	0.86
θ_m	-12.63 °	47.09 °	0.33	0.71	0.84
P_{wave}	-1.14 kW/m	23.34 kW/m	0.50	0.89	0.94

In order to compare the last parameter P_{wave}, α had to be ascertained. As the model performed well, it was opted to calculate α from the hindcast (Equation (4.19)) by utilising the relevant variables over the entire 20-year timespan. This resulted in α value of 1.29 (6% greater than the theoretical α), which had a standard deviation of 0.12 and a COV of only 0.09.

The value of P_{wave} was then calculated for both the hindcast and the wave buoy, which were compared by utilising the same five validation indicators (Table 4.2). As with the other three wave parameters, the high *r* and IoA values indicate good agreement between the numerical model and the wave buoy. The high SI value (0.5) was to be expected, since P_{wave} combines energy and frequency parameters; hence it is predicted with greater error.

These proposed validation metrics confirm that P_{wave} computed from the hindcast data is an accurate reflection of the measured wave resource. From this evaluation, it was also determined that the wave resource is predominantly underpredicted by 1.14 kW/m (Table

4.2). Therefore, it can be assumed that the wave energy resource estimated from the NZ Wave Data Tool wave parameters is conservative.

Furthermore, a time series of the observed and simulated wave parameters were plotted, which clearly shows that the model has captured the temporal variability of the wave climate (Figure 4.5).

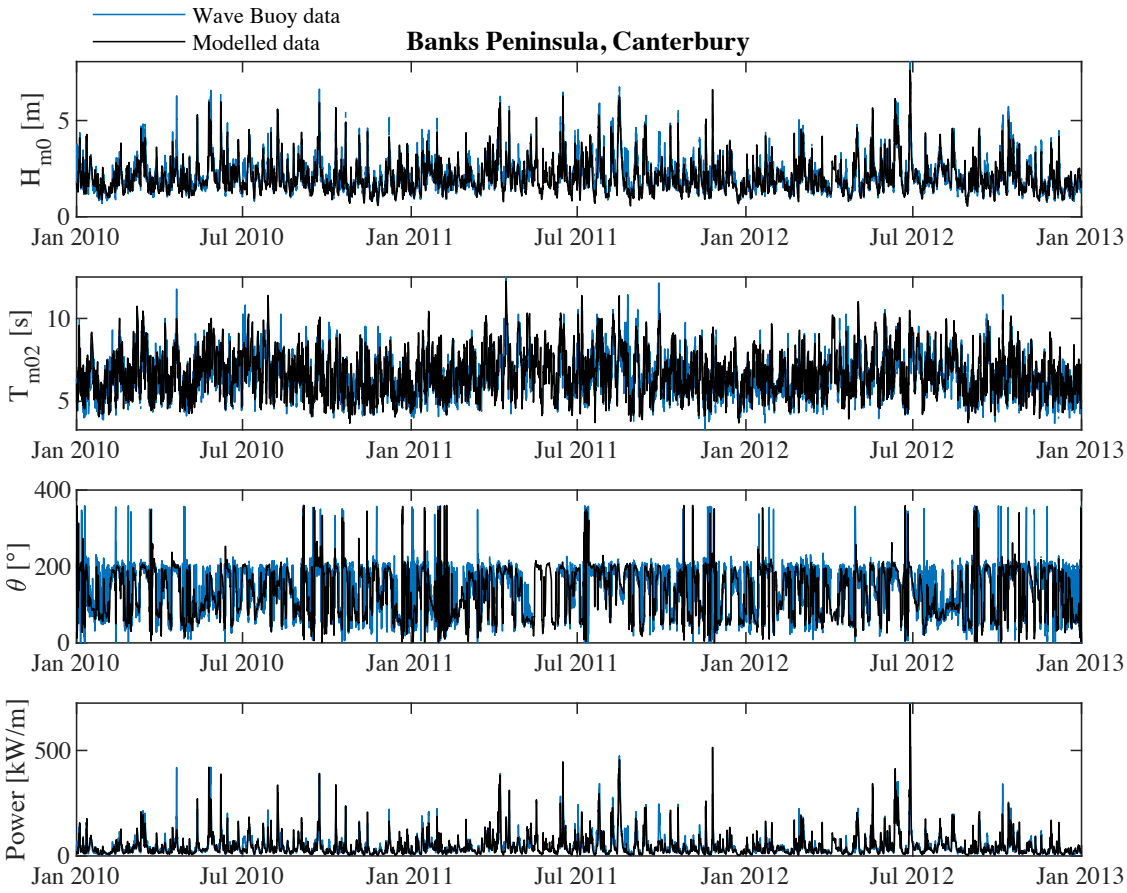

Figure 4.5. Time series plots of the observed and modelled H_{m0}, T_{m02}, θ_m, and P_{wave} wave parameters, from January 2010 to December 2012.

Whereas, the scatter plots show qualitatively that there is good agreement with H_{m0} (Figure 4.6(a)), T_{m02} (Figure 4.6(b)), and P_{wave} (Figure 4.6(d)) and more scatter in θ_m (Figure 4.6(c))—which is fairly typical in wave model simulations.

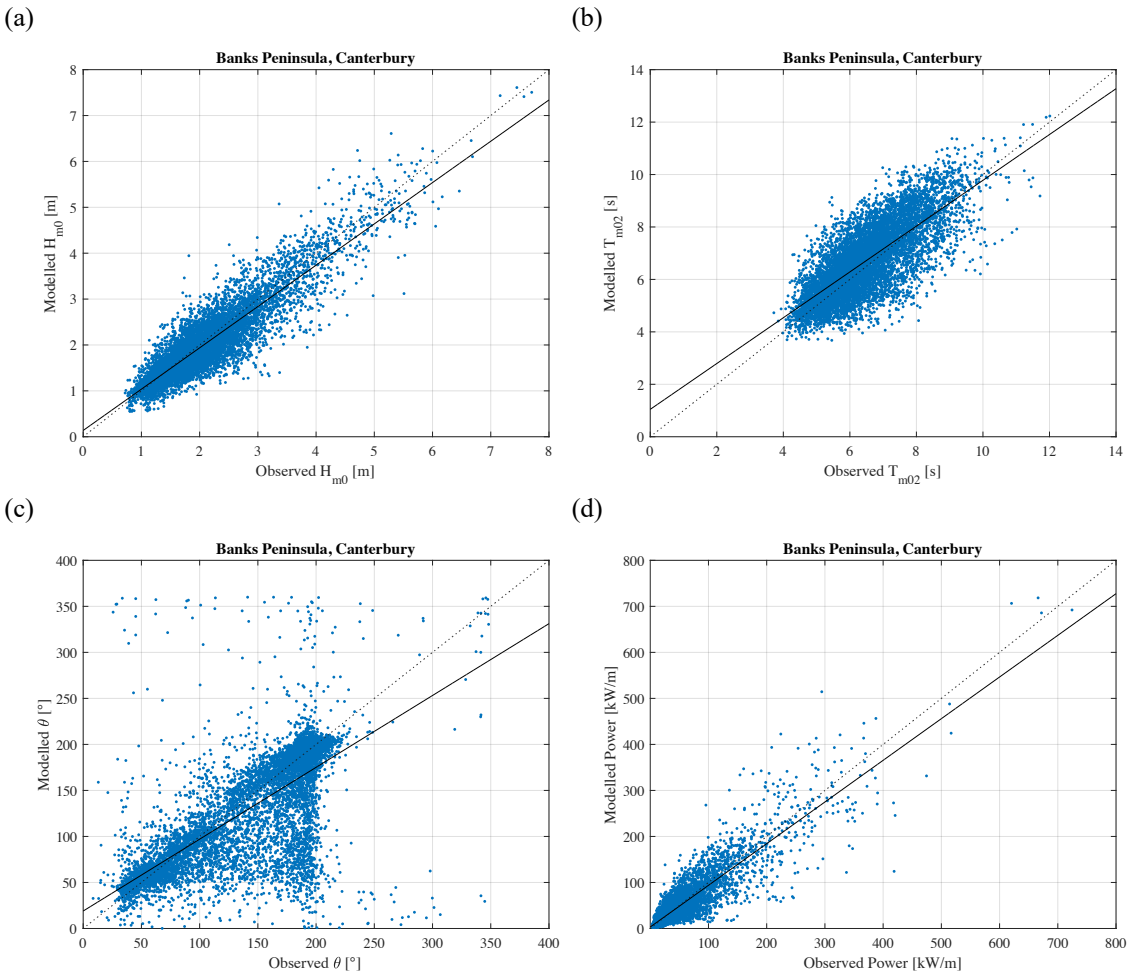

Figure 4.6. Correlation between the wave buoy (observed) data and the hindcast (modelled) data for (a) H_{m0}, (b) T_{m02}, (c) θ_m, and (d) P_{wave}. The line of best fit and the line of equality have been shown by solid and dashed lines, respectively.

From these analyses, the reliability of the NZ Wave Data Tool has been established, and therefore the parameters obtained from this hindcast were utilised in assessing the potential WEF sites.

The processing of the wave data and the evaluation of the performance of the NZ Wave Data Tool was undertaken in MATLAB, utilising the Main_WPR.m (Appendix A.1.1) and Main_Model_Validation_V1.m (Appendix A.1.2) scripts developed by the author.

4.3.3 Stage 2.1: Resource Quantification

The relevant details pertaining to the 12 sites identified as optimal WEF locations (Figure 3.32) are presented in Table 4.3. In order to quantify the available resource utilising the simplified power equation (Equation (4.2)), it had to be ascertained if the location being analysed was a deep-water site. As shown in Figure 2.6, a location is classified as a deep-water site, if d is greater or equal to half the λ measured at the region of interest. Therefore, a deep-water limit ($d_{critical}$) was established based on this definition:

$$d_{critical} = \frac{\lambda}{2} \tag{4.20}$$

where $d \geq d_{critical}$ denotes a deep-water site, and hence Equation (4.2) can be used to compute the theoretical P_{wave}.

Table 4.3. The coordinates, water depth, typical mean λ and $d_{critical}$ of each site considered suitable for the implementation of a WEF installation (Figure 3.32).

Site	Latitude [°]	Longitude [°]	d [m]	λ [m]	$d_{critical}$ [m]
Auckland 1 (A1)	-37.0	174.1	109.6	93.97	46.99
Auckland 2 (A2)	-37.1	174.2	90.6	93.08	46.54
Auckland 3 (A3)	-37.2	174.2	108.5	92.95	46.48
New Plymouth 1 (NP1)	-38.8	173.8	109.7	93.01	46.50
New Plymouth 2 (NP2)	-38.9	173.8	109.4	93.15	46.58
New Plymouth 3 (NP3)	-38.9	173.7	130.0	92.85	46.43
Greymouth 1 (G1)	-41.6	171.2	147.7	109.52	54.76
Greymouth 2 (G2)	-41.7	171.4	95.9	107.37	53.68
Greymouth 3 (G3)	-42.3	171.0	99.3	101.26	50.63
Invercargill 1 (I1)	-46.4	167.6	57.9	107.23	53.62
Invercargill 2 (I2)	-46.6	167.4	110.1	106.50	53.25
Invercargill 3 (I3)	-46.8	167.5	108.8	104.73	52.36

As seen in Table 4.3, d at each site is greater than $d_{critical}$, and so, therefore, P_{wave} at each of the proposed WEF locations was calculated utilising the deep-water equation.

The average available P_{wave} for each year, at each site, is depicted in Figure 4.7, where it is observed that the wave resource varied between locations (spatial variability). However, even though the available power differed from site to site, further inspection of the graph revealed that locations contained within a specific region of interest exhibited a similar trend. This similarity in trend is especially apparent for sites I1–I3 in the Invercargill region of interest.

The temporal variability of the wave resource is also clearly visible in Figure 4.7, as the wave resource varied from year to year at each of the locations. This inter-annual variation could be due to natural processes such as the El Niño-Southern Oscillation (ENSO) [197].

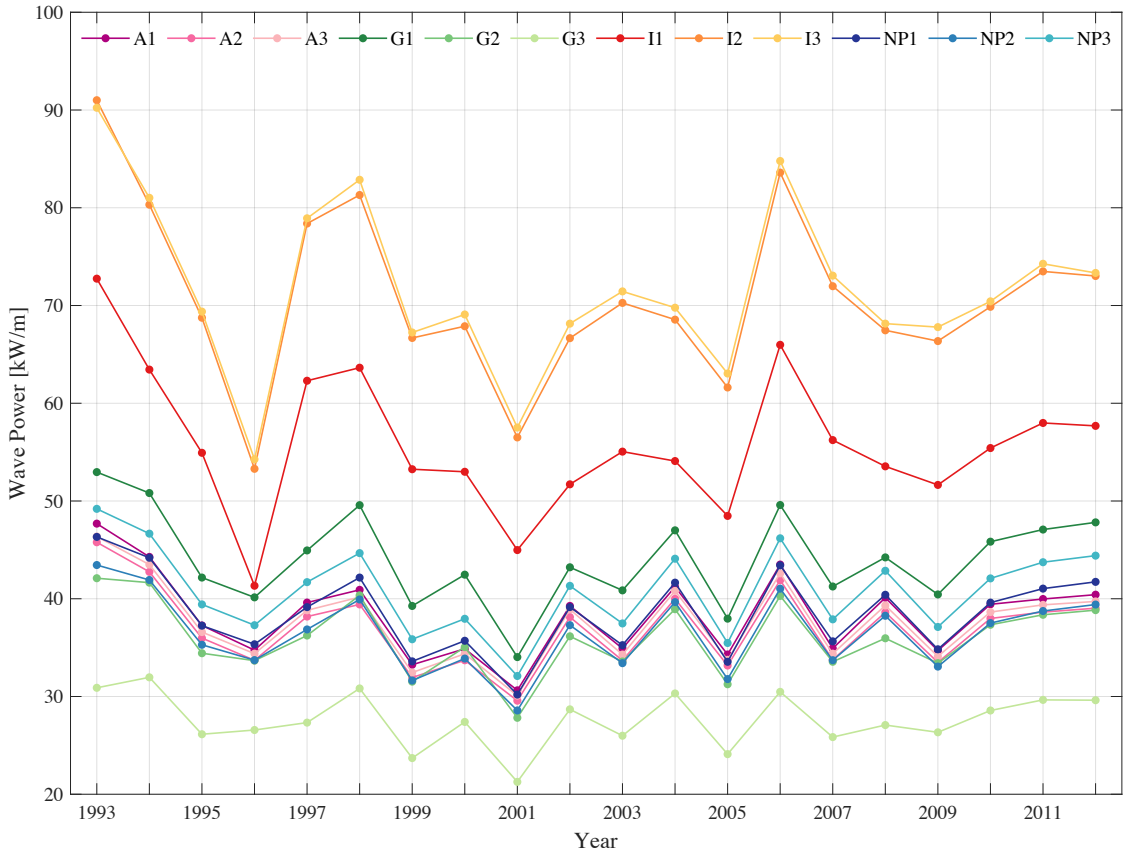

Figure 4.7. The inter-annual variation of the average yearly P_{wave} over a 20-year time horizon (January 1993–December 2012).

ENSO is a recurring global climate cycle that typically occurs every three to seven years for approximately 6–18 months. It involves the unusual warming (El Niño) and cooling (La Niña) of the equatorial water across the Pacific Ocean, coupled with atmospheric changes [198]. In NZ, La Niña events result in increasing wave heights off the northeast coast of North Island, whilst enhanced wave heights occur to the south and south-west of NZ during El Niño events [199]. This behaviour can be verified by comparing Figure 4.7 and Figure 4.8; as P_{wave} (the wave parameter depicted in Figure 4.7) is directly proportional to H_{m0}^2 (Equation (4.2)), it is considered to be representative of H_{m0}. It was observed that the available P_{wave} increased in all the years, which corresponded with El Niño events, with the exception of 2005. Closer examination of 2005 revealed that even though the largest El Niño event over the entire time horizon transpired in this year, this phase was limited to a single event, which occurred in what is typically considered a low energy month (February).

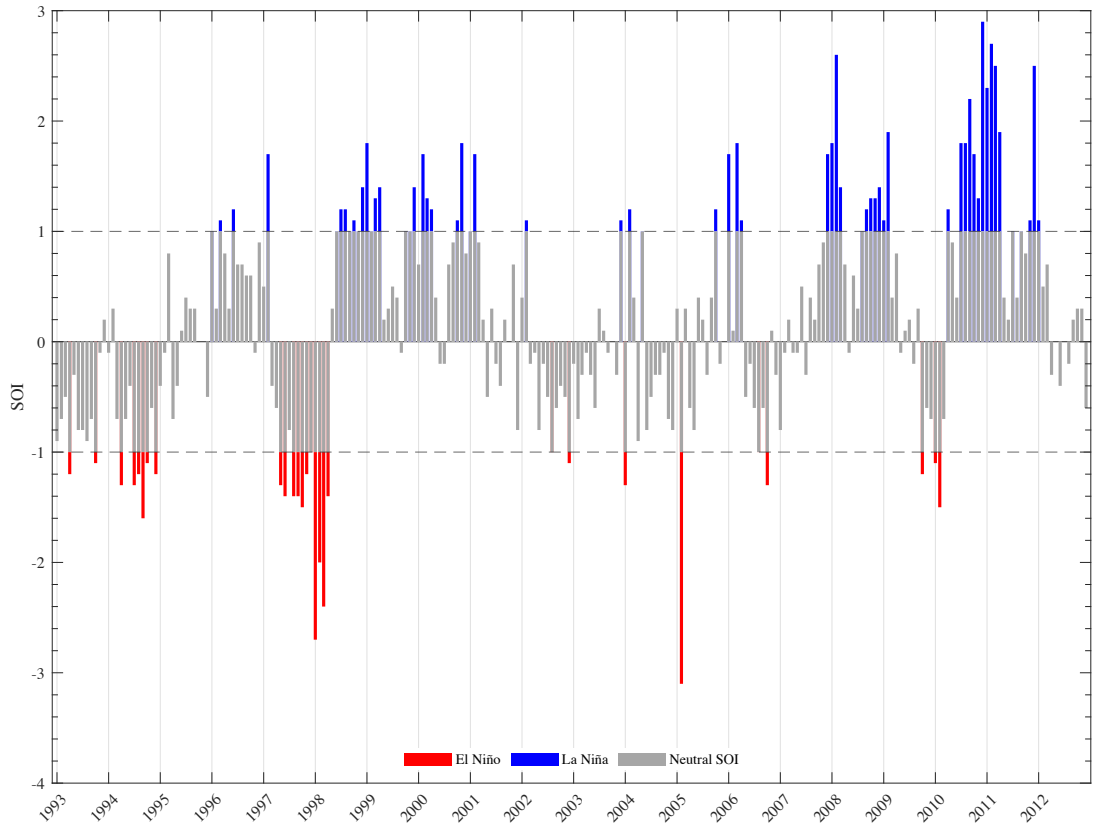

Figure 4.8. Time series of the Southern Oscillation Index (SOI) from January 1993 to December 2012. El Niño events correspond with SOI values below -1.0, and La Niña events correspond with SOI values above +1.0. (The data was obtained from NZ's Ministry for the Environment [200].)

Figure 4.9 (a) depicts the average P_{wave} available at each site for a typical year (where 'typical' is defined as the mean of the average P_{wave} available for a specific timescale—yearly, seasonal, monthly, daily—over the entire time interval being analysed). From this figure (and that of Figure 4.7), two main areas containing different wave energy distributions were clearly discernible. A higher-energy area comprising the south of NZ (sites I1–I3) with an annual average P_{wave} ranging from 55.9 (I1) to 71.7 kW/m (I3) and a yearly total wave energy ranging from 489.7 MWh/m to 628.8 MWh/m; and an intermediate-energy area along NZ's west coast (sites A1–A3, NP1–NP3, G1–G3) with an annual average P_{wave} ranging from 27.6 kW/m (G3) to 44.1 kW/m (G1) and a yearly total wave energy ranging from 242.3 MWh/m to 386.4 MWh/m.

These results correlate well with previous research conducted by Pickrill and Mitchell [201], Laing [202], Gorman et al. [199], and MetOcean Solutions [203]. These studies assessed the NZ wave climate by utilising wave data obtained from visual observations and in-situ (wave buoy) measurements [201], remote sensing (radar altimeters) measurements [202], as well as wave hindcasts [113, 199, 203]. Despite the use of

different wave data sources, each study established similar spatial distributions of $H_{m0,}$ where it was ascertained that the highest (and therefore most energetic) waves occurred along the south coast (due to exposure to the swell from the Southern Ocean [113]), followed by the west, east and north coasts, respectively (Appendix B). This is because the wave heights generally decreased from southwest to northeast as exposure to the Southern Ocean swell declined.

Figure 4.9 (a) also depicts the seasonal distribution of the average P_{wave} potential at all the locations, which behaved as expected; a maximum and minimum P_{wave} available in the winter (June, July, and August) and summer (December, January, and February) months, respectively. Across all the study sites, winter accounted for approximately 31% of the annual power, spring for 28 %, autumn for 25 %, whilst summer provided only about 16 % of the annual power output.

The typical monthly mean P_{wave} for each site is plotted in Figure 4.9(b), which shows that the annual minima generally occurs in December, January or February (corresponding to the least energetic season). Whilst the yearly maximum, however, occurs as bimodal maxima at all 12 sites, typically peaking in June (corresponding to the most energetic season) and then again in September (which explains the high contribution of spring to the annual P_{wave}). This behaviour was consistent with findings published by Gorman et al. [199] and Laing [202]. It should be noted that these findings were in terms of $H_{m0,}$ not P_{wave}. However, in cases where the values of power and/or energy are not presented, H_{m0} is considered representative of the wave resource.

(a)

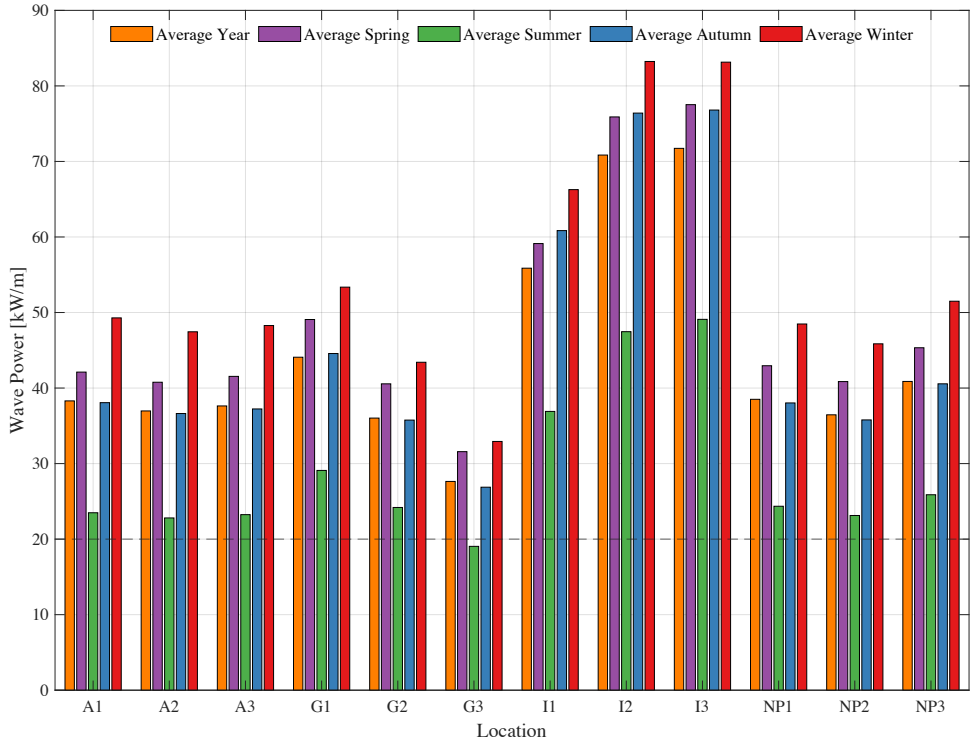

(b)

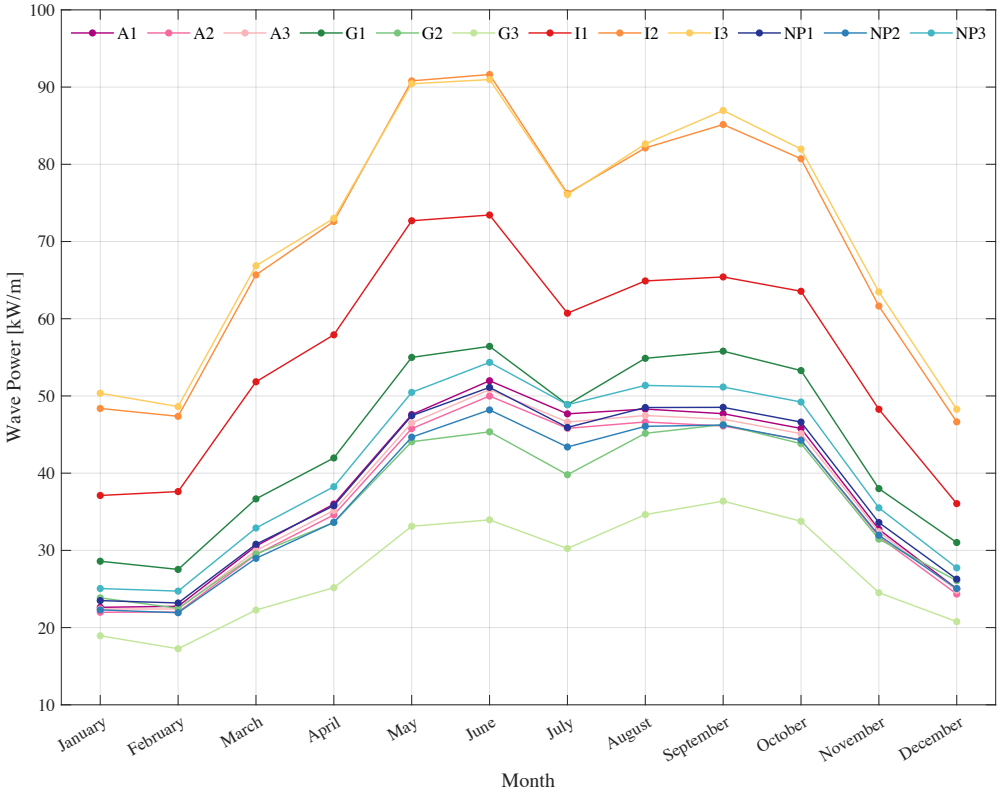

Figure 4.9. The intra-annual variation of the average yearly power over a 20-year time horizon (January 1993–December 2012) in terms of (a) typical yearly and seasonal wave power as well as (b) typical monthly power values.

The results relevant to this sub-stage were obtained from the Main_Wave_Power_V3.m (Appendix 0) and Main_Combine_Wave_Power_Sites_V2.m (Appendix A.2.2) MATLAB scripts developed by the author.

4.3.4 Stage 2.2: Resource Variability

Temporal Variability

The results pertaining to the variability of the wave resource at different timescales (yearly, seasonal and monthly) for each site is presented in Table 4.4. These values are consistent with Cornett's [21] global assessment of the temporal variability of P_{wave}, which indicated that the values of COV, SV, and MV ranged from 0.8–1.2, 0.25–0.75, and 0.3–0.9, respectively, depending on the location in NZ (Appendix C).

Table 4.4. Temporal variability indicators, COV, SV, and MV at each site, obtained for the 20-year time horizon (January 1993–December 2012).

Location	COV	SV	MV	Most Energetic		Least Energetic	
				Season	Month	Season	Month
A1	0.97	0.67	0.77	Winter	June	Summer	January
A2	0.97	0.67	0.76	Winter	June	Summer	January
A3	0.97	0.67	0.76	Winter	June	Summer	February
G1	0.99	0.55	0.66	Winter	June	Summer	February
G2	1.00	0.53	0.66	Winter	September	Summer	February
G3	1.06	0.50	0.69	Winter	September	Summer	February
I1	0.98	0.53	0.67	Winter	June	Summer	December
I2	0.96	0.50	0.63	Winter	June	Summer	December
I3	0.94	0.47	0.60	Winter	June	Summer	December
NP1	0.97	0.63	0.72	Winter	June	Summer	February
NP2	0.98	0.62	0.72	Winter	June	Summer	February
NP3	0.96	0.63	0.72	Winter	June	Summer	February

As seen in Table 4.4, the inter-annual fluctuations of average power flux corresponding to COV < 1.0 were observed at the majority of sites being analysed. The highest COV values, and so, therefore, the most significant yearly fluctuations, occurred at locations within the Greymouth region of interest (COV ≥ 1), followed by I1 (COV = 0.98). The other sites within the Invercargill region of interest (I2 and I3) had the mildest inter-annual fluctuations (with I3 having the lowest COV value compared to all the other sites). The higher yearly temporal variability experienced at I1 (in comparison to I2 and I3) confirms the findings from Liberti et al. [75], which showed that yearly fluctuations of P_{wave} tended to increase for sites in sheltered areas.

These results seem counterintuitive when compared with Figure 4.7, which indicated that the opposite was true; I1–I3 fluctuated the greatest in terms of the average yearly range, where I2 had the broadest range of 37.1 kW/m. Whilst, all the other study sites (A1–A3, NP1–NP2, G1–G3) appeared to fluctuate much less over the same period of time, with G3 only having a range of 10.7 kW/m. The issue with using the range as a measure of variability is that it is calculated from two extreme values, which makes it sensitive to outliers in the data. The error in the range values was then further compounded by the fact that the data being compared had been averaged; outliers in the dataset influence the mean to a large extent. Therefore, more robust methods should be utilised when quantifying the variability of the available P_{wave} at each site, such as those utilised in this thesis.

In terms of the intra-annual variability, the regions of interest along the coast of South Island fluctuated up to 35 % (with regards to seasonal variability) and 25 % (with regards to monthly variability) less than the sites along North Island. The lowest SV and MV values, and so, therefore, the mildest seasonal and monthly fluctuations occurred at site I3 (South Island), whereas the larger seasonal and monthly variations transpired at A1 (North Island).

The low COV, SV, and MV values, in combination with the substantial P_{wave} available at I3, indicates that this site is the most optimal location for stable wave energy production, as it contains both a strong and steady resource.

Similar to that of Stage 1.3.1, the findings relevant to this sub-stage were obtained from the MATLAB scripts developed by the author, namely Main_Wave_Power_V3.m (Appendix 0) and Main_Combine_Wave_Power_Sites_V2.m (Appendix A.2.2).

Directional Variability

As shown in Figure 4.10–Figure 4.13, wave power roses were constructed for each of the sites for a typical year and typical winter period. The addition of structuring the results in terms of winter is because it is the most energetic season and so, therefore, the most relevant timescale with regards to the available P_{wave} at a location [204]. Each wave rose was comprised of 36 direction bins (in 10° increments), which utilised the meteorological convention; the direction is measured in degrees, clockwise from north.

In NZ, the westerly wind flow ('westerlies') dominates wave generation and the direction of wave propagation, especially along the west and south coast [201]. Therefore, it is unsurprising that the prevailing wave approach direction (in terms of P_{wave}), at all the sites, was between South-South-West (SSW) and West-North-West (WNW).

For the sites located along the west coast of North Island, it was found that the directional variability of P_{wave} was very similar for areas within the same region of interest. At sites A1–A3 and NP1–NP3, it was established that the majority of the wave energy propagated from 220°–260° (Figure 4.10) and 230°–270° (Figure 4.11), respectively (at both timescales). It was also evident from the shape of the wave roses that the wave directions were unevenly spread within these ranges, with waves travelling from 230° (Auckland sites) and 240° (New Plymouth sites) contributing the greatest to the wave resource.

In the case of the Greymouth region of interest, it was found that the wave direction varied at each site as well as between the sites (Figure 4.12). For instance, at G1, the waves were predominately from 230°–270°, whereas the incoming P_{wave} at G2 and G3 were from 240°–270° and 250°–290°, respectively. This trend indicates that the prevailing wave direction increases as the sites move further down the west coast of South Island. The incoming P_{wave} was also unevenly distributed within these ranges, with waves travelling from 240° (G1) and 250° (G2 and G3) dominating the wave climate.

For I1–I3, which are located along the south coast of South Island, it was determined that the predominant wave direction was from 230°–270° and that, unlike the other sites, P_{wave} was relatively evenly distributed across 230°–250° (Figure 4.13).

It should be noted that, in general, deep-water sites tend to have a broad range of wave directions, thereby limiting its suitability for the installation of devices that are directionally sensitive (such as line absorbers) [57]. However, as just discussed, the wave climates of these proposed deep-water sites are dominated by waves propagating from a narrow range of directions, thereby making these locations ideal for the installation of omni-directional WECs (point absorbers) and line absorbers.

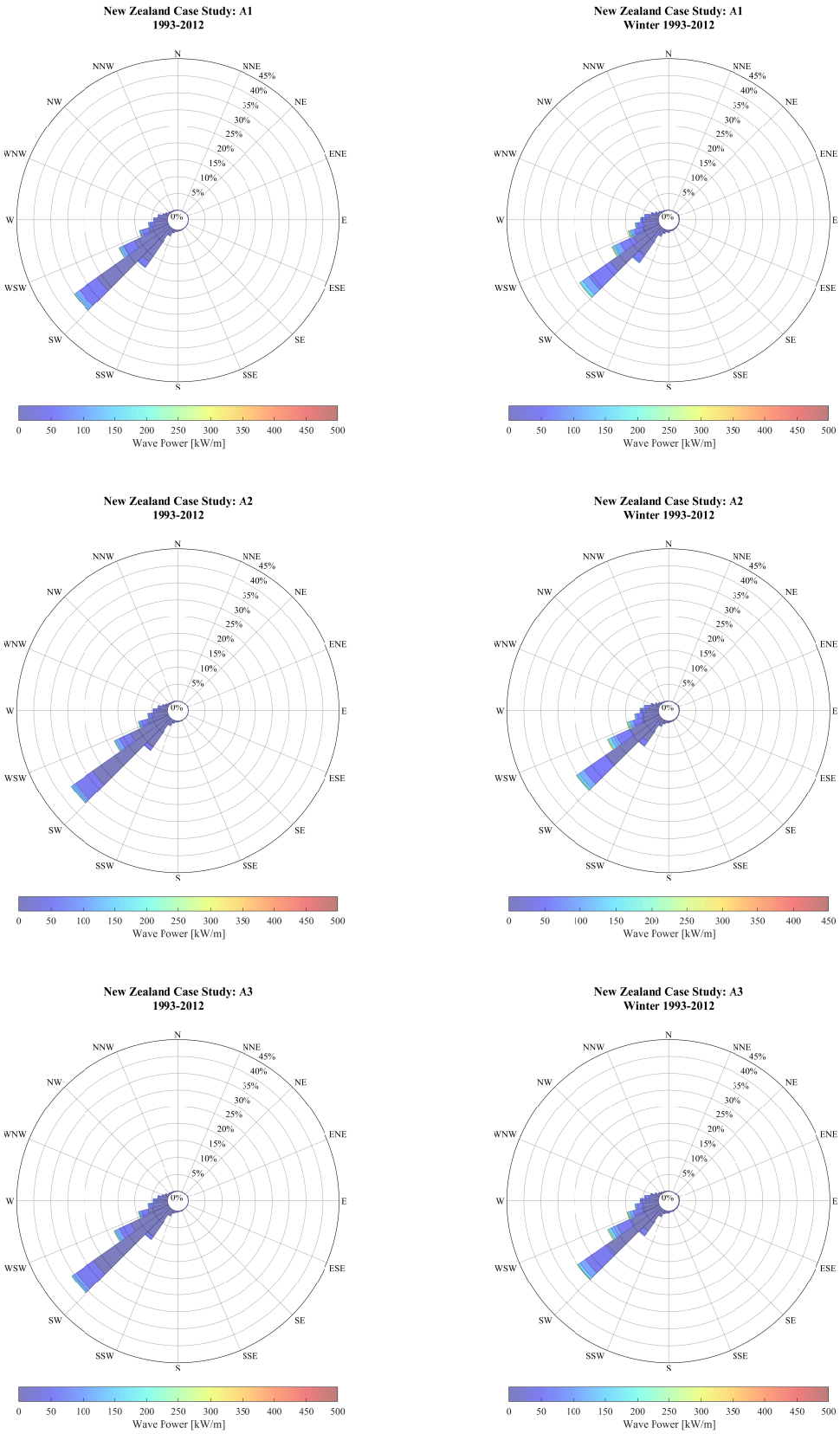

Figure 4.10. Wave roses depicting the joint occurrence of wave power and mean wave direction for a typical year (left panel) and typical winter (right panel) at the three sites located within the Auckland region of interest (A1–A3).

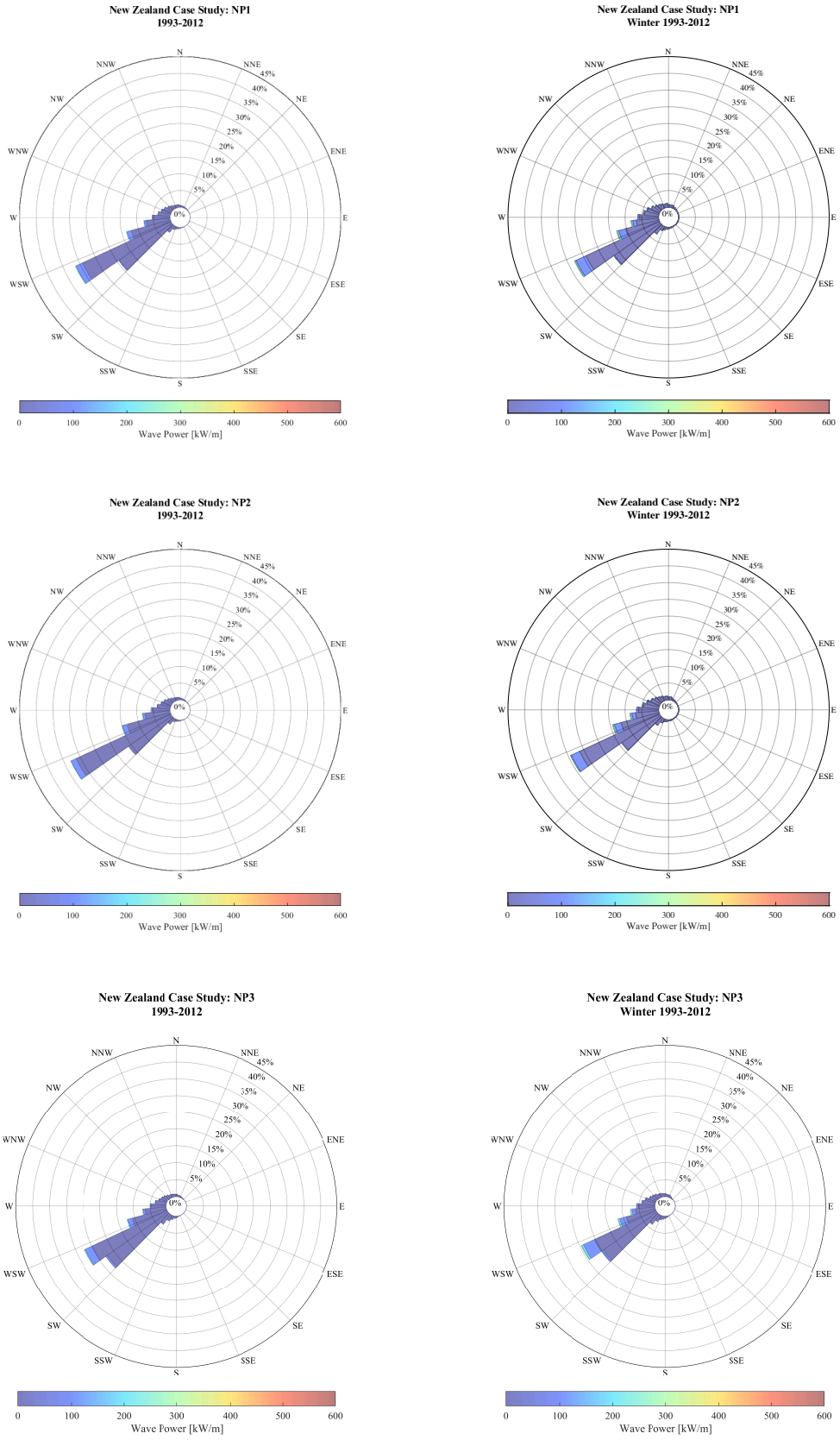

Figure 4.11. Wave roses depicting the joint occurrence of wave power and mean wave direction for a typical year (left panel) and typical winter (right panel) at the three sites located within the New Plymouth region of interest (NP1–NP3).

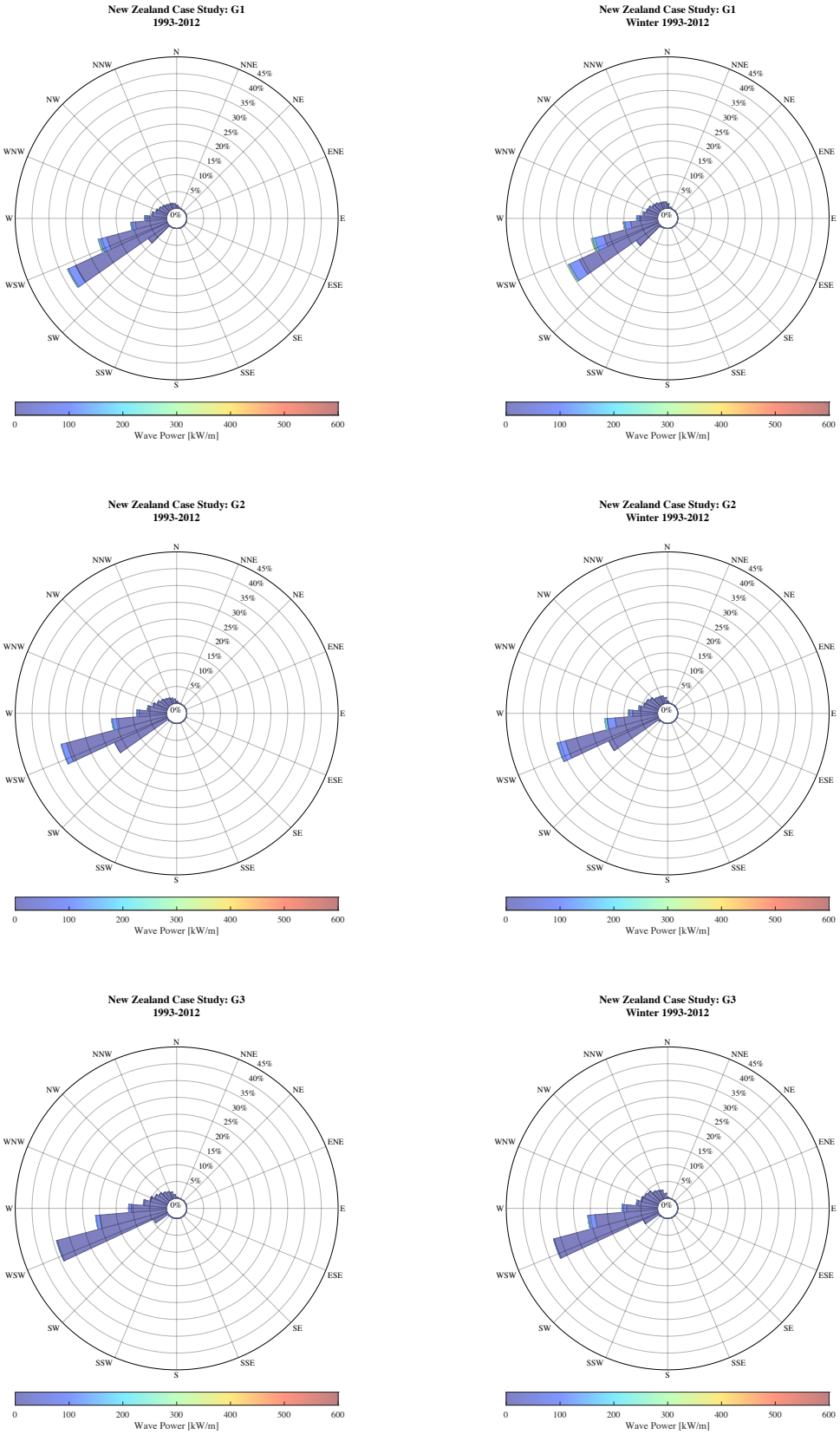

Figure 4.12. Wave roses depicting the joint occurrence of wave power and mean wave direction for a typical year (left panel) and typical winter (right panel) at the three sites located within the Greymouth region of interest (G1–G3).

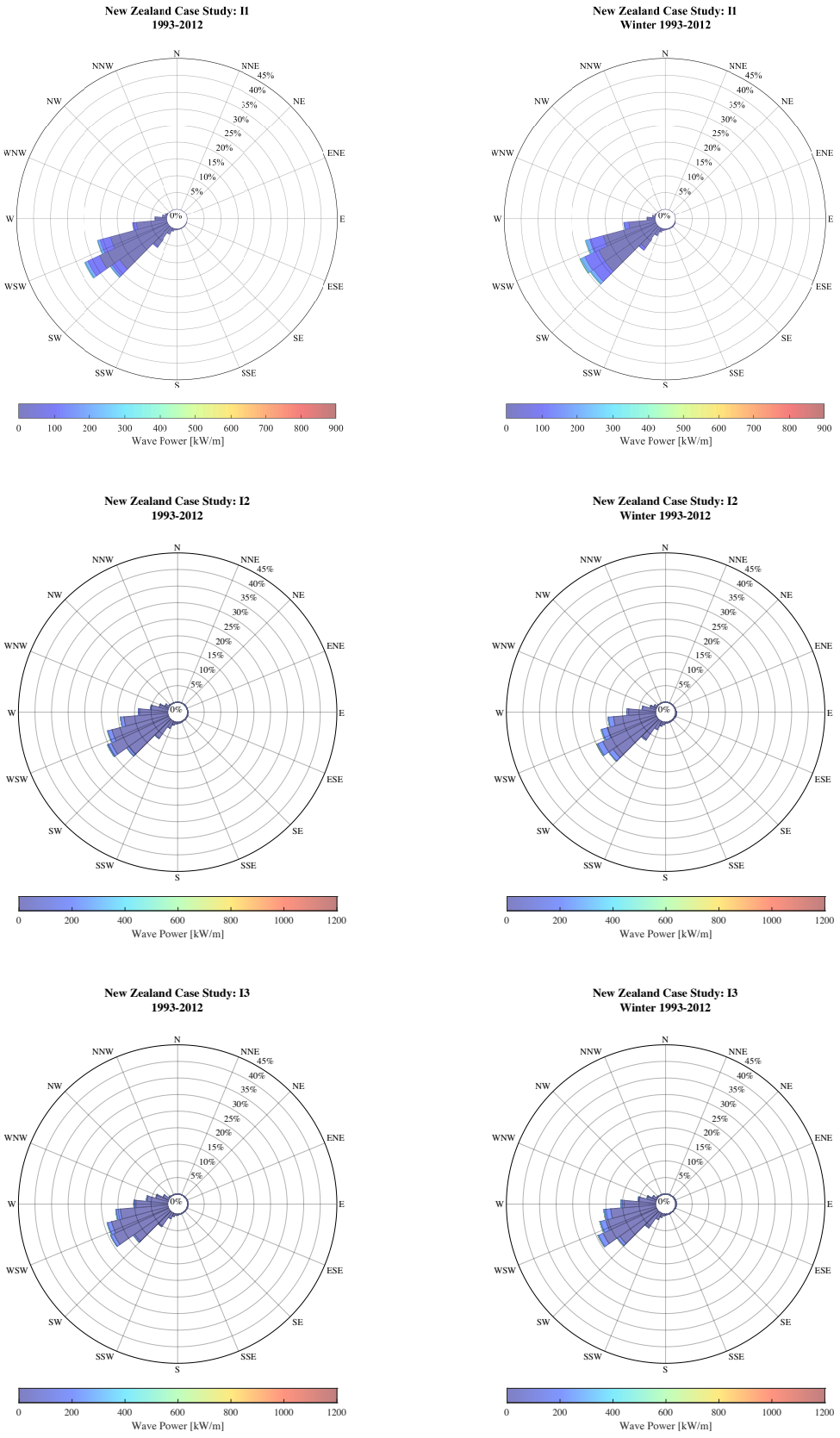

Figure 4.13. Wave roses depicting the joint occurrence of wave power and mean wave direction for a typical year (left panel) and typical winter (right panel) at the three sites located within the Invercargill region of interest (I1–I3).

Therefore, in terms of directionally sensitive WECs, sites A2, A3, G1, and G3 would be more favourable as these potential WEF locations have waves propagating from a dominant direction over 30 % of the time regardless of the timescale.

The results regarding the P_{wave} directional distribution were obtained from the Main_Export_Scatter_Data_V4.m (Appendix A.2.3) and Main_Wave_Roses.m (Appendix A.2.4) scripts created by the author.

4.3.5 Stage 2.3: Resource Characterisation

Resource-Characterisation Matrix

An overview of the variability of the distribution of H_{m0} and T_e at each of the locations in terms of a typical year and typical winter period are presented in Figure 4.14–Figure 4.25. In the lower left panel of each figure, the resource-characterisation matrix plotted the percentage occurrence of the H_{m0}–T_e pair. The H_{m0} bins were defined in 0.5 m intervals, which ranged from 0 to 16 m, and the T_e bins were defined in 1 s intervals that ranged from 0 to 20 s. On the upper and right panels of each resource characterisation matrix are two histograms that represent the distribution of T_e and H_{m0}, respectively.

As seen in the figures, NZ's wave climate is characterised by a widespread of wave conditions, with values of T_e occurring between 4 and 19 s at all the locations, whilst H_{m0} varied from waves just greater than 0 m to 9.5 m high at the majority of the study sites (A1–A3, NP1–NP3, G1–G3). The Invercargill locations (Figure 4.23, Figure 4.24, and Figure 4.25) experienced significantly higher H_{m0}, with waves reaching 12.5 m in height (at I2 and I3), which is unsurprising, because as previously stated, the wave environment south of NZ is highly energetic.

For the sites along the west coast of North Island (Figure 4.14–Figure 4.19), it was found that for the majority of the year sea states fell within a H_{m0} range of 1–3.5 m (~84 %) and a T_e range of 8–13 s (~84 %). As expected, during the wintertime, the values of H_{m0} increased to 1.5–4 m, which occurred ~82 % of the time, whilst the values and occurrence of T_e remained the same (Table 4.5).

(a)

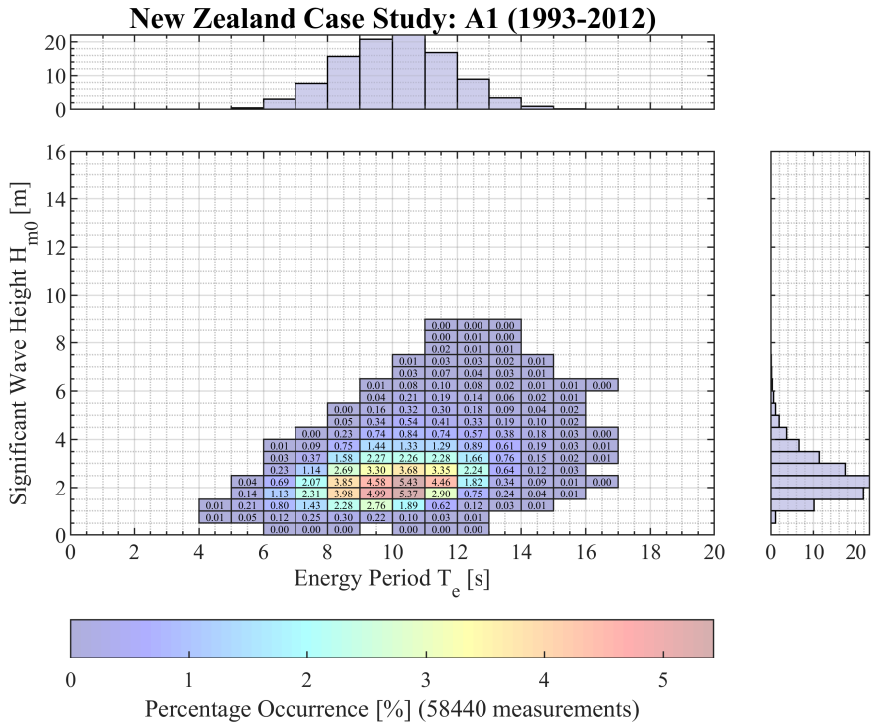

(b)

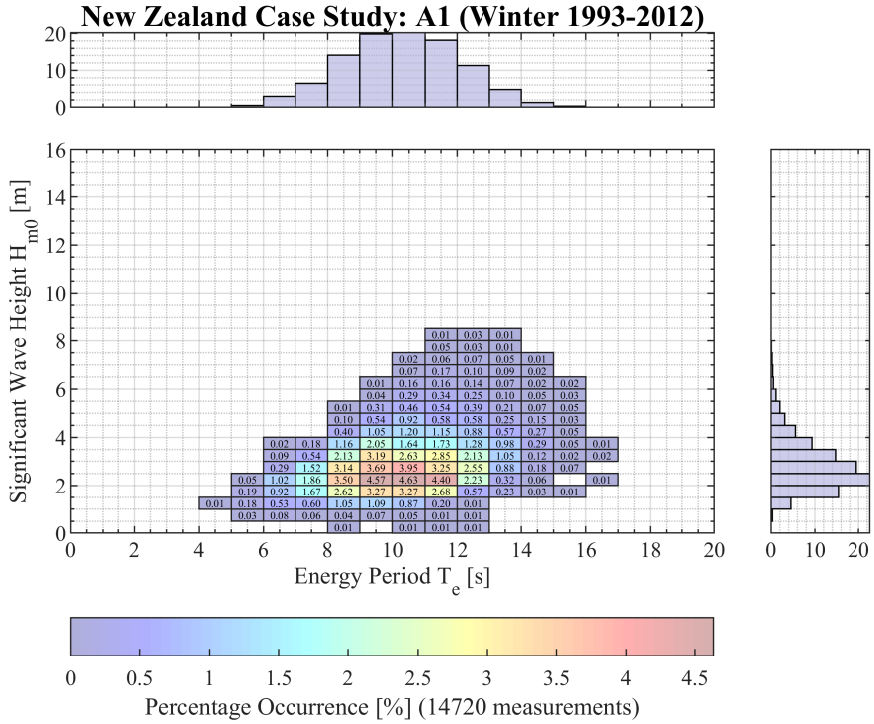

Figure 4.14. Distributions of H_{m0} and T_e as well as resource-characterisation matrices depicting the joint occurrence of H_{m0} and T_e for a (a) typical year and (b) typical winter at site A1 within the Auckland region of interest.

(a)

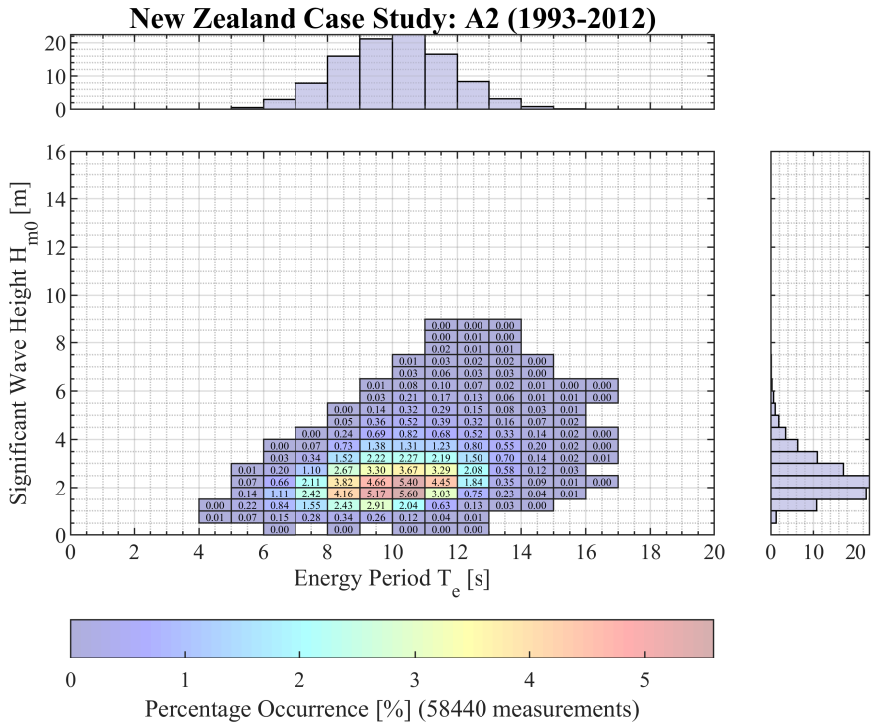

(b)

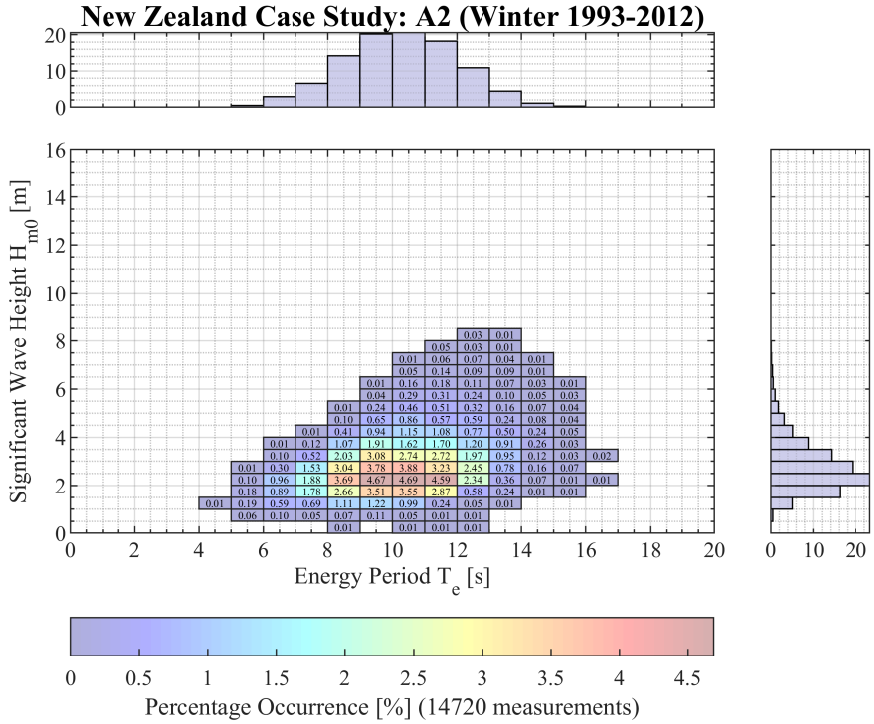

Figure 4.15. Distributions of H_{m0} and T_e as well as resource-characterisation matrices depicting the joint occurrence of H_{m0} and T_e for a (a) typical year and (b) typical winter at site A2 within the Auckland region of interest.

(a)

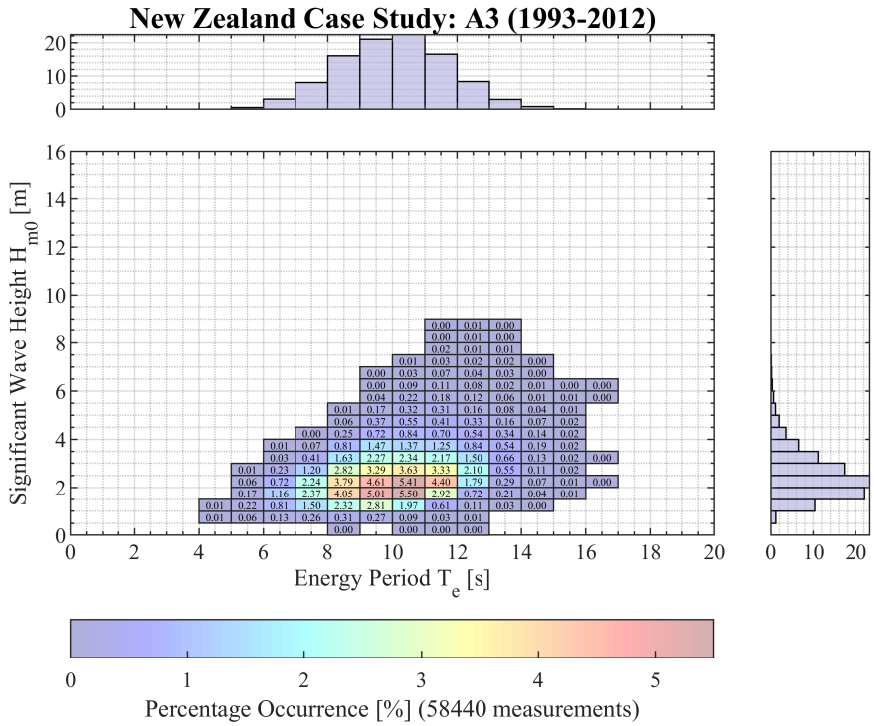

(b)

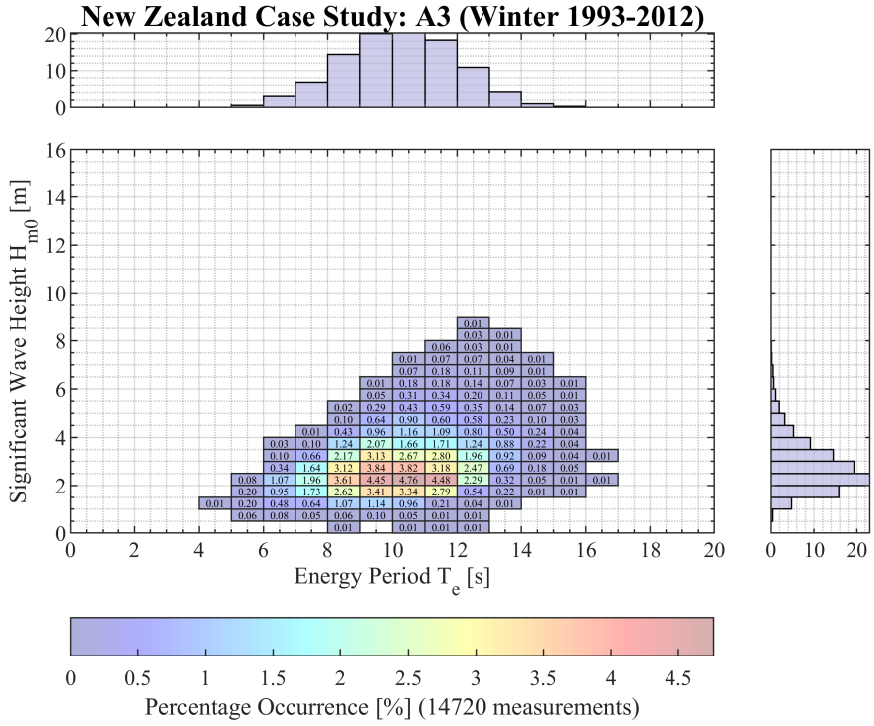

Figure 4.16. Distributions of H_{m0} and T_e as well as resource-characterisation matrices depicting the joint occurrence of H_{m0} and T_e for a (a) typical year and (b) typical winter at site A3 within the Auckland region of interest.

(a)

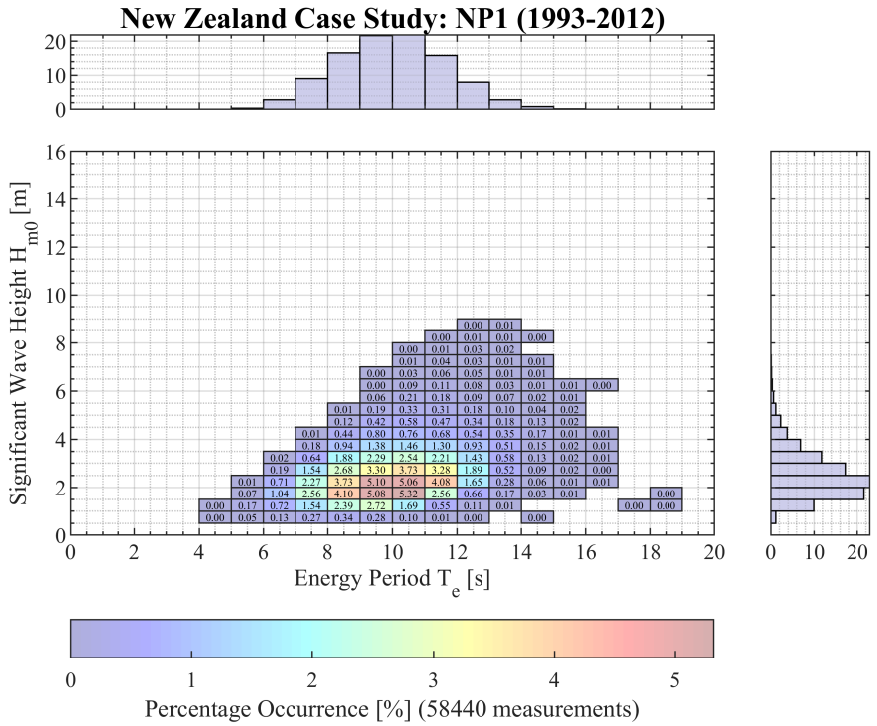

(b)

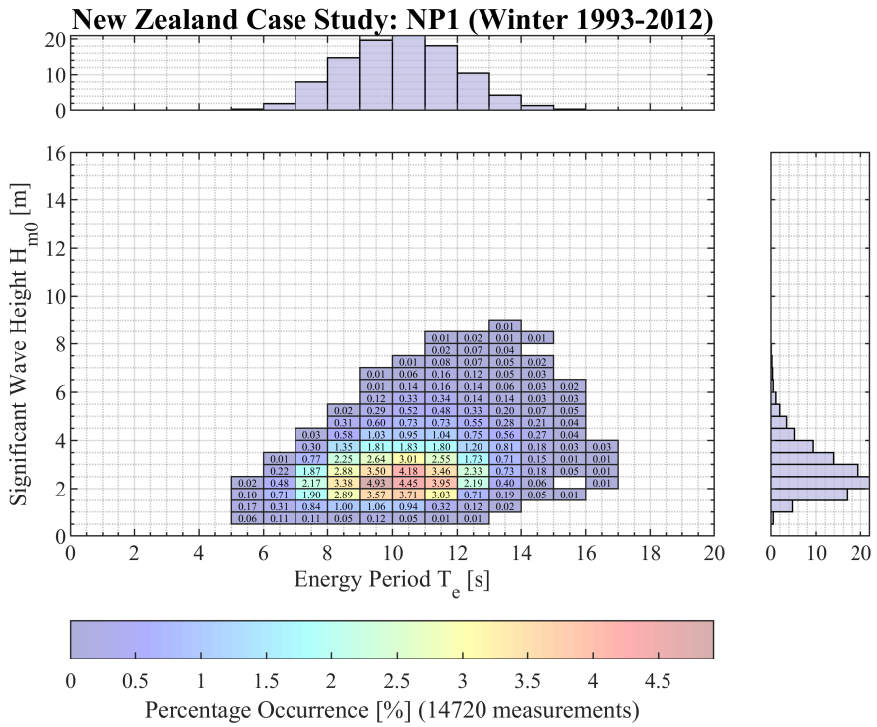

Figure 4.17. Distributions of H_{m0} and T_e as well as resource-characterisation matrices depicting the joint occurrence of H_{m0} and T_e for a (a) typical year and (b) typical winter at site NP1 within the New Plymouth region of interest.

(a)

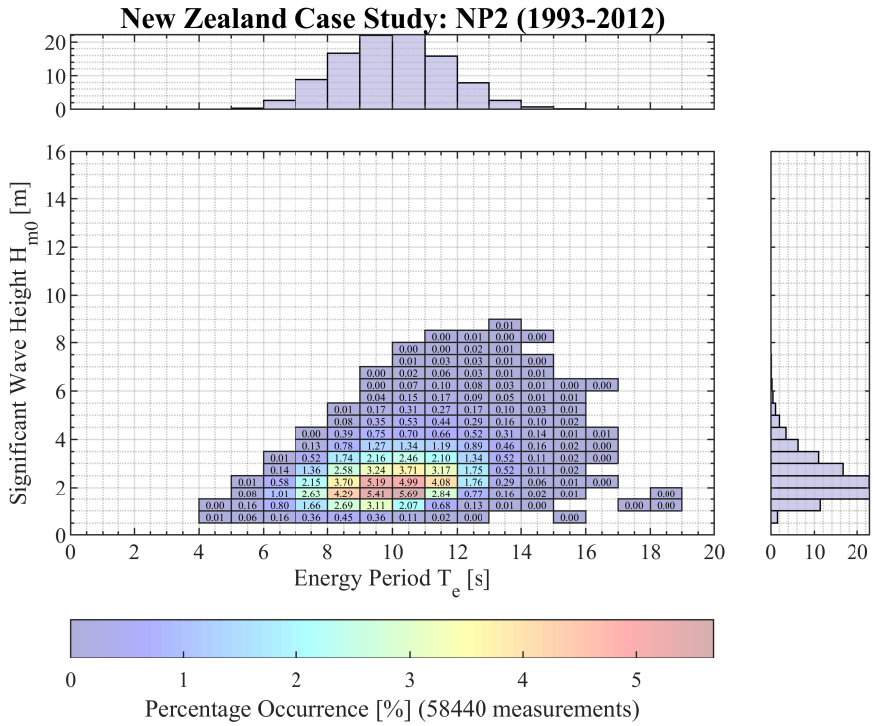

(b)

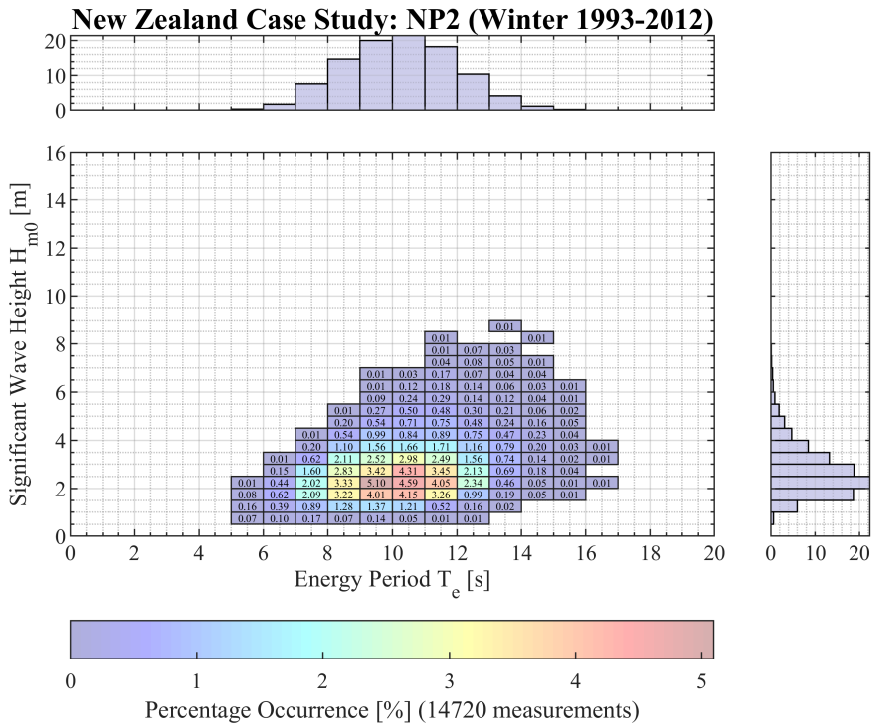

Figure 4.18 Distributions of H_{m0} and T_e as well as resource-characterisation matrices depicting the joint occurrence of H_{m0} and T_e for a (a) typical year and (b) typical winter at site NP2 within the New Plymouth region of interest.

(a)

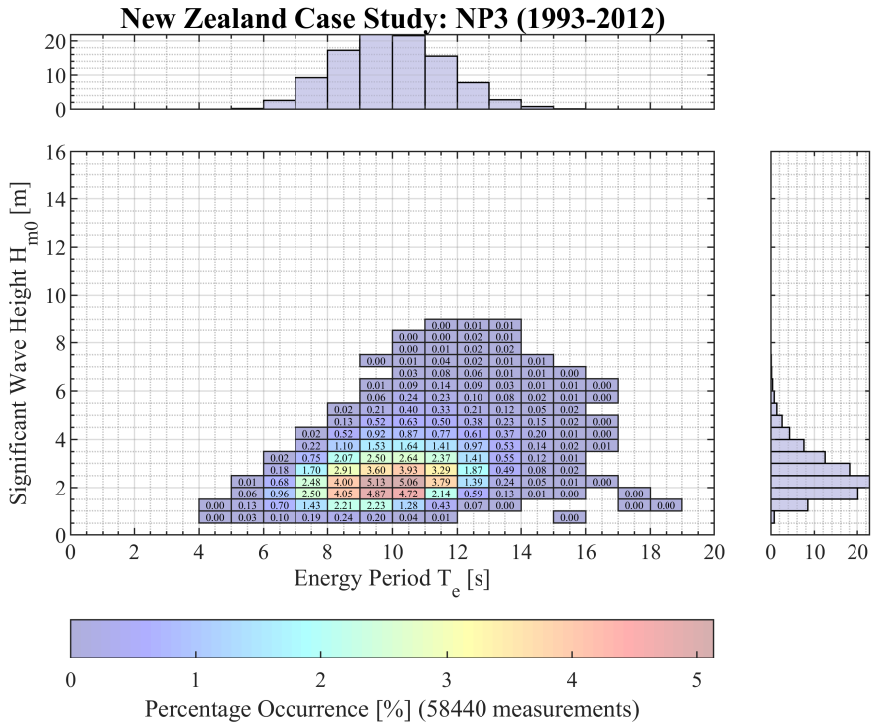

(b)

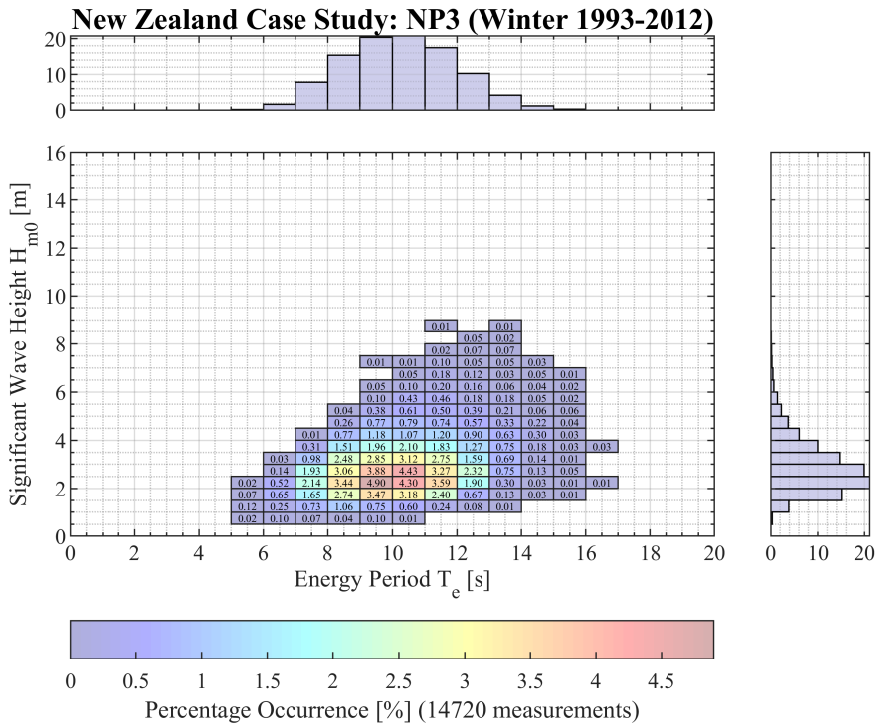

Figure 4.19. Distributions of H_{m0} and T_e as well as resource-characterisation matrices depicting the joint occurrence of H_{m0} and T_e for a (a) typical year and (b) typical winter at site NP3 within the New Plymouth region of interest.

(a)

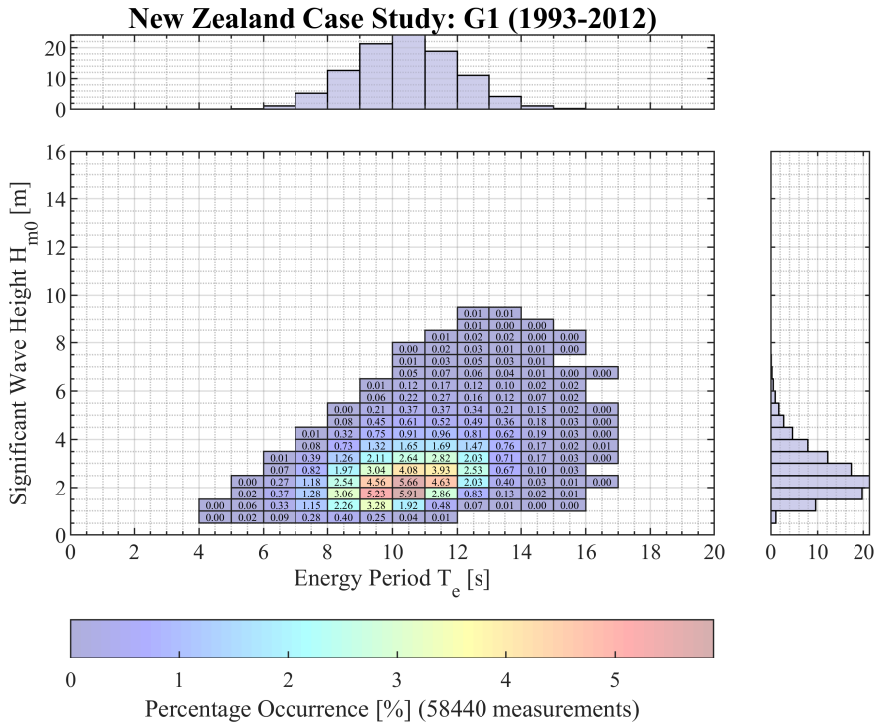

(b)

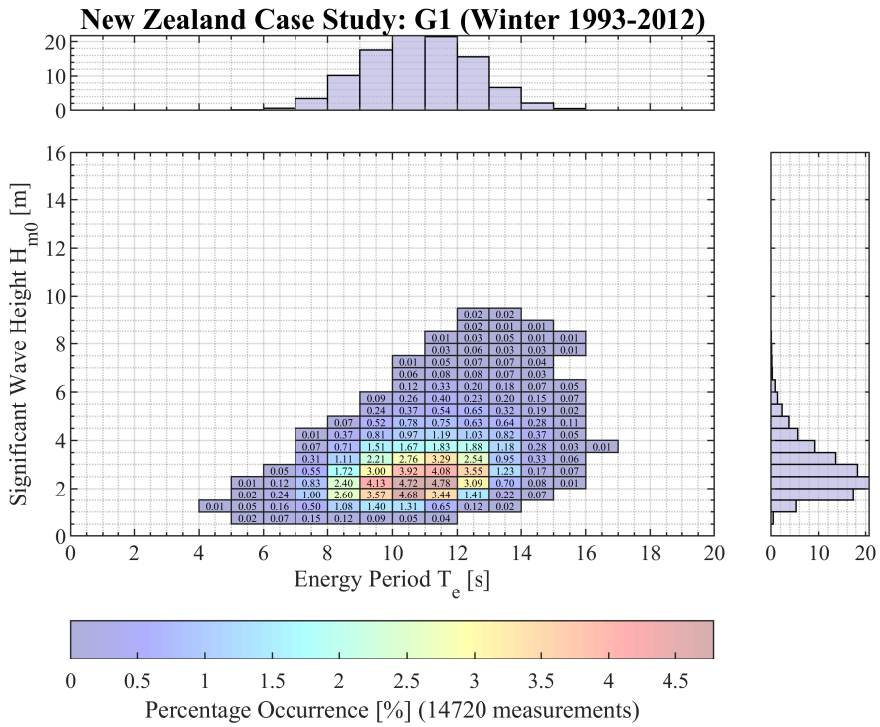

Figure 4.20. Distributions of H_{m0} and T_e as well as resource-characterisation matrices depicting the joint occurrence of H_{m0} and T_e for a (a) typical year and (b) typical winter at site G1 within the Greymouth region of interest.

(a)

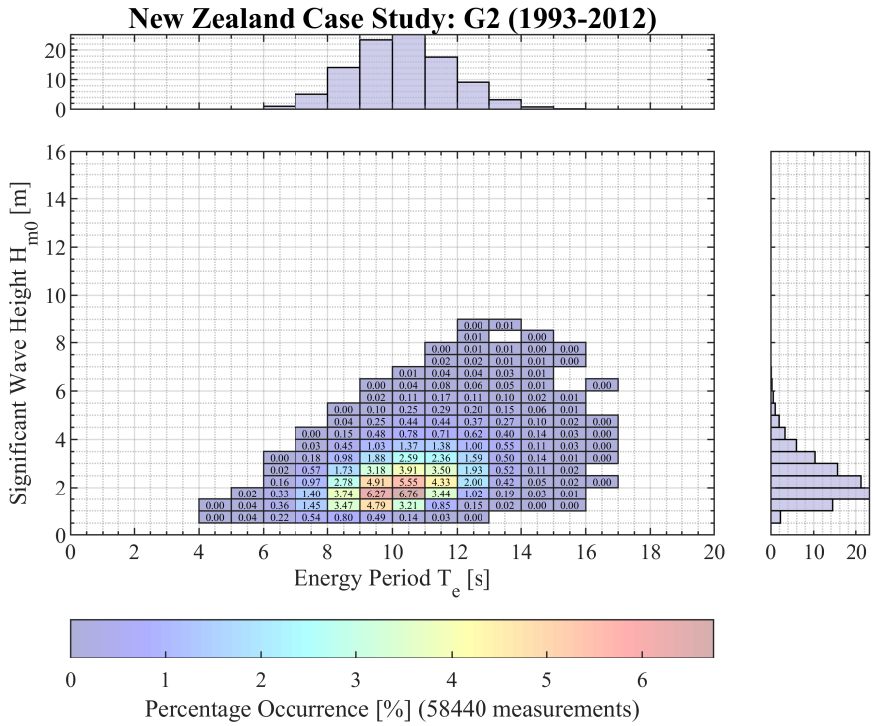

(b)

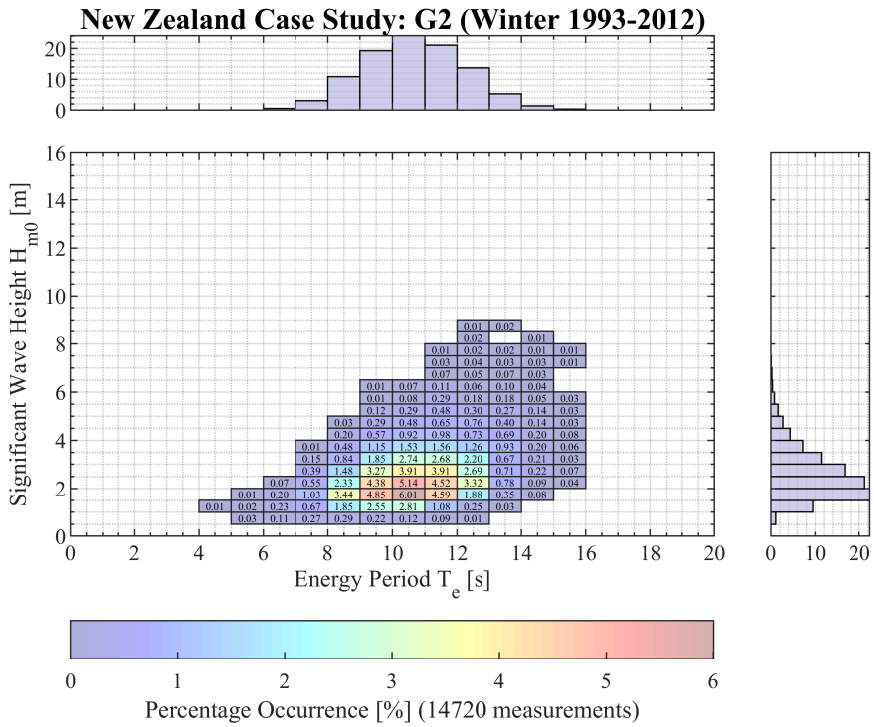

Figure 4.21. Distributions of H_{m0} and T_e as well as resource-characterisation matrices depicting the joint occurrence of H_{m0} and T_e for a (a) typical year and (b) typical winter at site G2 within the Greymouth region of interest.

(a)

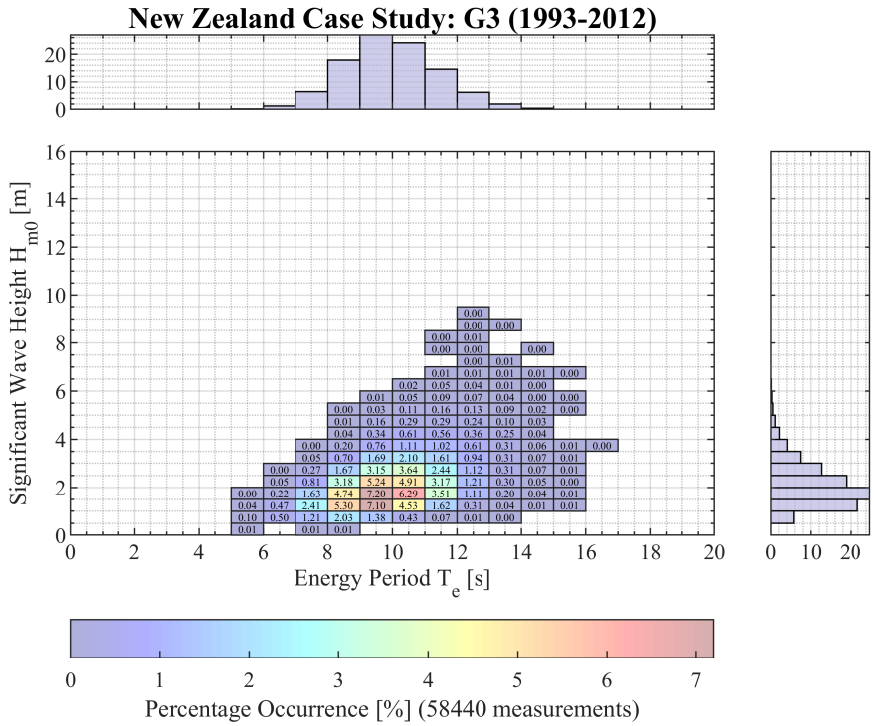

(b)

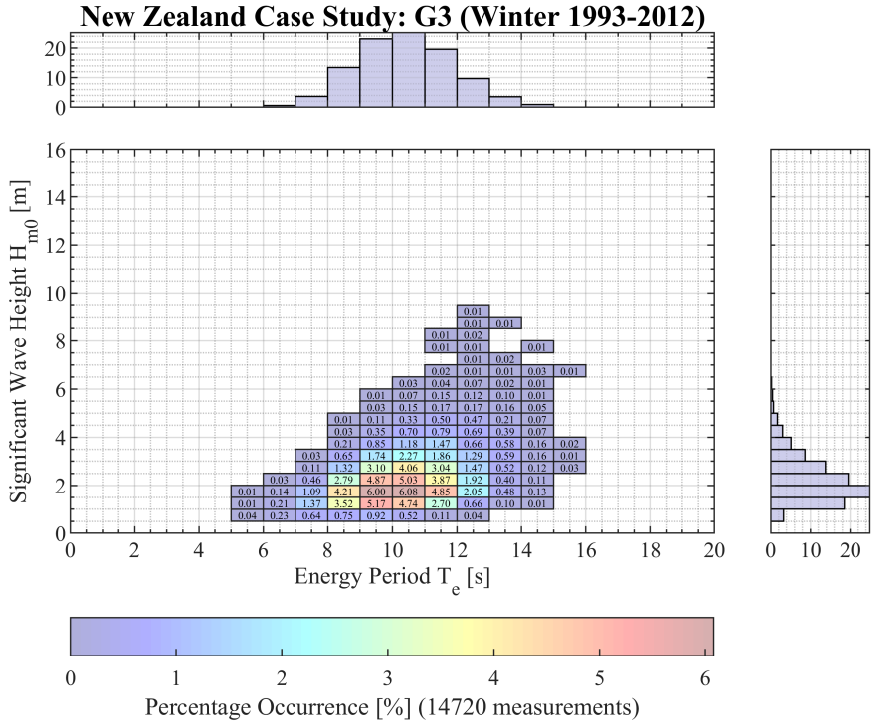

Figure 4.22. Distributions of H_{m0} and T_e as well as resource-characterisation matrices depicting the joint occurrence of H_{m0} and T_e for a (a) typical year and (b) typical winter at site G3 within the Greymouth region of interest.

(a)

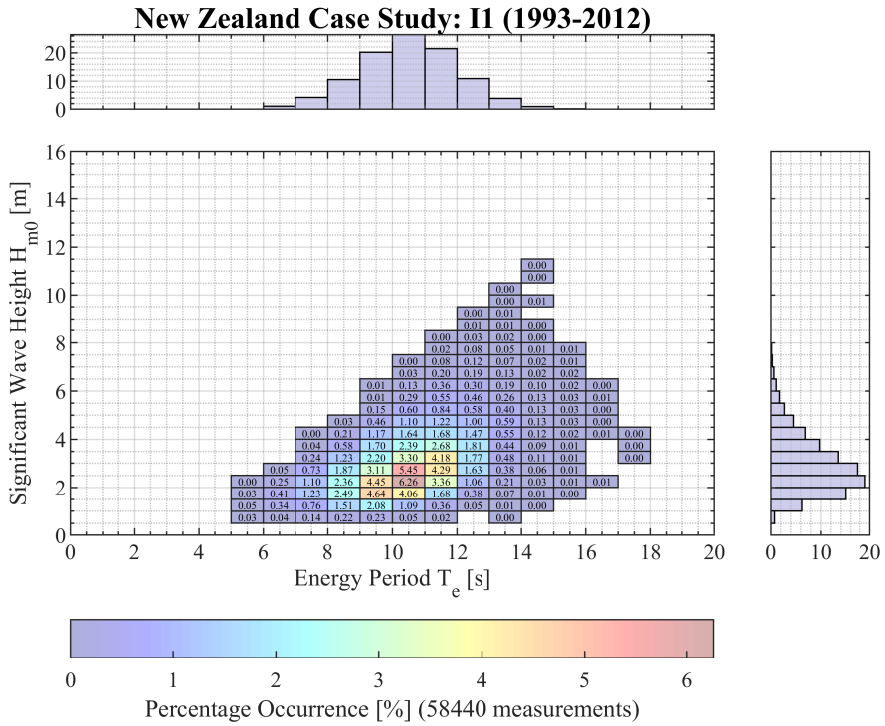

(b)

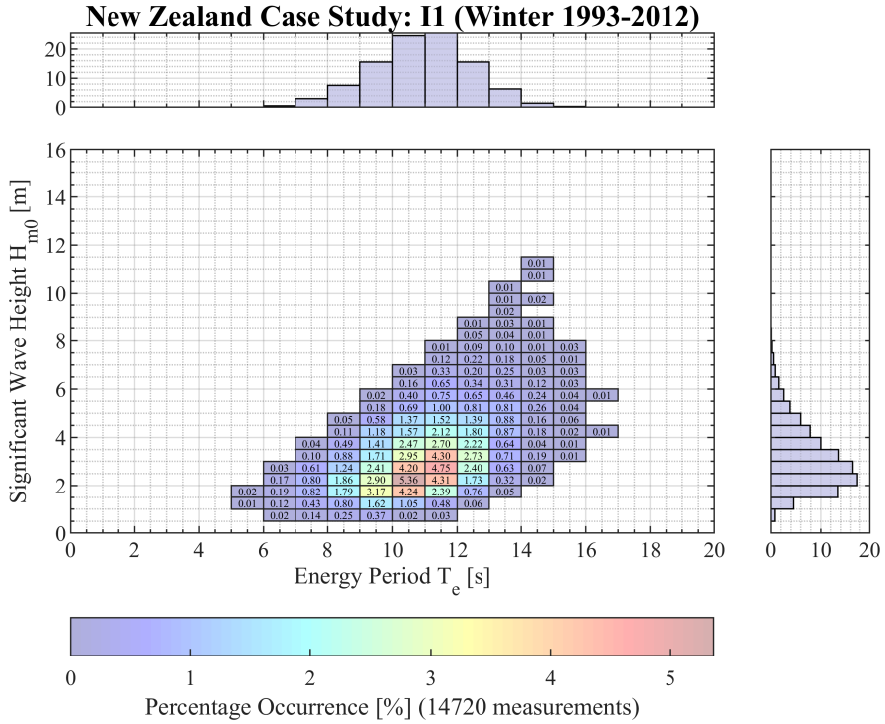

Figure 4.23. Distributions of H_{m0} and T_e as well as resource-characterisation matrices depicting the joint occurrence of H_{m0} and T_e for a (a) typical year and (b) typical winter at site I1 within the Invercargill region of interest.

(a)

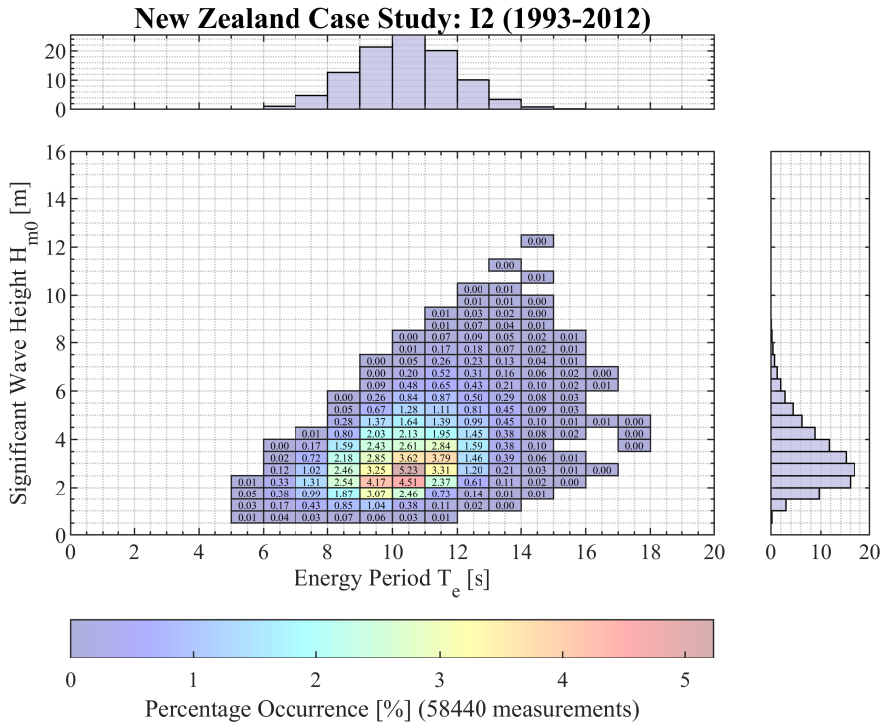

(b)

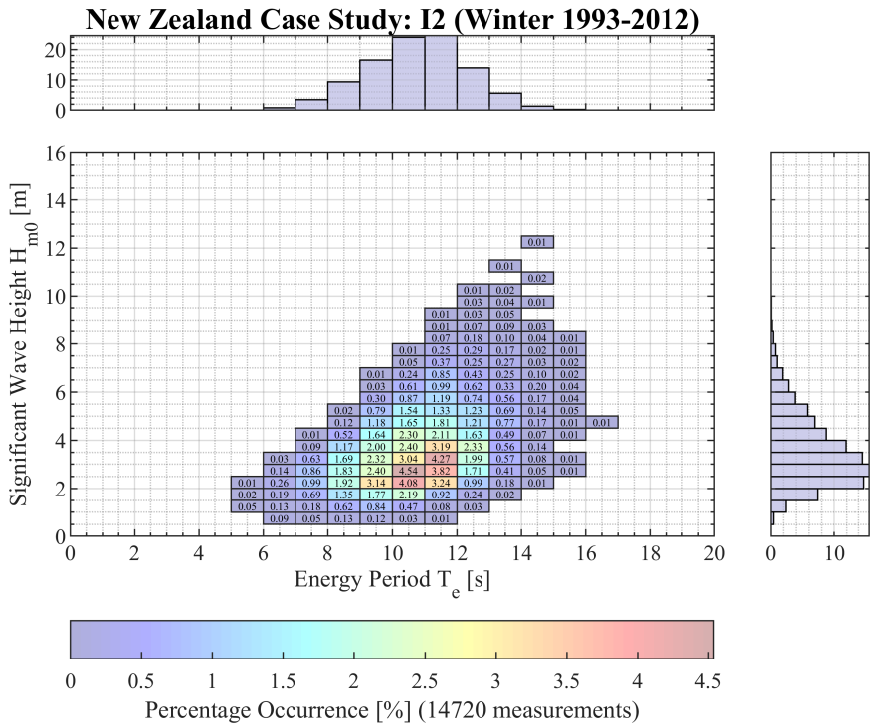

Figure 4.24. Distributions of H_{m0} and T_e as well as resource-characterisation matrices depicting the joint occurrence of H_{m0} and T_e for a (a) typical year and (b) typical winter at site I2 within the Invercargill region of interest.

(a)

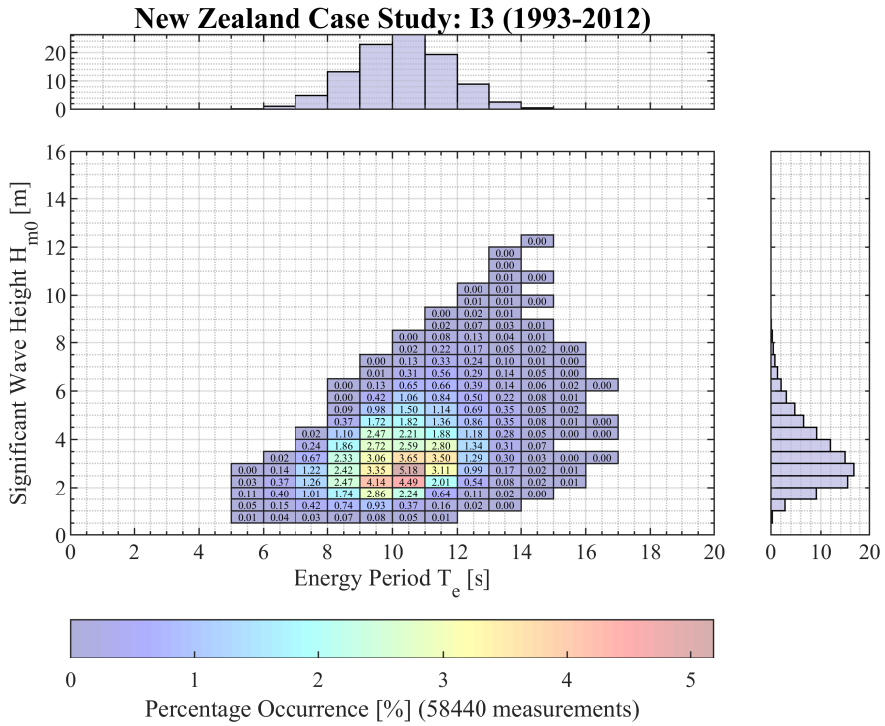

(b)

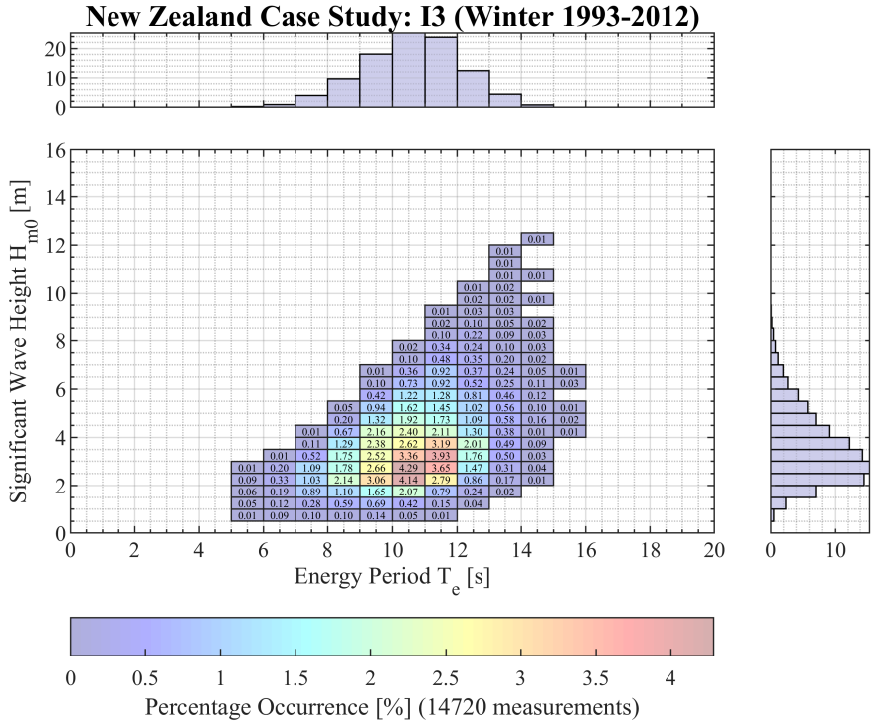

Figure 4.25. Distributions of H_{m0} and T_e as well as resource-characterisation matrices depicting the joint occurrence of H_{m0} and T_e for a (a) typical year and (b) typical winter at site I3 within the Invercargill region of interest.

In the case of the locations along the west coast of South Island (Figure 4.20, Figure 4.21, and Figure 4.22), it was established that although the majority of sea states within a year transpired between 1–3.5 m and 8–13 s for H_{m0} (≥ 80 %) and T_e (~89 %), respectively, that the frequency of these H_{m0} values varied quite widely from site to site (Table 4.5). In the winter period, it was found that similar to the Auckland and New Plymouth locations, T_e remained the same, whilst the H_{m0} values increased to 1–4 m (≥ 80 %), which also fluctuated considerably, in terms of occurrence, across the Greymouth sites (Table 4.5).

Table 4.5. The annual and wintertime sea states (with corresponding percentage probabilities of occurrence), which contribute the greatest to the wave climate at each of the locations as well as the probability of occurrence (%) of calm and extreme sea states, at both timescales, for all locations.

Site	H_{m0} [m]		T_e [s]		Calm [%]		Extreme [%]	
	Year	Winter	Year	Winter	Year	Winter	Year	Winter
A1	1–3.5 (84%)	1.5–4 (82%)	8–13 (84%)	8–13 (84%)	0.01	0.03	0.03	0.05
A2	1–3.5 (85%)	1.5–4 (82%)	8–13 (84%)	8–13 (84%)	0.01	0.03	0.02	0.03
A3	1–3.5 (84%)	1.5–4 (82%)	8–13 (84%)	8–13 (84%)	0.01	0.03	0.03	0.05
NP1	1–3.5 (83%)	1.5–4 (82%)	8–13 (84%)	8–13 (84%)	0.00	0.00	0.03	0.05
NP2	1–3.5 (85%)	1.5–4 (81%)	8–13 (85%)	8–13 (85%)	0.00	0.00	0.02	0.03
NP3	1–3.5 (82%)	1.5–4 (81%)	8–13 (84%)	8–13 (84%)	0.00	0.00	0.04	0.10
G1	1–3.5 (80%)	1–4 (84%)	8–13 (88%)	8–13 (87%)	0.00	0.00	0.07	0.18
G2	1–3.5 (84%)	1–4 (88%)	8–13 (89%)	8–13 (89%)	0.00	0.00	0.02	0.06
G3	1–3.5 (86%)	1–4 (90%)	8–13 (90%)	8–13 (91%)	0.02	0.00	0.01	0.05
I1	1–4 (81%)	1.5–4.5 (79%)	8–13 (90%)	8–13 (88%)	0.00	0.00	0.10	0.22
I2	1.5–5 (84%)	1.5–5 (80%)	8–13 (90%)	8–13 (88%)	0.00	0.00	0.46	0.83
I3	1.5–5 (84%)	1.5–5 (80%)	8–13 (91%)	8–13 (89%)	0.00	0.00	0.46	0.82

The distribution of the sea states at the Invercargill sites are depicted in Figure 4.23, Figure 4.24, and Figure 4.25. As seen from these plots and Table 4.5, the majority of the waves that occurred during a typical year were with H_{m0} that ranged from 1–4 m at I1 (81 %) to 1.5–5 m at I2 and I3 (84 %), and ~90 % of the waves were with T_e between 8 and 13 s at all the Invercargill locations. The H_{m0} values increased to 1.5–4.5 m (79 %) at I1 during the wintertime, whilst remaining the same at I2 and I3 (just for a lower duration

of time; 80 %). As with the other potential WEF locations, T_e remained unchanged whilst the occurrence of the values decreased slightly to ~88 %. Lower H_{m0} values occurred at I1, compared to that of I2 and I3, because it is a sheltered site and so, therefore, less exposed to the surrounding energetic wave climate.

Furthermore, it can be seen from Table 4.5 that the calm sea states rarely occurred and were limited to the Auckland locations at both timescales and G3 for a typical year. It was also determined that even though extreme sea states happened at all the locations, for both timescales, that these events, similar to that of the calm sea states, do not occur very often (less than 1 %).

Unlike the resource quantification and variability sub-stages, there is no most 'optimal' site(s) in terms of resource characterisation. In this case, the WEC's performance ultimately determines which site is 'best', as devices operate optimally, with high efficiency, when its operational range coincides with the dominant sea states at the location.

Sea State Contribution to Wave Power

A major limitation associated with resource-characterisation matrices is that these plots fail to fully describe which sea states contribute the greatest to the available wave power at a particular location [205]. Therefore, as recommended by Cahill and Lewis [205], the resource-characterisation matrices (Figure 4.14–Figure 4.25) were adapted by replacing the percentage occurrence of the H_{m0}-T_e pair with the percentage contribution of the sea state to the total wave power (Figure 4.26–Figure 4.37); enabling the identification of the most energy-rich sea states.

A comparison of the original resource-characterisation matrices (Figure 4.14–Figure 4.25) developed for each site with the corresponding revised plots (Figure 4.26–Figure 4.37) demonstrated that the most frequently occurring wave conditions were not necessarily the most energetic. In fact, it was observed that the positions of the most significant sea states shifted upwards at each site. The H_{m0} increased by a minimum of 0.5 m, whereas the majority of the sea states remained within the T_e range of 8–13 s, with the exception of the sites located along South Island (Table 4.6); values of T_e increased to 9–14 s in the wintertime.

(a)

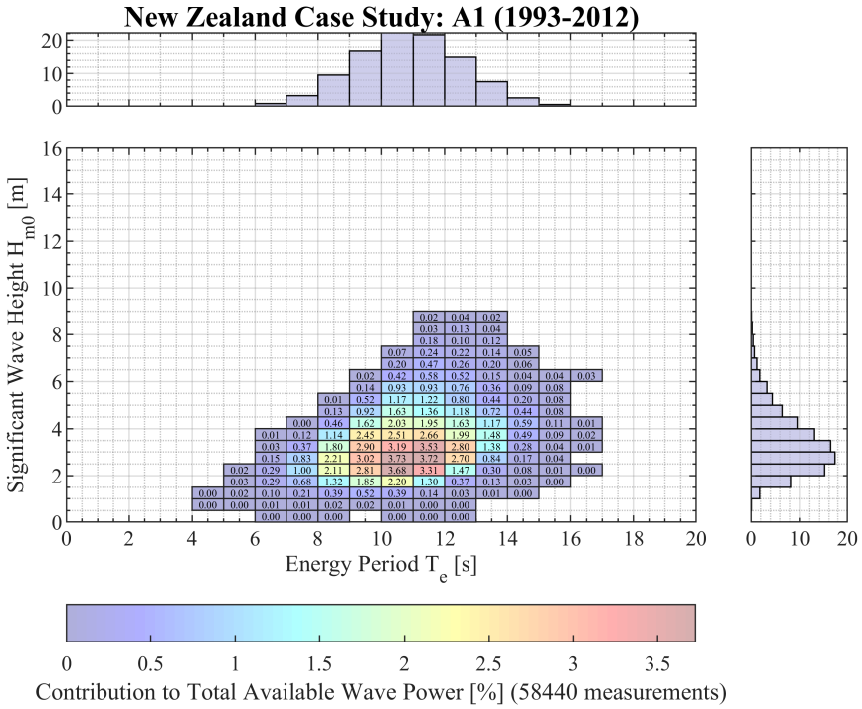

(b)

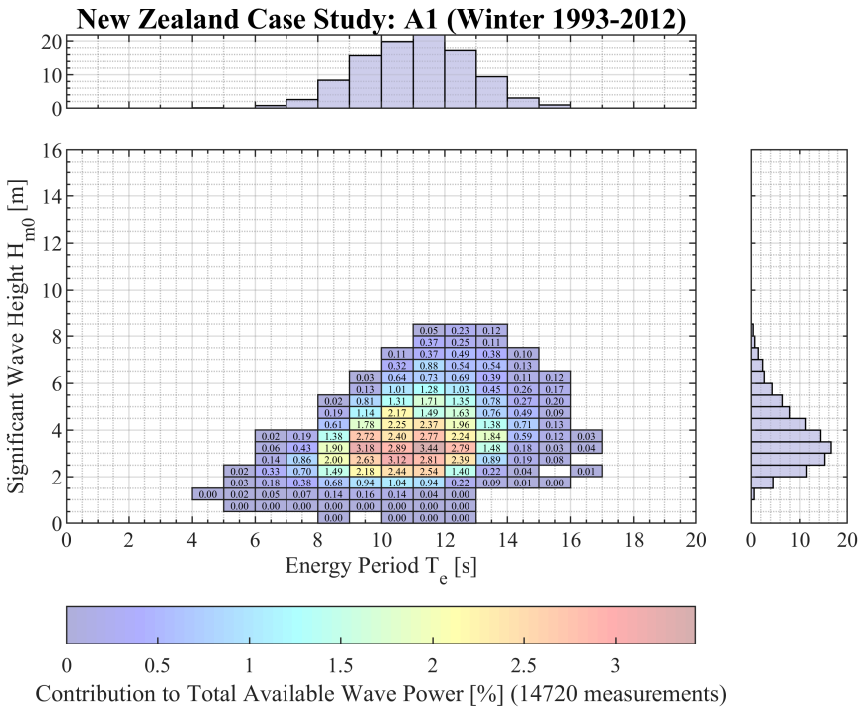

Figure 4.26. Percentage contribution of each sea state to the total available P_{wave} at A1 for a (a) typical year and (b) typical winter.

(a)

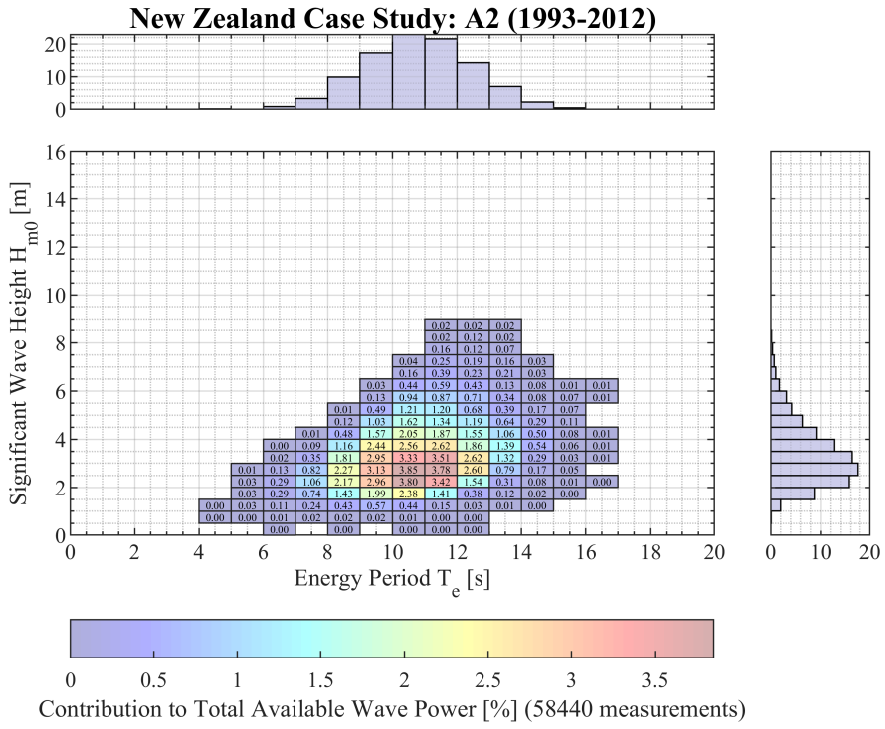

(b)

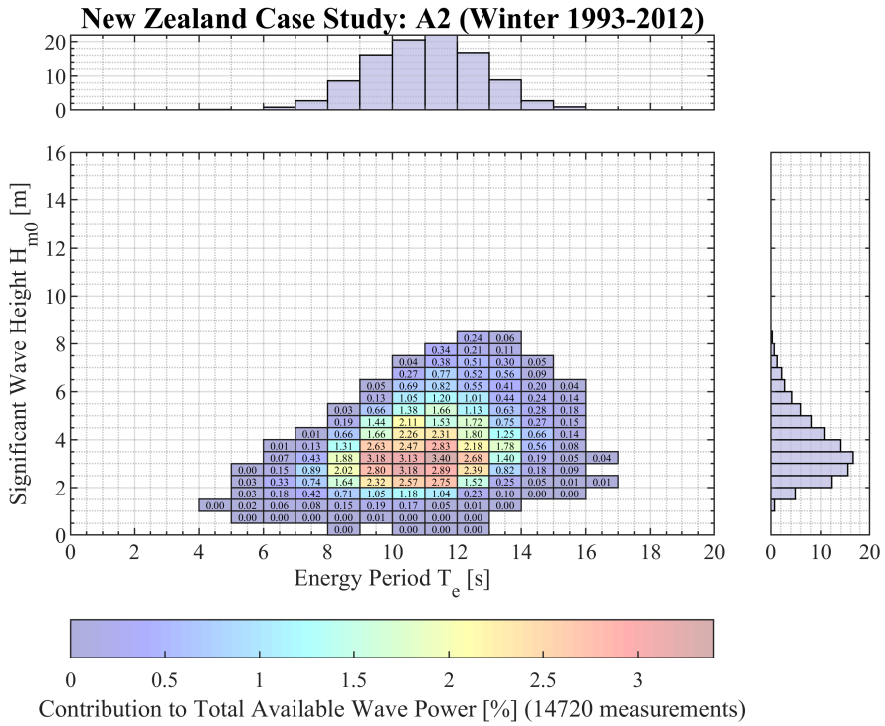

Figure 4.27. Percentage contribution of each sea state to the total available P_{wave} at A2 for a (a) typical year and (b) typical winter.

(a)

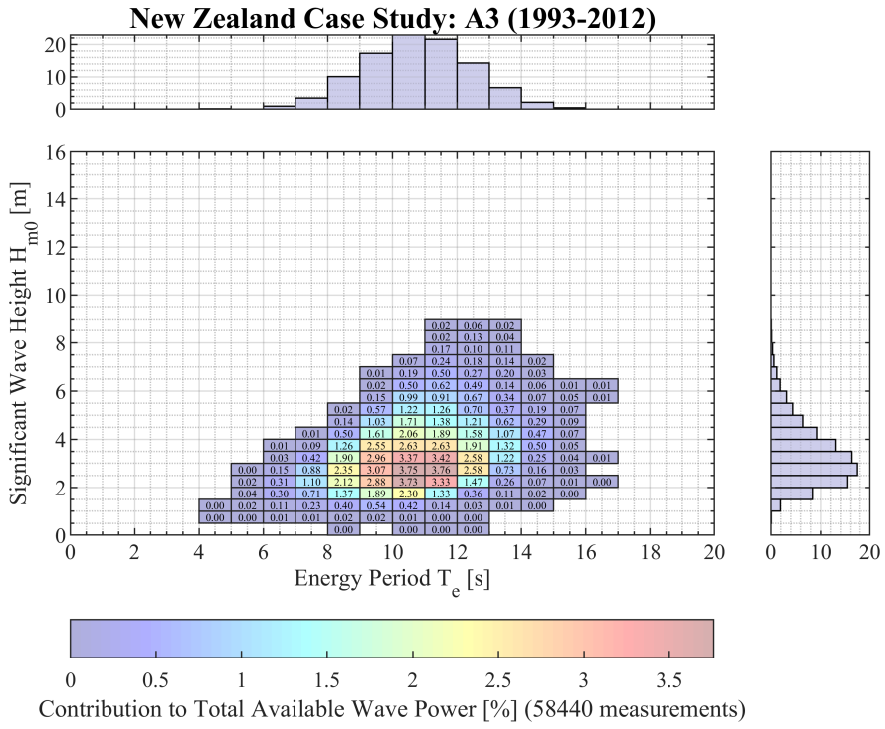

(b)

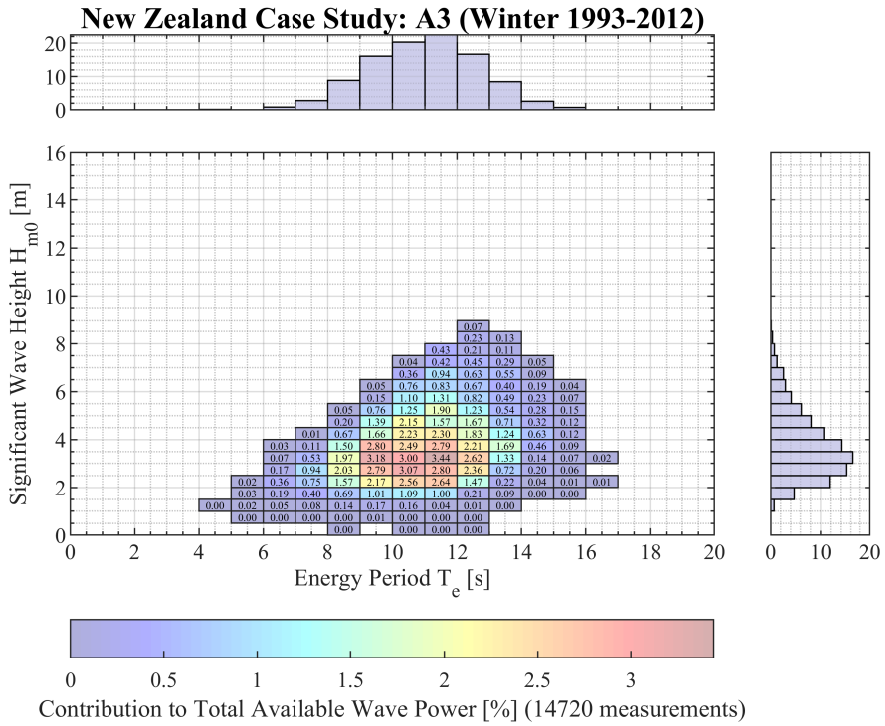

Figure 4.28. Percentage contribution of each sea state to the total available P_{wave} at A3 for a (a) typical year and (b) typical winter.

(a)

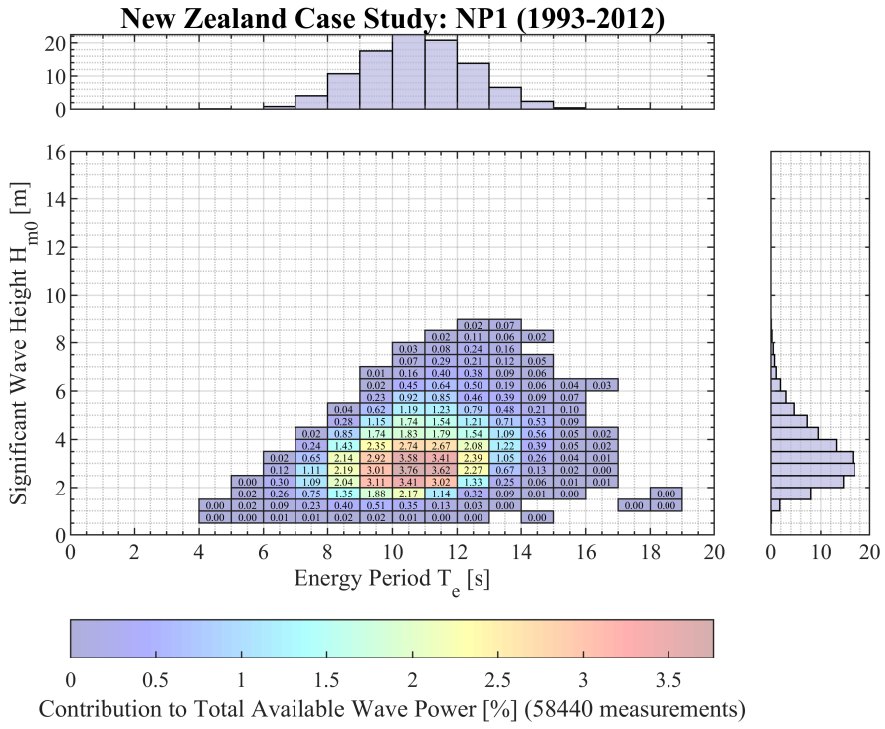

(b)

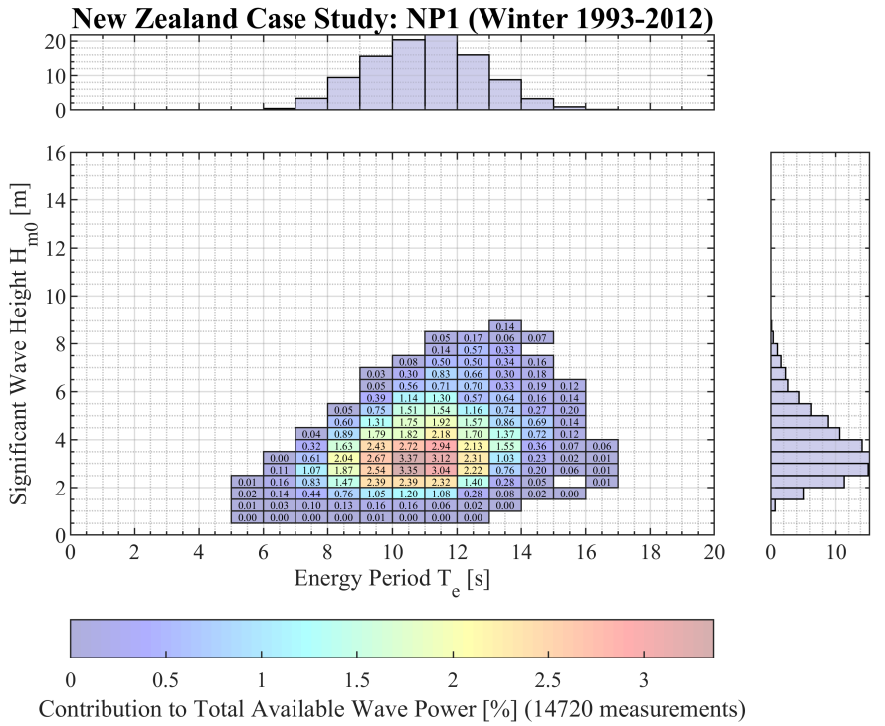

Figure 4.29. Percentage contribution of each sea state to the total available P_{wave} at NP1 for a (a) typical year and (b) typical winter.

(a)

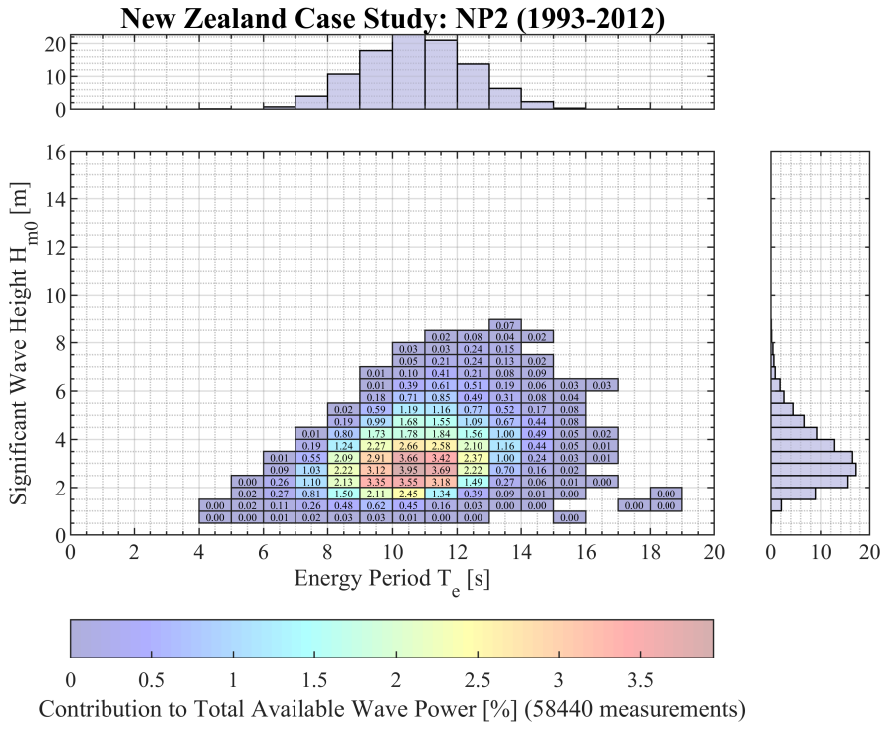

(b)

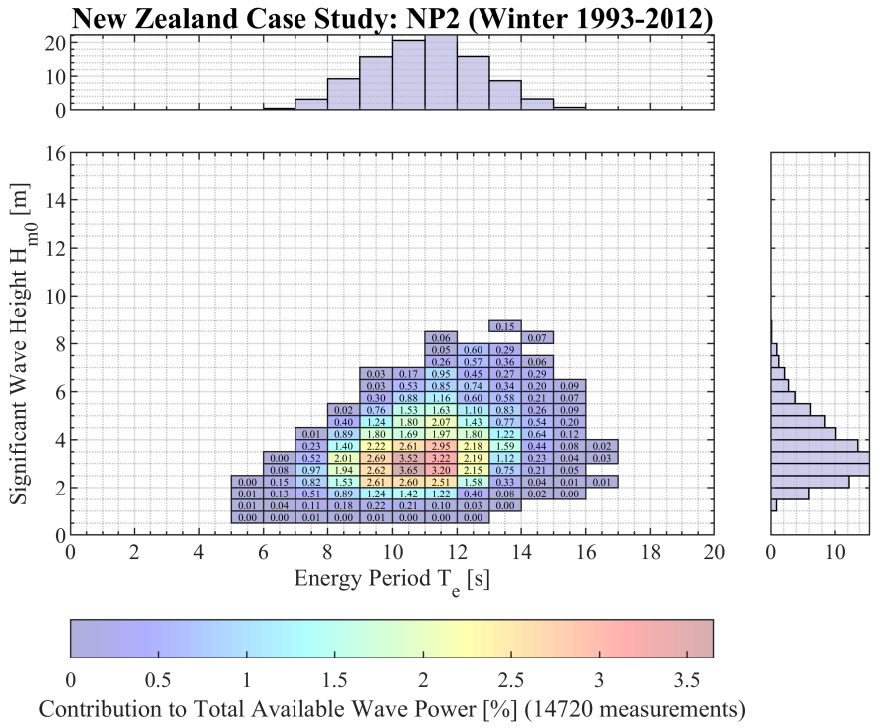

Figure 4.30. Percentage contribution of each sea state to the total available P_{wave} at NP2 for a (a) typical year and (b) typical winter.

(a)

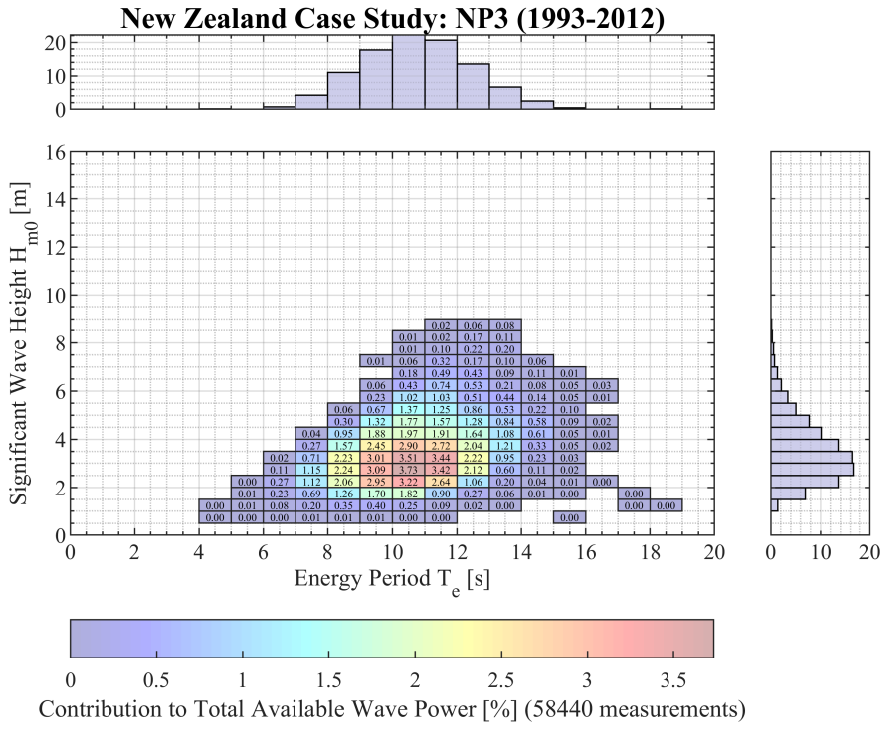

(b)

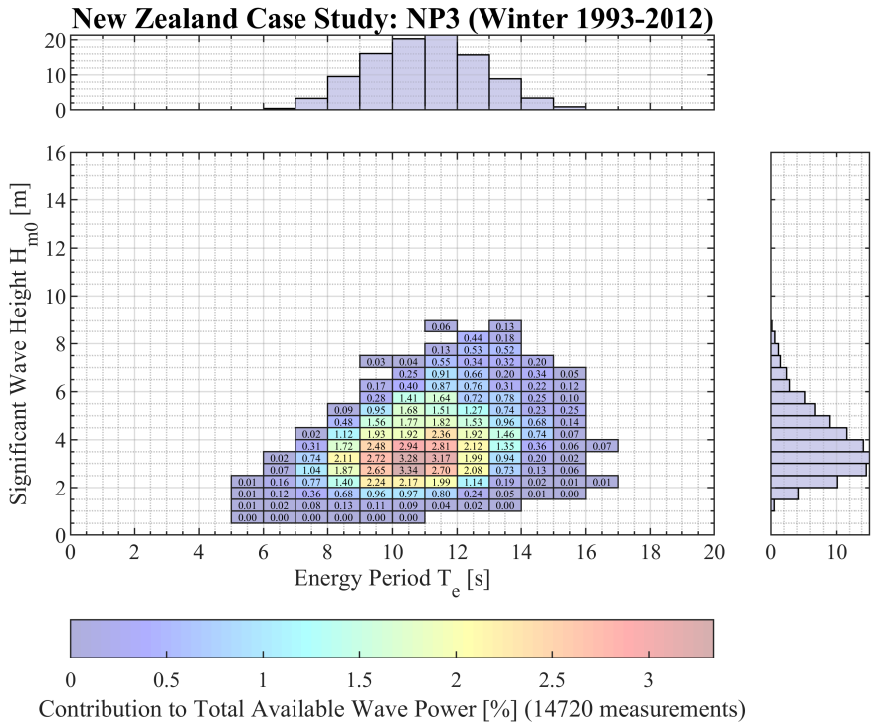

Figure 4.31. Percentage contribution of each sea state to the total available P_{wave} at NP3 for a (a) typical year and (b) typical winter.

(a)

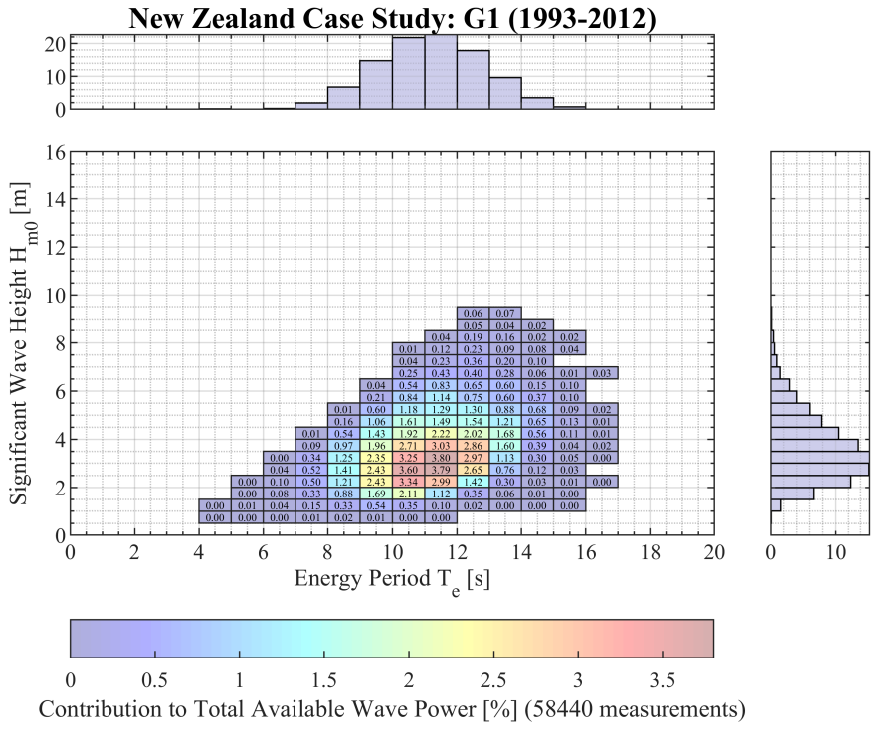

(b)

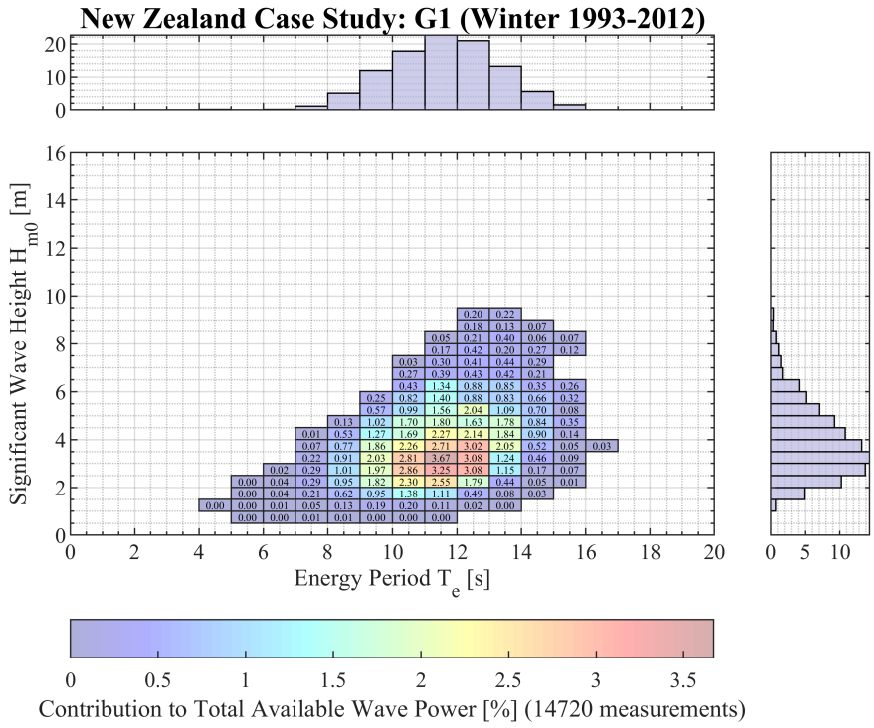

Figure 4.32. Percentage contribution of each sea state to the total available P_{wave} at G1 for a (a) typical year and (b) typical winter.

(a)

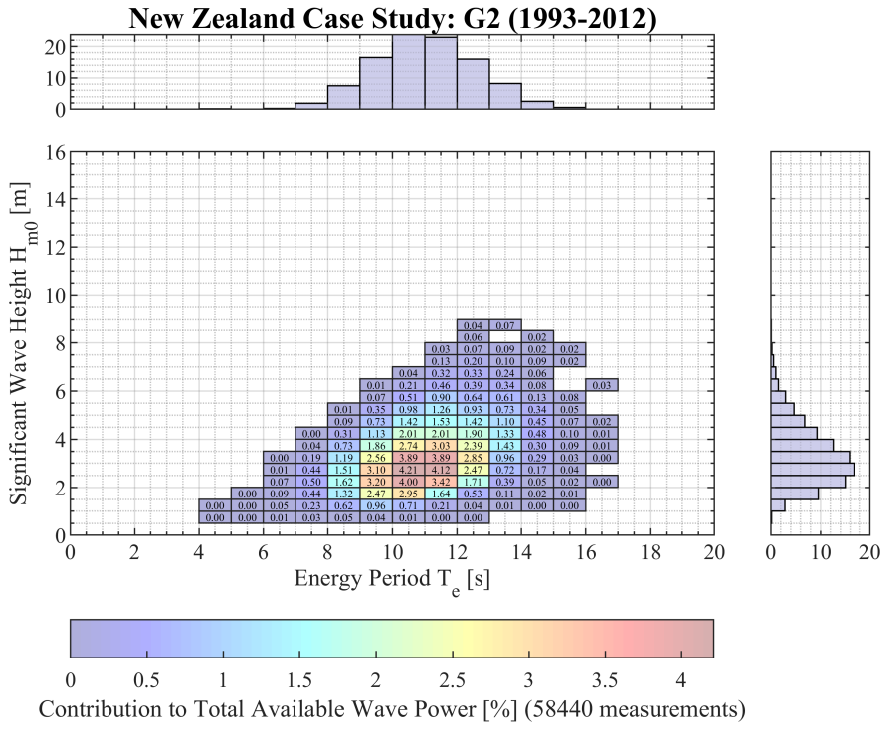

(b)

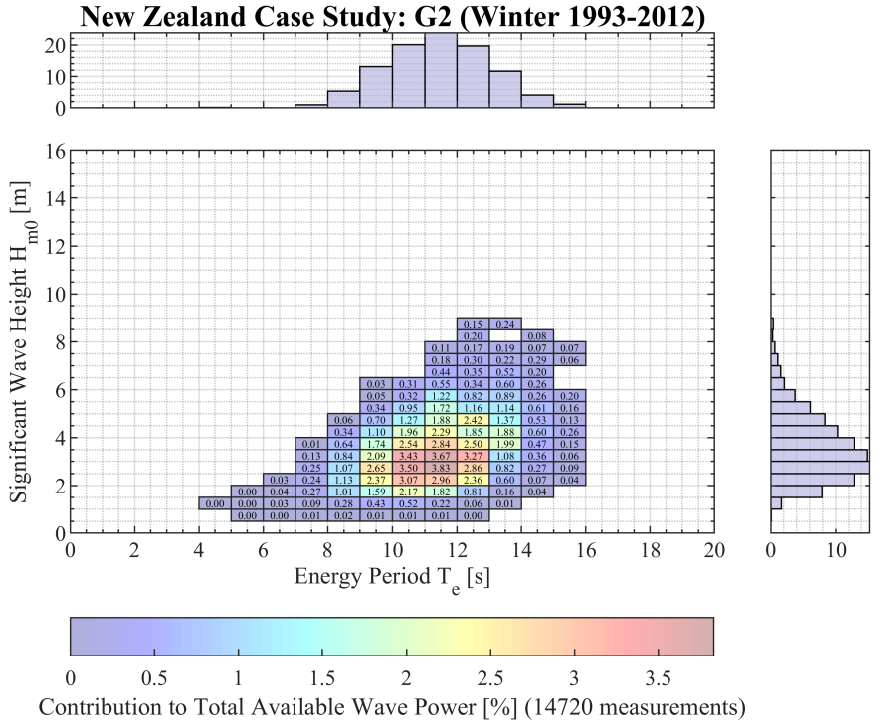

Figure 4.33. Percentage contribution of each sea state to the total available P_{wave} at G2 for a (a) typical year and (b) typical winter.

(a)

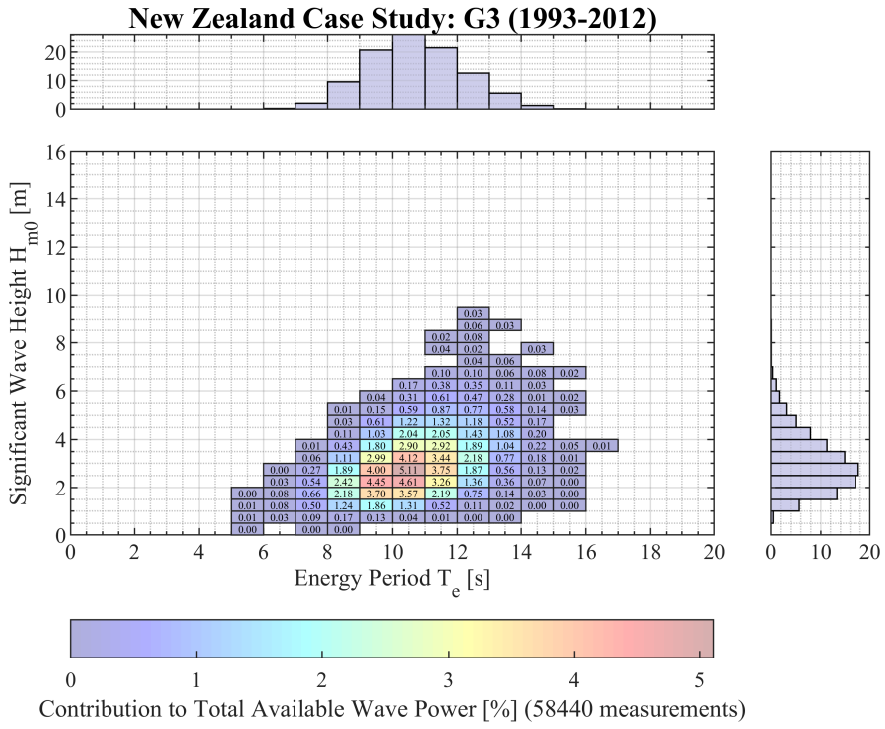

(b)

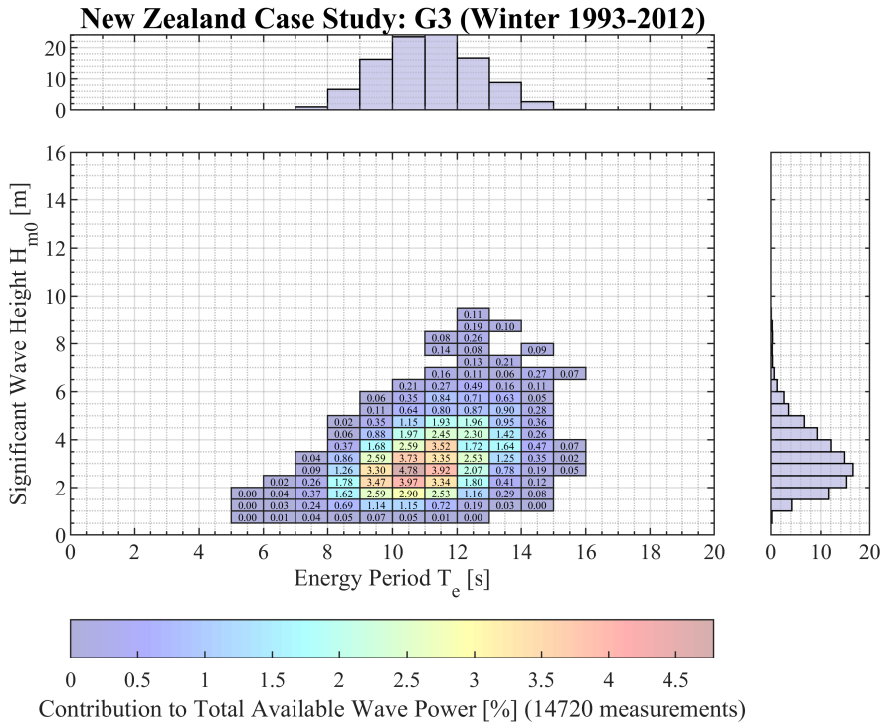

Figure 4.34. Percentage contribution of each sea state to the total available P_{wave} at G3 for a (a) typical year and (b) typical winter.

(a)

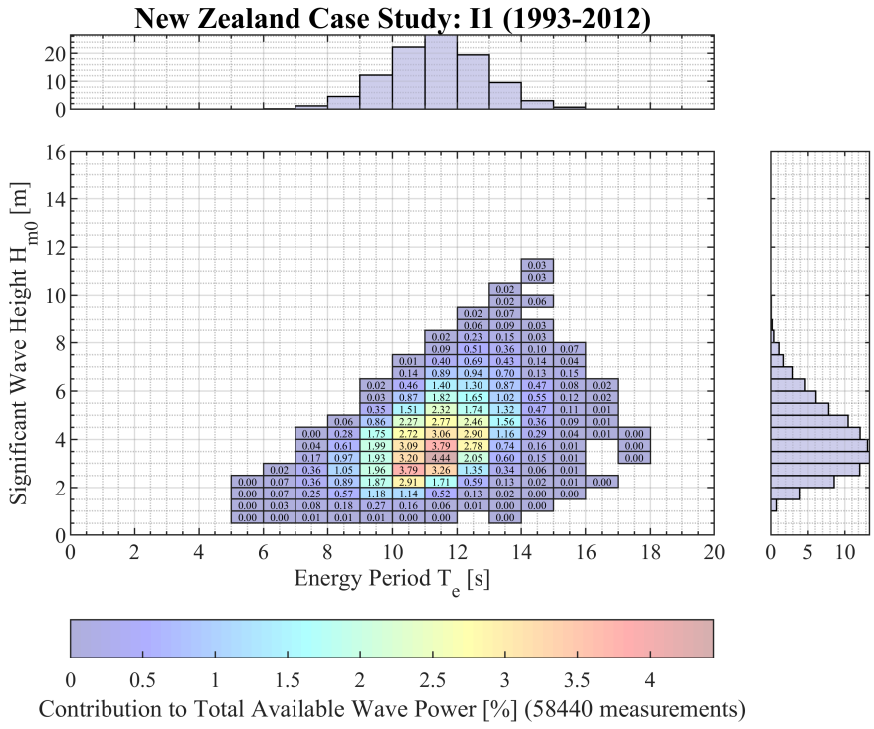

(b)

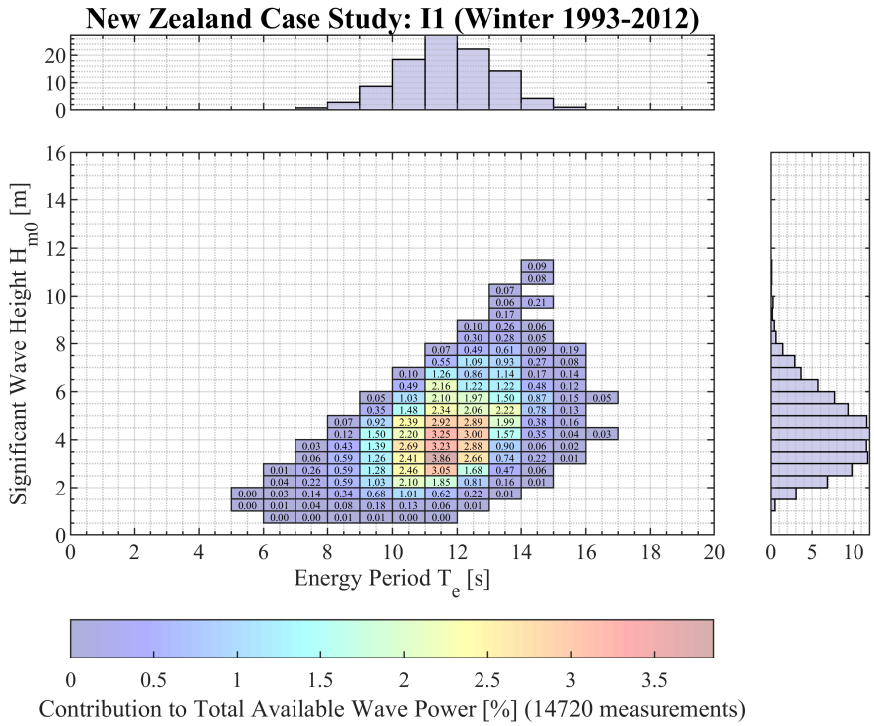

Figure 4.35. Percentage contribution of each sea state to the total available P_{wave} at I1 for a (a) typical year and (b) typical winter.

(a)

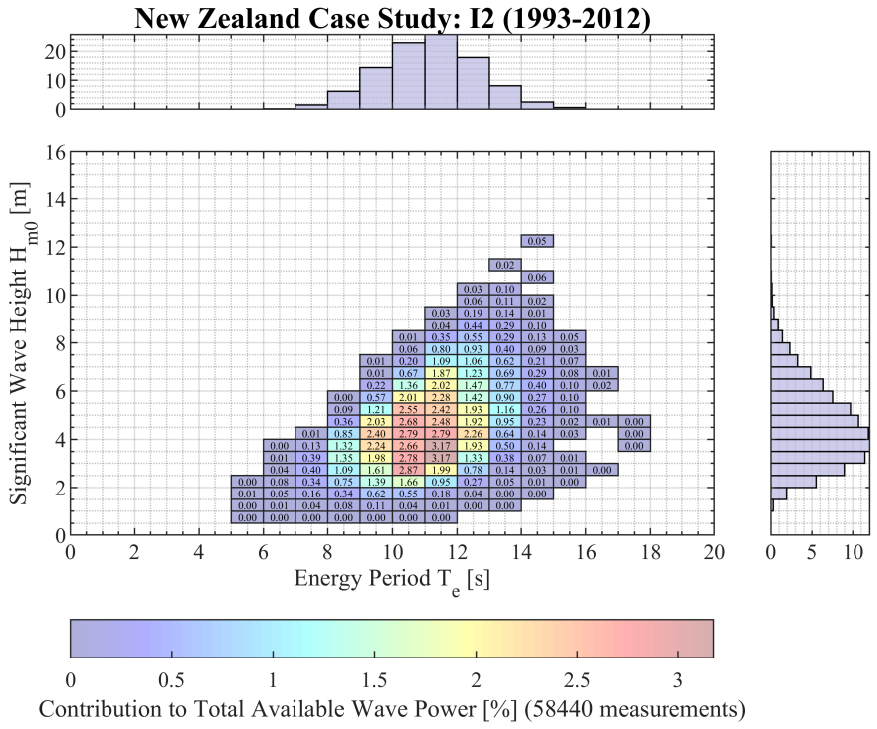

(b)

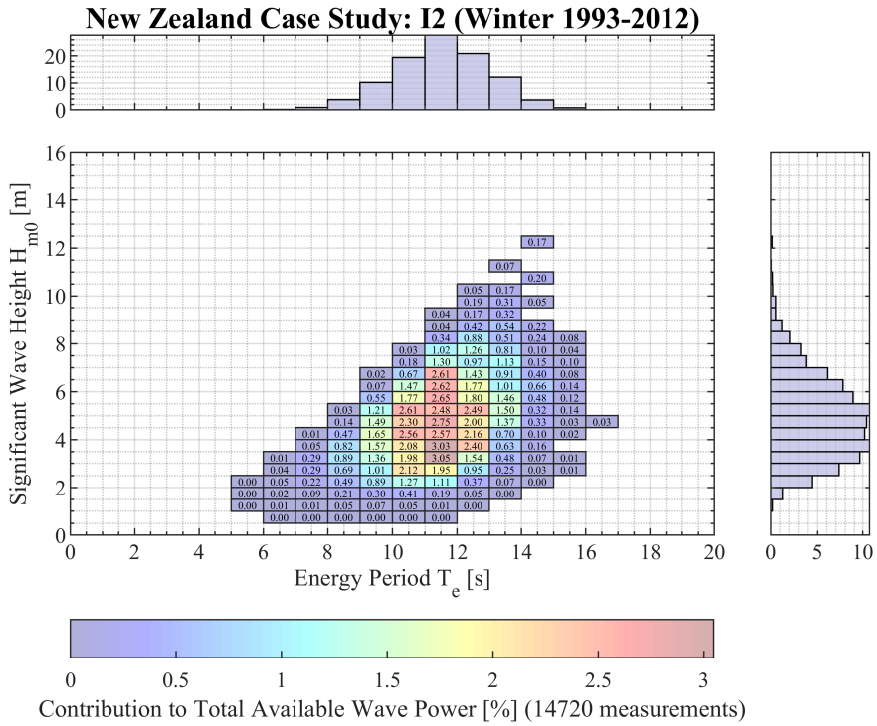

Figure 4.36. Percentage contribution of each sea state to the total available P_{wave} at I2 for a (a) typical year and (b) typical winter.

(a)

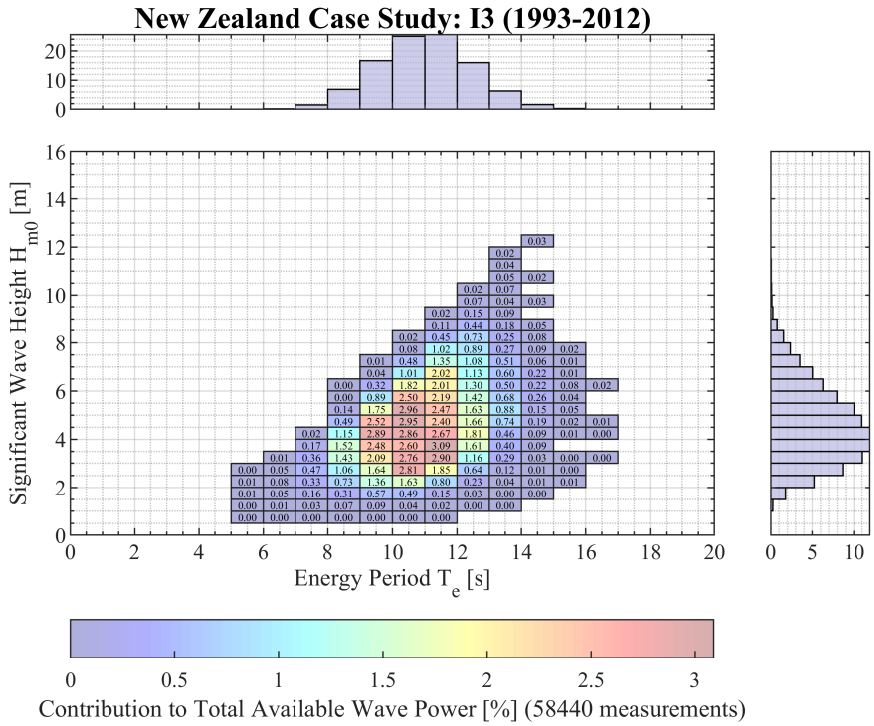

(b)

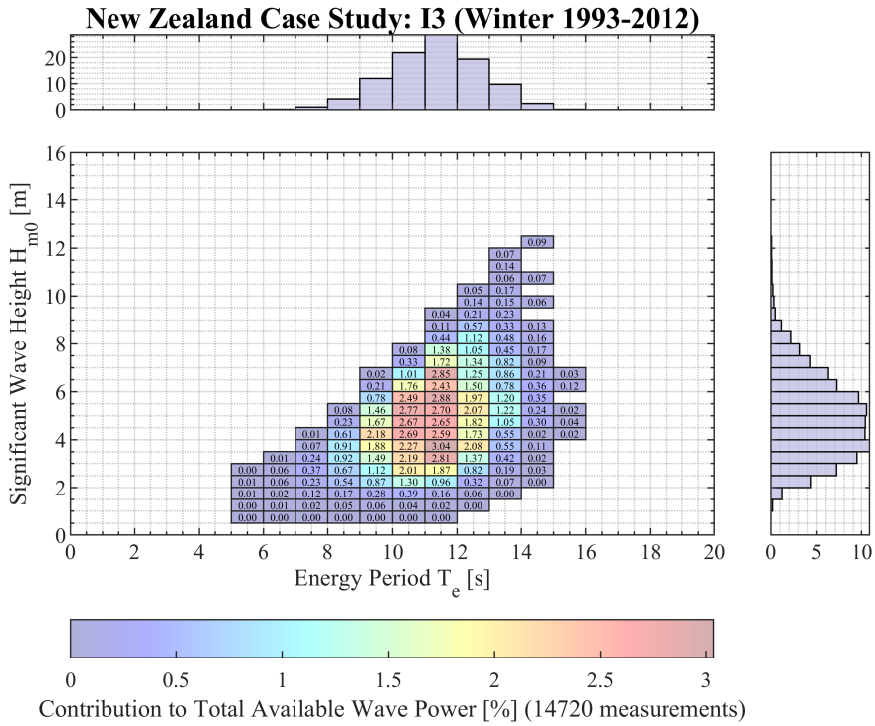

Figure 4.37. Percentage contribution of each sea state to the total available P_{wave} at I3 for a (a) typical year and (b) typical winter.

Therefore, at each location, there exists two significant clusters of sea states: the wave conditions that occur most frequently and the wave conditions which have the greatest contribution to the available resource. Both sets of sea states are important to developers, as the former is used to quantify the amount of power that can be produced by a WEC, whilst the latter can be used to optimise the performance of the device [205]. The adapted plots can also aid developers in selecting the most optimal locations for the deployment of their technology.

Table 4.6. The annual and wintertime sea states (with the corresponding percentage of occurrence) which contribute the greatest to the total wave power at each of the locations, at both timescales. The percentage contribution of calm and extreme sea states to the total wave power is also included.

Site	H_{m0} [m]		T_e [s]		Calm [%]		Extreme [%]	
	Year	Winter	Year	Winter	Year	Winter	Year	Winter
A1	1.5–5 (86 %)	2–5.5 (83 %)	8–13 (85 %)	8–13 (83 %)	0.00	0.00	0.29	0.41
A2	1.5–5 (87 %)	2–5.5 (83 %)	8–13 (86 %)	8–13 (84 %)	0.00	0.00	0.22	0.30
A3	1.5–5 (86 %)	2–5.5 (82 %)	8–13 (86 %)	8–13 (84 %)	0.00	0.00	0.30	0.43
NP1	1.5–5 (86 %)	2–5.5 (82 %)	8–13 (85 %)	8–13 (83 %)	0.00	0.00	0.30	0.50
NP2	1.5–5 (87 %)	2–5.5 (82 %)	8–13 (86 %)	8–13 (84 %)	0.00	0.00	0.23	0.28
NP3	1.5–5 (85 %)	2–5.5 (81 %)	8–13 (85 %)	8–13 (83 %)	0.00	0.00	0.48	0.81
G1	1.5–5 (82 %)	2–6 (84 %)	8–13 (84 %)	9–14 (86 %)	0.00	0.00	0.68	1.58
G2	1.5–5 (86 %)	1.5–5.5 (89 %)	8–13 (87 %)	9–14 (88 %)	0.00	0.00	0.20	0.65
G3	1.5–5 (87 %)	1.5–5 (86 %)	8–13 (91 %)	9–14 (89 %)	0.00	0.00	0.22	0.74
I1	2–6 (84 %)	2–6 (81 %)	8–13 (85 %)	9–14 (91 %)	0.00	0.00	0.86	1.73
I2	2–6.5 (84 %)	2.5–7 (82 %)	8–13 (87 %)	9–14 (91 %)	0.00	0.00	3.08	5.02
I3	2–6.5 (84 %)	2.5–7 (82 %)	8–13 (90 %)	9–14 (92 %)	0.00	0.00	2.96	4.83

Wave-Power Matrix

As the H_{m0} and T_e values from each site, across the different timescales, have been summarised into resource-characterisation matrices, it would be more convenient and cost-effective to translate these tables directly into values of mean P_{wave} [178]. However, there are disadvantages with this method in comparison with calculating the mean P_{wave}

directly from the 3-h sea states obtained from the NZ Wave Data Tool; the approach undertaken in Stage 2.1: Resource Quantification (Section 4.2.2).

Firstly, the sea-states can vary considerably within a single bin in the resource-characterisation matrix, depending on the resolution of the table, especially for the bins indexed by small values of H_{m0} [61]. Secondly, rounding errors are introduced in the wave-power matrix as the theoretical power in each cell is derived from a single H_{m0} and T_e value, which are considered representative for the range of values ascribed to that bin [50, 93, 178]. Therefore, to reduce the error associated with this method, a higher resolution was used for the H_{m0} intervals (increments of 0.5) compared to that utilised for the T_e intervals (increments of 1).

The implementation of this approach required the development of a table that contained the theoretical P_{wave} for each H_{m0}-T_e combination (Figure 4.38). For a particular sea state, the theoretical P_{wave} was computed by utilising Equation (4.2), where the values of H_{m0} and T_e corresponded with the centre of the bin being analysed. This table was multiplied by the resource-characterisation matrix (Figure 4.39), resulting in a wave-power matrix (Figure 4.40) containing the contribution of each sea state to the mean P_{wave} [86, 206].

H_{mo} [m] \ T_e [s]	0	1	2	3	4	5	6	7	8	9	10	11	12	13	14	15	16	17	18	19	20
16																	60.78	182.33	303.88	425.43	546.98
15																	56.98	170.93	284.89	398.84	512.80
14																	53.30	159.91	266.51	373.12	479.73
13																	49.75	149.25	248.75	348.25	447.75
12																	46.32	138.96	231.60	324.24	416.88
11																	43.01	129.04	215.06	301.09	387.12
10																	39.83	119.48	199.14	278.79	358.45
9																	36.77	110.30	183.83	257.36	330.89
8																	33.83	101.48	169.13	236.78	304.43
7																	31.01	93.02	155.04	217.05	279.07
6																	28.31	84.94	141.56	198.19	254.82
5																	25.74	77.22	128.70	180.18	231.66
4																	23.29	69.87	116.45	163.03	209.61
3																	20.96	62.89	104.81	146.74	188.67
2																	18.76	56.27	93.79	131.30	168.82
1																	16.68	50.03	83.38	116.73	150.08
0																	14.72	44.15	73.58	103.01	132.44
																	12.88	38.63	64.39	90.14	115.90
																	11.16	33.49	55.81	78.14	100.47
																	9.57	28.71	47.85	66.99	86.13
																	8.10	24.30	40.50	56.70	72.90
																	6.75	20.26	33.76	47.27	60.78
																	5.53	16.58	27.64	38.69	49.75
																	4.43	13.28	22.13	30.98	39.83
																	3.45	10.34	17.23	24.12	31.01
																	2.59	7.76	12.94	18.11	23.29
																	1.85	5.56	9.26	12.97	16.68
																	1.24	3.72	6.20	8.68	11.16
																	0.75	2.25	3.75	5.25	6.75
																	0.38	1.15	1.91	2.68	3.45
																	0.14	0.41	0.69	0.96	1.24
																	0.02	0.05	0.08	0.11	0.14

H_{mo} [m] \ T_e [s]	22	23	24	25	26	27	28	29	30	31	32	33	34	35	36	37	38	39	40	41	42
16	1640.93	1762.48	1884.03	2005.59	2127.14	2248.69	2370.24														
15	1538.40	1652.36	1766.31	1880.27	1994.22	2108.18	2222.13														
14	1439.18	1545.78	1652.39	1758.99	1865.60	1972.20	2078.81														
13	1343.26	1442.76	1542.26	1641.76	1741.26	1840.76	1940.26														
12	1250.65	1343.29	1435.93	1528.57	1621.21	1713.85	1806.49														
11	1161.35	1247.37	1333.40	1419.42	1505.45	1591.47	1677.50														
10	1075.35	1155.01	1234.66	1314.32	1393.97	1473.63	1553.28														
9	992.66	1066.19	1139.72	1213.26	1286.79	1360.32	1433.85														
8	913.28	980.93	1048.58	1116.24	1183.89	1251.54	1319.19														
7	837.21	899.23	961.24	1023.26	1085.27	1147.29	1209.30														
6	764.45	821.07	877.70	934.32	990.95	1047.57	1104.20														
5	694.99	746.47	797.95	849.43	900.91	952.39	1003.87														
4	628.84	675.42	722.00	768.58	815.16	861.74	908.32														
3	566.00	607.92	649.85	691.77	733.70	775.62	817.55														
2	506.46	543.98	581.49	619.01	656.52	694.04	731.55														
1	450.23	483.58	516.93	550.29	583.64	616.99	650.34														
0	397.31	426.74	456.17	485.61	515.04	544.47	573.90														
	347.70	373.46	399.21	424.97	450.72	476.48	502.23														
	301.40	323.72	346.05	368.37	390.70	413.02	435.35														
	258.40	277.54	296.68	315.82	334.96	354.10	373.24														
	218.71	234.91	251.11	267.31	283.51	299.71	315.91														
	182.33	195.83	209.34	222.84	236.35	249.85	263.36														
	149.25	160.31	171.36	182.42	193.47	204.53	215.58														
	119.48	128.33	137.18	146.04	154.89	163.74	172.59														
	93.02	99.91	106.80	113.70	120.59	127.48	134.37														
	69.87	75.05	80.22	85.40	90.57	95.75	100.92														
	50.03	53.73	57.44	61.14	64.85	68.55	72.26														
	33.49	35.97	38.45	40.93	43.41	45.89	48.37														
	20.26	21.76	23.26	24.76	26.26	27.76	29.26														
	10.34	11.10	11.87	12.63	13.40	14.16	14.93														
	3.72	4.00	4.27	4.55	4.82	5.10	5.37														
	0.41	0.44	0.47	0.51	0.54	0.57	0.60														

Figure 4.38. Theoretical P_{wave} (in kW/m) computed for each sea state by utilising Equation (4.2).

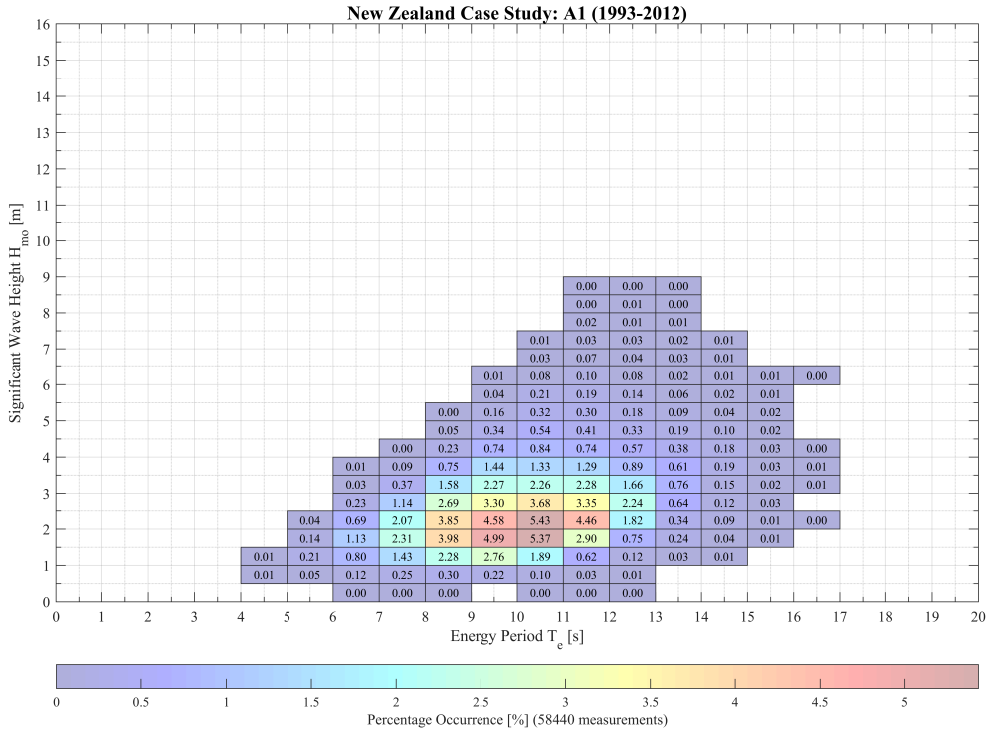

Figure 4.39. Resource-characterisation matrix depicting the probability of occurrence (%) of H_{m0} and T_e, for a typical year, at site A1 (similar to Figure 4.14(a)).

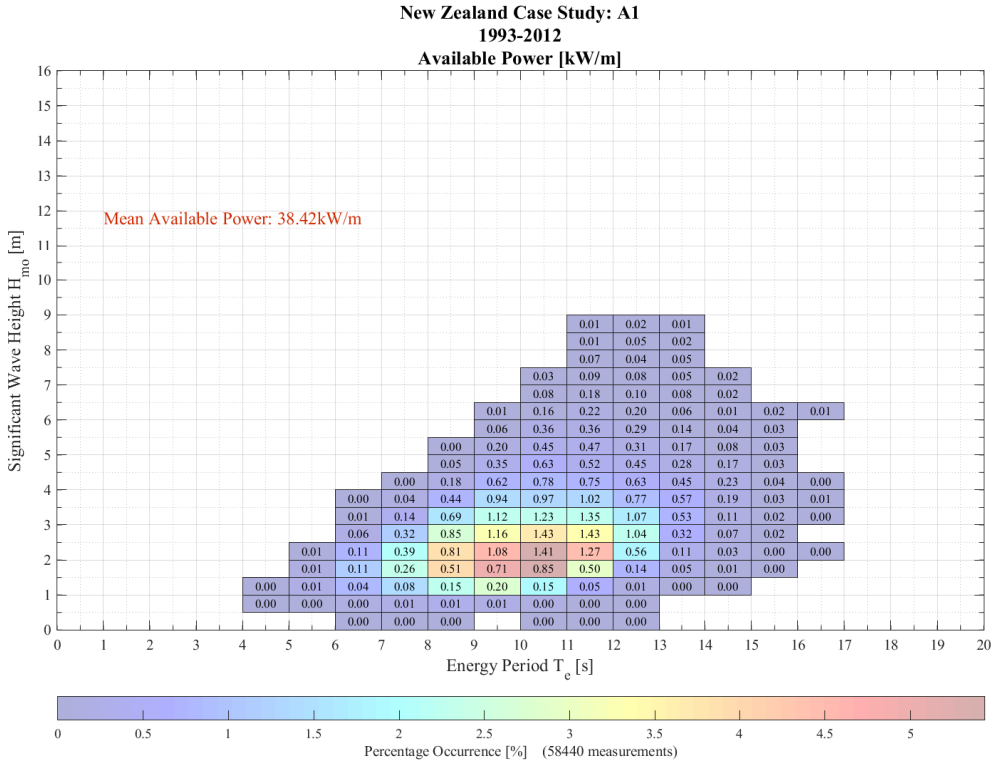

Figure 4.40. Wave-power matrix depicting the contribution of each bin (in kW/m) to the annual mean P_{wave} at site A1.

The average P_{wave} is then computed by summing the entries in the wave-power matrix:

$$Average\ P_{wave} = \frac{1}{100}\sum_{i=1}^{n_H}\sum_{j=1}^{n_V} P_{occ,ij}P_{T,ij} \tag{4.21}$$

where $P_{occ,ij}$ indicates the percentage occurrence of the $H_{m0}-T_e$ pair that corresponds to the bin defined by row i and column j of the resource-characterisation matrix. $P_{T,ij}$ refers to the theoretical power associated with the same sea state of the wave-power matrix, while n_H and n_V refer to the number of horizontal and vertical bins, respectively.

As depicted by Figure 4.39 and Figure 4.40, this approach was demonstrated by computing the mean P_{wave} directly from site A1's resource characterisation matrix. The application of this method resulted in a mean P_{wave} of 38.42 kW/m (Figure 4.40), for a typical year, whereas the mean power production calculated directly from the 3-h sea states, for the same time and location, was 38.30 kW/m (Figure 4.9(a)); a difference of only 0.32 % (Table 4.7).

Table 4.7. Comparison of the mean P_{wave} computed (i) directly from the 3-h modelled data and (ii) from the resource-characterisation matrix, at each site for typical timescales (monthly, seasonal and yearly).

	Percentage Error [%]												
	A1	**A2**	**A3**	**NP1**	**NP2**	**NP3**	**G1**	**G2**	**G3**	**I1**	**I2**	**I3**	**Average**
Jan	0.29	0.29	0.36	0.29	0.26	0.29	0.61	0.39	0.14	0.19	0.26	0.30	**0.31**
Feb	0.87	0.71	0.63	0.26	0.40	0.13	0.56	0.44	0.74	0.38	0.28	0.38	**0.48**
Mar	0.04	0.37	0.20	0.31	0.28	0.23	0.20	0.37	0.35	0.27	0.25	0.08	**0.24**
Apr	0.81	0.35	0.42	0.10	0.54	0.26	0.14	0.54	0.40	0.37	0.09	0.03	**0.30**
May	0.24	0.13	0.26	0.38	0.24	0.34	0.22	0.50	0.66	0.12	0.24	0.27	**0.30**
Jun	0.06	0.22	0.06	0.11	0.34	0.29	0.05	0.05	0.29	0.32	0.10	0.13	**0.16**
Jul	0.21	0.00	0.13	0.26	0.09	0.24	0.33	0.33	0.55	0.13	0.50	0.13	**0.24**
Aug	0.44	0.32	0.43	0.28	0.46	0.18	0.10	0.46	0.32	0.07	0.23	0.12	**0.24**
Sep	0.30	0.19	0.20	0.05	0.26	0.04	0.30	0.05	0.03	0.13	0.01	0.25	**0.15**
Oct	0.45	0.44	0.41	0.10	0.24	0.04	0.08	0.37	0.24	0.20	0.17	0.21	**0.25**
Nov	0.20	0.32	0.21	0.28	0.23	0.11	0.57	0.01	0.62	0.37	0.02	0.11	**0.25**
Dec	0.40	0.48	0.42	0.82	0.73	0.38	0.12	0.67	0.20	0.44	0.20	0.19	**0.42**
Summer	0.57	0.56	0.53	0.52	0.51	0.36	0.53	0.55	0.37	0.39	0.25	0.27	**0.45**
Autumn	0.36	0.26	0.29	0.28	0.34	0.28	0.10	0.48	0.49	0.24	0.14	0.14	**0.28**
Winter	0.19	0.18	0.21	0.21	0.30	0.24	0.08	0.28	0.38	0.13	0.27	0.04	**0.21**
Spring	0.33	0.32	0.28	0.13	0.24	0.06	0.29	0.15	0.26	0.22	0.06	0.20	**0.21**
Yearly	**0.32**	**0.28**	**0.29**	**0.25**	**0.32**	**0.20**	**0.20**	**0.33**	**0.37**	**0.22**	**0.17**	**0.15**	0.26

Furthermore, it can be clearly seen from Table 4.7 that the error associated with calculating the mean P_{wave} directly from the resource-characterisation matrix is minimal;

less than 0.3 % on average, per timescale, with the exception of summer (the least energetic season) and the corresponding summer months (December, January, and February). The slight increase in error for the summer months is to be expected because summer is characterised by smaller H_{m0}'s, which occur more often, and as previously stated sea-states can vary significantly in the bins containing small H_{m0} values. This is especially true for the interval that defines a calm sea state (H_{m0} between 0 m and 0.5 m), which has a potential 25:1 variation in wave power for the range of H_{m0} values contained within that bin.

It should also be noted that calculating the mean P_{wave} by utilising the wave-power matrix results in a slight overprediction of the wave resource; 0.3 % on average, per timescale, with the exception of summer (0.45 %) and the corresponding summer months (~0.40 %). However, this slight overprediction is balanced by the slight underprediction of the power due to the modelled data (Section 4.3.2).

The results pertaining to the Resource-Characterisation Matrix, the Sea State Contribution to Wave Power, and Wave-Power Matrix sections were obtained from the following scripts that were developed by the author: Main_Export_Scatter_Data_V4.m (Appendix A.2.3), and Main_Export_Hist_and_Scatter.m (Appendix A.2.5).

4.4 Conclusions

A site assessment procedure has been developed and demonstrated using an NZ case study in this chapter. This approach was comprised of three main sub-stages, which were implemented by utilising 20 years (January 1993–December 2012) of hindcast data, which were validated against 36 months of wave buoy measurements.

The first sub-stage quantified the available resource at three different timescales (yearly, seasonal and monthly) for the 12 sites that were identified as suitable WEF locations in NZ. It was observed that the available resource at all the sites was subjected to both spatial and temporal variability. In terms of spatial variability, two main areas containing different wave energy distributions were discernible: a higher-energy area comprising the south of NZ with the highest annual average P_{wave} occurring at I3 (71.7 kW/m); and an intermediate-energy area along NZ's west coast with the lowest annual average P_{wave} occurring at G3 (27.6 kW/m).

It was also evident from the results that the resource was subjected to seasonal variability at each of the sites, with a maximum and minimum P_{wave} available in the winter (June, July, and August) and summer (December, January, and February) months, respectively.

The second sub-stage determined the magnitude of the temporal variability and the directional distribution of the available wave power. From this analysis, it was ascertained that I3 was the most optimal site with regards to temporal variability, as it contains both a strong and steady resource. Whereas A2, A3, G1, and G3 would be more favourable locations for the deployment of line absorbers, as these sites have waves propagating from a narrow band of directions.

The third and final sub-stage developed resource-characterisation matrices in order to observe the wide range of wave conditions that were experienced at each site. These matrices were then redrawn by replacing the percentage occurrence of the sea states with the percentage contribution of the sea states to the available power, which showed that the most prevalent wave conditions were not the most energy rich. Furthermore, it was demonstrated that P_{wave} could be quantified from the resource-characterisation matrix (with minimal error), which was computationally less expensive than calculating the power directly from the 3-h sea states.

Chapter 5

Stage 3: Device Selection

5.1 Introduction

A wide variety of wave energy technologies have been proposed to extract energy from the waves, and the particular characteristics of these devices are critical in quantifying the amount of energy that can be harvested [207]. Therefore, an important aspect to consider when selecting a suitable location for the deployment of a WEF is determining which WEC would be more appropriate for the particular conditions encountered at that potential site [20].

However, it is widely reported that there are over 200 WECs currently in development [208]. Hence, in order to select the most suitable WEC for a potential WEF location, an initial screening based on technology maturity should be undertaken. It should be noted that as this industry is continually evolving, the actual number of devices in development is in a constant state of flux, which has resulted in obsolete classification schemes (Section 2.3).

The aim of this chapter is, therefore, to identify all WECs that are currently in development, establish a flexible taxonomy that is able to classify both current and future technology, as well as identify appropriate metrics for evaluating and ranking devices, in terms of suitability, at potential WEF sites.

5.2 Methodology

The proposed device selection methodology was comprised of three main sub-stages: Stage 3.1: WEC Identification, Stage 3.2: WEC Classification, and Stage 3.3: Site Matching. The first sub-stage identified all WECs currently in development, which were then further classified according to five proposed main categories in the second sub-stage. Whereas the third and final sub-stage utilised an advanced technical maturity to reduce the number of devices identified in the first sub-stage, and then discussed which techno-economic metrics would be appropriate for the evaluation of the WEC's performance, and therefore, its suitability for potential WEF locations.

5.2.1 Stage 3.1: WEC Identification

In order to select the most appropriate device for potential WEF locations, all the WECs currently under development had to be identified. Technologies that utilise ocean waves to generate electricity, desalinate seawater, pump or heat water, propel ships [42], and produce liquid fuel [209] have been proposed in the literature, patented and developed in industry. However, for the purpose of this study, only devices that generate electricity were considered.

Therefore, this stage required the development of a database, which was created by combining the relevant information available on the European Marine Energy Centre [208], Open Energy Information [210], and Open Wave Energy Project [211] websites. Only the developer's name, location, and device(s) were recorded. However, once this initial database was compiled then each company was investigated further to ensure that they were actively developing a WEC. This required the status of the company to be determined (active, dissolved, etc. —not possible for all countries), as well as undertaking a review of the developer's website and social media platforms (Twitter, Facebook, LinkedIn, and YouTube). An Excel spreadsheet was utilised to collate all this information.

For companies that had little to no online footprint, the relevant patents, journal publications, and online newspaper articles were examined. If the aforementioned methods could not be applied, then the WEC developers were emailed directly. Developers were considered 'inactive' if they did not respond, no explicit information could be found regarding the status of the device/developer, and/or social media platforms and websites had not been updated within the last five years.

5.2.2 Stage 3.2: WEC Classification

The database was then expanded, by recording the classification of the technology, for companies that were established as actively developing a device (or devices). As stated in Section 2.3, WECs are most commonly classified according to directional alignment, location, operating principle, and PTO system. The approach proposed in this thesis utilised an adapted (and, in some cases, redefined) version of these categories with the addition of a class that described the device's maturity (Figure 5.1).

Operating Principle

The mode of energy extraction employed by a WEC is referred to as its operating principle. The methods for harvesting wave energy vary widely, which has led to an extensive range of device types that, according to Falcão [41], can be grouped into three main categories. Namely, wave-activated bodies (also referred to as oscillating bodies), overtopping devices, and OWCs.

Wave-Activated Bodies. A wave-activated device is comprised of one or more bodies, which oscillate around a reference point when subjected to the incoming waves [18]. The relative motion of the bodies to a fixed reference point (such as the sea bottom) or between the bodies themselves are utilised to extract energy from ocean waves [212]. These devices are generally located offshore, either floating or (less common) fully submerged [23].

Overtopping Device. The overtopping device is designed in such a manner that as the waves break across the structure, the seawater is collected in a storage reservoir located above the free water surface [212]. The potential energy of the stored water is then converted into electricity by utilising a low-head hydraulic turbine [23]. The main advantage of this device is its ability to produce a relatively smooth power output due to the built-in storage reservoir [24]. Whilst a key disadvantage is that a large structure is required for the reservoir [24]. These devices can be located onshore as part of a shoreline structure or offshore as floating devices [213].

Oscillating Water Column. An OWC is a partly submerged structure that contains an air chamber. This air chamber is open to the sea below the water level resulting in a volume of air being trapped above an enclosed column of water. As the waves rise and fall, the water enclosed in the chamber rises and falls [212]. This results in the trapped air being compressed (and exhausted from the chamber via a turbine) and decompressed (drawn back into the chamber via the same turbine) [212]. These devices can be located: onshore, enclosed within a fixed structure on the shoreline or within a human-made breakwater; nearshore, as a bottom-mounted structure; or offshore, as a moored floating system [23].

The review of current WECs in Stage 3.1 led to the discovery of a new class of devices, which convert wave energy directly into rotational work (in either the vertical or horizontal plane), therefore leading to the formation of the ‘Rotational Conversion System’ category. Furthermore, a ‘Pressure Differential’ category was also established in place of the OWC, as only devices that utilise a difference in air pressure are included in

the OWC class. Whereas the new pressure differential category consists of any device that uses a fluid (gas and/or liquid) pressure difference. Therefore WECs that were classified as submerged pressure differential, bulge wave [44], and membrane [45] form part of this new category.

Directional Alignment

Wave energy technologies may also be classified according to size and orientation [42]. If the device has small dimensions with respect to a typical wavelength, the WEC is called a point absorber. Whereas a large device with the longest dimension comparable to or larger than a typical wavelength is referred to as a line absorber. A line absorber is further classified as an attenuator (longest dimension aligned parallel to the prevailing wave direction) or terminator (longest dimension aligned perpendicular to the prevailing wave direction). When reviewing the devices currently in development, a new descriptor was required to define line absorbers that were neither parallel nor perpendicular to the wave propagation direction, but positioned at an angle, hence the addition of the 'Angled' sub-category.

Device Maturity

Given the nascent state of the ocean wave energy sector, the addition of a category that specifies the maturity of devices in development will provide insight into the global market status as well as identify WECs that are near or at commercialisation. This category was primarily based on the TRLs proposed by ESBI and Vattenfall (Figure 2.1) [39], which have been integrated into a seven-stage developmental plan. The inclusion of two additional stages accounts for yet-to-be-proven device ideas/concepts ('Stage 0'-TRL 1) and commercially viable technology ('Stage 6'-TRL 9). Devices identified as being at Stage 0 were not included in the database.

TPLs were not incorporated into this category as this metric is not yet widely implemented (or even known), and funding opportunities, as well as the commercial ability of WECs, are currently defined in terms of TRLs [104]. However, funding agencies such as the USA's Department of Energy are transitioning towards a more holistic evaluation process, which would include incorporating performance indicators such as TPLs [214]. Therefore, once TPLs become more commonplace in this industry, the Device Maturity category will be expanded to include this metric.

PTO System

The mechanism which converts energy harvested from ocean waves into useable electricity is referred to as the PTO system. The PTO system is of great importance as it affects the power conversion efficiency of the device, thereby impacting its economic performance. A number of PTO systems exist; however, for this category, seven main types, five of which were identified by Têtu [215], have been incorporated into the four general energy conversion mechanisms (electrical, pneumatic, mechanical, and hydraulic) proposed by Falnes [42]. The addition of the sixth and the seventh PTO takes into account the 'Piezoelectric Material' utilised by the technology formerly referred to as bulge wave as well as the recently identified 'Pneumatic System', which is mainly comprised of a compressor and pneumatic motor.

Location

The fundamental design of the device is dependent on the installation site and resource availability at that location [213]. The intended WEC location (shoreline, nearshore, and offshore) will also determine the type of mooring system/foundations to be used. This category was based on the nomenclature proposed by the Strategic Initiative for Ocean Energy [213].

Shoreline (waves breaking at the shore). Onshore wave energy devices are constructed directly onto the shoreline or into a fixed shoreline structure (for instance, a sea defence wall or human-made breakwater) [24] and require considerable civil engineering works [213]. The advantage of these WECs is that the civil works are land-based, and therefore, cable connections are easier [24]. The disadvantage is that the energy resource available at the shoreline is greatly reduced compared to that available offshore [43]. In order to reduce the capital civil costs, it has been proposed that these onshore devices be constructed into new breakwater developments [24].

Nearshore (shallow water). Nearshore devices are constructed near the shore but outside the surf zone [24]. The depth of water at this location is approximately 20 m [24]. In the marine energy industry, this is typically referred to as shallow water [43] (as opposed to the more scientifically correct definition provided in Section 2.4.1.). These devices are usually held in place either with pinned pile foundations or gravity-based foundations and have the added benefit of short cable runs [24, 213].

The nearshore environment has the advantage of being more accessible and less severe than the offshore environment [213]. However, the advantage of working in this limited water depth can be overshadowed by civil and installation costs [24]. A further disadvantage of nearshore devices, similar to that of onshore devices, is the reduced energy resource compared to that available in the offshore environment [24].

Offshore (intermediate and deep water). Offshore floating devices are either tight- or slack-moored in intermediate and deep water depths, depending on the type and PTO system of the device [213]. (Assuming that intermediate and deep water refers to the typical design depths depicted in Figure 5.1, as opposed to the scientific definitions presented in Section 2.4.1). The advantage of the offshore environment is that the resource is undiminished [24], as the wave transformation processes that dissipate energy (Section 2.4.1) occur in the nearshore environment (shallow water) [18]. However, the depth to which device deployment can occur is restricted by the current technology and financial limitations [213].

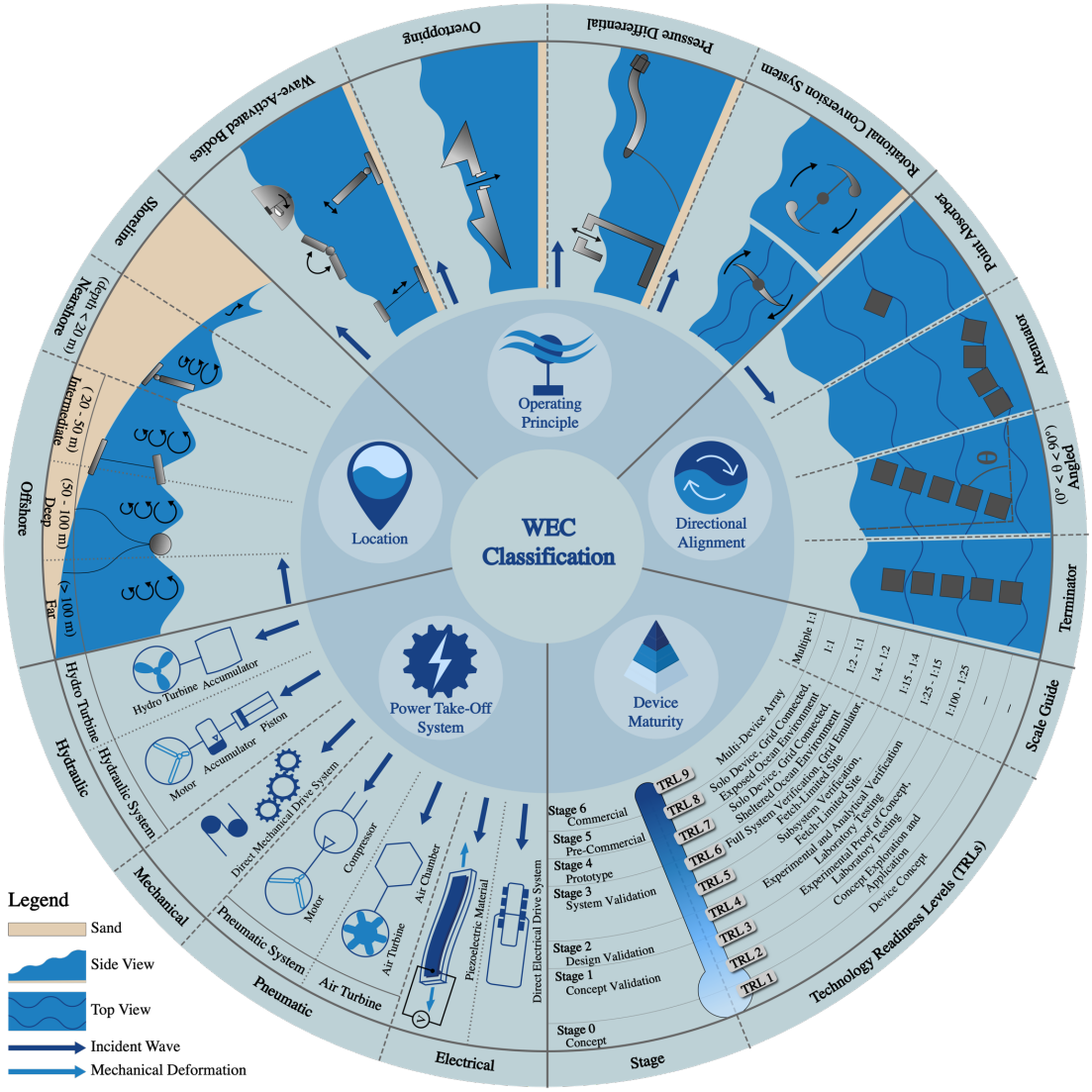

Figure 5.1. Proposed WEC classification system comprised of five main categories: Operating Principle, Directional Alignment, Device Maturity, PTO System, and Location.

5.2.3 Stage 3.3: Site Matching

Preliminary WEC Screening

Once all the relevant information had been recorded in the developer database (Stage 3.1), WECs that had reached TRL 7 (Stage 4) or above were selected for further analysis. At this TRL, the device and its subsystems (PTO and control systems, foundations and moorings, and primary mover) have been validated; energy production has been verified; and survivability has been demonstrated [39]. It should be noted that in this thesis, survivability has been defined in terms of storm survivability and operational survivability. Where storm survivability refers to the WEC's ability to avoid structural damage during extreme sea states, and operational survivability refers to the device's

ability to generate electricity over the project lifetime whilst being exposed to long-term conditions such as cumulative wave loading [216].

The devices can then be screened further once the locations of potential WEFs have been determined (shoreline, nearshore, and offshore).

WEC Assessment

As the wave energy sector is characterised by a wide range of technologies, appropriate performance metrics are required in order to compare and rank the devices. Since the ultimate objective of any power generating plant is to produce and supply electricity, an integral parameter to consider would be the average power output (P_E) of the WEC. This is dependent on its geometry, PTO, and control strategies, as well as the local wave resource [90], and is calculated as follows [85]:

$$P_E = \frac{1}{100}\sum_{i=1}^{n_H}\sum_{j=1}^{n_V} P_{occ,ij}P_{WEC,ij} \tag{5.1}$$

where $P_{WEC,ij}$ indicates the expected power output for the $H_{m0}-T_e$ pair that corresponds to the bin defined by row i and column j of the WEC's power matrix, while n_H and n_V refer to the number of horizontal and vertical bins, respectively.

However, devices vary in terms of size and rated capacity, and so, therefore, it would be more appropriate to compare normalised power performance by utilising indicators such as the Capture Width Ratio (CWR) and capacity factor (C_f).

Capture Width Ratio. This parameter represents the effectiveness of the WEC to capture the energy contained within the ocean waves [217] and is determined by [218] :

$$CWR = \frac{P_E}{BP_{Wave}} \tag{5.2}$$

where B is the characteristic dimension of the WEC (most commonly the device's width [218]).

Capacity Factor. The average usage of the WEC's installed capacity is described by the C_f [217], which corresponds to the ratio between the average electrical power generated and the rated peak power [219]. This commonly used metric is computed by [220]:

$$C_f = 100.\frac{P_E}{R_C} \tag{5.3}$$

Whilst these power performance metrics are essential in assisting in the selection of an appropriate device for a particular location, it does not include cost and so, therefore, are insufficient for evaluating the technology's investment potential [219].

LCOE (Equation (3.2)) is a well-established economic measure, which evaluates the project costs (Table 3.2) in relation to the amount of power generated during the lifetime of the WEF [104]. In addition, this metric is commonly used to compare various generation technologies, to determine the most cost-effective option [103]. Therefore, it will be used to measure the cost-performance of the selected WECs.

As the methodology compares conflicting criteria, it will be necessary to utilise multi-criteria decision-making analysis to prioritise and rank the most optimal (WEC) solutions for a proposed WEF site.

5.3 Results

5.3.1 Stage 3.1: WEC Identification

The initial database identified 272 companies that were developing a total of 295 WECs. However, once each of these companies was reviewed, this number significantly reduced to 116 companies developing a total of 130 devices—with 11 of these companies developing more than one WEC (Table 5.1).

Table 5.1. Companies that were identified as actively developing WECs.

Developer	Location	Device Name
2mike	Ukraine	Energy Absorbing Breakwater
40 South Energy	Italy	H-type
40 South Energy	Italy	R-type
Accumulated Ocean Energy, Inc. (AOE)	Canada	pneumatic WEC (pWEC)
Albatern Ltd	UK	WaveNET
Applied Technologies Company Ltd (ATC)	Russia	Float Wave Electric Power Station (FWEPS)
Aqua Power Technologies	UK	MANTA
Aqua-Magnetics, Inc. (AMI)	USA	Ocean Swell Wave Energy Conversion (OSWEC)
AquaHarmonics	USA	AquaHarmonics Wave Energy Device
Aquanet Power	Hong Kong	aquaWAVE
Aquanet Power	Hong Kong	blueWAVE
AQUSYS Corporation	Japan	Mitsui WEC
Arrecife Energy Systems	Spain	Arrecife
Atargis Energy Corporation	USA	Cycloidal Wave Energy Converter (CycWEC)

Developer	Location	Device Name
Australian Marine & Offshore Group (AMOG)	Australia	AMOG WEC
AW-Energy OY	Finland	MegaRoller
AW-Energy OY	Finland	WaveRoller
AWS Ocean Energy Ltd	UK	Archimedes Waveswing™
AWS Ocean Energy Ltd	UK	AWS-III
AWS Ocean Energy Ltd	UK	Electric Eel™
BioPower Systems Pty Ltd	Australia	bioWAVE™
Blu-tility Wave Power, Inc.	Canada	Blu-Dino™
Blue Power Energy Ltd	Ireland	BPE Buoy
Bombora Wave Power	Australia	mWave™
Brimes Energy	USA	Jellyfish
CalWave Power Technologies	USA	CalWave WEC
CalWave Power Technologies	USA	Wave Carpet
Carnegie Clean Energy Ltd	Australia	CETO
Checkmate Seaenergy Ltd	UK	Anaconda
Columbia Power Technologies, Inc. (C.Power)	USA	StingRAY
CorPower Ocean AB	Sweden	CorPower WEC
Crestwing ApS	Denmark	Crestwing
Cyan Technologies Ltd	Ireland	CyanWave WEC
Ecomerit Technologies, LLC	USA	Centipod
Earth by Design	USA	Coastal Wave Energy Capture and Conversion System
Eco Wave Power Ltd	Sweden / Israel	Eco Wave Power WEC
Embley Energy Ltd	UK	SPERBOY™
Energystics Ltd	USA	Vibristor®
Enorasy, LLC	USA	Robotic Juggler™
EnSea SRL	Italy	SWATHS
Etymol Ocean Power SpA	Chile	Etymol Alfa
Exowave ApS	Denmark	Exowave WEC
Fazzini Meccanica SNC	Italy	ECOWEC
Finima Innovations Company Ltd	Hong Kong / USA	Aimmer WEC
Float, Inc.	USA	Rho-Cee
Floating Power Plant (FPP) A/S	Denmark	P80 Commercial Platform
Fred. Olsen Ltd	Norway	BOLT Lifesaver
Geps Techno	France	IHES
Geps Techno	France	MLINER
Geps Techno	France	PH4S
Geps Techno	France	PMH
Group Captain SM Ghouse	India	Free Floating Wave Energy Convertor (FFWEC)
Gwave, LLC	USA	Power Generation Vessel (PGV)
Hann-Ocean Energy	Singapore	Drakoo
Healy Wave Energy, LLC	USA	Healy Wave Energy Convert (HWEC)
Hydro Air Concept Energie (HACE)	France	HACE WEC
Hydrocap Energy	France	Seacap
Hydrokinetic Energy, Inc.	USA	Poseidon
HydroWave AS	Norway	Havkraft Wave Energy Converter (H-WEC)
Ingine, Inc.	South Korea	INWave™

Developer	Location	Device Name
Joules Energy Efficiency Services Ltd	UK	WaveTrain
Kinetic Wave Power, LLC	USA	PowerGin™
Laminaria	Belgium	Deep water version
Laminaria	Belgium	Undeep water version
M3 Wave, LLC	USA	Delos-Reyes Morrow Pressure device (DMP)
Marine Energy Corporation (MEC)	USA	Super Watt Wave Catcher Barge©
Marine Hydroelectric Company	USA	Marine Hydroelectric Generator (MHG)
Marine Power Systems	UK	DualSub
Marine Power Systems	UK	WaveSub
Martin, Ottaway, van Hemmen & Dolan, Inc.	USA	SurfWEC
Mighty Waves Energy, LLC	USA	Mighty Waves Energy WEC
Mocean Energy Ltd	UK	Blue Horizon
NEMOS GmbH	Germany	NEMOS WEC
Neptune Energy Ltd	UK	Neptune Energy WEC
NeptuneWave.ca	Canada	Neptune Wave Engine
Northwest Energy Innovations, LLC (NWEI)	USA / NZ	Azura
Novige AB	Sweden	NoviOcean WEC
Ocean Energy Industries	USA	WaveSurfer ™
Ocean Energy Ltd	Ireland	OE Buoy
Ocean Grazer BV	Netherlands	Ocean Grazer 3.0
Ocean Harvesting Technologies	Sweden	InfinityWEC
Ocean Motion International	USA	WavePump
Ocean Power Technologies (OPT)	USA	PowerBuoy
Ocean Wave Energy Company (OWEC)	USA	OWEC WEC
Oceantec- IDOM	Spain	MARMOK-A-5
Oscilla Power, Inc. (OPI)	USA	Triton™ WEC
Paradyme Systems USA	USA	GyroGen™
Pearl Clean Energy	Australia	Duelling SPAR (D-SPAR)
Pearl Clean Energy	Australia	Pearl Island WEC
Pelagic Power AS	Norway	W2Power
Pontoon Power AS	Norway	Ponton Power Converter (PPC)
Protean Wave Technology Ltd	UK	WaveShip
Pure Marine Gen Ltd	UK	DUO WEC
Resen Waves	Denmark	Resen Waves Power Buoy
Rotary Wave SL	Spain	Butterfly Device
Rotary Wave SL	Spain	Rotary Device
RTI Wave Energy	USA	RTI F2MS
RVP1985, LLC	USA	Low Cost Multi Point WEC
RWPower AS	Norway	Wave Pump
SBM Offshore	France	S3 WEC
Sea Energies Ocean Power	Ireland	SeaEnergies WEC (SE-WEC)
Sea Power Ltd	Ireland	Seapower Platform™
Sea Wave Energy Ltd (SWEL)	UK	Waveline Magnet
Seabased AB	Norway	Seabased WEC

Developer	Location	Device Name
SeaDog Systems, Inc.	USA	SeaDog™ Pump
SeaNergy Electric Ltd	Israel	Turbo Outburst Power Buoy (TOP Buoy)
Seatricity Ltd	UK	Oceanus 2
Sigma Energy	Slovenia	Sigma WEC
SINN Power GmbH	Germany	SINN Power WEC
Slow Mill Sustainable Projects BV	Netherlands	Slow Mill
Teamwork Technology BV	Netherlands	Symphony WEC
Treadwater Energy, Inc	USA	
Vortex Wave Power Ltd	Argentina / Chile	Vortex Wave Power Converter
Wave Dragon ApS	Denmark	Wave Dragon
Wave for Energy (W4E)	Italy	IOWEC
Wave for Energy (W4E)	Italy	ISWEC
Wave Power Engineering	Australia	Wave Mill (WM)
Wave Rider Energy Pty Ltd	Australia	Wave Rider™
Wave Swell Energy Ltd	Australia	UniWave®
Waveco AS	Norway	Subwave Turbine
WaveForce Energy Ltd	Ireland	WFE Buoys
Wavenergy.it SRL	Italy	REsonant WEC (REWEC3)
Wavepiston A/S	Denmark	Wavepiston
Wavergy	USA	Wavergy WEC
Waves4Power AB	Sweden	WaveEL
Wedge Global SL	Spain	W1 WEC
Wello Oy	Finland	Penguin
Weptos A/S	Denmark	Weptos WEC
Yam Pro Energy	Israel	YPE Technology

5.3.2 Stage 3.2: WEC Classification

The majority of these devices are currently being developed specifically for the offshore ocean environment (Figure 5.2(a)). The advantage of these offshore WECs is that they can extract greater amounts of energy due to the higher energy content in deeper water waves [18]. In addition, suitable areas for wave device installation in deep water are considerably greater than the areas available for nearshore and shoreline device deployment [213], which has led to a growing market for these types of devices. However, these devices are more challenging to construct, operate and maintain and therefore, costs are significantly increased [43]. Furthermore, these devices need to be designed to survive the most extreme conditions due to the increased wave height and energy content in deep water waves. These complications have hindered their development, and as a result, almost 64 % of the WECs currently being developed for the offshore environment are only at Stage 3 or below with regards to device maturity.

Offshore devices are predominately based on the wave-activated bodies working principle [41]. This principle of operation also encompasses a broad range of WECs, that

vary from single- to multi-body systems, which can be either floating or fully submerged [41]. Therefore, as seen in Figure 5.2(b), this is currently the prevailing technology type in the ocean wave sector.

In terms of directional alignment (Figure 5.2(c)), the most common WEC currently in development is the point absorber (with a 54 % majority). This device is able to capture energy from all directions, which is usually converted by a mechanical and/or hydraulic PTO system to a linear or rotational motion to drive electrical generators [18]. Consequently, as seen in Figure 5.2(d), the most common methods of energy conversion are based on the hydraulic (hydro turbine or hydraulic system) and mechanical (direct drive system) PTO systems.

(a) Distribution of WEC locations

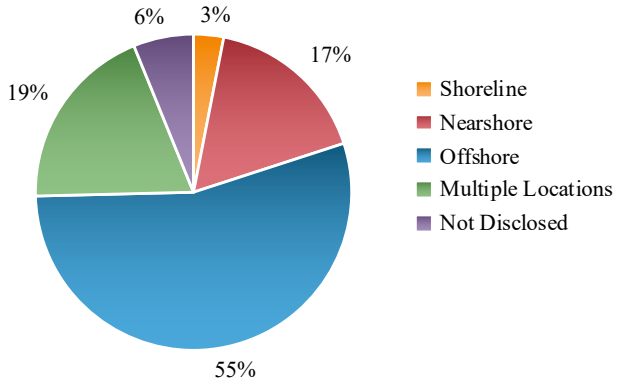

(b) Distribution of WEC operating principles

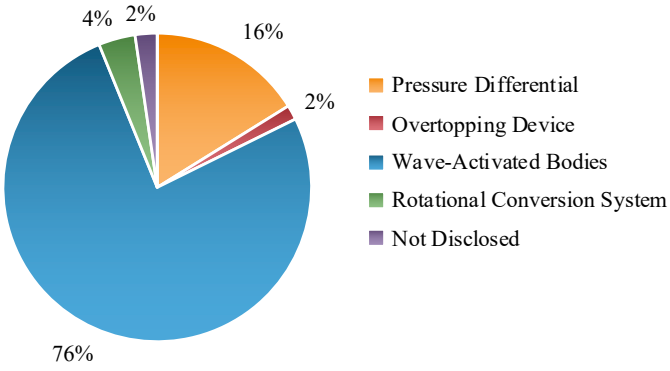

(c) Distribution of WEC directional alignments

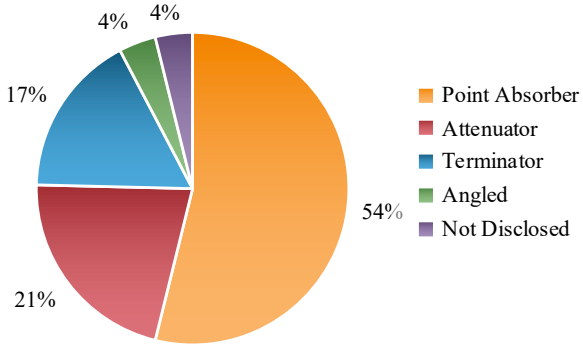

(d) Distribution of WEC PTO systems

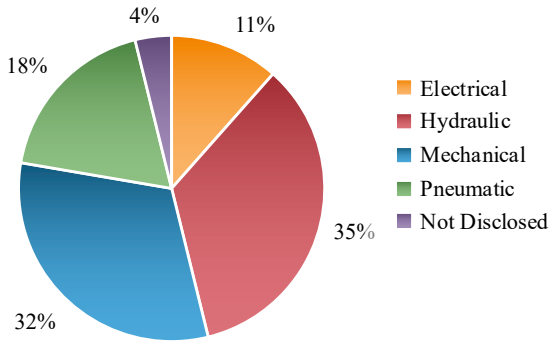

Figure 5.2. The distribution of wave energy technology, identified as active, according to four of the proposed classification categories: (a) Location; (b) Operating Principle; (c) Directional Alignment; and (d) PTO System.

The international development status of WECs, based on the proposed seven-staged approach, is depicted in Figure 5.3(a). As seen in this figure, the majority of devices (64 %) are currently only at Stage 3 (TRL 5–6) or below. This can be attributed to the exponential increase in costs associated with advancing the technology readiness of the device from Stage 3 (TRL 5–6) to Stage 4 (TRL 7), as a twofold increase in spending is expected [39]. Also, in some cases, the developer will deliberately remain at laboratory testing scale (1:100–1:15) in order to optimise the WEC's technical and economic performance, rather than devoting the resources to prematurely scaling-up the device for ocean deployment (J. Rohrer[9], personal communication, April 7, 2019).

Figure 5.3(b) also shows the global distribution of individual WEC development. As shown in this graph, the industry is currently dominated by the USA (with 33 devices) and the UK (with 15 devices), both of which have significant wave energy resources coupled with the manufacturing capability [31]. However, in terms of technology maturity, Denmark is in the lead with five devices at Stage 4 or above, followed by the UK, France, and Italy, with four devices each (also at Stage 4 or above). It should be noted that in this study, if a developer was based in two or more countries, 0.5 of the device was allocated to each of these countries.

[9] John Rohrer, President at RTI Wave Energy.

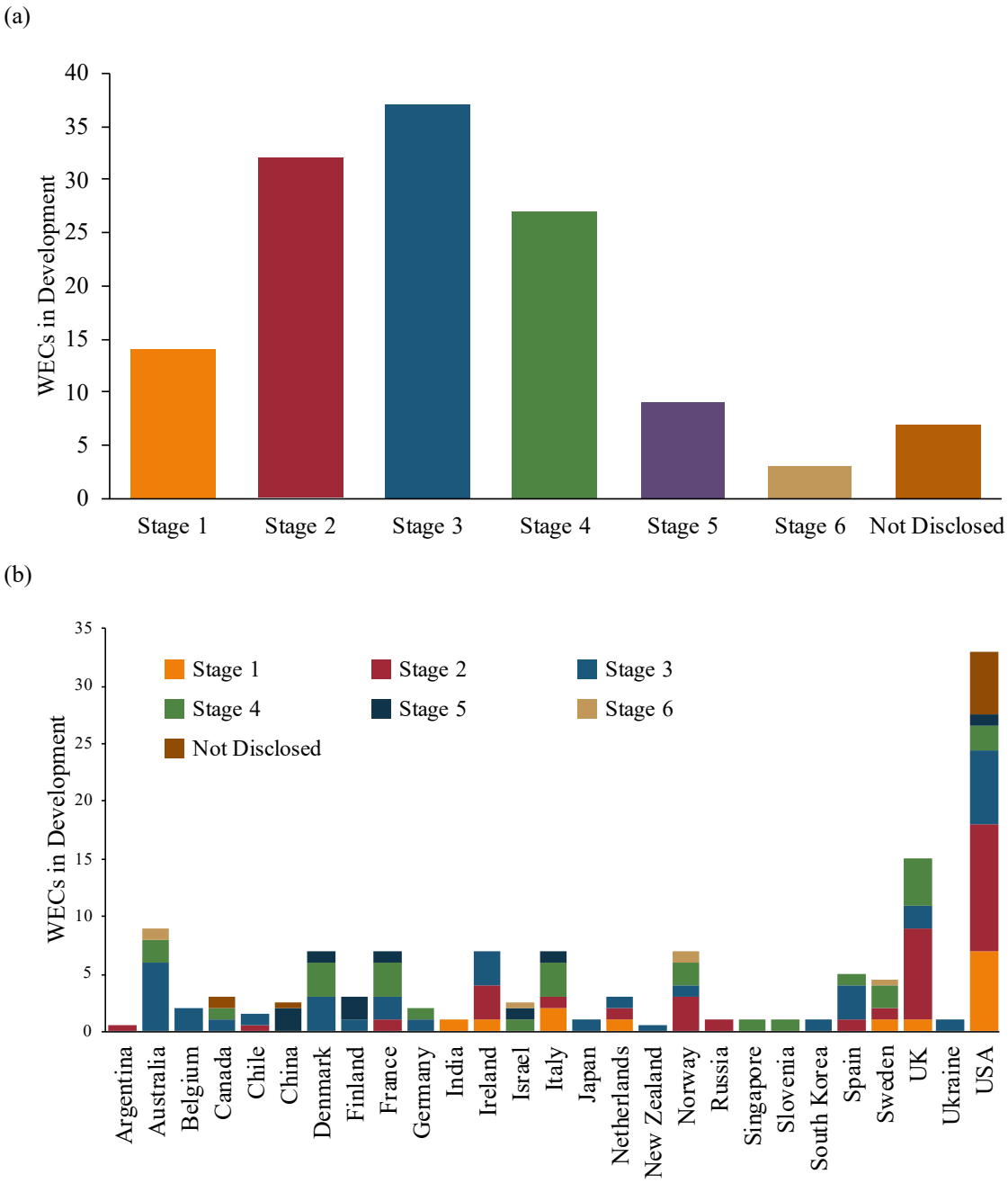

Figure 5.3. Current wave energy technology based on the (a) proposed seven-staged approach (with the exclusion of Stage 0—TRL 1), and (b) global distribution by country.

As the wave energy sector is continually evolving, it is recommended that in order to maintain the database, it should be updated continuously (at least once a year, but preferably every six months).

5.3.3 Stage 3.3: Site Matching

Preliminary WEC Screening

A total of 41 devices were identified as being at Stage 4 (TRL 7) or above from the 130 WECs currently in development. This included the Azura and WEPTOS WECs, which were between Stage 3 and 4 (TRL 6–7). The developers of these devices are predominately based in the European Union[10] (50 %), and the majority of these WECs are offshore (Figure 5.4(a)), wave-activated (Figure 5.4(b)), point absorbers (Figure 5.4(c)) that either utilise a hydraulic (42 %), or mechanical (34 %) PTO system (Figure 5.4(d)).

It should be noted that the 0 % depicted in Figure 5.4(a), Figure 5.4(b) and Figure 5.4(d) specifies that for these specific categories, the relevant information was disclosed, either directly from the developers or it was inferred from the company website (or other legitimate online sources).

(a) Distribution of WEC locations

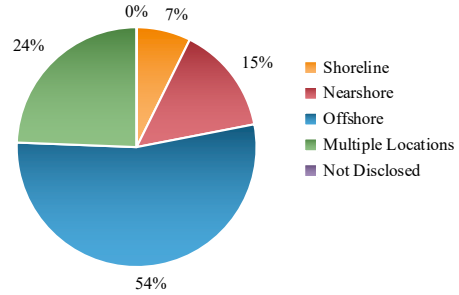

(b) Distribution of WEC operating principles

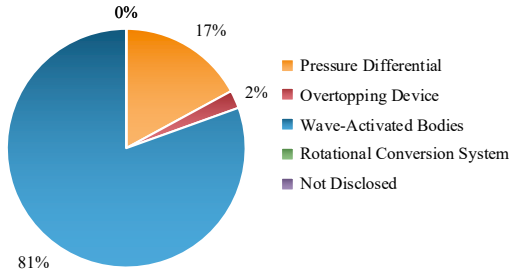

(c) Distribution of WEC directional alignments

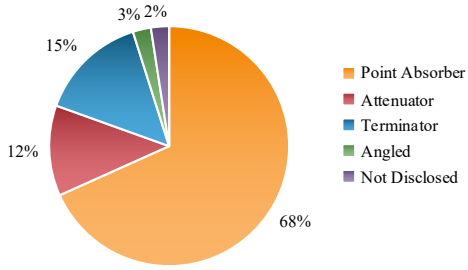

(d) Distribution of WEC PTO systems

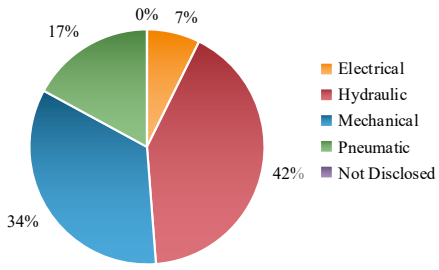

Figure 5.4. The distribution of current wave energy technology at an advanced maturity level, according to four of the proposed classification categories: (a) Location; (b) Operating Principle; (c) Directional Alignment; and (d) PTO System.

[10] As the UK withdrew from the European Union on 31 January 2020, the four UK WECs at an advanced technological maturity were not included in this percentage.

Furthermore, in terms of the NZ case study, the 12 proposed WEF sites are located in deep water (in terms of both the industry and scientific definition provided in Figure 5.1 and Section 2.4.1, respectively). Therefore, WECs considered for these specific locations would have to be able to operate in offshore conditions. This new consideration reduced the number of WECs for analysis even further, resulting in a total of 32 devices that are potentially suitable for wave energy projects in NZ (Table 5.2).

Table 5.2. Devices that are suitable for wave energy projects in NZ. The technology has been listed from least mature to most advanced.

Developer	Location	Device Name	Deployment Location	Development Stage
Northwest Energy Innovations, LLC (NWEI)	USA / NZ	Azura	Offshore	TRL 6-7
Weptos A/S	Denmark	WEPTOS WEC	Offshore	TRL 6-7
40 South Energy	Italy	R-type	Offshore	TRL 7
Albatern Ltd	UK	WaveNET	Offshore	TRL 7
Aqua Power Technologies	UK	MANTA	Nearshore / Offshore	TRL 7
Exowave ApS	Denmark	Exowave WEC	Offshore (Intermediate)	TRL 7
Geps Techno	France	IHES	Nearshore / Offshore	TRL 7
Geps Techno	France	MLINER	Nearshore / Offshore	TRL 7
Geps Techno	France	PH4S	Nearshore / Offshore	TRL 7
Hann-Ocean Energy	Singapore	Drakoo	Any Location	TRL 7
Healy Wave Energy, LLC	USA	Healy Wave Energy Convert (HWEC)	Offshore	TRL 7
Ocean Power Technologies (OPT)	USA	PowerBuoy	Offshore	TRL 7
SeaNergy Electric Ltd	Israel	Turbo Outburst Power Buoy (TOP Buoy)	Nearshore / Offshore	TRL 7
Seatricity Ltd	UK	Oceanus 2	Offshore	TRL 7
Sigma Energy	Slovenia	Sigma WEC	Offshore	TRL 7
SINN Power GmbH	Germany	SINN Power WEC	Any location	TRL 7
Wave Dragon ApS	Denmark	Wave Dragon	Offshore	TRL 7
Wave Power Engineering	Australia	Wave Mill	Nearshore / Offshore	TRL 7
Wedge Global SL	Spain	W1 WEC	Offshore	TRL 7
AWS Ocean Energy Ltd	UK	AWS-III	Offshore	TRL 7-8
CorPower Ocean AB	Sweden	CorPower WEC	Offshore	TRL 7-8
Crestwing ApS	Denmark	Crestwing	Offshore	TRL 7-8
Fred. Olsen Ltd	Norway	BOLT Lifesaver	Offshore	TRL 7-8
HydroWave AS	Norway	Havkraft Wave Energy Converter (H-WEC)	Offshore	TRL 7-8
Waves4Power AB	Sweden	WaveEL	Offshore	TRL 7-8

Developer	Location	Device Name	Deployment Location	Development Stage
Aquanet Power	Hong Kong	blueWAVE	Offshore	TRL 8
Geps Techno	France	PMH	Nearshore / Offshore	TRL 8
Ocean Energy Industries	USA	WaveSurfer™	Offshore	TRL 8
Resen Waves	Denmark	Resen Waves Power Buoy	Offshore	TRL 8
Wave for Energy (W4E)	Italy	ISWEC	Offshore	TRL 8
Wello Oy	Finland	Penguin	Nearshore / Offshore	TRL 8

WEC Assessment

In order to evaluate the devices in terms of the proposed techno-economic performance metrics, an initial Request for Information (RfI) will be sent to the developers who pass the screening process. For the NZ case study, an RfI will be sent to the companies identified in Table 5.2. This initial RfI will collect information from developers regarding the device's: power matrix, rated capacity, and dimensions. Thereafter, a second RfI will be sent to obtain details about the device's: installation site requirements (water depth, mooring type, and foundation); features (total mass and survivability mechanism); and the deployment and maintenance strategy. This is discussed further in recommended future work.

5.4 Conclusions

A device selection procedure has been developed and demonstrated in this chapter, which was comprised of three main sub-stages. The first sub-stage identified 130 WECs currently in development, whilst the second stage utilised five main categories, including a technology maturity category, to classify current and future devices in a practical and meaningful manner. As part of the third sub-stage, 41 devices were selected for further analysis based on a high technology maturity level. This number was reduced to 32 once site-specific factors for the NZ case study were taken into consideration. Thereafter, four conflicting techno-economic performance metrics were proposed to quantitatively compare and rank the WECs, which will be applied, in future work, to the 12 sites identified as being suitable for the installation of WEFs in NZ.

Chapter 6
Conclusions

An integrated site and device selection methodology has been developed and demonstrated in this thesis, which was comprised of three main stages.

The first stage implemented a robust site selection methodology that was applicable at any scale and was applied to an NZ case study. For this stage: (1) five main dimensions were utilised, which included a new cultural dimension, in order to determine the relevant site selection criteria; (2) limiting conditions were introduced to reduce the study area; (3) site selection criteria were classified as exclusion or weighted factors, and the exclusion factors were eliminated from further analysis; and (4) a SS, which represented the spatial distribution of each area's suitability for a WEF, was developed by combining the relevant weighted factors. Based on these analyses, 12 optimal WEF locations, clustered in four regions, were identified along NZ's west and south coast. Namely, offshore Auckland (North Island), New Plymouth (North Island), Greymouth (South Island), and Invercargill (South Island).

The second stage developed a suite of MATLAB tools in order to thoroughly assess the wave climate at potential WEF sites. The main capabilities of the tools included: (1) quantifying the available resource at various timescales; (2) determining the magnitude of the temporal variability; (3) generating wave roses at various timescales in order to examine the directional variability; and (4) creating resource-characterisation matrices at various timescales to analyse the spectral characteristics of the wave climate, for a particular location.

For the NZ case study, it was established that the available resource at all 12 sites was subjected to both spatial and temporal variability. In terms of spatial variability, two main areas containing different wave energy distributions were discernible; a higher-energy area comprising the south of NZ and an intermediate-energy area along NZ's west coast. It was also evident from the results that the resource was subjected to seasonal variability at each of the sites, with a maximum and minimum P_{wave} available in the winter and summer months, respectively. Furthermore, it was ascertained that site I3 was the most optimal in terms of temporal variability, whereas sites A2, A3, G1, and G3 were more favourable in terms of directional characteristics, as the waves propagated from a narrow band of directions.

In order to observe the wide range of wave conditions experienced at each site, resource characterisation matrices were generated. Additional capabilities of the MATLAB tools were the ability to redraw these matrices by replacing the percentage occurrence of the sea states with the percentage contribution of the sea states to the available power, which showed that the most prevalent wave conditions were not the most energy rich. Moreover, the tools were adapted in order to demonstrate that P_{wave} could be quantified from the resource-characterisation matrix (with minimal error), which is computationally less expensive than calculating the power directly from the 3-h sea states.

The third stage identified 130 WECs currently in development and utilised five main categories, including a technology maturity category, to classify current and future devices in a practical and meaningful manner. In addition, 41 devices were selected for further analysis based on a high technology maturity level. It was then shown that the devices to be evaluated could be reduced even further by taking into consideration site-specific factors, such as the deployment location. For the NZ case study, the number of devices appropriate for the sites identified as suitable for WEFs reduced to 32. Thereafter, four conflicting techno-economic performance metrics were proposed to quantitatively compare and rank the WECs, which will be applied, in future work, to the 12 potential WEF sites in NZ.

6.1 Recommended Future Work

6.1.1 WEC Assessment

The natural progression following this research is to conduct the WEC Assessment for a range of device types that are suitable for the NZ wave climate. This will require an initial RfI to be sent to the developers identified in Table 5.2. Once the relevant information has been received, then the performance metrics identified in Stage 3.3 can be quantified. Thereafter, it is recommended that the Analytical Hierarchy Process (a multi-criteria decision-making technique) is utilised to rank the devices, as it provides a structure that prevents double counting [221].

6.1.2 WEF Modelling

As developers at an advanced maturity level have been identified in Table 5.2, potential future research could focus on modelling a WEF for a particular wave climate in NZ. Key challenges that would have to be addressed are as follows: geometrical layout of the farm

(array clusters), electrical arrangements (on- and offshore), mooring configurations, control systems, as well as the hydrodynamic interactions between the individual WECs in the array clusters [222]. All the factors that would have an impact on the amount of electricity generated by the WEF [222].

Furthermore, wind and wave energy systems could be integrated into a hybrid energy system, as there is a strong connection between offshore wind and wave conditions (Section 2.4.1). Developing these hybrid energy systems could reduce the overall cost associated with the project and provide a combined steady energy supply.

6.1.3 Sustainability Assessment

The most widely accepted definition of sustainable development is stated in the 1987 Brundtland Report: 'Sustainable development is development that meets the needs of the present without compromising the ability of future generations to meet their own' [100]. Since the publication of this report, considerable research has been conducted into the concept of sustainable development; however, there is still no broad consensus regarding the best approach to measure sustainability [223, 224].

There has been a number of studies published on the topic of sustainability of energy systems. However, these vary substantially with regards to the scope of the study and the evaluation methods implemented [225, 226]. These studies vary with respect to factors such as the selection of system boundaries; time scales; the type and amount of sustainability indicators analysed (technical, environmental, economic and social dimensions [223]); evaluation approaches (such as input-output approach [227], emergy accounting [227], life cycle assessment [225], life cycle cost analysis [225] and environmental/social/economic footprints [223]); and methodologies to quantitatively measure energy sustainability (such as multi-criteria decision analysis [225], system dynamics [227] and energy return on energy investment [227]).

Therefore, in order to assess if the installation of a WEF is sustainable, it is proposed that an Energy System Sustainability Index be developed, which will compare renewable and non-renewable energy systems. This can potentially be achieved by developing sets of indicators: to measure and assess the three major dimensions of sustainable development (social, economic and environmental [228, 229]); take into account the multi-dimensional and integrated nature of sustainable development; and assess the proposed WEF and a

select number of current electricity generation systems (both renewable and non-renewable) in NZ.

References

[1] Bertram DV, Tarighaleslami AH, Walmsley MRW, Atkins MJ, Glasgow GDE. A systematic approach for selecting suitable wave energy converters for potential wave energy farm sites. Renewable and Sustainable Energy Reviews. 2020;132:110011.
[2] Bertram DV, Bostock H, Walmsley MR, Atkins MJ, Glasgow G. Geospatial multi-criteria analysis for site selection of wave energy farms in New Zealand. Australasian Coasts and Ports 2019 Conference: Future directions from 40 [degrees] S and beyond; 2019 10-13 Sep; Hobart, Australia: Engineers Australia.
[3] Bertram DV, Oskartiz O, Tarighaleslami AH, Walmsley MRW, Atkins MJ, Glasgow GDE. A systematic approach for selecting suitable wave energy converters for potential wave energy farm sites. In: Varbanov PS, Seferlis P, Voutetakis SS, Walmsley TG, Klemeš JJ, editors. PRES'19: Proceedings of the 22nd Conference on Process Integration, Modelling and Optimisation for Energy Saving and Pollution Reduction; 2019 20–23 Oct; Crete, Greece.
[4] Bertram DV. Selecting suitable wave energy converters for the New Zealand wave climate. Waikato Young Research Engineers Symposium 2018 1 Nov; Hamilton, New Zealand.
[5] Bertram DV. Geospatial multi-criteria analysis for site selection of wave energy farms in New Zealand. Australasian Coasts and Ports 2019 Conference: Future directions from 40 [degrees] S and beyond; 2019 10-13 Sep; Hobart, Australia.
[6] Ritchie H, Roser M. Energy. Our world in data. 2018.
[7] Heffron RJ, Talus K. The development of energy law in the 21st century: a paradigm shift? The Journal of World Energy Law & Business. 2016;9(3):189-202.
[8] International Energy Agency (IEA). Global energy & CO2 status report. Paris, France; 2019.
[9] International Energy Agency. Data and statistics, 2020. https://www.iea.org/data-and-statistics?country=WORLD&fuel=Energy%20supply&indicator=Total%20primary%20energy%20supply%20(TPES)%20by%20source
[10] International Energy Agency, International Renewable Energy Agency, United Nations Statistics Division, World Bank, World Health Organization. Tracking SDG7: the energy progress report. Washington: The World Bank; 2018.
[11] Castán Broto V, Kirshner J. Energy access is needed to maintain health during pandemics. Nature Energy. 2020;5(6):419-21.
[12] Xie J, Zuo L. Dynamics and control of ocean wave energy converters. International Journal of Dynamics and Control. 2013;1(3):262-76.
[13] Chakraborty T. A MCDM-NBO approach for selection of installation location for wave energy power plants. Application of Geographical Information Systems and Soft Computation Techniques in Water and Water Based Renewable Energy Problems. Springer; 2018, p. 121-40.
[14] Edenhofer O, Pichs-Madruga R, Sokona Y, Seyboth K, Kadner S, Zwickel T, et al. Renewable energy sources and climate change mitigation: special report of the Intergovernmental Panel on Climate Change: Cambridge University Press; 2011.
[15] Looney B. BP statistical review of world energy. 2020.
[16] United Nations. Factsheet: people and oceans [Internet]. New York; 2017. [cited: 2019 7 June]. Available from: https://www.un.org/sustainabledevelopment/wp-content/uploads/2017/05/Ocean-fact-sheet-package.pdf
[17] Ghosh S. Wave energy potential site selection based on MCDM and neural network analysis. Application of Geographical Information Systems and Soft

Computation Techniques in Water and Water Based Renewable Energy Problems. Springer; 2018, p. 107-20.
[18] Czech B, Bauer P. Wave energy converter concepts: design challenges and classification. IEEE Industrial Electronics Magazine. 2012;6(2):4-16.
[19] Hannon M, van Diemen R, Skea J. Examining the effectiveness of support for UK wave energy innovation since 2000: lost at sea or a new wave of innovation? Glasgow: University of Strathclyde, International Public Policy Institute; 2017.
[20] O'Connor M, Lewis T, Dalton G. Techno-economic performance of the Pelamis P1 and Wavestar at different ratings and various locations in Europe. Renewable Energy. 2013;50:889-900.
[21] Cornett AM. A global wave energy resource assessment. The Eighteenth International Offshore and Polar Engineering Conference; 2008: International Society of Offshore and Polar Engineers.
[22] Ingram D, Smith G, Bittencourt-Ferreira C, Smith H. Protocols for the equitable assessment of marine energy converters. 1st ed. United Kingdom: The Institute for Energy Systems; 2011.
[23] Falcão AF. Modelling of wave energy conversion. Instituto Superior Técnico, Universidade Técnica de Lisboa. 2014.
[24] Alcorn R. Wave energy. In: Letcher TM, editor. Future energy: improved, sustainable and clean options for our planet. 2nd ed. London, UK: Elsevier; 2014, p. 357-82.
[25] Setoguchi T, Takao M. Current status of self rectifying air turbines for wave energy conversion. Energy Conversion and Management. 2006;47(15):2382-96.
[26] Salter SH. Wave power. Nature. 1974;249:720.
[27] Salter S. Looking back. In: Cruz J, editor. Ocean wave energy: current status and future perspectives. Springer; 2007, p. 7-40.
[28] Cruz J. Introduction. In: Cruz J, editor. Ocean wave energy: current status and future perspectives. Springer; 2007, p. 1-6.
[29] McGowin C. Ocean tidal and wave energy: renewable energy technical assessment guide. Electric Power Research Institute, Palo Alto, CA, Paper No TAG-RE. 2005.
[30] Bedard R, Previsic M, Hagerman G, Polagye B, Musial W, Klure J, et al. North American ocean energy status—March 2007. Electric Power Research Institute (EPRI) Tidal Power (TP). 2007;8:17.
[31] Koca K, Kortenhaus A, Oumeraci H, Zanuttigh B, Angelelli E, Cantù M, et al. Recent advances in the development of wave energy converters. Proceedings of the 10th European Wave and Tidal Energy Conference (EWTEC). 2013 Sep 2-5; Aalborg, Denmark.
[32] Kempener R, Neumann F. Wave energy technology brief. International Renewable Energy Agency (IRENA). 2014.
[33] AWTEC. The Asian Wave and Tidal Energy Conference (AWTEC) [Internet]. 2012. [cited: 2018 7 February]. Available from: https://www.awtec-headoffice.com/awtec-2012
[34] Magagna D, Monfardini R, Uihlein A. JRC ocean energy status report 2016 edition. Luxembourg: Publications Office of the European Union; 2016.
[35] O'Halloran B. Ocean energy developer Wavebob set to go under. The Irish Times. 2013 3 April;Sect. 03 April 2013.
[36] Vorrath S. Wave energy company Oceanlinx goes into receivership. Renew Economy. 2 April 2014.
[37] Holmes B, Nielsen K. Guidelines for the development & testing of wave energy systems. OES-IA Annex II Task 2.1; 2010. Contract No.: Report T02.1.

[38] Fitzgerald J, Bolund B. Technology readiness for wave energy projects; ESB and Vattenfall classification system. Proceedings of the 4th International Conference on Ocean Energy. 2012 Oct 17 -19; Dublin, Ireland.
[39] Fitzgerald J. ESB wave energy systems: technology readiness levels. 2012. Contract No.: ESBIoe-WAV-12-091 Rev.2.
[40] Weber J. WEC technology readiness and performance matrix–finding the best research technology development trajectory. The 4th International Conference on Ocean Energy. 2012 Oct 17 -19; Dublin, Ireland.
[41] Falcão AF. Wave energy utilization: a review of the technologies. Renewable and Sustainable Energy Reviews. 2010;14(3):899-918.
[42] Falnes J. A review of wave-energy extraction. Marine structures. 2007;20(4):185-201.
[43] Drew B, Plummer AR, Sahinkaya MN. A review of wave energy converter technology. 2009.
[44] EMEC. Wave devices [Internet]. 2019. [cited: 2019 9 June]. Available from: http://www.emec.org.uk/marine-energy/wave-developers/
[45] Li Y, Yu Y-H. A synthesis of numerical methods for modeling wave energy converter-point absorbers. Renewable and Sustainable Energy Reviews. 2012;16(6):4352-64.
[46] Lehmann M, Karimpour F, Goudey CA, Jacobson PT, Alam M-R. Ocean wave energy in the United States: current status and future perspectives. Renewable and Sustainable Energy Reviews. 2017;74:1300-13.
[47] Myers LE, Bahaj AS, Retzler C, Pizer D, Gardner F, Bittencourt C, et al. EquiMar Deliverable D5. 2: device classification template. 2011.
[48] Margheritini L, Hansen AM, Frigaard P. A method for EIA scoping of wave energy converters-based on classification of the used technology. Environmental Impact Assessment Review. 2012;32(1):33-44.
[49] Doyle S, Aggidis GA. Development of multi-oscillating water columns as wave energy converters. Renewable and Sustainable Energy Reviews. 2019;107:75-86.
[50] Dunnett D, Wallace JS. Electricity generation from wave power in Canada. Renewable Energy. 2009;34(1):179-95.
[51] Coe RG, Michelen C, Eckert-Gallup A, Sallaberry C. Full long-term design response analysis of a wave energy converter. Renewable Energy. 2018;116:356-66.
[52] Bedard R, Hagerman G, Previsic M, Siddiqui O, Thresher R, Ram B. Final summary report, project definition study, offshore wave power feasibility demonstration project. Electric Power Research Institute Inc. 2005.
[53] Zubiate L, Villate J, Torre-Enciso Y, Soerensen H, Holmes B, Panagiotopoulos M, et al. Methodology for site selection for wave energy projects. Proceeding at the 8th European Wave and Tidal Energy Conference (EWTEC08); 2009.
[54] Kim C-K, Toft JE, Papenfus M, Verutes G, Guerry AD, Ruckelshaus MH, et al. Catching the right wave: evaluating wave energy resources and potential compatibility with existing marine and coastal uses. PLOS ONE. 2012;7(11).
[55] Lynch K, Murphy J, Serri L, Airoldi D. Site selection methodology for combined wind and ocean energy technologies in Europe. 4th International Conference on Ocean Energy; 2012, Oct 17-19; Dublin, Ireland.
[56] Bahaj AS. Generating electricity from the oceans. Renewable and Sustainable Energy Reviews. 2011;15(7):3399-416.
[57] Neill SP, Hashemi MR. Fundamentals of ocean renewable energy: generating electricity from the sea: Academic Press; 2018.
[58] Bouws E, Draper L, Shearman E, Laing A, Feit D, Mass W, et al. Guide to wave analysis and forecasting. WMO-No. 702. World Meteorological Organization. 1998.
[59] Garrison TS. Essentials of oceanography: Cengage Learning; 2012.

[60] Sorensen RM. Basic coastal engineering: Springer Science & Business Media; 2005.
[61] Folley M. The wave energy resource. In: Pecher A, Kofoed JP, editors. Handbook of Ocean Wave Energy. London: Springer; 2017, p. 203-20.
[62] Brooke J. Wave energy conversion: Elsevier; 2003.
[63] Reeve D, Chadwick A, Fleming C. Coastal engineering: processes, theory and design practice: CRC Press; 2012.
[64] Pinet PR. Invitation to oceanography: Jones & Bartlett Learning; 2019.
[65] Duckers L. Wave power. Engineering Science & Education Journal. 2000;9(3):113-22.
[66] Thurman HV, Trujillo AP. Essentials of oceanography. 7th ed: Prentice hall; 2008, p. 236-64.
[67] Iglesias G. The marine resource. In: Greaves D, Iglesias G, editors. Wave and Tidal Energy. 1st ed. Hoboken, USA: John Wiley & Sons Ltd; 2018, p. 35-71.
[68] Schwartz M. Encyclopedia of coastal science: Springer Science & Business Media; 2006.
[69] Davis Jr RA, FitzGerald DM. Beaches and coasts: John Wiley & Sons Ltd; 2020.
[70] Benassai G. Introduction to coastal dynamics and shoreline protection. Southampton, UK: WIT Press; 2006.
[71] Bozzi S, Archetti R, Passoni G. Wave electricity production in Italian offshore: a preliminary investigation. Renewable Energy. 2014;62:407-16.
[72] Morim J, Cartwright N, Etemad-Shahidi A, Strauss D, Hemer M. Wave energy resource assessment along the Southeast coast of Australia on the basis of a 31-year hindcast. Applied Energy. 2016;184:276-97.
[73] Rusu L, Onea F. Assessment of the performances of various wave energy converters along the European continental coasts. Energy. 2015;82:889-904.
[74] Arena F, Barbaro G, Romolo A. Return period of a sea storm with at least two waves higher than a fixed threshold. Mathematical Problems in Engineering. 2013;2013:6.
[75] Liberti L, Carillo A, Sannino G. Wave energy resource assessment in the Mediterranean, the Italian perspective. Renewable Energy. 2013;50:938-49.
[76] Amrutha M, Kumar VS, Bhaskaran H, Naseef M. Consistency of wave power at a location in the coastal waters of Central Eastern Arabian Sea. Ocean Dynamics. 2019;69(5):543-60.
[77] Zheng CW, Zhou L, Jia BK, Pan J, Li X. Wave characteristic analysis and wave energy resource evaluation in the China Sea. Journal of Renewable and Sustainable Energy. 2014;6(4):043101.
[78] Mota P, Pinto JP. Wave energy potential along the western Portuguese coast. Renewable Energy. 2014;71:8-17.
[79] Folley M, Whittaker T. Analysis of the nearshore wave energy resource. Renewable Energy. 2009;34(7):1709-15.
[80] Morim J, Cartwright N, Hemer M, Etemad-Shahidi A, Strauss D. Inter-and intra-annual variability of potential power production from wave energy converters. Energy. 2019;169:1224-41.
[81] Nobre A, Pacheco M, Jorge R, Lopes MFP, Gato LMC. Geo-spatial multi-criteria analysis for wave energy conversion system deployment. Renewable Energy. 2008;34(1):97-111.
[82] Galparsoro I, Liria P, Legorburu I, Bald J, Chust G, Ruiz-Minguela P, et al. A marine spatial planning approach to select suitable areas for installing Wave Energy Converters (WECs), on the Basque Continental Shelf (Bay of Biscay). Coastal Management. 2012;40(1):1-19.
[83] EU WAVEPLAM Project. D3.1 Methodology for site selection. 2009.

[84] Le P, Fischer A, Penesis I, Rahimi R. Aggregating GIS and MCDM to optimize wave energy converters location in Tasmania, Australia. Soft Computing Applications for Renewable Energy and Energy Efficiency. IGI Global; 2015, p. 141-64.
[85] Rusu E. Evaluation of the wave energy conversion efficiency in various coastal environments. Energies. 2014;7(6):4002-18.
[86] Margheritini L, Kofoed JP. Weptos wave energy converters to cover the energy needs of a small island. Energies. 2019;12(3):423.
[87] Carballo R, Iglesias G. A methodology to determine the power performance of wave energy converters at a particular coastal location. Energy Conversion and Management. 2012;61:8-18.
[88] Dalton GJ, Alcorn R, Lewis T. Case study feasibility analysis of the Pelamis wave energy convertor in Ireland, Portugal and North America. Renewable Energy. 2010;35(2):443-55.
[89] Iuppa C, Cavallaro L, Foti E, Vicinanza D. Potential wave energy production by different wave energy converters around Sicily. Journal of Renewable and Sustainable Energy. 2015;7(6):061701.
[90] Babarit A, Hals J, Muliawan MJ, Kurniawan A, Moan T, Krokstad J. Numerical benchmarking study of a selection of wave energy converters. Renewable Energy. 2012;41:44-63.
[91] Veigas M, López M, Romillo P, Carballo R, Castro A, Iglesias G. A proposed wave farm on the Galician coast. Energy Conversion and Management. 2015;99:102-11.
[92] Sierra JP, Mösso C, González-Marco D. Wave energy resource assessment in Menorca (Spain). Renewable Energy. 2014;71:51-60.
[93] Aoun NS, Harajli HA, Queffeulou P. Preliminary appraisal of wave power prospects in Lebanon. Renewable Energy. 2013;53:165-73.
[94] Silva D, Rusu E, Soares CG. Evaluation of various technologies for wave energy conversion in the Portuguese nearshore. Energies. 2013;6(3):1344-64.
[95] Vaquero AM, Ruiz FC, Rusu E. Evaluation of the wave power potential in the northwestern side of the Iberian nearshore. Developments in Maritime Transportation and Exploitation of Sea Resources–Guedes Soares & López Peña (eds)© 2014 Taylor & Francis Group, London, ISBN 978-1-138-00124. 2013;4:1012-9.
[96] Rusu L, Onea F. The performance of some state-of-the-art wave energy converters in locations with the worldwide highest wave power. Renewable and Sustainable Energy Reviews. 2017;75:1348-62.
[97] Vannucchi V, Cappietti L. Wave energy assessment and performance estimation of state of the art wave energy converters in Italian hotspots. Sustainability. 2016;8(12):1300.
[98] ArcGIS Desktop. version 10.5.1. Redlands, USA: Environmental Systems Research Institue Inc.; 2017.
[99] Crosier S, Booth B, Dalton K, Mitchell A, Clark K. ARGIS 9 Getting started with ArcGIS. United States: ESRI; 2004.
[100] Brundtland G, Khalid M, Agnelli S, Al-Athel S, Chidzero B, Fadika L, et al. Our common future. 1987.
[101] Strange T, Bayley A. Sustainable development: linking economy, society, environment. Paris: OECD Publishing; 2008.
[102] Cisneros-Montemayor AM, Pauly D, Weatherdon LV, Ota Y. A global estimate of seafood consumption by coastal indigenous peoples. PLOS ONE. 2016;11(12).
[103] Heck N, Smith C, Hittinger E. A Monte Carlo approach to integrating uncertainty into the levelized cost of electricity. The Electricity Journal. 2016;29(3):21-30.
[104] Chozas J. International levelised cost of energy for ocean energy technologies.: Ocean Energy Systems; 2015.

[105] Lee C-Y, Ahn J. Stochastic modeling of the levelized cost of electricity for solar PV. Energies. 2020;13(11):3017.
[106] SI Ocean. Ocean energy: cost of energy and cost reduction opportunities.; 2013.
[107] de Andres A, Medina-Lopez E, Crooks D, Roberts O, Jeffrey H. On the reversed LCOE calculation: design constraints for wave energy commercialization. International Journal of Marine Energy. 2017;18:88-108.
[108] Guardiola Moliner E. Cost analysis of the UGEN [master's thesis]. Lisbon, Portugal: Instituto Superior Técnico; 2016.
[109] Ocean Energy Systems. Annual report 2012. 2012.
[110] Carbon Trust. Accelerating marine energy. London, UK; 2011.
[111] Walrond C. Natural environment - geography and geology. 2005. In: Te Ara - The Encyclopedia of New Zealand [Internet]. Available from: http://www.TeAra.govt.nz/en/natural-environment/page-1.
[112] Stevens C, Smith M, Gorman R. Ocean bounty: energy from waves and tides. Water & Atmosphere. 2005;13(4).
[113] Gorman RM, Bryan KR, Laing AK. Wave hindcast for the New Zealand region: nearshore validation and coastal wave climate. New Zealand Journal of Marine and Freshwater Research. 2003;37(3):567-88.
[114] Power Projects Limited. Development of marine energy in New Zealand. 2008.
[115] The Economist. Pocket world in figures 2019: Profile Books; 2018.
[116] Statistics New Zealand. Are New Zealanders living closer to the coast? ; 2006.
[117] National Topographic Office. NZ coastlines and islands polygons (Topo 1:50k), LINZ Data Service, v38; 2018. https://data.linz.govt.nz/layer/51153-nz-coastlines-and-islands-polygons-topo-150k/
[118] New Zealand Hydrographic Authority. 200 mile exclusive economic zone outer limits, LINZ Data Service, v5; 2015. https://data.linz.govt.nz/layer/50842-200-mile-exclusive-economic-zone-outer-limits/
[119] Ministry for Primary Industries Geospatial Management. Taiapure, ArcGIS REST Services, 2017. https://maps.mpi.govt.nz/wss/service/ags-relay/arcgis1/guest/arcgis/rest/services/MARINE/MARINE_RestrictionsCustomary/MapServer/10
[120] Ministry for Primary Industries Geospatial Management. Current marine farms, ArcGIS REST Services, 2017. https://maps.mpi.govt.nz/wss/service/ags-relay/arcgis1/guest/arcgis/rest/services/MARINE/MARINE_Aquaculture/MapServer/1
[121] Ministry for Primary Industries Geospatial Management. Settlement areas, ArcGIS REST Services, 2017. https://maps.mpi.govt.nz/wss/service/ags-relay/arcgis1/guest/arcgis/rest/services/MARINE/MARINE_Aquaculture/MapServer/6
[122] New Zealand Hydrographic Authority. Offshore platform points (Hydro, 1:90k - 1:350k), LINZ Data Service, v18; 2018. https://data.linz.govt.nz/layer/50480-offshore-platform-points-hydro-190k-1350k/
[123] New Zealand Petroleum and Minerals. Petroleum wells, Permit Maps - Petroleum, 2019. http://data.nzpam.govt.nz/permitwebmaps?commodity=petroleum
[124] New Zealand Petroleum and Minerals. Mineral active permits, Permit Maps - Minerals, 2018. http://data.nzpam.govt.nz/permitwebmaps?commodity=minerals
[125] Ministry for the Environment (MfE). Benthic protection areas (2016 report), MfE Data Service, v8; 2016. https://data.mfe.govt.nz/layer/53494-benthic-protection-areas-2016-report/
[126] Ministry for the Environment (MfE). DoC marine mammal sanctuaries (2016 report), MfE Data Service, v6; 2016. https://data.mfe.govt.nz/layer/53495-doc-marine-mammal-sanctuaries-2016-report/history/
[127] Kaikōura (Te Tai o Marokura) marine management act 2014 (NZ).

[128] Ministry for the Environment (MfE). Type 2 marine protected areas, MfE Data Service, v7; 2016. https://data.mfe.govt.nz/layer/52762-type2-marine-protected-areas/
[129] Ministry for the Environment (MfE). Marine reserves, MfE Data Service, v9; 2016. https://data.mfe.govt.nz/layer/52760-marine-reserves/
[130] Ministry for the Environment (MfE). Seamount closures (2016 report), MfE Data Service, v6; 2016. https://data.mfe.govt.nz/layer/53496-seamount-closures-2016-report/
[131] National Topographic Office. NZ Chatham Island wreck points (Topo, 1:50k), LINZ Data Service, v10; 2018. https://data.linz.govt.nz/layer/50118-nz-chatham-island-wreck-points-topo-150k/
[132] National Topographic Office. NZ wreck points (Topo, 1:50k), LINZ Data Service, v40; 2018. https://data.linz.govt.nz/layer/50379-nz-wreck-points-topo-150k/
[133] New Zealand Hydrographic Authority. Wreck points (Hydro, 1:4k - 1:22k), LINZ Data Service, v20; 2019. https://data.linz.govt.nz/layer/50763-wreck-points-hydro-14k-122k/
[134] New Zealand Hydrographic Authority. Wreck points (Hydro, 1:22k - 1:90k), LINZ Data Service, v22; 2019. https://data.linz.govt.nz/layer/50633-wreck-points-hydro-122k-190k/
[135] New Zealand Hydrographic Authority. Wreck points (Hydro, 1:90k - 1:350k), LINZ Data Service, v22; 2019. https://data.linz.govt.nz/layer/50518-wreck-points-hydro-190k-1350k/
[136] New Zealand Hydrographic Authority. Wreck points (Hydro, 1:350k - 1:1500k), LINZ Data Service, v20; 2019. https://data.linz.govt.nz/layer/50424-wreck-points-hydro-1350k-11500k/
[137] National Institue of Water and Air (NIWA). New Zealand regional bathymetry (2016), NIWA, 2016. https://www.niwa.co.nz/our-science/oceans/bathymetry
[138] New Zealand Hydrographic Authority. Dredged area polygon (Hydro, 1:22k - 1:90k), LINZ Data Service, v21; 2018. https://data.linz.govt.nz/layer/50557-dredged-area-polygon-hydro-122k-190k/
[139] New Zealand Hydrographic Authority. Dredged area polygon (Hydro, 1:90k - 1:350k), LINZ Data Service, v20; 2018. https://data.linz.govt.nz/layer/50450-dredged-area-polygon-hydro-190k-1350k/
[140] New Zealand Hydrographic Authority. Dredged area polygon (Hydro, 1:4k - 1:22k), LINZ Data Service, 2017. https://data.linz.govt.nz/layer/50676-dredged-area-polygons-hydro-14k-122k/
[141] New Zealand Hydrographic Authority. Dumping ground polygons (Hydro, 1:4k - 1:22k), LINZ Data Service, v18; 2018. https://data.linz.govt.nz/layer/50449-dumping-ground-polygon-hydro-190k-1350k/
[142] New Zealand Hydrographic Authority. Dumping ground polygon (Hydro, 1:90k - 1:350k), LINZ Data Service, v18; 2018. https://data.linz.govt.nz/layer/50449-dumping-ground-polygon-hydro-190k-1350k/
[143] New Zealand Hydrographic Authority. Dumping ground polygon (Hydro, 1:22k - 1:90k), LINZ Data Service, v18; 2018. https://data.linz.govt.nz/layer/50555-dumping-ground-polygon-hydro-122k-190k/
[144] Land Information New Zealand (LINZ). 5 Firing practice, exercise and submarine safe bottoming areas. New Zealand Nautical Almanac 2018/19. Wellington2018, p. 222 - 8.
[145] Pilois J. NZ commercial ports, ArcGIS REST Services, 2018. https://services.arcgis.com/hLRlshaEMEYQG5A8/arcgis/rest/services/NZ_Commercial_Ports_(View_Layer)/FeatureServer
[146] New Zealand Hydrographic Authority. Cable, submarine polyline (Hydro, 1:350k - 1:1,500k), LINZ Data Service, v13; 2017. https://data.linz.govt.nz/layer/51091-cable-submarine-polyline-hydro-1350k-11500k/

[147] Submarine cables and pipelines protection (Tui Area Development) order 2007 (NZ).
[148] Submarine cables and pipelines protection (Kupe Gas Project) order 2008 (NZ).
[149] Submarine cables and pipelines protection (Maari Development) order 2008 (NZ).
[150] Submarine cables and pipelines protection order 2009 (NZ).
[151] De Freitas CR, Perry M. New environmentalism: managing New Zealand's environmental diversity: Springer Science & Business Media; 2012.
[152] Ministry of Fisheries, Department of Conservation. Marine protected areas: classification, protection standard and implementation guidelines. Wellington, New Zealand; 2008.
[153] Department of Conservation. New Zealand coastal policy statement 2010. Wellington; 2010.
[154] Parliamentary Counsel Office. New Zealand legislation [Internet]. Department of Internal Affairs; 2020. [cited: 2020 21 August]. Available from: http://www.legislation.govt.nz/
[155] New Zealand Gazette Office. New Zealand Gazette *Te Kāhiti o Aotearoa* [Internet]. Department of Internal Affairs. Available from: https://gazette.govt.nz/
[156] Office of the Surveyor-General. LINZS25002: standard for New Zealand geodetic datum 2000 projections: version 2. 2008.
[157] Humboldt State University. Introduction to coordinate systems / spatial reference systems [Internet]. 2018. [cited: 2020 25 August]. Available from: http://gis.humboldt.edu/OLM/Lessons/GIS/03%20Projections/IntroductionToCoordinateSystems1.html
[158] (ESRI) ESRI. ArcGIS 10.5.0 Geographic and vertical transformation tables. Available from: http://downloads2.esri.com/support/TechArticles/geographic_transformations_105.pdf.
[159] Office of the Surveyor-General. LINZS25002: standard for New Zealand geodetic datum 2000. 2007.
[160] Official information act 1982 (NZ).
[161] Ministry for Primary Industries. Fishery maps [Internet]. 2020. [cited: 2020 22 August]. Available from: https://www.mpi.govt.nz/law-and-policy/legal-overviews/fisheries/fishery-maps/
[162] United Nations convention on the law of the sea, 1982 (UN General Assembly).
[163] Continental shelf act 1964 (NZ).
[164] ArcGIS Desktop. ArcMap: hot spot analysis (Getis-Ord Gi*) [Internet]. 2018. [cited: 2020 23 August]. Available from: https://desktop.arcgis.com/en/arcmap/10.3/tools/spatial-statistics-toolbox/hot-spot-analysis.htm
[165] Marine Traffic. Density maps [Internet]. 2020. [cited: 2020 23 August]. Available from: https://www.marinetraffic.com/en/ais/home/centerx:163.2/centery:-43.6/zoom:4
[166] Ministry for Primary Industries. Marine parks, https://maps.mpi.govt.nz/wss/service/ags-relay/arcgis1/guest/arcgis/rest/services/MARINE/MARINE_MarineProtectedAreas/MapServer/1
[167] Department of Conservation, Ministry of Fisheries. Coastal marine habitats and marine protected areas in the New Zealand Territorial Sea: a broad scale gap analysis. Wellington, New Zealand; 2011.
[168] McSaveney E. Landscapes – overview – offshore islands. 2007. In: Te Ara - The Encyclopedia of New Zealand [Internet]. Available from: http://www.TeAra.govt.nz/en/landscapes-overview/page-10.
[169] National Geospatial-Intelligence Agency. World port index. 27th ed. USA: National Geospatial-Intelligence Agency; 2019.

[170] Submarine cables and pipelines protection act 1996 (NZ).
[171] Land Information New Zealand (LINZ). 13 Submarine cables and pipelines. New Zealand Nautical Almanac 2018/19. Wellington2018, p. 255 - 8.
[172] ArcGIS Desktop. Splitting a polygon by an overlapping feature [Internet]. 2016. [cited: 2021 9 May]. Available from: https://desktop.arcgis.com/en/arcmap/10.3/manage-data/editing-fundamentals/splitting-a-polygon-by-an-overlapping-line-feature.htm
[173] Hozo SP, Djulbegovic B, Hozo I. Estimating the mean and variance from the median, range, and the size of a sample. BMC medical research methodology. 2005;5(1):1-10.
[174] MATLAB. version 9.6.0.1072779 (R2019a). Natick, USA: The MathWorks Inc.; 2019.
[175] Cohan K. What is MATLAB? [Internet]. MathWorks; 2020. [cited: 2020 4 July]. Available from: https://www.mathworks.com/videos/matlab-overview-61923.html
[176] Kent E, Hall A, Leader VTT. The Voluntary Observing Ship (VOS) scheme. Proceedings from the 2010 AGU Ocean Sciences Meeting; 2010: American Geophysical Union, 2000 Florida Ave., N. W. Washington DC 20009 USA.
[177] Gulev SK, Grigorieva V, Sterl A, Woolf D. Assessment of the reliability of wave observations from voluntary observing ships: Insights from the validation of a global wind wave climatology based on voluntary observing ship data. Journal of Geophysical Research: Oceans. 2003;108(C7).
[178] Pitt E. Assessment of wave energy resource. UK: The European Marine Energy Centre Ltd 2009; 2009.
[179] Reikard G, Robertson B, Buckham B, Bidlot J-R, Hiles C. Simulating and forecasting ocean wave energy in western Canada. Ocean Engineering. 2015;103:223-36.
[180] Venugopal V, Davey T, Smith H, Smith G, Holmes B, Barrett S, et al. Deliverable D2.2 Wave and tidal resource characterisation. Equitable Testing and Evaluation of Marine Energy Extraction Devices in terms of Performance, Cost and Environmental Impact (EquiMar): European Community's Seventh Framework Programme; 2011. p. 79.
[181] Vicinanza D, Contestabile P, Ferrante V. Wave energy potential in the north-west of Sardinia (Italy). Renewable Energy. 2013;50:506-21.
[182] Greaves D, Iglesias G. Wave and tidal energy: John Wiley & Sons; 2018.
[183] Akpınar A, Bingölbali B, Van Vledder GP. Long-term analysis of wave power potential in the Black Sea, based on 31-year SWAN simulations. Ocean Engineering. 2017;130:482-97.
[184] WindRose Excel. How to: interpret a wind rose diagram [Internet]. 2020. [cited: 2020 3 July]. Available from: https://windroseexcel.com/guides/how-to-interpret-a-wind-rose-diagram/
[185] Sierra JP, González-Marco D, Sospedra J, Gironella X, Mösso C, Sánchez-Arcilla A. Wave energy resource assessment in Lanzarote (Spain). Renewable Energy. 2013;55:480-9.
[186] International Electrotechnical Commission. Marine energy—wave, tidal and other water current converters-part 101: wave energy resource assessment and characterization. International Electrotechnical Commission: London, UK2015.
[187] MetOcean Solutions. Historical datasets available [Internet]. [cited: 2019 5 June]. Available from: https://static1.squarespace.com/static/57070436f699bbcfa154423d/t/5b762d79cd8366dcb3b5a1d1/1534471548997/MetOcean-Solutions-Historical-datasets-available.pdf

[188] MetOcean Solutions. MetOceanView: operations and planning system, Meteorological Service of New Zealand Ltd, 2019. https://app.metoceanview.com/hindcast/
[189] Albuquerque J, Antolínez JAA, Gorman R, Méndez FJ, Coco G. A high resolution 20-year partitioned hindcast for the New Zealand area, Coast and Ocean Collective, 2019. https://uoa-eresearch.github.io/waves/#NZ-HIST-000-HSIGN-Hsig@1993-01-01%2000:00
[190] Saulter A. Operational wave models. In: Bruns T, editor. Guide to Wave Analysis and Forecasting (Draft Version for Approval) WMO-No 702. World Meterological Organization; 2018, p. 126-40.
[191] Zhang A, Hess KW, Aikman F. User-based skill assessment techniques for operational hydrodynamic forecast systems. Journal of Operational Oceanography. 2010;3(2):11-24.
[192] Willmott CJ. On the validation of models. Physical Geography. 1981;2(2):184-94.
[193] Chiswell S, Kibblewhite A. Spectra of the fully developed wind‐generated ocean wave field west of central New Zealand. New Zealand journal of marine and freshwater research. 1981;15(1):81-4.
[194] Huckerby J, Johnson D. New Zealand's wave and tidal energy resources and their timetable for development. International Conference on Ocean Energy. 2008; Brest, France.
[195] Gorman R. Cantebury wave conditions [Internet]. [cited: 2020 10 July]. Available from: https://niwa.co.nz/our-services/online-services/canterbury-wave-conditions
[196] Cahill B, Lewis T. Wave periods and the calculation of wave power. 2014.
[197] Ministry for the Environment. Climate change projections for New Zealand: atmospheric projections based on simulations undertaken for the IPCC 5th assessment. Wellington, New Zealand: Ministry for the Environmment; 2018. Report No.: ME 1385.
[198] Mullan B, Wratt D, Dean S, Hollis M, Allan S, Williams T, et al. Climate change effects and impacts assessment: a guidance manual for local government in New Zealand. Wellington, New Zealand: Ministry for the Environmment; 2008. Report No.: ME 870.
[199] Gorman RM, Bryan KR, Laing AK. Wave hindcast for the New Zealand region: deep‐water wave climate. New Zealand Journal of Marine and Freshwater Research. 2003;37(3):589-612.
[200] Ministry for the Environment (MfE). Monthly El Niño southern oscillation index, 1986–2016, MfE Data Service, v3; 2017. https://data.mfe.govt.nz/layer/52762-type2-marine-protected-areas/
[201] Pickrill RA, Mitchell JS. Ocean wave characteristics around New Zealand. New Zealand Journal of Marine and Freshwater Research. 1979;13(4):501-20.
[202] Laing AK. New Zealand wave climate from satellite observations. New Zealand Journal of Marine and Freshwater Research. 2000;34(4):727-44.
[203] MetOcean Solutions. Appendix C: "marine energy resources: ocean wave and tidal current resources in New Zealand". In: Power Projects Limited, editor. Development of marine energy in New Zealand. 2008.
[204] Rusu E, Guedes Soares C. Numerical modelling to estimate the spatial distribution of the wave energy in the Portuguese nearshore. Renewable Energy. 2009;34(6):1501-16.
[205] Cahill BG, Lewis T. Wave energy resource characterisation of the Atlantic Marine Energy Test Site. International Journal of Marine Energy. 2013;1:3-15.
[206] Thorpe TW. A brief review of wave energy: Harwell Laboratory, Energy Technology Support Unit London; 1999.

[207] Sharp R, Tallis H, Ricketts T, Guerry A, Wood S, Chaplin-Kramer R, et al. InVEST user guide. The Natural Capital Project, Stanford University, University of Minnesota, The Nature Conservancy, and World Wildlife Fund. 2016.
[208] EMEC. Wave developers [Internet]. 2020. [cited: 2018 21 February]. Available from: http://www.emec.org.uk/marine-energy/wave-developers/
[209] Leung S-F, Fu H-C, Zhang M, Hassan AH, Jiang T, Salama KN, et al. Blue energy fuels: converting ocean wave energy to carbon-based liquid fuels via CO2 reduction. Energy & Environmental Science. 2020.
[210] OpenEI. Marine and hydrokinetic technology database [Internet]. 2018. [cited: 2018 21 February]. Available from: https://openei.org/wiki/Marine_and_Hydrokinetic_Technology_Database
[211] OWEP. Wave energy developers & projects [Internet]. 2018. [cited: 2018 21 February]. Available from: http://openwaveenergy.org/open-wave-energy-project-resource-and-industry/wave-energy-developers-a-projects.html
[212] Day A, Babarit A, Fontaine A, He Y-P, Kraskowski M, Murai M, et al. Hydrodynamic modelling of marine renewable energy devices: A state of the art review. Ocean Engineering. 2015;108:46-69.
[213] SI Ocean. Ocean energy: state of the art. 2012.
[214] Ocean Energy Systems. Annual report 2018. 2018.
[215] Têtu A. Power take-off systems for WECs. In: Pecher A, Kofoed JP, editors. Handbook of Ocean Wave Energy. London: Springer; 2017, p. 203-20.
[216] Starling M. Guidelines for reliability, maintainability and survivability of marine energy conversion systems: marine renewable energy guides. European Marine Energy Centre; 2009.
[217] Pecher A, Kofoed JP. Handbook of ocean wave energy: Springer London; 2017.
[218] Babarit A. A database of capture width ratio of wave energy converters. Renewable Energy. 2015;80:610-28.
[219] Dallman A, Jenne DS, Neary V, Driscoll F, Thresher R, Gunawan B. Evaluation of performance metrics for the wave energy prize converters tested at 1/20th scale. Renewable and Sustainable Energy Reviews. 2018;98:79-91.
[220] Rusu E, Onea F. A review of the technologies for wave energy extraction. Clean Energy. 2018;2(1):10-9.
[221] Saaty TL. How to make a decision: the analytic hierarchy process. European journal of operational research. 1990;48(1):9-26.
[222] Cruz J, Sykes R, Siddorn P, Taylor RE. Wave farm design: preliminary studies on the influences of wave climate, array layout and farm control. Proc EWTEC. 2009.
[223] Čuček L, Klemeš JJ, Kravanja Z. A review of footprint analysis tools for monitoring impacts on sustainability. Journal of Cleaner Production. 2012;34:9-20.
[224] Klemeš JJ. Assessing and measuring environmental impact and sustainability: Butterworth-Heinemann; 2015.
[225] Santoyo-Castelazo E, Azapagic A. Sustainability assessment of energy systems: integrating environmental, economic and social aspects. Journal of Cleaner Production. 2014;80:119-38.
[226] Li J, Geng X, Li J. A comparison of electricity generation system sustainability among G20 countries. Sustainability. 2016;8(12):1276.
[227] Maxim A. Sustainability assessment of electricity generation technologies using weighted multi-criteria decision analysis. Energy Policy. 2014;65:284-97.
[228] Dinçer İ, Colpan CO, Kadioglu F. Causes, impacts and solutions to global warming: Springer Science & Business Media; 2013.
[229] International Atomic Energy Agency, United Nations Department of Economic and Social Affairs, International Energy Agency, Eurostat, European Environment

Agency. Energy indicators for sustainable development: guidelines and methodologies. Vienna2005.
[230] Perreira D. Wind rose. version 1.6.0.2 MATLAB Central File Exchange; 2020.

Appendix A
MATLAB Processing Tools

The suite of MATLAB tools developed in order to assess the potential WEF sites in Stage 2: Site Assessment (Chapter 4) are detailed below. These programs consisted of scripts and dependencies, where a dependency referred to a function (which was not a MATLAB built-in function) that was called on in the script. The naming convention of these MATLAB programs included a brief description of the program's purpose and the version which was implemented in order to obtain the results in this thesis. The version of the program was denoted by the letter 'V' followed by the version number (if more than one version exists) at the end of the program name. Scripts were distinguished from dependencies by including the word 'Main' at the start of the program name. For example, in order to verify the performance of a numerical model (Section A.1.2), the MATLAB program Main_Model_Validation_V1.m was developed by the author. 'Main' denotes that the program is a script, 'Model_Validation' states the purpose of the program, and 'V1' specifies that this is the second iteration of the program.

Unless stated otherwise, the author developed all the MATLAB programs (scripts and dependencies). It should be noted that the programs were extensively debugged, and the results verified by comparing randomly selected outputs with values computed in Excel. When a new version of a program was developed, this process was repeated.

The suite of MATLAB scripts developed by the author are as follows:

1. Main_WPR.m
2. Main_Model_Validation_V1
3. Main_Wave_Power_V3.m
4. Main_Combine_Wave_Power_Sites_V2.m
5. Main_Export_Scatter_Data_V4
6. Main_Wave_Roses.m
7. Main_Export_Hist_and_Scatter.m

A.1 Model Validation

The performance of the numerical model was validated by developing two MATLAB scripts. The first MATLAB script, Main_WPR.m, calculated the wave period ratio α, whilst the second MATLAB script, Main_Model_Validation_V1.m, produced qualitative and quantitative performance results.

A.1.1 Main_WPR.m

The Main_WPR.m MATLAB script (Figure A.1) determines the fixed conversion factor α that can be utilised to calculate T_e from T_{m02}. The script prompts the user to select a .csv file containing the relevant wave data. It then divides all the T_e values by the corresponding T_{m02} values. Thereafter, the mean of these values is obtained, which corresponds to the wave period ratio α. The standard deviation and coefficient of variation are also calculated. This programme does not have any dependencies.

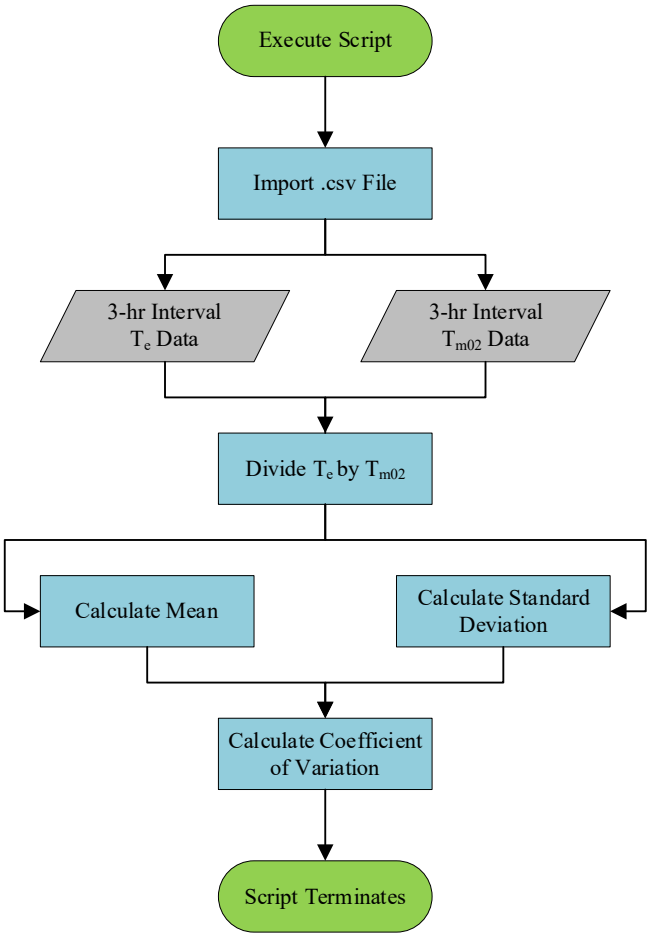

Figure A.1. Programming flow chart for the Main_WPR.m script, outlining the main processes.

A.1.2 Main_Model_Validation_V1

The Main_Model_Validation_V1.m (Figure A.2) script prompts the user to select two .csv files. First, the user is prompted to select the hindcast data, and then the user is prompted to select the corresponding wave buoy data (for the same location and time interval). The code then pre-processes the wave buoy data (changes irregular timesteps to regular time steps, finds missing timestamps, and downsamples the wave buoy data from 30-min intervals to 3-h intervals). T_e and then subsequently P_{wave} are calculated by utilising the α computed by Main_WPR.m. Thereafter, time series and scatter plots comparing the hindcast and wave buoy data for T_{m02}, H_{m0}, θ_m, and P_{wave} are graphed, and the following validation metrics calculated: Bias, RMSE, SI, *r*, and AoI, to determine the performance of the hindcast model.

Dependencies

a) wave_power.m: calculates the available wave power, utilising the fixed conversion factor α calculated in Main_WPR.m.
b) L_Regression.m: accepts the wave buoy and modelled data in order to fit a linear trendline similar to that of Excel.
c) bias.m: calculates the bias of the model.
d) RMSE.m: calculates the root mean square error of the model.
e) IoA.m: calculates the IoA of the model.
f) save_figure.m: accepts the figure handle and full path and saves the relevant figure as a high resolution pdf.

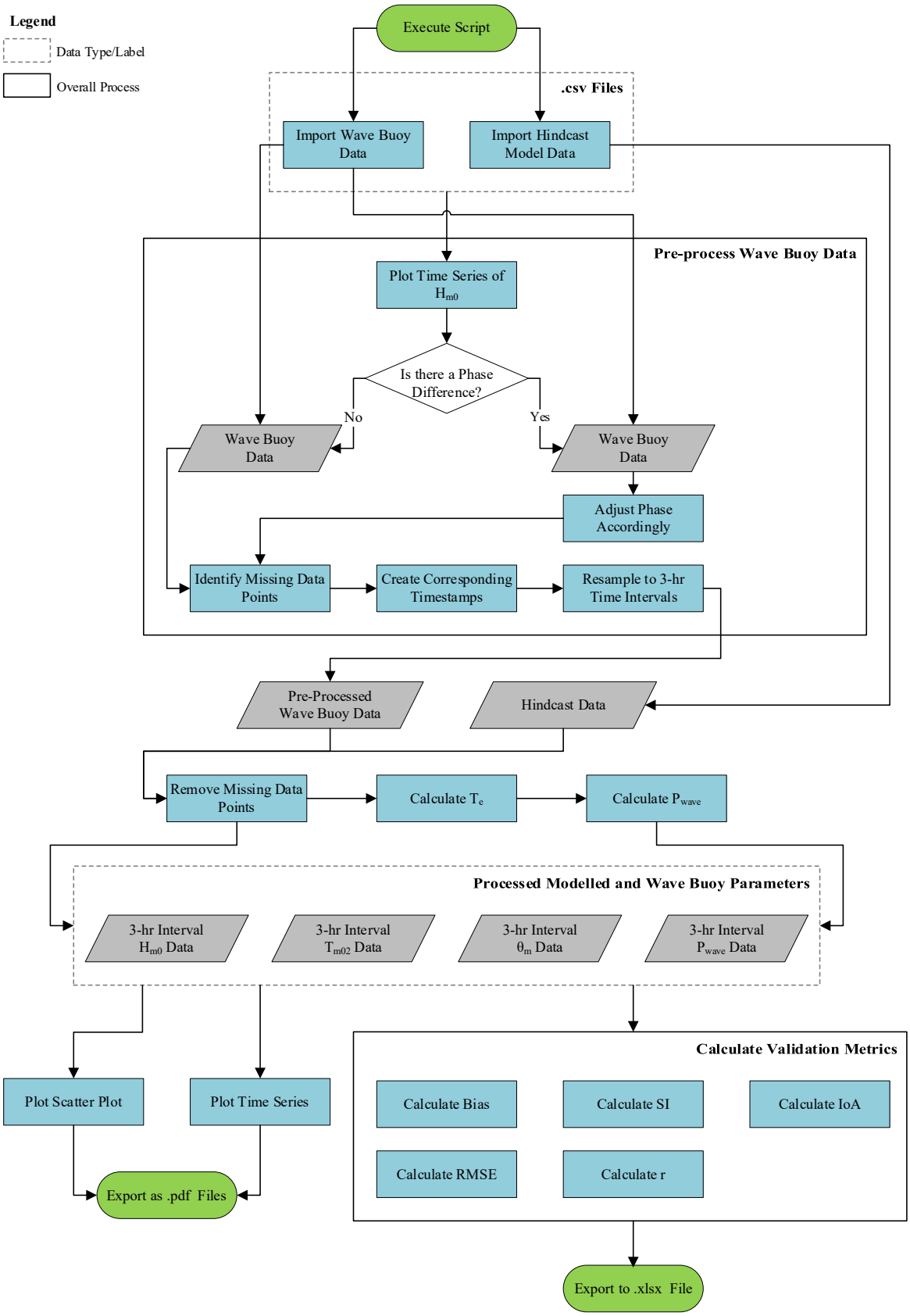

Figure A.2. Programming flow chart for Main_Model_Validation_V1.m script, outlining the main processes.

A.2 Resource Quantification, Variability, and Characterisation

The available resource was quantified, and the temporal, directional, and spectral characteristics of the wave climate were determined, at the potential deployment sites, by developing a range of MATLAB tools (which are discussed below). It should be noted that outputs in terms of a 'timescale' refer to both the particular and typical timescale throughout the time horizon being analysed. For instance, if analysing data for a monthly timescale, the programs will produce outputs for every single month for the entire time horizon being examined ('particular'), as well as the averaged monthly values over the number of years being considered ('typical'). In this case, the time horizon is 20 years. Therefore, the number of outputs in terms of a monthly timescale will be 252 (20 years × 12 months/year = 240 monthly outputs, with the addition of the averaged monthly outputs, 240 + 12, results in a total of 252 outputs).

A.2.1 Main_Wave_Power_V3.m

The Main_Wave_Power_V3.m (Figure A.3) script prompts the user to select a .csv file containing the wave parameters for a specific location, including but not limited to H_{m0}, T_e, T_{m02}, T_p, λ, and θ_m. The H_{m0} and T_e values are used to calculate the available yearly, seasonal, monthly, daily, and hourly theoretical wave power and energy. Thereafter, the following parameters are computed: mean, maximum, and standard deviation of H_{m0}, T_e, θ_m, and P_{wave}, total E_{wave}, and mean λ and $d_{critical}$ (Figure A.4). These calculated parameters are then exported to a user-selected folder in a .mat file format.

Dependencies

a) calculate_power.m: calculates the theoretical wave power based on Equation (4.2).
b) Create_Wave_Table.m: accepts a placeholder table containing H_{mo}, T_e, θ_m, P_{wave}, E_{wave}, and λ values for a specific timescale, and then returns a table comprised of the: mean, maximum and standard deviation of H_{mo}, T_e, θ_m, and P_{wave}; total E_{wave}; and the mean λ.

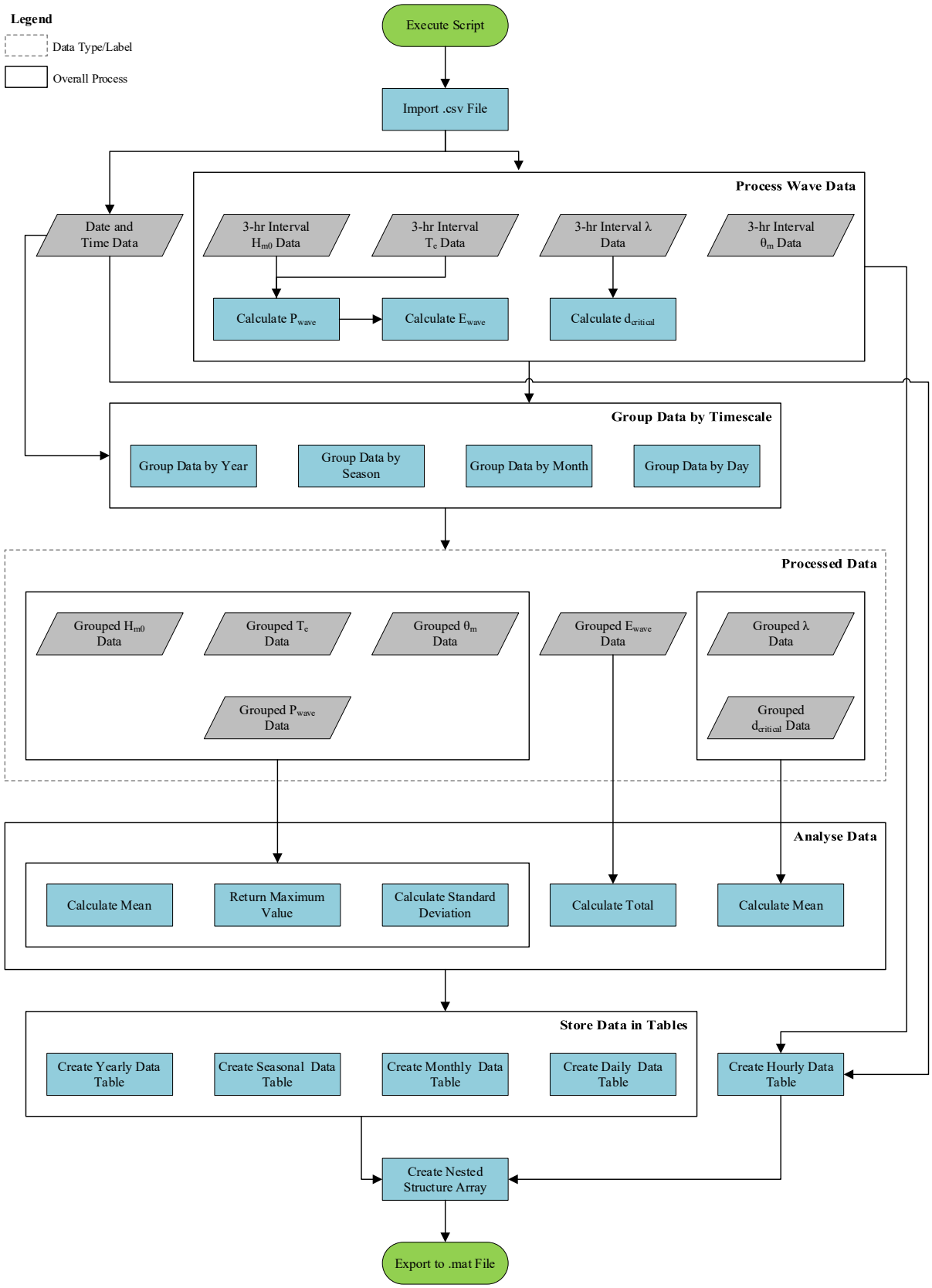

Figure A.3. Programming flow chart for Main_Wave_Power_V3.m script, outlining the main processes.

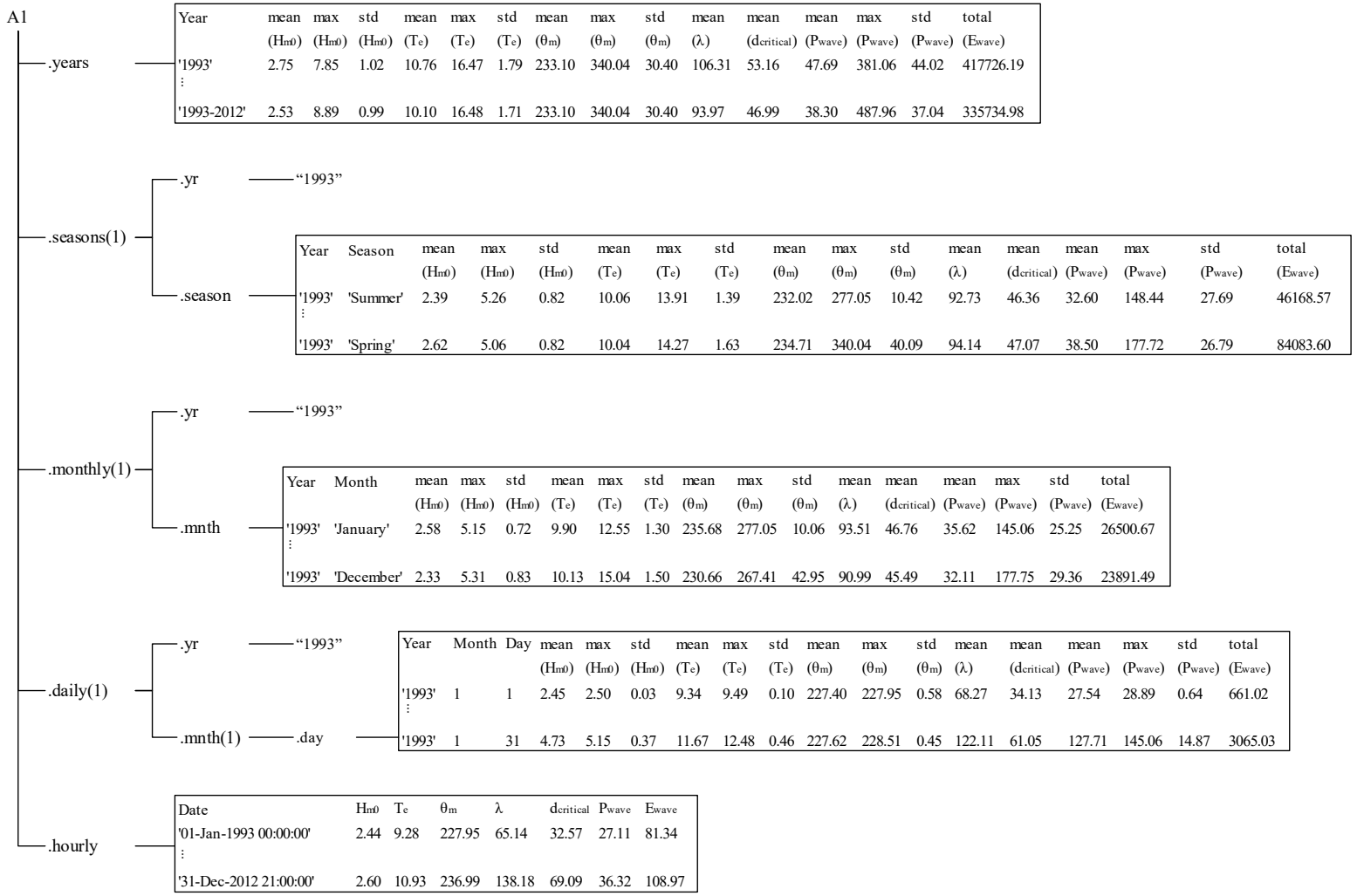

Figure A.4. Nested structure array utilised in MATLAB processing script for each site (Site A1 in this case). The first level of the structure array contains fields years, seasons, monthly, daily, and hourly.

A.2.2 Main_Combine_Wave_Power_Sites_V2.m

The Main_Combine_Wave_Power_Sites_V2.m script (Figure A.5) prompts the user to select the folder of .mat files that were generated from the Main_Wave_Power_V3.m script. The .mat files for each site are combined into a single nested structure array which utilised the site names (i.e., A1, A2, A3…) as the primary fields. This nested structure array is then exported (in a .mat file extension) to a user selected folder. Thereafter, two line charts and a clustered column chart are generated and saved as pdfs to the same user selected folder. The first line chart displays the average yearly power, for each year, over the 20-year time horizon for all the sites. The second line chart depicts the monthly values averaged over the 20 years for each site. Lastly, the clustered column chart depicts the average yearly and seasonal power averaged over the 20 year time period, which is available at each site.

Dependencies

a) save_figure.m: accepts the figure handle and full path and saves the relevant figure as a high resolution pdf.

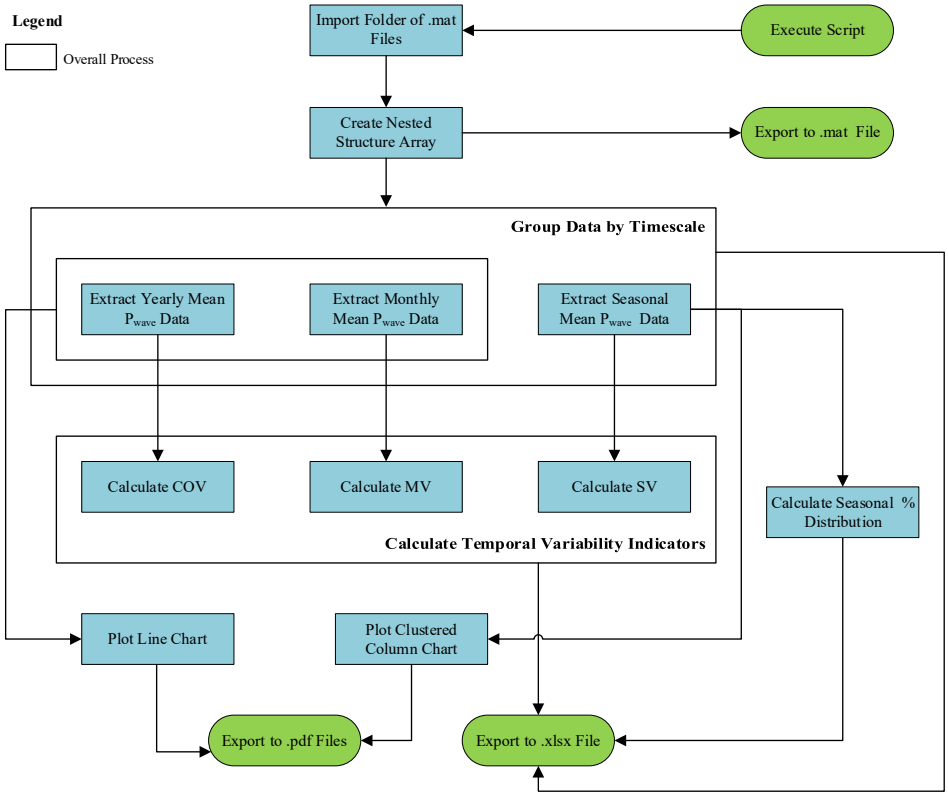

Figure A.5. Programming flow chart for Main_Combine_Wave_Power_Sites_V2.m, outlining the main processes.

A.2.3 Main_Export_Scatter_Data_V4

The Main_Export_Scatter_Data_V4.m script (Figure A.6) prompts the user to select a .csv file containing the wave parameters for a specific location, including but not limited to H_{m0}, T_e, T_{m02}, T_p, λ, and θ_m. The H_{m0}, T_e, and θ_m values are then separated according to years, seasons, months, and days and these datasets are exported to a .mat files. Thereafter, H_{m0}-T_e bivariate distributions are generated for each timescale (years, seasons, months, and days) in terms of: (i) count (frequency of observations in each bin), (ii) normalised count (count in a bin divided by the total number of observations), (iii) percentage occurrence (normalised count in bin x 100), (iv) mean P_{wave} occurrence for each sea state, and (v) percentage contribution of each sea state to the mean P_{wave}. The average P_{wave} for each timescale is also calculated. These outputs are then saved in a structure array, which is exported as a .mat file to a user selected folder.

Dependencies

a) separate_years_V2.m: sorts through the data and separates H_{m0}, T_e, and θ_m according to the year and returns a structure array containing these data.
b) separate_mnths_days_V2.m: sorts through the structure array generated from the separate_years_V2.m function and creates two new structure arrays containing H_{m0}, T_e, and θ_m data according to the: (i) months in the year and (ii) days in a month.
c) find_season_V3.m: sorts through the structure array containing the monthly data and creates a new structure array containing H_{m0}, T_e, and θ_m according to the seasons in a year.
d) create_scatter_V2.m: imports H_{m0} and T_e for a specific timescale (yearly, seasonal, and monthly) and generates bivariate distributions in terms of (i) count, (ii) normalised count, (iii) percentage occurrence, (iv) P_{wave} occurrence, and (v) percentage contribution. This function also calculates the average P_{wave} for each timescale. These values are returned to the main script in a structure array.
e) coordinates.m: determines the x and y coordinates of the bins, which is based on the centre of each cell (called in the create_scatter_V2.m function).
f) power_kW_m.m: creates a table populated with the theoretical P_{wave} for each sea state. For a particular wave condition, the theoretical P_{wave} was computed by utilising Equation (4.2), where the values of H_{m0} and T_e corresponded with the

centre of the bin being analysed. This function was called in the create_scatter_V2.m function.

g) name_mnth.m: accepts a number from 1–12 and returns the corresponding month name as a character data type (i.e., 1 = 'January' etc.). This function is called on in the main script as well as the separate_mnths_days_V2.m and find_season_V3.m function.

h) name_season.m: accepts a number from 1–4 and returns the corresponding season name as a character data type (1 = ‘Summer’; 2 = ‘Autumn’; 3 = ‘Winter’; 4 = ‘Spring’). This function is called on in the main script as well as in the find_season_V3.m function.

i) find_days.m: imports the monthly data and returns the H_{m0} and T_e values relating to a particular day for a specific year.

j) available_wave_data.m: imports the monthly data and plots a bar chart of the wave data availability for each month of a specific year.

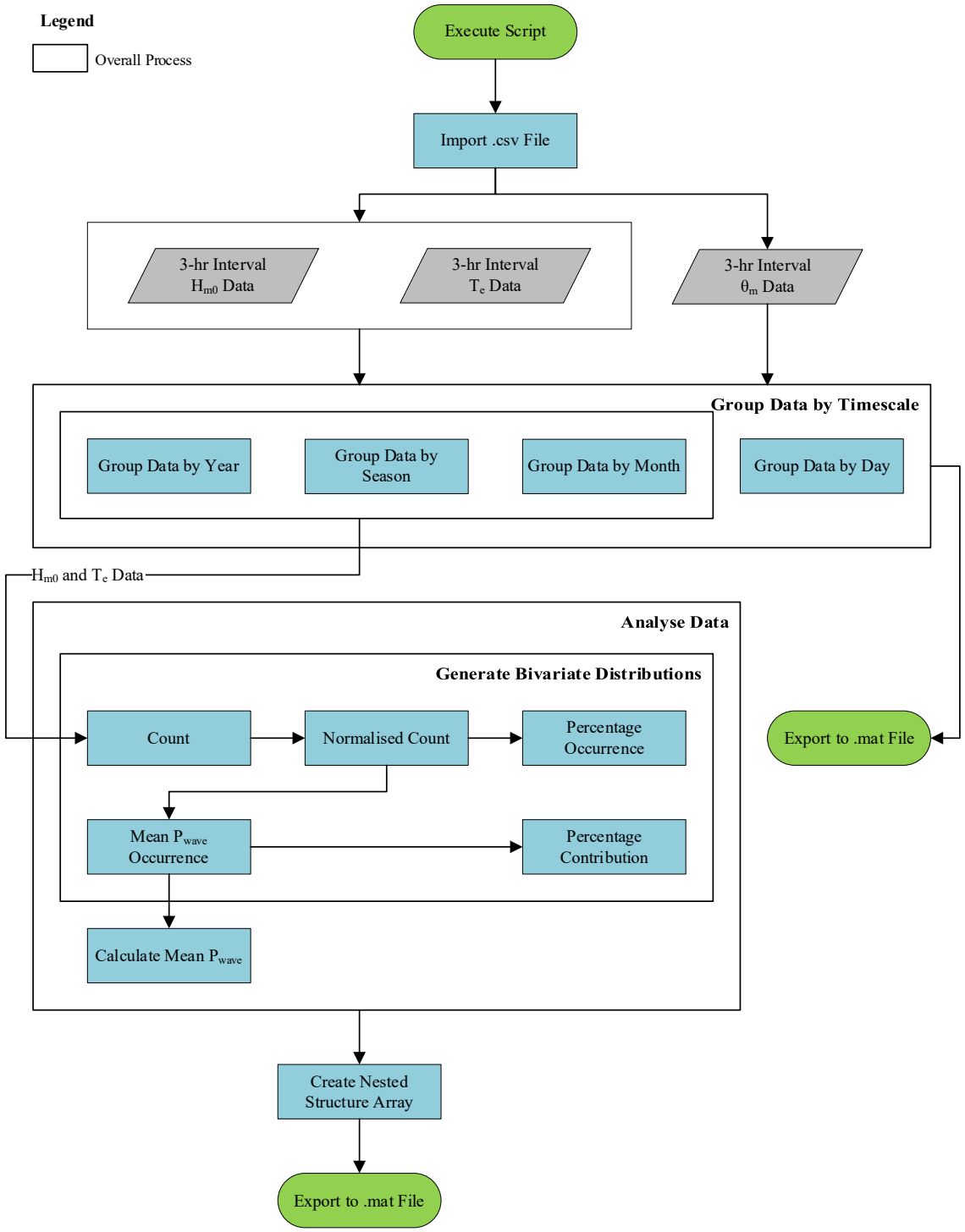

Figure A.6. Programming flow chart for Main_Export_Scatter_Data_V4.m, outlining the main processes.

A.2.4 Main_Wave_Roses.m

The Main_Wave_Roses.m script (Figure A.7) prompts the user to select a folder containing .mat files, for a specific location, that was generated from the Main_Export_Scatter_Data_V4.m script. For each timescale (yearly, seasonal, and monthly), H_{m0}, T_e, and θ_m values are extracted from the relevant .mat files. The H_{m0} and T_e values are used to calculate P_{wave}, utilising Equation (4.2). Thereafter, wave roses are generated for each timescale, from the P_{wave} and θ_m data, which are then exported as .pdf files to the initial folder selected by the user. Furthermore, the bivariate distribution data relating to each wave rose is extracted and exported as a .mat file to the same folder.

Dependencies

a) WindRose.m [230]: accepts P_{wave} and θ_m values and plots a corresponding polar bar chart ('wave rose') as well as return a table of the bivariate distribution data to the main script.
b) name_season.m: accepts a number from 1–4 and returns the corresponding season name as a character data type (1 = 'Summer'; 2 = 'Autumn'; 3 = 'Winter'; 4 = 'Spring').
c) name_mnth.m: accepts a number from 1–12 and returns the corresponding month name as a character data type (i.e. 1 = 'January' etc.).
b) save_figure.m: accepts the figure handle and full path and saves the relevant figure as a high resolution pdf.

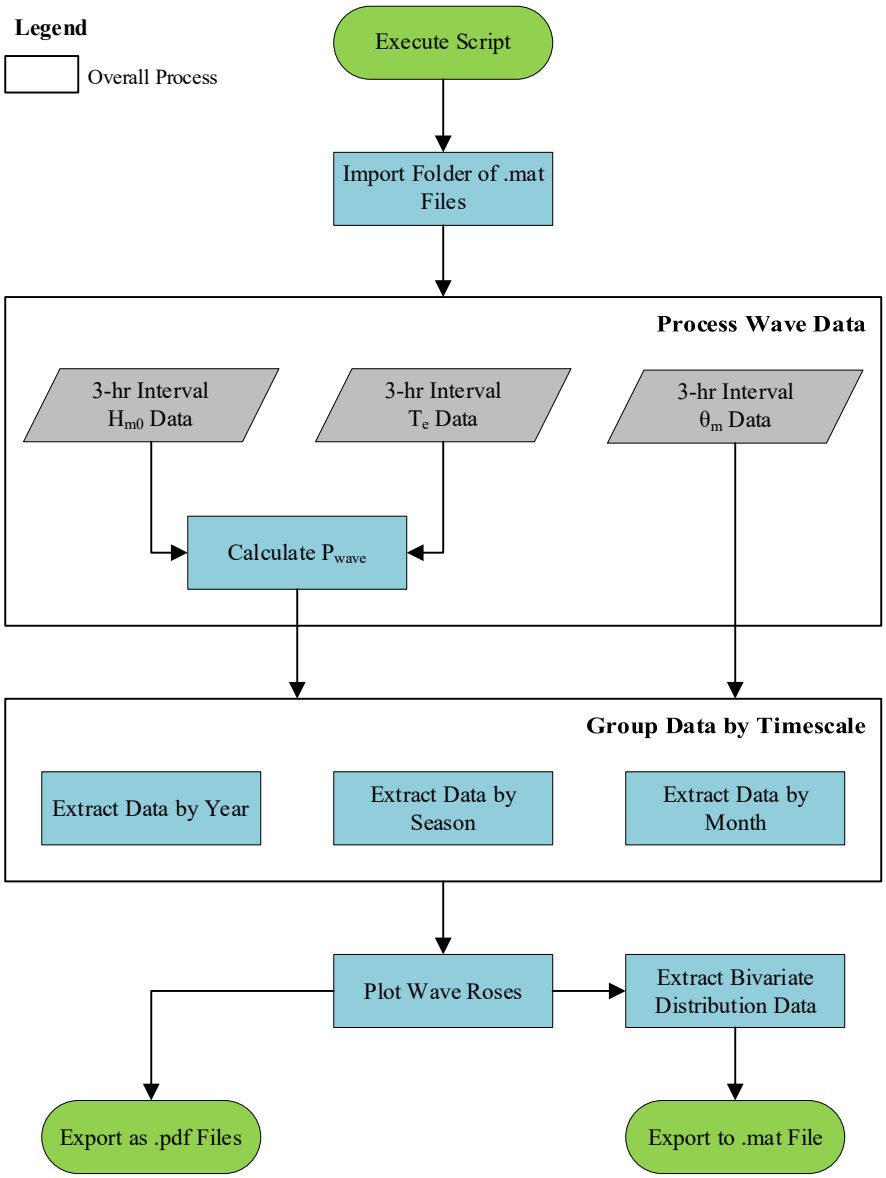

Figure A.7. Programming flow chart for Main_Wave_Roses.m, outlining the main processes.

A.2.5 Main_Export_Hist_and_Scatter.m

The Main_Export_Hist_and_Scatter.m script (Figure A.8) prompts the user to select a folder containing .mat files, for a specific location, that was generated from the Main_Export_Scatter_Data_V4.m script. For each timescale (yearly, seasonal, and monthly), the percentage occurrence and percentage contribution tabulated values are extracted from the relevant .mat files. A H_{m0} histogram, T_e histogram and bivariate histogram are generated (for each timescale and bivariate distribution), which are then exported as .pdf files to the initial folder selected by the user. Furthermore, the H_{m0} and T_e histogram data are extracted and exported as a .mat file to the same folder.

Dependencies

a) plot_scatter_histogram.m: generates a H_{m0} histogram, T_e histogram, and bivariate histogram for a specific timeframe. This function then returns the histogram data to the main script, and exports a single figure containing these three diagrams to a user selected folder.
b) name_season.m: accepts a number from 1–4 and returns the corresponding season name as a character data type (1 = ‘Summer’; 2 = ‘Autumn’; 3 = ‘Winter’; 4 = ‘Spring’).
c) name_mnth.m: accepts a number from 1–12 and returns the corresponding month name as a character data type (i.e. 1 = 'January' etc.).

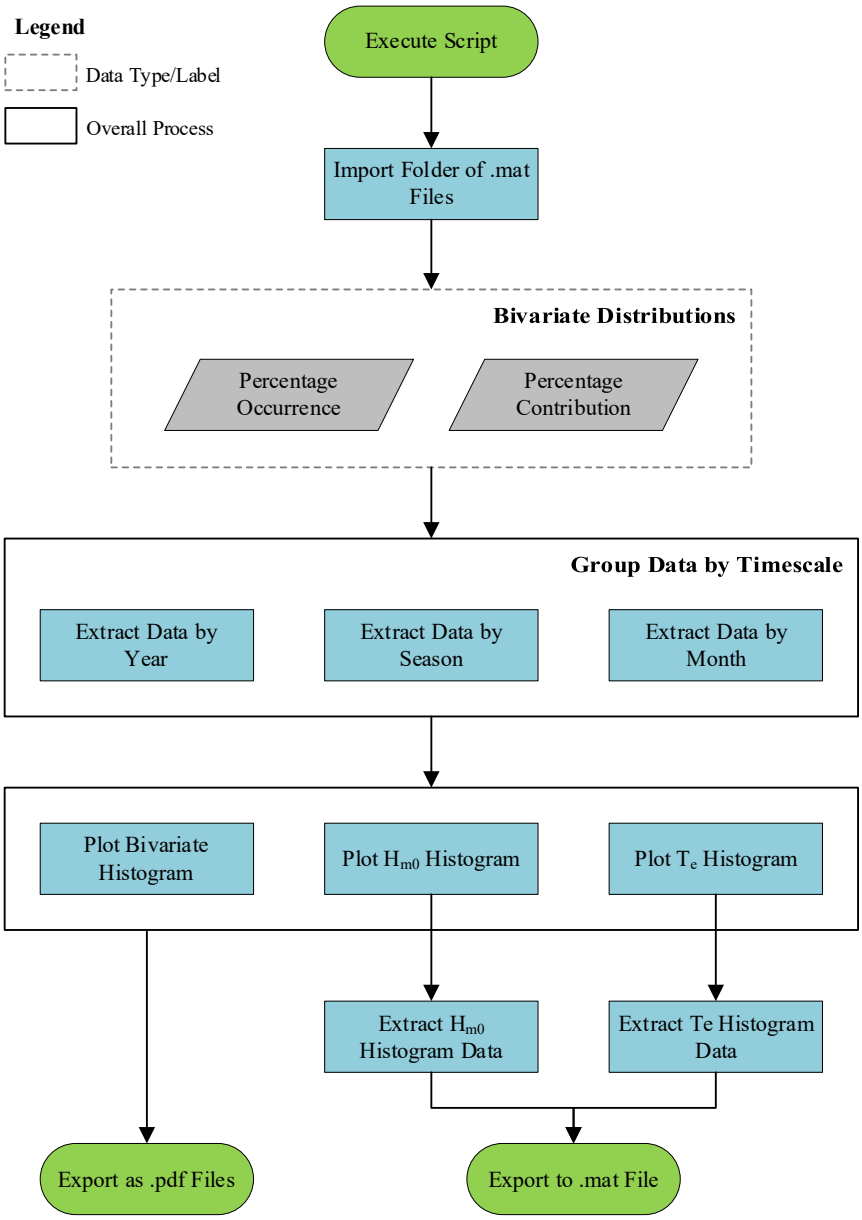

Figure A.8. Programming flow chart for Main_Export_Hist_and_Scatter.m, outlining the main processes.

Appendix B

Mapping of Significant Wave Height

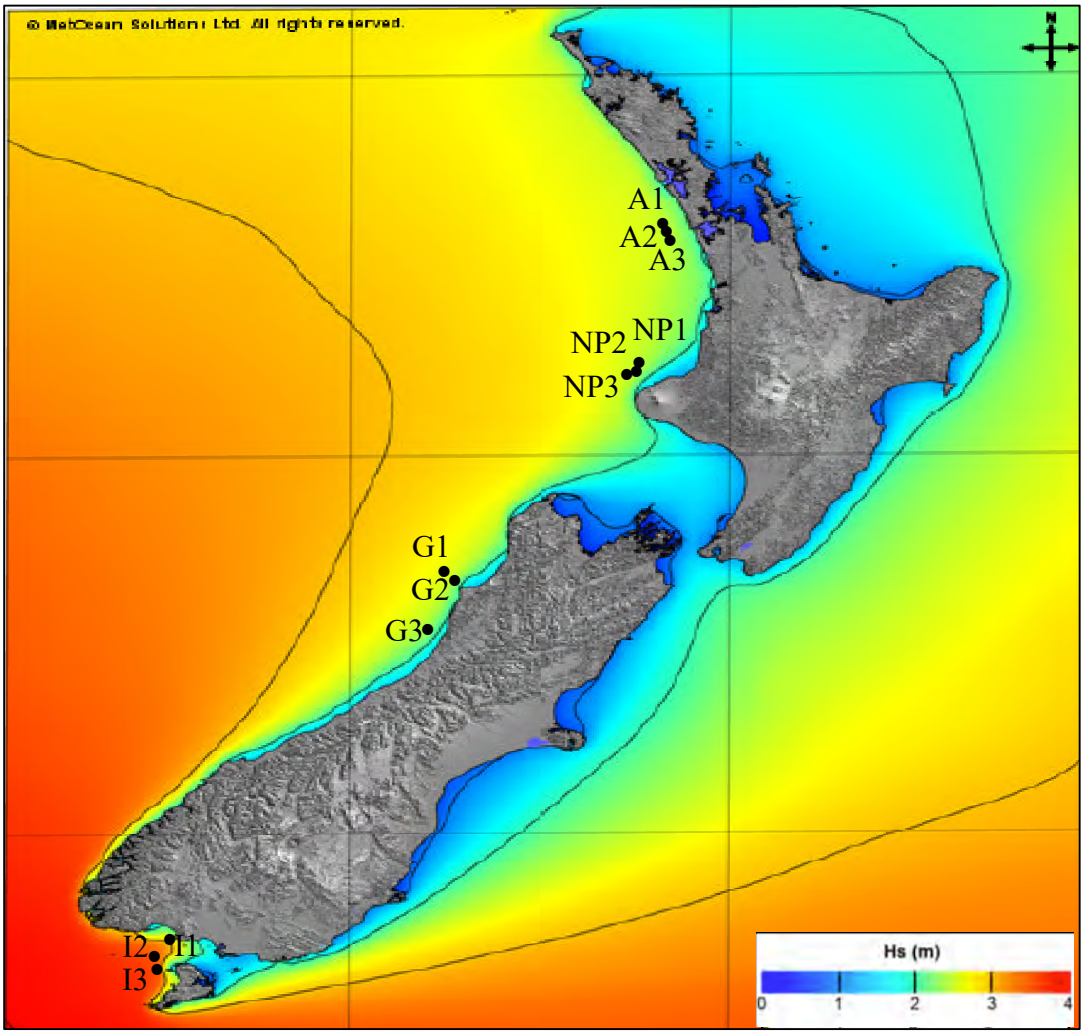

Figure B.1. Distribution of mean H_{m0} in NZ, from 1998–2007 [114]. Image has been adapted with the addition of the proposed NZ WEF sites. Reprinted with permission from MetOcean Solutions Ltd. (personal communication, July 24, 2020).

Table B.1. Typical H_{m0} and T_e values determined from the NZ Wave Data Tool (for the time horizon 1993–2012).

Sites	A1	A2	A3	NP1	NP2	NP3	G1	G2	G3	I1	I2	I3
H_{m0} [m]	2.5	2.5	2.5	2.5	2.5	2.6	2.7	2.4	2.1	3.0	3.4	3.4
T_e [s]	10.1	10.1	10.0	10.0	10.0	10.0	10.4	10.3	10.0	10.5	10.4	10.3

Appendix C

Global Distribution of Temporal Variability Indicators

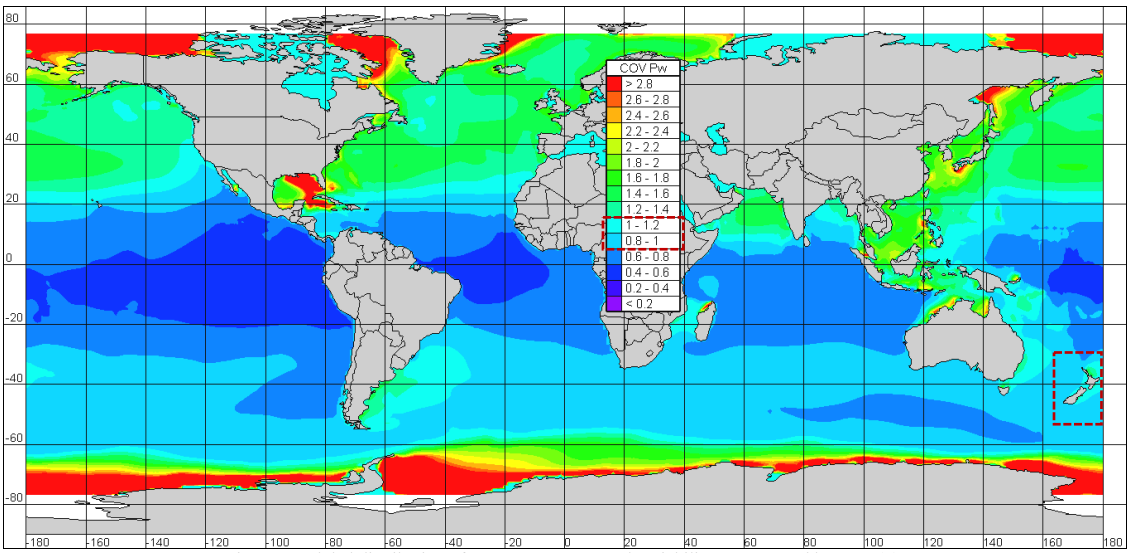

Figure C.1. Global distribution of wave power in terms of COV [21]. Image has been adapted by enclosing NZ (bottom right) and the values pertaining to the proposed NZ WEF sites (centre) in red dashed boxes. Reprinted with permission from A. Cornett (personal communication, June 26, 2020).

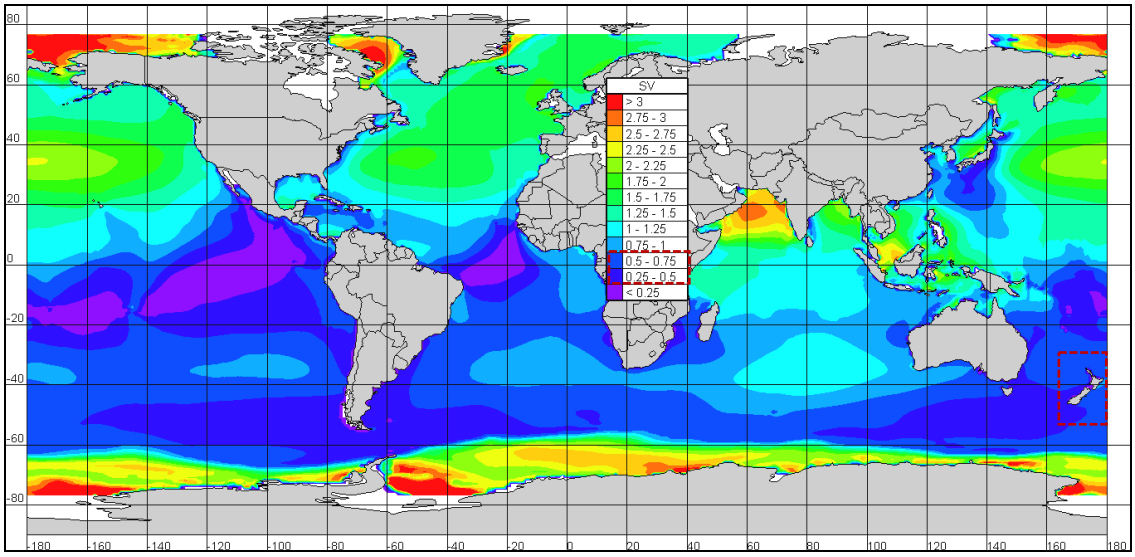

Figure C.2. Global distribution of wave power in terms of SV [21]. Image has been adapted by enclosing NZ (bottom right) and the values pertaining to the proposed NZ WEF sites (centre) in red dashed boxes. Reprinted with permission from A. Cornett (personal communication, June 26, 2020).

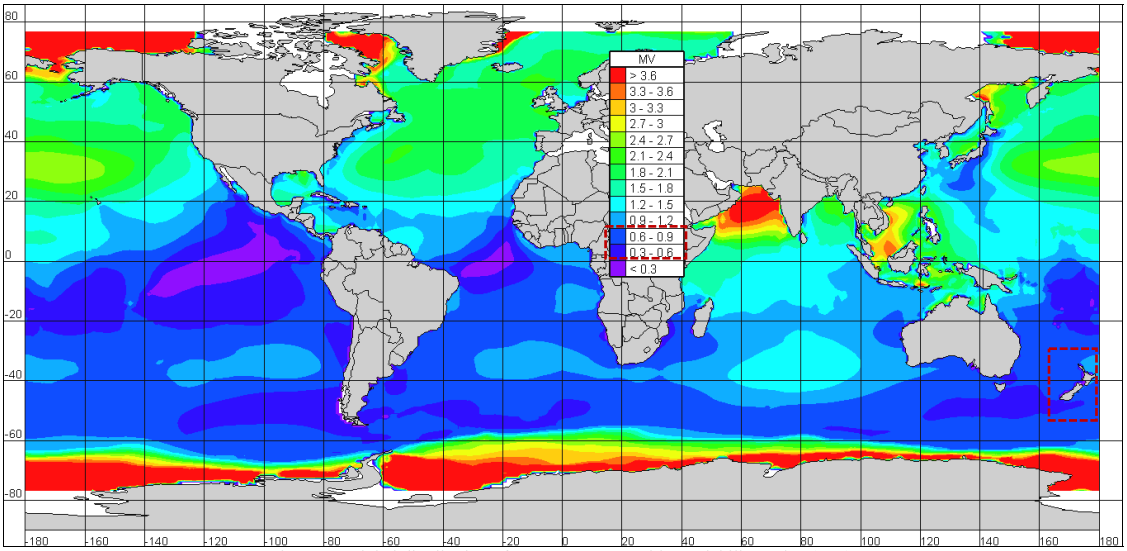

Figure C.3. Global distribution of wave power in terms of MV [21]. Image has been adapted by enclosing NZ (bottom right) and the values pertaining to the proposed NZ WEF sites (centre) in red dashed boxes. Reprinted with permission from A. Cornett (personal communication, June 26, 2020).